UNIVERSITÀ
DEGLI STUDI
DI PADOVA

Sede Amministrativa: Università degli Studi di Padova

Dipartimento **TERRITORIO E SISTEMI AGRO-FORESTALI (TESAF)**

SCUOLA DI DOTTORATO DI RICERCA IN :

"TERRITORIO, AMBIENTE, RISORSE E SALUTE"

CICLO XXVII

GEOMORPHOMETRIC ANALYSIS AND SEDIMENT DYNAMICS IN MOUNTAINOUS BASINS: SPATIAL AND TEMPORAL SCALES

Direttore della Scuola : Ch.mo Prof. Mario Aristide Lenzi

Supervisore : Dr. Lorenzo Marchi

Co-supervisore: Dr. Marco Cavalli

Dottoranda : Beatrice Goldin

ACKNOWLEDGEMENTS

I would like to thank the following people and institutions that make this work possible:

- My supervisor, Dr. Lorenzo Marchi, for giving me the opportunity to obtain my PhD at the IRPI-CNR institute, which funded this project, and for numerous helpful discussions on the main topics. His advices helped me grow to be a more mature researcher;
- My co-supervisor, Dr. Marco Cavalli, for the huge help throughout these years, for teaching me the essential skills for conducting a high-level research and for fruitful discussions, for being a guide and having transmitted the passion for research;
- Pierpaolo Macconi and Omar Formaggioni, who kindly provided technical information on the database of natural hazard phenomena, one of the sources of information of this work;
- Dr. Eric Bardou, research scientist at CREALP, for his precious advices related to ongoing research activity and for having kindly worked together on the interpretation of sediment connectivity variability on glacierized catchments. I would also like to thank all the people working at the CREALP for their support and pleasant coffee breaks;
- My office mate Stefano Crema, for his help and suggestions, and for sharing opinions about PhD activity;
- My colleagues at IRPI for the good time we spent together, drinking and eating, talking and laughing;
- Giacomo Blasone for sharing ideas about DoD improvements;
- My family, for their encouragements and advices throughout the PhD formation, for believing me and for inspiring me to follow my dreams;

- My boyfriend Andrea for his patience and support during all these years, for making me smile during hard times, for his understanding and sharing my mountain passion. Thanks for everything.

RIASSUNTO

Il presente lavoro è consistito nello sviluppo e nell'applicazione di metodi geomorfometrici per l'analisi della dinamica del sedimento legata a processi di trasporto solido e colate detritiche a diverse scale temporali e spaziali in ambiente alpino.

L'analisi ha riguardato due aspetti principali. Nella prima parte, sono state analizzate, da un punto di vista quantitativo (variazioni areali e volumetriche) e qualitativo (pattern di distribuzione spaziale dei processi erosivi e di deposizione), le variazioni morfologiche avvenute in un arco temporale di sei anni in due piccoli bacini (Gadria e Strimm) della Val Venosta (Alpi Orientali, Italia). L'analisi dei cambiamenti geomorfologici è stata effettuata determinando i DTM delle Differenze (*DTM of Difference*, DoD) ottenuti dal confronto di modelli digitali ad alta risoluzione (2 m) derivati da rilievi LiDAR ripetuti nel tempo disponibili per entrambi i bacini.

Per la determinazione del DoD è stato applicato un metodo di spazializzazione dell'errore verticale basato sulla logica *fuzzy* che ha previsto l'utilizzo di parametri legati alla qualità ed accuratezza dei DTM e alla complessità topografica dell'area di interesse, quali la densità della nuvola di punti al suolo e la pendenza.

I volumi di sedimento erosi e depositati dagli eventi verificatisi nell'arco temporale analizzato, ottenuti dall'applicazione del metodo descritto, sono stati confrontati con i dati di campo presenti in un sistema integrato e aggiornato di documentazione dei fenomeni torrentizi e fluviali gestito dalla Provincia Autonoma di Bolzano. L'utilizzo di un approccio basato sulla spazializzazione dell'incertezza verticale per l'analisi DoD ha consentito di recuperare parte dell'informazione relativa a variazioni morfologiche di piccola entità in aree a bassa pendenza che sarebbero andate perdute nel caso fosse stata considerata una spazializzazione spazialmente uniforme. L'analisi ha inoltre evidenziato la possibilità di utilizzare il

DoD per l'identificazione di processi erosivi e deposizionali in aree non facilmente accessibili e di eventi non rilevati mediante osservazioni di terreno.

L'analisi delle relazioni tra parametri geomorfometrici, come la curvatura (planare e di profilo), la pendenza e l'area drenata, e i cambiamenti geomorfologici rilevati col DoD ha apportato un valido contributo all'interpretazione qualitativa delle variazioni occorse a completamento delle stime volumetriche di erosione e deposito. Queste relazioni possono essere utilizzate per valutare quantitativamente le variazioni dell'assetto morfologico conseguenti ad eventi di erosione e deposito.

La seconda parte è stata dedicata all'analisi della connettività del sedimento a diverse scale spaziali sia in termini di risoluzione del DTM che di estensione geografica. L'analisi è stata condotta utilizzando un indice di connettività del sedimento a base morfometrica (IC) proposto da Borselli et al. (2009) e adattato da Cavalli et al. (2013) all'ambito montano. IC applicato a DTM ad alta risoluzione consente di caratterizzare spazialmente la potenziale connettività del sedimento tra versante e aree di particolare interesse (e.g. strade, sezione di chiusura del bacino, corsi d'acqua). È stata valutata l'applicabilità del modello in un contesto regionale (alta e media Val Venosta) che presenta un'alta variabilità in termini topografici e di uso del suolo. In particolare, sono stati analizzati gli effetti della risoluzione del DTM sui risultati di IC e la variabilità dell'indice stesso applicato a bacini selezionati all'interno dell'area della Val Venosta caratterizzati da diversa forma, dimensione, pendenza e dinamiche di trasporto del sedimento. La dipendenza dell'indice dall'area del bacino, dovuta soprattutto alla componente *downslope* che considera la lunghezza del percorso che il sedimento deve affrontare per raggiungere un *sink*, suggerisce che il modello applicato consente il confronto principalmente tra bacini che presentano dimensioni simili. La risoluzione sembra invece influire non solo in termini di valori medi ma anche, ed in misura più evidente, sulla distribuzione spaziale della connettività sia a scala di bacino sia a scala regionale. D'altra parte i risultati ottenuti hanno evidenziato la possibilità di utilizzare l'indice

di connettività come strumento per una rapida caratterizzazione spaziale della connettività del sedimento su ampie aree ed in aree morfologicamente complesse interessate da diversi processi di trasporto del sedimento come colate detritiche e trasporto solido canalizzato.

Le due tipologie d'analisi finalizzate allo studio a diverse scale spaziali e temporali delle aree di studio, presentate in modo distinto nella presente tesi, possono considerarsi tuttavia connesse. L'applicazione, infatti, di IC in un bacino caratterizzato dalla presenza di un ghiacciaio soggetto a ritiro (Zinal, Svizzera) ha consentito di valutare l'effetto del processo di scioglimento del ghiacciaio stesso sulla potenziale connettività del sedimento dopo un periodo di circa quarant'anni. L'analisi qualitativa della variazione dell'indice di connettività in relazione al ritiro del ghiacciaio ha dimostrato come il grado di connettività del sedimento sia un fattore chiave nel controllare il rilascio di sedimento tra versanti e canale principale e come i flussi sedimentari futuri provenienti dalla zona soggetta a scioglimento dipendano in modo critico dallo sviluppo di morene laterali.

Nel complesso, l'elevata risoluzione dei DTM derivati da rilievi LiDAR, valorizzata tramite l'impiego di idonei strumenti per l'analisi geomorfometrica, ha consentito sia di cogliere le variazioni, dovute al succedersi di più eventi a scala di bacino sia di ottenere mappe di previsione sulla potenziale connettività del sedimento a diverse scale spaziali in aree caratterizzate da diversa morfologia e processi di trasporto.

ABSTRACT

In this work geomorphometric methods were applied at different spatial and temporal scales for the analysis of the sediment dynamic related to debris flows and bedload sediment transport in alpine environments.

The thesis involves two kinds of analysis. The first is aimed at investigating morphological changes occurred in a six years period in two catchments (Gadria and Strimm) of Venosta valley (Eastern Alps, Italy). The study areas were analyzed from both a quantitative (volumetric and areal variations) and qualitative (spatial distribution pattern of erosion and deposition) perspective. The multitemporal analysis was performed by calculating the digital terrain model (DTM) of Difference (DoD) obtained from the comparison of high resolution DTMs (2m), related to both studied catchments, derived from successive LiDAR surveys.

A method based on fuzzy logic that takes into account the spatial variability of DTM vertical error was applied to derive the DoD. To evaluate the uncertainty in both pre-event and post-event DTMs, two geomorphometric parameters, i.e., ground point density and slope, approximating the quality of the DTM and the topographic complexity of the study area, respectively, were considered.

Volumes of sediment eroded and deposited by events occurred in the analyzed period, as computed by the DoD, were compared to field survey data derived from a database of historical events provided by the Autonomous Province of Bolzano.

The use of a spatially variable uncertainty permitted both to recover the information related to low magnitude changes in gentle slope areas that would be lost if a uniform threshold was applied. The analysis also highlighted the possibility to use the DoD for the identification of erosion and deposition processes in uneasily accessible areas and of events that could not be detected through field surveys.

The analysis of the relationship between geomorphometric parameters, such as curvature (planform and profile), slope and drainage area, and geomorphologic changes detected by the DoD, improved the qualitative interpretation of surface variations, integrating the volumetric estimates of erosion and deposition.

The second analysis involves the investigation of sediment connectivity at different spatial scales both in terms of DTM resolution and geographic extent. The analysis was carried out by using the index of connectivity (IC) proposed by Borselli et al. (2009) and modified by Cavalli et al. (2013) for the analysis of alpine catchments. IC applied to high resolution DTMs allows the spatial characterization of the potential sediment connectivity between hillslope and areas of particular interest (e.g. road, basin outlet, channel). The feasibility of applying IC at regional area (Venosta valley) presenting high topographic and land use variability was tested. In particular, the effect of the DTM resolution on IC results and the variability of the index applied to selected basins of Venosta valley characterized by different shape, size, slope and sediment dynamics, was investigated. The dependence of the sediment connectivity index on the drainage area, mainly due to the downslope component of the index that considers the length of sediment pathways to reach a target or a sink, implies that only basins of similar size can be compared. DTM resolution affects not only mean values of IC but also the spatial distribution of the sediment connectivity both at basin and regional scale.

Nevertheless, the obtained results highlight the possibility to apply the connectivity index for a rapid spatial characterization of the sediment connectivity at large scale and in areas characterized by complex morphology and different sediment transport processes such as debris flows and bedload transport.

The two analyzed scales, spatial and temporal, even if presented separately in the thesis, can be considered connected. The application of the connectivity index in a basin undergoing glacier retreat (Zinal glacier, Switzerland) allowed the evaluation in a future scenario of the melting process on the potential sediment connectivity

after a period of fourty years. Qualitative analysis of the variation of the geomorphologic index suggested that the degree of sediment connectivity is a key factor in controlling the release of sediment between hillslopes and main channel and that future sediment fluxes coming from the melting zone critically depend on the lateral moraines development.

As a general conclusion of this study, the high resolution of digital terrain models derived from LiDAR surveys, coupled with the use of suitable tools for geomorphometric analysis, permitted both to evaluate geomorphic changes, caused by multiple events, occurred at basin scale and to create scenario map of the potential sediment connectivity at different spatial scales, in areas characterized by different morphology and sediment transport processes.

CONTENTS

LIST OF FIGURES

LIST OF TABLES

CHAPTER 1

INTRODUCTION

Natural processes related to sediment erosion, transport and deposition play a major role in shaping the morphology of mountainous catchments and may result in severe hazard when sediment transport occurs in paroxysmal ways, as in the case of debris flows and debris floods.

Uncertainties in the evaluation of sediment dynamics in mountainous catchments are due to both the complexity of the processes and to the difficulty of gathering reliable experimental data. Regarding the issue of field data collection, both technical problems (e.g. the difficulty in evaluating the depth of erosion and the thickness of the deposits) and economical and time resources constraints hamper sediment monitoring on large areas.

High-resolution DEMs can help overcoming the limits mentioned above on sediment data in mountainous catchments, permitting the analysis of sediment dynamics on large areas and favoring the development of new analytical techniques. Among remote sensing technique, LiDAR (or laser scanning), providing a high-resolution description of the topography, opened new perspective in the investigation of natural processes, especially in mountain basins where complex morphology plays a fundamental role in the geomorphological and hydrological response. The availability of high accuracy and high resolution DEMs allowed the development and the update of quantitative methods for the description of different processes. Geomorphometry emerges thus as a new analytical approach for the quantification of the surface morphology and related building processes at various spatial and temporal scales.

In this work, the main objective is the analysis of the feasibility of different geomorphometric indices, derived from LiDAR derived high-resolution DTMs, to

evaluate the sediment dynamic in mountain basins linked to bedload and debris flow processes. The research involves the analysis of the sediment connectivity carried out at regional and basin scale and the estimation of morphological variations occurred at basin scale. Further analysis between investigated processes and morphometric relationship was also investigated. The following questions will be answered in detail:

1) Can potential sediment connectivity be modeled by applying a topographic index to high-resolution data at large scale?
2) Is the sediment connectivity index dependant from the computational scale?
3) Which are the main factors (impedance to sediment transport, catchment area, shape and slope) that influence the sediment topographic index at basin scale?
4) How geomorphic changes resulting from the DTM of Difference between two LiDAR surveys can be compared with post-event field surveys?
5) How could glacier retreat influence the sediment connectivity in an alpine catchment?

The work is structured as follows:

– Chapter 2 recalls some basic issues of geomorphometry, including the main parameters used in this thesis, and summarizes the state of the art of sediment connectivity and geomorphologic changes analysis;
– Chapter 3 describes the main characteristics of study areas (Venosta Valley, Gadria and Strimm catchments, in Eastern Italian Alps, and Navizence catchment in Swiss Alps) giving necessary information on geomorphology that had to be considered for the application of geomorphometric methods;
– Chapter 4 presents the data collected and the methods applied for the analysis of sediment connectivity and of geomorphologic variations;
– Chapter 5 reports and discussed obtained results;
– Chapter 6 draws the main conclusions of the research, stressing the important findings of the present work.

CHAPTER 2
LITERATURE REVIEW

2.1 Geomorphometry

Geomorphological and hydrological processes are closely linked to the topography of a landscape. The need to incorporate a quantitative measure of topography for hydro-geomorphological analysis dates back to the mid-twentieth century when an interdisciplinary science, named geomorphometry, evolving from mathematics and earth sciences, appeared (Pike et al., 2009). Defined as "the science of quantitative land surface analysis that deals with the recognition and quantification of landform and surface processes" (Rasemann, 2004), geomorphometry is nowadays a modern analytical and cartographic approach revolutioned by the advent of computers and the development of Geographic Information System (GIS) and modern data acquisition techniques.

The most widely used data structure employed to store and accurately characterize information about topography in a GIS environment is a land-surface model, i.e. the Digital Elevation Model (DEM) usually in a form of a grid or vector map of elevation points (Pike et al., 2009).

From the literature, different model definitions exist according to the variety of their applications in terrain modelling. The three most common models used are (Cavalli, 2009; Bishop, 2013; Wasklewicz et al., 2013):

- DEM (Digital Elevation Model), which describes the altitude of land topography;
- DSM (Digital Surface Model), that relates to the actual structure of the land surface, including human-built structures, vegetation and other objects on the surface (Fig. 2.1);

- DTM (Digital Terrain Model), that is the result of a workflow process of sampling elevations, preprocessing data to obtain a DEM, and analyzing and removing errors. Unlike DSM, DTM is defined only by ground points (i.e. filtered from vegetation and human structures).

Although raster DEM require large amounts of storage, they are the main structure used for geomorphometric applications. The widespread use of gridded DEMs derives firstly from their simple structure; as it is spatially uniform, the main controlling factor of its properties is represented only by the cell size. Thanks to these characteristics, raster DEMs are more suitable for images processing and geomorphometric analysis than other model structure (e.g. vector data) since easier algorithms can be applied (Hengl and Evans, 2009).

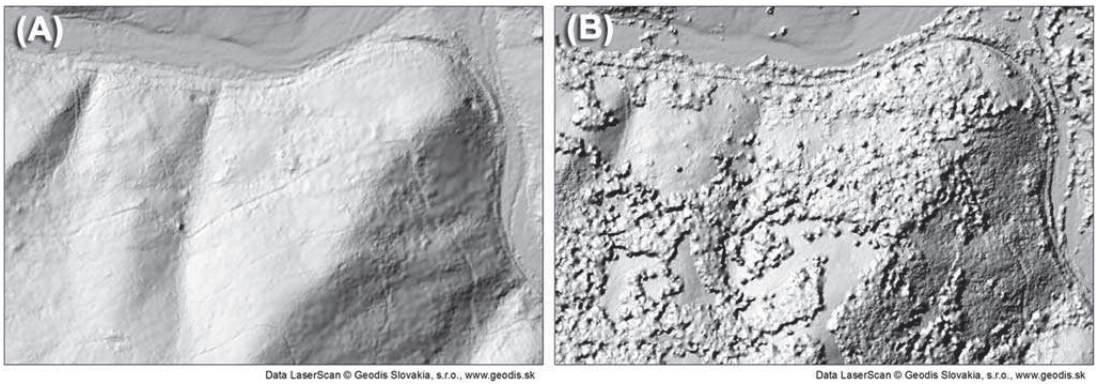

Figure 2. 1: Examples of a DEM (A) and a DSM (B) of a same area (Smrecek et al., 2013).

In the present study the term DEM is referred to a general model of the terrain whereas DTM is used only for bare ground models derived from LiDAR data.

2.1.1 Geomorphometric analysis: parameters and indices

The main purpose of geomorphometry is the extraction from a DEM of topographic elements describing the morphology of the surface. Principal steps of geomorphometric analysis, summarized in Figure 2.2, are (Pike et al., 2009):

- Land surface sampling (i.e. elevation measurements acquisition);
- Derivation of a digital model (DEM) from sampled elevations;
- DEM processing and error assessment;
- Derivation of landform parameters and indices from processed DEM;
- Geomorphic analysis applying calculated index and parameters.

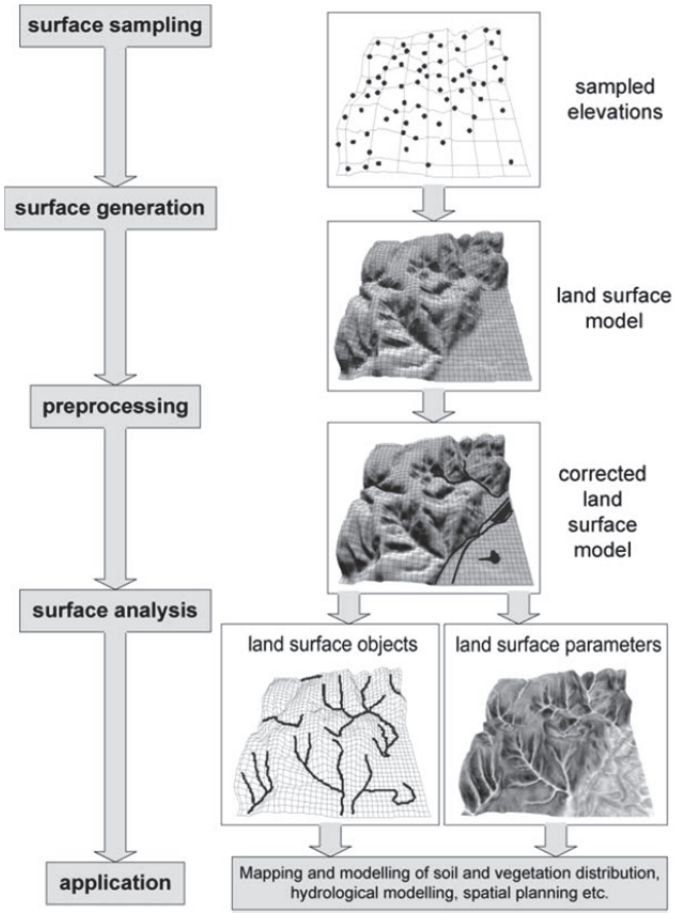

Figure 2. 2: Synthetic diagram of geomorphometric analysis process (Pike et al., 2009).

According to Pike et al. (2009) DEM derived topographic elements and indices can be differentiated into:

- Parameter (or attribute): descriptive measure of landforms (e.g. slope, curvature, wetness index), generally described by continuous value (i.e. raster image);
- Object: discrete spatial feature (e.g. watershed line, cirque, alluvial fan, drainage network), generally represented on a vector map consisting of points, lines or polygons.

Wilson and Gallant (2000) applied a further distinction between primary and secondary attributes (Tab. 2.1). Primary attributes can be derived directly from the DEM (e.g. slope, aspect, curvature) whereas secondary attributes are computed from two or more primary topographic attributes.

Primary attributes, calculated as derivatives of a surface, are useful for the description of the morphometry and surface attributes of hillslope and channels or for landform classification. Secondary attributes plays a fundamental role for hydrological and geomorphological analysis since they describe and quantify the spatial variability of a process occurring in the landscape (Wilson and Gallant, 2000).

Table 2. 1: Selection of commonly used primary and secondary parameters (Wilson and Gallant, 2000, modified).

Category	Parameter	Processes involved
Primary parameters	Aspect	Evapotranspiration, flora and fauna distribution and abundance, snowmelt
	Slope	Overland and subsurface flow velocity, vegetation, soil water
	Catchment area	Runoff volume
	Flow path length	Erosion rate, sediment yield
	Profile curvature (i.e. parallel to the direction of the maximum slope)	Erosion/deposition rates
	Planar curvature (i.e. perpendicular to the direction of the maximum slope)	Converging/diverging flow, soil characteristics
Secondary parameters	Wetness index $W_T = ln\left(\frac{A}{Ttan\,\beta}\right)$ $W = ln\left(\frac{A_s}{tan\,\beta}\right)$	Soil saturation
	Stream power indexes $SPI = A_s \tan\beta$ $LS = (m+1)\left(\frac{A}{22.13}\right)^m \left(\frac{sin\beta}{0.0896}\right)^n$ $CIT = A_s(\tan\beta)^2$	Runoff erosion, sediment transport capacity, headwaters prediction

Morphometric analyses on a raster DEM are generally computed through the application of a neighborhood function based on the concept of the moving window, i.e. a regular matrix of n x n cells of different size and form that repeats an algorithm on the entire grid shifting from upper left to lower right corner. By using

the moving window it is possible to extract parameters and indices (e.g. slope) from local scale to greater extensions (Pike et al., 2009).
The parameters used in this study are described in more detail in the following sections.

Slope. Slope is the measure of steepness or the degree of inclination of a feature relative to the horizontal plan. The slope can be considered one of the most important aspect of the surface form since "it controls the gravitational force available for geomorphic work" (Evans, 1972). Expressed as the percent gradient or the angle of the slope, this parameter can be both calculated from field measurements and derived from DTMs. Several mathematical algorithms are available in the scientific literature for the computation of slope from DTMs (Ritter, 1987; Horn, 1981; Unwin, 1981; Zevenbergen and Thorne, 1987; Sharpnack and Akin, 1969; Wood, 1996; Travis et al., 1975). Most of these methods are based on the computation of the local slope for each cell on the DTM within a cell moving window (Vianello et al., 2009). The choice of a method can depend on the different morphology represented by the DTM: for example the slope algorithm developed by Horn (1981) is suited for rough surfaces whereas that presented by Zevenbergen and Thorne (1987) performs better on smoother surfaces (Burrough and McDonnell, 1998).

Drainage area. The drainage or contributing area is the total area flowing into a given point (outlet). The computation of the drainage area depends on the calculation of the flow direction i.e. the direction that water would flow through every cell of the DEM. Different algorithms can be applied to determine the flow direction:

- The single-flow direction D8: this method, introduce by O'Callaghan and Mark (1984), assigns flow from each cell to one of its 8 neighbors, either

adjacent or diagonal, in the direction of the steepest downslope gradient (Gruber and Peckham, 2009). Since flow can accumulate into a cell from several cells and can be distributed only into a single cell, this algorithm can be used to model the flow convergence in streamlines and channels, but not the divergence on convex surfaces (Gallant and Wilson, 2000);

- Multiple-flow-direction (MFD): this method overcomes the limits of the D8 by partitioning the flow out of one cell into all of the neighbor cells. MFD methods allow both the evaluation of the flow dispersion from a ridge and the modeling of complex hydrology of a segmented hillside (Gruber and Peckham, 2009);
- D infinity (D∞): proposed by Tarboton (1997), this method defines the flow direction as the angle of the steepest descent determined by the analysis of 8 triangular facets formed by the 3x3 cell neighborhood. An infinite number or flow directions, represented as an angle between 0 and 2π, are possible. Flow from a grid cell is shared between the two downslope grid cells closest to the vector flow angle based on angle proportioning. The D∞ algorithm allows a better representation of water flow on divergent slopes since from a cell it will either go to one or two of the neighboring cells (Tarboton, 1997)

Slope and drainage area are considered important parameters in the study of erosion since they control the nature and efficiency of transport processes (Lague et al., 2000, Tarolli and Dalla Fontana, 2009). In particular, the **relationship between slope and drainage area** can be used to analyze the relation between landforms and erosion processes (Hack, 1957; Tarboton et al., 1989; Montgomery and Foufoula-Georgiou, 1993; Tucker and Bras, 1998; Montgomery, 2001). Based on different patterns of slope-area relation in a log-log diagram it is possible to depict a partitioning of the landscape into different patterns (Fig. 2.3) defining hillslopes, unchanneled valleys, debris flow-dominated channels and alluvial channels

(Montgomery and Foufoula-Georgiou, 1993). The log-log diagram of slope-area relationship has been used to define both the threshold between erosion and landslide processes (Tucker and Bras, 1998) and the topographic signature of valley incision by debris flows (Stock and Dietrich, 2003).

Using slope-area relationship, several studies proposed threshold criteria to determine the network sources locations from DTM (Tarboton 1991, O'Callaghan and Mark, 1984; Band, 1986; Mark, 1988; Montgomery and Dietrich, 1992; Dietrich et al., 1993). Threshold criteria based on the relation between local slope and contributing area have also been proposed to identify the threshold for debris flow potential initiation sites (Cavalli and Grisotto, 2006).

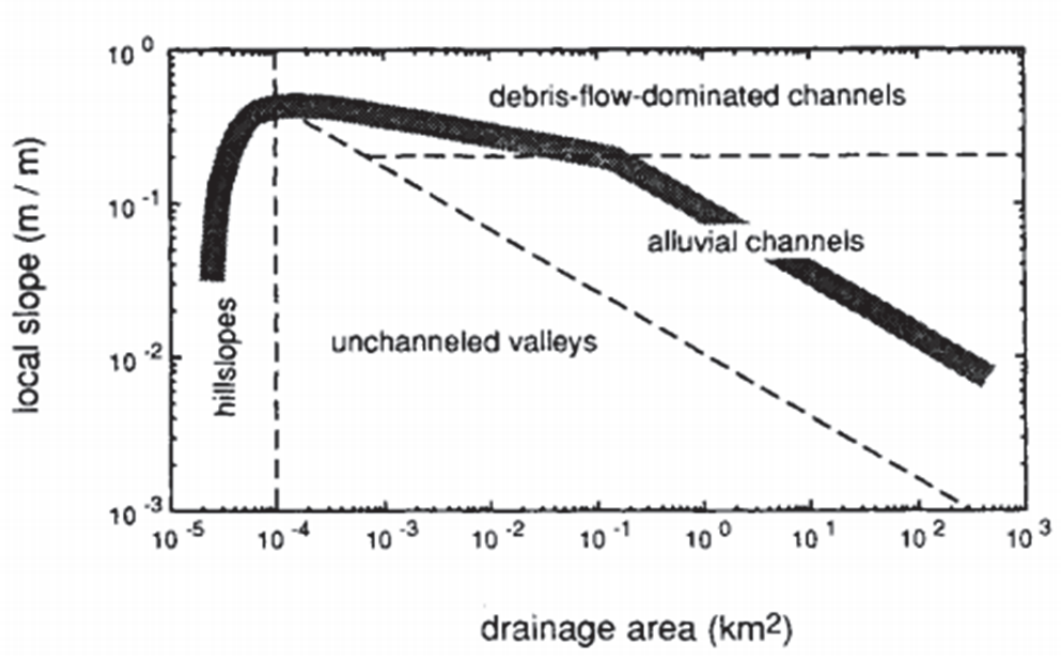

Figure 2. 3: Schematic illustration of relationship between slope and drainage area defining hillslope-valley transition and channel initiation (Montgomery and Foufoula-Georgiou, 1993).

Hillshade is a representation of a surface exposed to a hypothetical illumination of a surface. The hillshade can be calculated by simulating the presence of a hypothetical light source whose position is determined by specifying the azimuth angle (i.e. the angle from which the terrain is illuminated ranging from 0 to 360°).

The hillshade map can greatly enhance the visualization and understanding of a topographic surface derived from a DEM.

Topographic roughness refers to the irregularity of a topographic surface, implying the variation of slope in a terrain. Several algorithms have been proposed in the literature to compute topographic roughness (Shepard et al., 2001; McKean and Roering, 2004; Glenn et al., 2006; Frankel and Dolan, 2007; Booth et al., 2009; Hani et al., 2011). In this thesis the roughness was calculated as the standard deviation of the residual topography on a moving window (Cavalli et al., 2008; Cavalli and Marchi, 2008; Cavalli, 2009):

$$\sigma = \sqrt{\frac{\sum_{i=1}^{25}(x_i - x_m)^2}{25}} \qquad [2.1]$$

where σ is the roughness index-elevation or the standard deviation of residual topography, 25 is the number of the processing cells within the 5-cells moving window, x_i is the value of one specific cell within the moving window, x_m is the mean of the 25 cells values.

Curvature. The surface curvature represents the rate of change of the slope or of the orientation per unit length, in the XY plan (Gallant & Wilson, 2000). The unit of measure is 1/m and in some cases the curvature values are multiplying by 100 to simplify the calculation and the understanding of this parameter.
Curvature maps have been widely used for the automatic extraction of channel network from digital elevation models (e.g. Band, 1986; Gallant and Wilson, 2000; Pirotti and Tarolli, 2010; Sofia et al., 2011). Tarolli and Dalla Fontana (2009) applied an objective method to recognize channel heads based on a threshold range identified as n-times the standard deviation of landform curvature. Numerous

studies proved curvature effectiveness for other geomorphic feature extraction (e.g. Molloy and Stepinski, 2007; Lashermes et al., 2007; Tarolli et al., 2012; Thommeret et al., 2010; Pirotti and Tarolli, 2010; Passalacqua et al., 2010). Curvature has also been used for the characterization of surface morphology and landforms. For example, Cavalli and Marchi (2008) applied a procedure based on curvature to characterize the topography of an alpine alluvial fan. Morphological types of landform elements such as crests, troughs, depression, enclosed basins, can been identified by using the curvature (Blaszczynski, 1997). An objective classification of elemental landform features completely based on consideration of signs of curvatures has been proposed by Dikau (1989), Shary (1995) and Shary et al. (2005). Surface curvature analysis has proved to be helpful in the interpretation of processes producing landforms such as hillslope processes (erosion and denudation, accumulation and deposition) or geomorphic processes (alluvial or glacial deposition) (MacMillan and Shary, 2009). For instance, Maggioni and Gruber (2003) used surface curvature to characterize a large potential avalanche release areas whereas Adams et al. (2003) proved curvature to be very efficient in the identification of landforms associated with debris slide occurrences.

Different types of curvature can be found in the literature, depending on the aim of the morphometric analysis; in this study plan and profile curvature, the most frequently calculated forms, were applied. Plan curvature is the curvature of a hypothetical contour line passing through a specific cell. It gives information about convergent and divergent flow, helping in the differentiation between ridges and valleys. Profile curvature is the curvature of the surface in the direction of the steepest slope. It describes the changing rate of the slope on the hillslope profile direction and it can be useful to highlight convex and concave slopes across the surface (Olaya, 2009). Surface curvature affects the accumulation of the flow: with response to horizontal convexity and concavity, divergence and convergence flow

can occur respectively, while changes in profile curvature from convex to concave shape can lead to a deceleration of the flow in the downslope direction (Fig. 2.4).

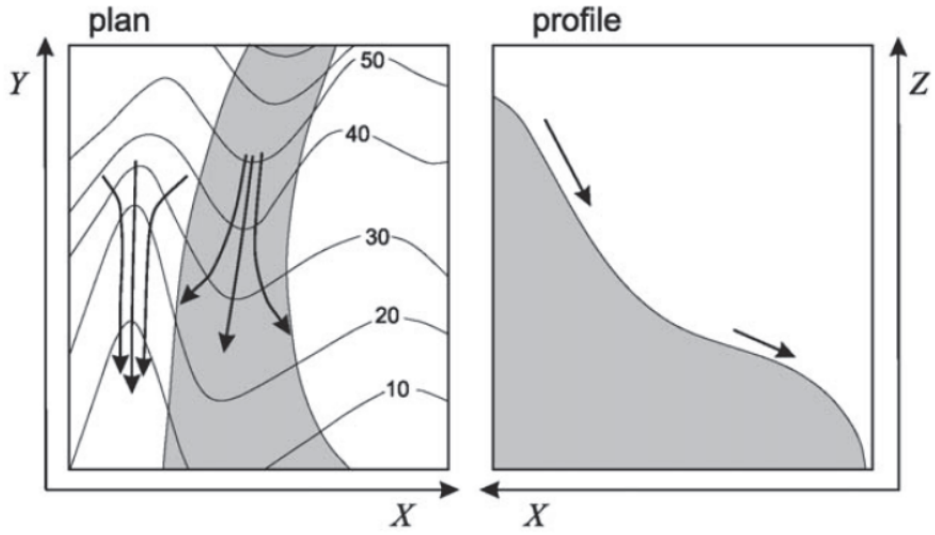

Figure 2. 4: Illustration of plan and profile curvature.

Melton index. It is an indicator of basin ruggedness (Melton, 1965), calculated as:

$$\mathrm{Me} = \mathrm{H_b}\sqrt{\mathrm{A_b}} \qquad [2.2]$$

where H_b is the basin relief, i.e. the difference between the maximum and minimum elevation of the catchment, and A_b is the catchment area.

The elongation ratio (*Re*) is defined as (Schumm, 1956):

$$Re = \frac{D_c}{L_b} \qquad [2.3]$$

where D_c is the diameter of the circle with the same area as that of the basin and L_b is the maximum length of the watershed. *Re* is an important areal parameter that helps in defining watershed discharge characteristics: circular basins are more efficient in run-off discharge than elongated basins (Singh and Singh, 1997). The value of elongation ratio may vary from values close to 0 (highly elongated shape) to 1 (circular shape) over a wide variety of climatic and geologic types. Values close to 1 are typical of regions of very low relief, whereas that of 0.6 to 0.8 are usually associated with high relief and steep ground slope (Strahler, 1964).

Circularity ratio (*Rc*) is defined as:

$$Rc = \frac{4\pi A}{P^2} \quad [2.4]$$

where *A* is the area of the basin and *P* the perimeter of a circle having the same circumference as the perimeter of the basin (Miller,1953). The value of circularity ratio varies from values close to 0 (in a line) to 1 (in a circle). *Rc* depends on basin geomorphometric characteristics (stream length, slope), geological structure, land use and climate.

Basin relief ratio index (*Rh*) is calculated as (Schumm, 1956):

$$R_H = \frac{H_{max} - H_{min}}{L} \quad [2.5]$$

where H_{max} and H_{min} are the highest and lowest point respectively in the basin and *L* is the basin length measured along the longest main stream.

2.1.2 DTM sources

For the derivation of DEMs, which represent the primary input of geomorphometric analysis, different sources are available, including ground survey techniques (e.g. differential Global Positioning System, Total Station), topographic maps and remote sensing (RS) technologies (e.g. aerial photographs, LiDAR, RADAR). Active sensors, such as LiDAR and RADAR, have permitted to overcome many of the limitations of "historical" available techniques. For instance, these technologies are able to capture subtle features that cannot be observed by human eyes or to acquire data at relative low time/cost-benefits (Wasklewicz et al., 2013). The development of modern geospatial technologies has permitted also the generation of DEMs at increased spatial extent and temporal frequencies, allowing an accurate detection of landforms and geomorphic changes in a very rapid way. The terrestrial laser scanner (TLS) has opened new perspective in the geomorphological field leading to the development of DTMs at scales (millimeters to centimeters) that are close to the operational scale of many processes (Wasklewicz et al., 2013). High resolution and accuracy DTMs can be generated from Airborne Laser Scanning (ALS) especially for hardly accessible areas (e.g. steep terrain in mountain basins, ice and snow covered area) and forested areas (Wehr and Lohr, 1999).

The Shuttle Radar Topographic Mission (SRTM) acquired topographic data for almost the 80% of the Earth surface, deriving the first DEM at global scale. The Advanced Spaceborn Thermal Emission and Reflection Radiometer (ASTER), launched onboard the flagship satellite Terra of NASA Earth Observing System, is able to create detailed and high resolution data (30 m) on large and heterogeneous areas. DSMs derived from ASTER and SRTM have been used to characterize the surface morphology (Bubenzer and Bolten, 2008), to map shallow landslides (Fourniadis et al., 2007), to estimate volumetric changes in glacial environments

(Miller et al., 2009) and to assess hazard risk associated with volcanic activity (Hubbard et al., 2007; Tralli et al., 2005).

DEMs derived from modern geospatial technologies have proved to be an effective tool not only in the framework of scientific knowledge of landforms and processes but also for supporting political decision-making in the field of environmental management since these products can address requirements at local, regional and global scale (Gianinetto and Villa, 2006). The availability of a cartographic database covering the Earth surface can be useful both for emergency prevention measures (e.g. hydraulic modelling for flood simulation) and for rapid post event assessment (e.g. orthophotos acquisition). In Italy, a very high resolution national database has been created in the framework of The Extraordinary Plan of Environmental Remote Sensing aiming to contribute to government activities and political decision-making in all areas subject to hydrogeological risk, supporting topographic, cartographic and photogrammetric activities, modelling and Territorial Information Systems (http://www.pcn.minambiente.it/GN/progetto_pst.php)

2.2 Sediment connectivity

The concept of connectivity has been widely used in geomorphology, hydrology and ecology but up to now there is not an uniform scientifically based definition. In geomorphological studies the term connectivity is generally used in relation to the transfer of material (sediment, water and nutrients) across a system (Jain and Tandon, 2010). In particular, sediment connectivity is defined as the degree of linkage which controls sediment transport through a landscape, focusing on the potential that sediment particles are routed from hillslope and headwater sources to river system and finally to basin outlet (Harvey, 2001; Harvey, 2002; Hooke, 2003; Brierley et al., 2006; Fryirs, 2007a).

Although not explicitly mentioned, the concept of sediment connectivity is implicit in approaches for sediment budget estimation as the “sediment delivery ratio”

which consider the transfer of material throughout the analyzed system (Bracken and Croke, 2007). Starting from first studies by Brunsden and Thornes (1979) and Caine and Swanson (1989), sediment connectivity has received increasing attention in the last decades. Brunsden (1993) identified different types of connectivity, differentiating between coupled, not coupled and decoupled systems, while Croke et al. (2005) outlined the spatial distribution within a catchment of both direct connectivity, via channels or gullies, and diffuse connectivity, which contributes to sediment transport thanks to overland flow and surface runoff. Brierley et al. (2006) and Fryirs (2013) considered different types of landscape linkages, stressing the importance of spatial scale in influencing the activity of different geomorphic processes in a catchment (Fig. 2.5):

- lateral, including slope–channel and channel–floodplain linkages;
- longitudinal, including upstream–downstream and tributary–trunk stream interactions;
- vertical, including surface–subsurface interactions of water and sediment.

Hooke (2003), focusing on the assessment of connectivity in a river-channel system, proposed a classification of coarse sediment connectivity based on the temporal variation of sediment transfer, distinguishing between "partially" connected system, in which sediment transport occurs only during extreme events, and "potentially" connected system, influenced by system configuration changes.

Spatial and temporal variation of coupling mechanism have been widely recognized. These two dimensions represent important aspects of connectivity since they can be integrated in a framework system to estimate the contribution of a given part of a landscape as sediment source and the relative sediment paths (Borselli et al., 2008). As the scale changes, ranging from local (i.e. hillslope-channel, channel-reach) to large scale (i.e. fluvial system, regional scale) coupling mechanism are controlled by different factors. For instance, large scale are more influenced by regional tectonic and geomorphic history than local scale in which local variations (e.g. climate) or

other environmental factors controlling runoff and sediment generation are likely to dominate (Harvey, 2002). Investigations on local scale have shown that the connectivity can depend not only on the channel morphology but also on the characteristics of transported sediment whereas for larger systems coupling mechanism takes into account relationships between upslope and downslope components of the system (Harvey, 2002).

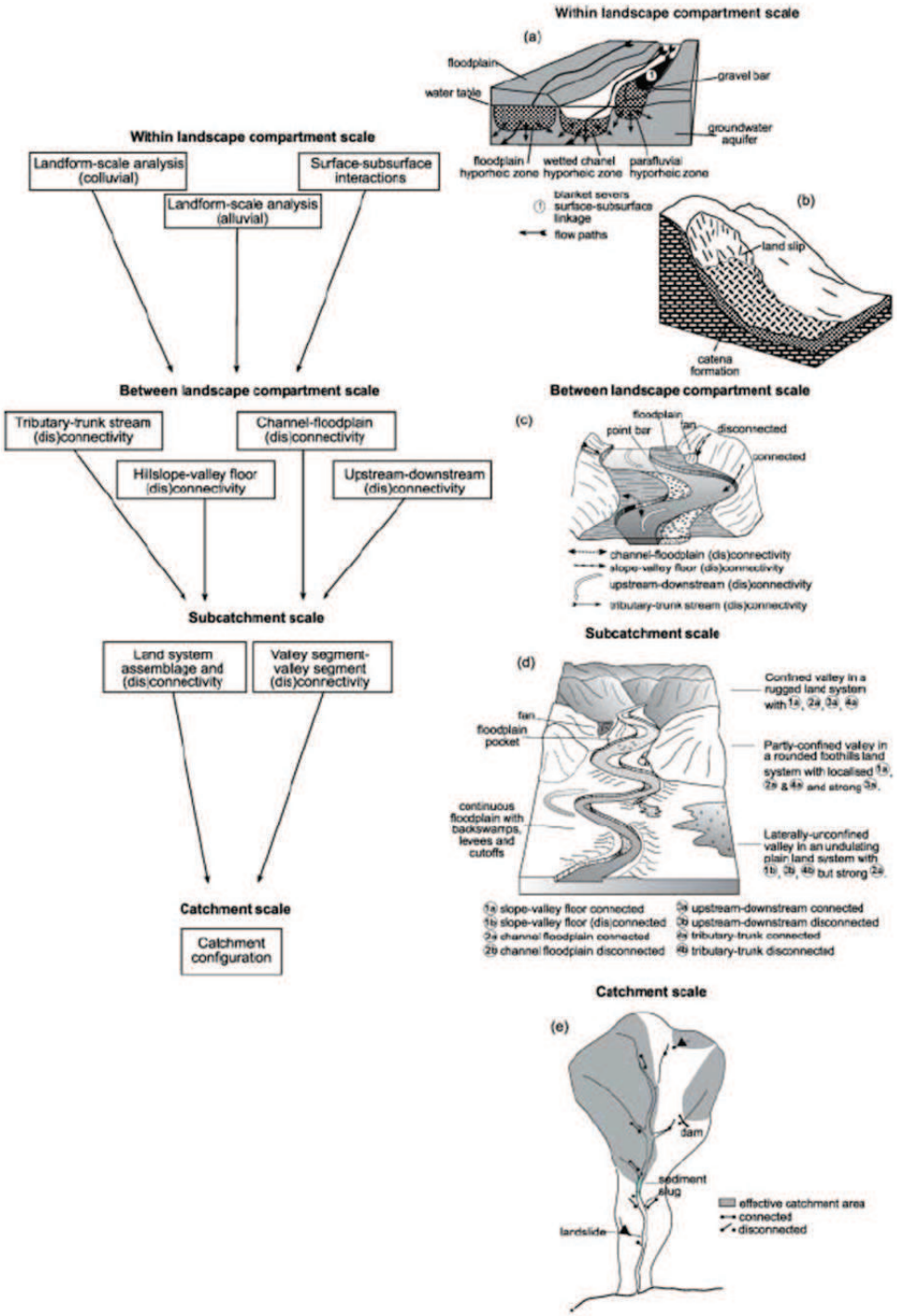

Figure 2. 5: Example of spatial scale of connectivity in a catchment (from Brierley et al., 2006).

The presence of natural (e.g. alluvial fans, low slope areas, bedrock outcrops) or anthropogenic (e.g. dams, embankment) barriers can impact water and sediment

flow at different spatial scale at different intensities (Fryirs et al., 2007b). For instance, land surfaces (terraces, floodplain) or water bodies (lakes) can interrupt the transport of landslide debris to the hydrographic network (Korup et al., 2013). On the other hand, the installation of dams can alter the sediment connectivity at reach scale which can further involve geomorphic channel changes (e.g. upstream aggradation and downstream degradation) (Poeppl et al., 2013).

Alluvial fans and debris cones can instead play a dual role within the sediment cascade of mountain fluvial systems: they can act as coupling features, for example linking hillslope gully systems to stream channels or mountain catchment sediment source areas to main river systems or as buffering elements, for instance preventing the coarse sediment, coming from mountain source areas, from reaching downstream channels (Harvey, 2012). The effect of alluvial fans and debris cones in the sediment connectivity are also influenced by temporal scale: on short scale debris cones can affect sediment supply to the channel, whereas on longer period, coupling-fans allow the supply of sediment to the downstream system from erosion of the distal areas of the fan or the valley-floor aggradation (Harvey, 2012).

Furthermore, the position of buffering elements in the system influence the different types of linkages. Thus, going from headwaters to lowland plain, longitudinal and lateral connectivity tend to be inhibited while vertical linkages tend to increase (Fryirs, 2013).

Sediment connectivity is also an important factor in geomorphologic analysis since internal linkages influence the sensitivity of a geomorphic system to natural and anthropogenic induced changes (Brunsden and Thornes, 1979; Brunsden, 2001; Harvey, 2001; Heckmann and Schwanghart, 2013). Well-connected systems allow the transfer of the sediment generated by an environmental perturbation between landscape units, whereas in poorly connected systems such effect may be spatially restricted (Harvey, 2001; Fuller and Marden, 2011). For instance, in connected systems an increase in the erosion on hillslopes can cause an increase in sediment

input to the channels whereas in buffered systems, where there's no linkages between two component of the system, the same effect may lead to local aggradation without any propagation in the downsystem. Disconnected system are so more sensitive to spatial and temporal variability of sediment dynamics than well-connected system that can response to environmental changes in a more uniform way (Harvey, 2001).

Temporal variability of sediment connectivity deals mainly with the magnitude and frequency characteristics of sediment transfer processes and the evolution of land use and management (Wolman and Miller, 1960; Borselli et al., 2008). Extreme events, linked, for example, to climate changes, may lead to an increase of sediment supply deriving from erosion of terrace and floodplains and so to an increase in hillslope-channel-coupling (Jain and Tandon, 2010). Land use changes, such as road building or cultivated area planting, can increase soil erosion and sediment connectivity at large temporal scale (Bracken and Croke, 2007).

Methods applied to analyze sediment connectivity, aimed to identify sediment sources and storages areas, are often based on qualitative approaches, including geomorphological field studies and mapping (Harvey, 2001; Schlunegger et al., 2005; Theler et al., 2010; Beel et al., 2011; Fuller and Marden, 2011) and geophysical surveys (Harvey, 2001; Schrott et al., 2003; Beel et al., 2011).

More recently, thanks to the development of GIS technologies, advances have been made in quantifying and modelling sediment connectivity. Morphometric GIS-based methods, compared to traditional geomorphic mapping, provide a feasible approach for the evaluation of sediment connectivity allowing the research in inaccessible areas (e.g. very steep mountain basins) and over large geographical extents, thanks to the availability of remote sensing technology, and the analysis of spatio-temporal variability of coupling processes on long term period (Meßenzehl et al., 2014).

Borselli et al. (2008) developed a connectivity index, based on topographic characteristics and land use management, for the assessment of connectivity in forest and agricultural catchments. Borselli's index showed promising results for the evaluation of hillslope sediment delivery ratio on semi-arid catchments, allowing the characterization of sediment connectivity at different scale (from hillslope up to medium size basins scale) (Vigiak et al., 2012).The same index proved to be useful for the characterization of connectivity in other catchments with ad hoc modifications. For instance Sougnez et al. (2011) modify Borselli's algorithm using an erosion index to model interill and rill erosion, whereas Cavalli et al. (2013) applied a topographic surface roughness to model impedance to sediment flux in alpine environment. The connectivity index developed by Cavalli (2013) proved also reliable estimate and characterization of coupling mechanisms of hillslope to main stream in a small deglaciated alpine catchment (Meßenzehl et al., 2014).

A numerical GIS-based model have been used to investigate coupling processes in mountain environment through the application of graph theory (Hechmann and Schwanghart, 2013). Carrivick et al. (2013) applied a DTM differencing approach to quantify geomorphological activity of sediment fluxes in proglacial areas of an alpine catchment.

Despite the availability of high resolution DTMs covering large spatial extents, to date quantitative morphometric methods have mainly focused on the assessment of spatial connectivity at relative small scales (i.e. patch, hillslope, gullies, small and medium basin), with few exceptions. For instance, Walling and Zhang (2004) reported a first attempt of the application of a connectivity index related to sediment transport capacity, land use, slope-shape and drainage pattern factors, to evaluate the efficiency of slope-channel sediment transfer at regional scale deriving mostly from agricultural land erosion.

An indicator of processes at large scale (e.g. large river basins), where instrumental measurements installation would be impractical or the application of physically

based models would require a large amounts of input data, can contribute to the development of a rapid and cost effective method for the management of sediment related risk.

2.3 Geomorphic change detection

The identification of temporal variations of processes causing changes on Earth surface and of the related landform developments represent one of the main challenge in geomorphology. Quantification of morphological changes can be considered the main research topic for many investigations concerning temporal analysis (Williams, 2012). The process of estimating geomorphological changes from repeated field surveys has first been applied to cross section and longitudinal profile monitoring in order to quantify sediment transfer rates along rivers and infer volumetric estimates mainly at bar and reach scale (Martin and Church, 1995; Ham and Church, 2000; Brewer and Passmore, 2002; Vale and Fuller, 2009; Wheaton, 2008). Thanks to the development of newer geomatic technologies and high resolution remote sensing techniques (e.g. terrestrial and airborne LiDAR, close-range photogrammetry), this method has been extended to gridded elevation models that allow the evaluation and quantification of landform change patterns at high spatial resolution and geographical extension and at a range of temporal frequencies comparable to the rates of landform evolution (Williams, 2012).

In the case of digital terrain models, if repeated surveys are available, the geomorphological change in time is inferred by subtracting the elevation cells of the old surface from the cells of the new surface (Fig. 2.6). The resulting DEM of Difference (DoD) deriving from the application of geomorphic change detection shows the spatial pattern of geomorphic dynamics that can be converted to volumetric change by multiplying them by the area of grid cells (Wheaton, 2008).

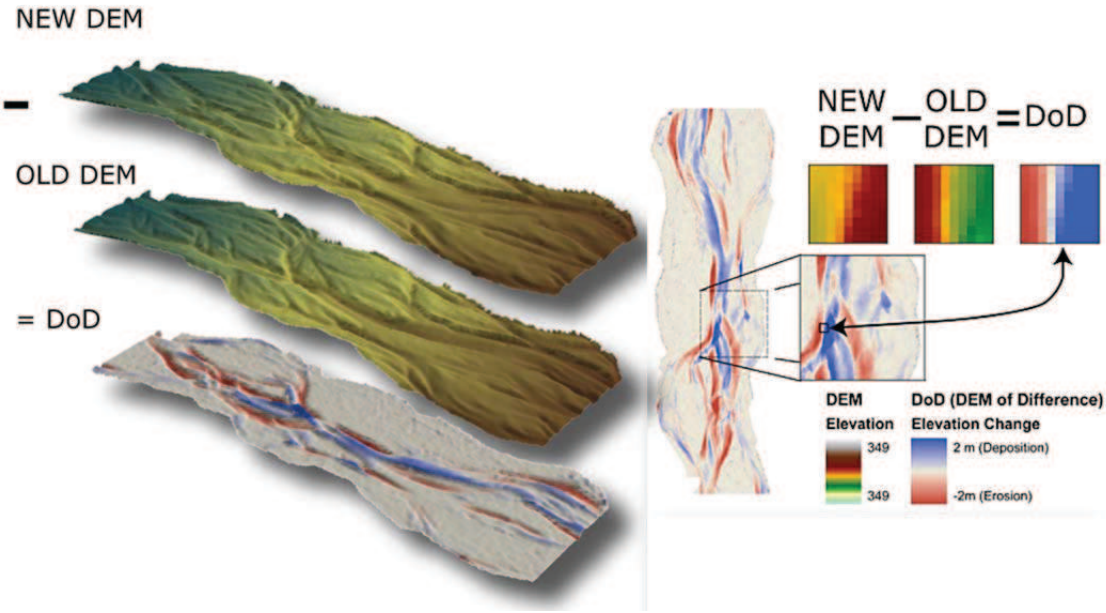

Figure 2. 6: Scheme of DTM differencing method (Wheaton, 2008, modified). New and old DTM refer respectively to the new and old surface surveyed.

The DEM differencing has become an adaptable technique that has been exploited in different geomorphological contexts since it can be applied to DTM derived from different topographic survey techniques. Table 2.2 summarizes experiences from existing studies on river systems, landslide and glaciers, pointing out how the uncertainty in DEM differencing (as explained in the paragraph 2.3.1) was considered. Several analysis of topographic variations based on DEM differencing deal with the application of this method within the fluvial system. In this context, DoD has been shown to improve sediment budgeting at reach scale avoiding problems that arise from traditional morphologic approach, based upon cross sections technique (Ham and Church, 2000), linked to the uncertainty deriving from the interpolation of cross section data over larger distances and to the difficult representation of downstream effects of geomorphic changes (Brasington et al., 2000; Fuller et al., 2003; Bangen et al., 2014). Fuller et al, (2003) demonstrate that DTM differencing also provide a reliable estimate of sediment transfer calculation whereas cross-section approach can lead to underestimation of the magnitude of

erosion processes. DoD have facilitated the estimate of bed load transport especially in gravel bed rivers where measurements of sediment transport rates may be inaccurate if calculated with formulae or difficult when derived from field campaigns that require a large effort and may not achieve acceptable accuracy (Gomez, 1991; Wilcock, 2001).

Table 2. 2: Examples of DEM differencing application in geomorphology disciplines. StD: Standard Deviation; CI: Confidence Interval; ALS: Airborne Laser Scanning; TLS: Terrestrial Laser Scanning; AP: Aerial Photogrammetry.

Research topic	Survey technology	Uncertainty estimation	Scale of analysis	Reference
Alluvial fan deposition	dGPS	-	Fan	Fuller and Marden, 2010
Debris flow and Flood	ALS	-	Basin	Bull et al., 2010
	ALS	Slope grid segregation	Basin	Scheidl et al., 2008
	TLS	StD and slope	Reach	Schurch et al., 2011
	Stereographic photographs	-	Hillslope	Coe et al., 1997
	TLS, ALS	Pre-DoD processing (alignment and filtering DTM)	Hillslope	Bremer and Sass, 2012
	TLS	FIS	Basin	Blasone et al., 2014
	ALS	Fuzzy logic	Basin	Croke et al., 2013
Glacier	ASTER, ALS, AP	-	Basin	Karimi et al., 2012
	AP, ALS	-	Basin	Hubbard et al. 2000
	AP, cartographic data	-	Basin	Rippin et al 2003
	AP, ALS	-	Basin	Barrand et al., 2009
	ALS	-	Basin	Abermann et al., 2010

Research topic	Survey technology	Uncertainty estimation	Scale of analysis	Reference
Interpolation and point density analysis	TLS	Local roughness	Gravel bar	Heritage et al., 2009
Landslide and earth slide-earth flow	ALS	-	Hillslope	Corsini et al., 2009a
	ALS	-	Hillslope	Corsini et al., 2009b
	AP, ALS	-	Hillslope	Dewitte et al., 2008
	ALS	-	Basin	Baldo et al., 2009
	AP	-	Hillslope	Walstra et al., 2004
	ALSM	LoD_{min}	Basin	De Long et al., 2012
	LiDAR	LoD	Hillslope	Bennett et al., 2012
River system	Rtk-GPS	LoD at CI	Reach	Brasington et al., 2003
	ALS, TLS	-	Basin	Carrivick et al. 2013
	ALS	-	Reach	De Rose and Basher, 2011
	AP, ALS	Probabilistic threshold based on CI, StD errors	Reach	Lane et al., 2003
	ALS	Fuzzy logic	Sub-reach	Moretto et al., 2012
	GPS	LoD threshold with StD at CI	Reach	Rumsby et al., 2008
	TLS	-	Channel	Hughes et al., 2006
	Contour, ALS	LoD at CI	Reach	Carley et al., 2012
	TLS	Probabilistic threshold based on CI, StD errors	Reach	Milan et al., 2007
	AP, GPS	LoD at CI	Reach	Rumsby et al., 2008
	TLS	Fuzzy logic	Sub-reach scale	Picco et al., 2012
	Theodolite (Total Station)	LoD_{min} with covariance	Reach	Fuller et al., 2003

Research topic	Survey technology	Uncertainty estimation	Scale of analysis	Reference
	GPS	Fuzzy logic	Reach	Wheaton et al., 2010
River system	TLS	Probabilistic threshold based on CI, StD of errors	Reach	Milan et al., 2007
	LiDAR, AP	Fuzzy logic	Reach	Thompson et al., 2013
	Total Station	Spatially variable uncertainty with StD errors, local roughness	Reach	Milan et al., 2011
	TLS, ALS	-	Reach	Theule et al., 2012
	AP, SONAR	-	Reach	Ghoshal et al., 2010
Wildfire	TLS	-	Sub-basin	Wester et al., 2014

Other important applications in river environments include the quantification of river channel changes, such as bank and bar erosion, lobe deposition or bed level modification (e.g. Brasington, 2003; Fuller et al., 2003; Lane et al., 2003; Barker et al., 1997; Heritage et al., 2009; Milan et al., 2011; Picco et al., 2012,). In fluvial geomorphology, DoD has also been used to validate morphological and physical models and to interpret their results (Wheaton, 2008; Williams, 2012).

DTM differencing proved to be an effective and feasible tool for monitoring mass movements, i.e. landslide, rock falls and debris and earth flows. This method can be used not only to spatially identify sediment deposition and erosion areas, that can be confirmed by field observations, but also to quantify sediment volumes transported by analyzed processes (e.g. Baldo et al., 2008, Bremer and Sass, 2012 Bull et al., 2012; DeLong et al., 2012). Combined use of remote sensing technique and DTM differencing can improve the assessment of volumetric sediment budget of debris flows helping the prediction of the magnitude of response of such events

that are better characterized using measures of total volume (Scheidl et al., 2008; Blasone et al., 2014). Coe et al (1997) findings prove that DoD can help characterize and quantify hillslope erosion even in semiarid regions where field measurements are usually difficult due to the low frequency and localized occurrence of precipitation events causing erosion.

The analysis of geomorphic changes has been also widely applied in glacial, proglacial and periglacial environments. Karimi et al (2012) used multitemporal DTMs acquired from different topographic surveys to quantify morphometric changes of a glacier over a 50 years period, whereas Hubbard et al. (2000) and Rippin et al. (2003) used DTMs derived only from aerial photography to infer changes in glacial ice from repeated surveys. The comparison of multitemporal LiDAR derived DTMs comparison provides satisfactory performance on different glacial areas for the quantification of Permafrost extent and volume changes and for the identification of dead ice, debris-covered ice or permafrost from its rocky surroundings (Abermann et al., 2009).

2.3.1 Uncertainty analysis of Geomorphic Change Detection

Taking into account uncertainty in the terrain representation of DTMs used in geomorphic changes detection contributes to high accuracy and satisfactory quality of the analysis. Meeting such requirements enables the possibility of using DoD as supporting tool for hazard assessment studies and for planning of land use and mitigation measures. Therefore, when applying DTM differencing particular attention has to be focused on the uncertainty that can arise from the topographic surfaces involved and that can be amplified by the raw differencing and propagated into the DoD. Digital elevation model errors can arise from different sources (Lane, 1998; Pike, 2002; Fisher and Tate, 2006; Wechsler, 2007; Hebeler and Purves, 2009; Heritage et al., 2009):

- Data acquisition (i.e. point density, accuracy and distribution);

- Survey strategy (e.g. sampling patterns, instrument precision);
- Data post processing (e.g. interpolation method errors for DTM derivation, resolution);
- Topographic roughness.

A correct application of DoD method must distinguish real changes from noise that can arise from these errors in order to address to a meaningful interpretation of geomorphological changes (Wheaton, 2008; James et al., 2012). This is more important when the order of magnitude of geomorphic changes detected by DTM differencing and of the noise are comparable. Therefore the quantification of errors is a fundamental step in order to obtain a reliable and robust method.

To date, different methods have been proposed to assess topographic surface quality for the application of DTM differencing and to analyze the propagation of uncertainties into the DoD. The most common procedure used to evaluate uncertainties is represented by the application of a constant threshold, called Minimum Level of Detection (LoD_{min}), based on the standard deviation of errors of both surfaces implied, above which elevation change can be considered reliable (Wheaton et al.2010). An improvement of LoD_{min} has been proposed by Fuller et al. (2003) study that adds the covariance between DEM to better estimate propagation of error for the evaluation of sediment budget of gravel-bed rivers. Riverbed conditions (i.e. dry or wet) have been used to spatially segregate estimates of errors across DTM surface (Lane et al., 2003; Milan et al., 2007).

As pointed out by Brasington et al. (2000) and Wheaton et al. (2010), the application of a spatially uniform threshold can lead to misleading interpretation of real changes according to different topographic and morphologic characteristics (e.g. underestimation of geomorphic changes for high gradient features such as bans). To remove systematic bias due to a constant LoD_{min}, a method based on a probabilistic thresholding has been developed (Brasington et al. 2000; Brasington et al. 2003; Lane et al., 2003). Through the application of a variable threshold, based

on a chosen confidence interval (CI), it is possible to derive a more reliable DoD discarding all elevation changes featuring a lower probability with respect to chosen threshold.

Methods based on a spatial uniform threshold can lead to the occurrence into the calculated DoD of areas characterized by error values supposed to be greater or lower than the calculated threshold value. These approaches can discard relevant information on examined processes, for instance discarding areas characterized by geomorphologic change where the uncertainty is low. Furthermore, elevations characterized by small magnitude of changes but widespread in the analyzed area can be classified as noise (Williams, 2012). Therefore, spatial structure of uncertainty is a fundamental issue in geomorphic change analysis. The incorporation of a spatially variable uncertainty has been proposed by Wheaton et al. (2010) whose approach, applied on a channel scale, is based on the application of the fuzzy logic to estimate errors for DTMs involved, taking into account different parameters linked to the study area (e.g. slope, surveyed point density, topographic roughness, vegetation presence). The advantages of using a fuzzy approach relies on the fact that, unlike probabilistic methods, requires few assumptions and that variables do not show a deterministic and simple relationship with DTM associated uncertainty (Wheaton, 2008). Uncertainty spatial assessment as described by Heritage et al. (2009) is based on the relationship between survey techniques and interpolation methods to topographic variability (i.e. surface roughness). Milan et al. (2011) improved this method introducing the relationship between standard deviations of elevation errors and local topographic roughness for scour and fill volume estimate. However, by using surface roughness as the main component for uncertainty assessment, underestimation of elevation changes in area featuring low variability can occur (Carley et al., 2012). When original points data are limited or unknown, as in the case of contour lines or other historical data sets, Carley et al. (2012) proved that a spatially variable uncertainty can be assessed

by applying a threshold with confidence limit to an artificial point grid with standard deviation representing surface variability.

The examples of change detection applications over different geomorphologic contexts reported in this chapter (see Tab. 2.1) show that uncertainty analysis has received considerable attention especially within the fluvial geomorphology discipline, probably due to the fact that river changes have similar magnitude of survey technique errors (Williams, 2012). Furthermore, current scale analysis have been so far limited to small scale (e.g. reach, sub-reach). Croke et al. (2013) reported the largest application of DTM differencing to date, using a spatial variable errors estimate on a smooth large catchment .

The wide availability of large, high resolution DTMs should imply the need to shift spatial error research toward larger systems, especially in alpine catchments that are more sensitive to natural and anthropogenic disturbance.

CHAPTER 3
STUDY AREAS

The study areas, located in the Italian and Swiss Alps, encompass:

- Venosta Valley, located in the upper Adige river basin, limited to the confluence of main channel with Senales river;
- Gadria and Strimm basins, included in the upper Venosta Valley;
- Navizence catchment, located in the Anniviers Valley (Valais, Switzerland).

The Venosta Valley has been selected to analyze sediment connectivity at different DTM resolutions and on catchment of different size, allowing, in particular, to study connectivity pattern on basins showing different sediment transport processes and size.

Within the Venosta Valley, the Gadria and Strimm basins have been chosen for sediment connectivity and geomorphic changes analysis because of the availability of repeated LiDAR surveys and their different morphology and sediment transfer processes that makes these areas suitable for the aims of the research.

The Navizence catchment, characterized by the presence of a large glacial system, represents a significant example of the sediment deliver issue associated with glacier melting process, which can be analyzed by means of morphometric indexes of sediment connectivity.

3.1 Venosta Valley

The Venosta Valley is a mountainous region of the Northern Italy (Fig. 3.1 and Tab. 3.1). Drained by the Adige river, the area is bordered by Austria to the north and by Switzerland to the west.

The selected study area covers about 1200 m^2: it includes the Upper Venosta Valley, going from Resia Lake to the alluvial fan of Malser Haide near Malles, the Middle

Venosta Valley, extending from Malles to Silandro, and only a small part of the Low Venosta Valley that reaches Senales. Two important reservoirs are present in the Valley, the Resia and San Valentino alla Muta lakes. With its capacity of 118 million m^3 and a surface of 6.6 km^2, Resia lake is the largest one in the Autonomous Province of Bolzano (Gumiero et al., 2009).

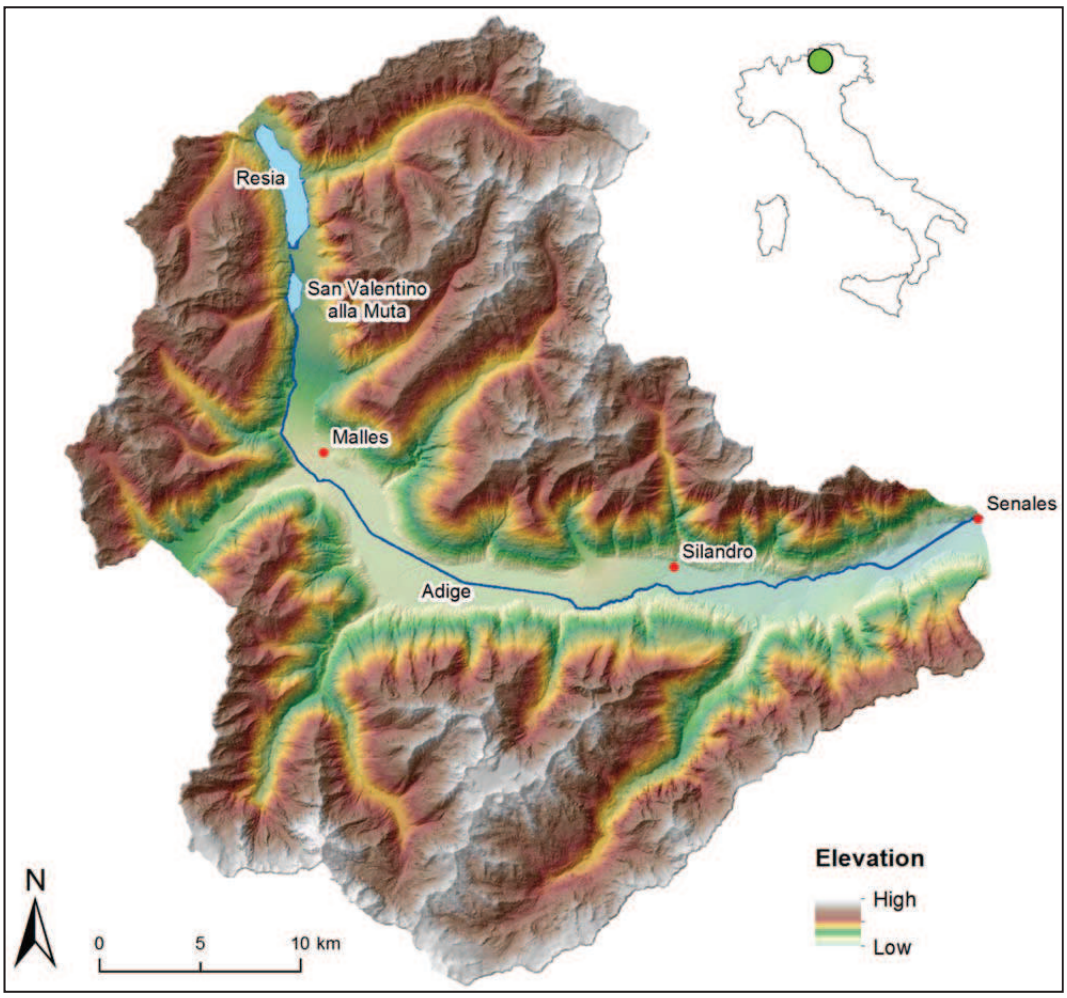

Figure 3. 1: Map of selected area within Venosta Valley.

Table 3. 1: Main morphometric parameters of selected area of Venosta Valley.

Area (km^2)	Elevation (m)			Mean slope (%)	Length main channel (km)
	Min	Max	Mean		
1209	547	3896	2110	55.1	57.4

The area below 1000 m is only the 8.5 % of the Venosta Valley, whereas the 31.5% of the territory lays between 1000 and 2000 m and more than half of the surface, the 60%, is above 2000 m altitude (Fig. 3.2).

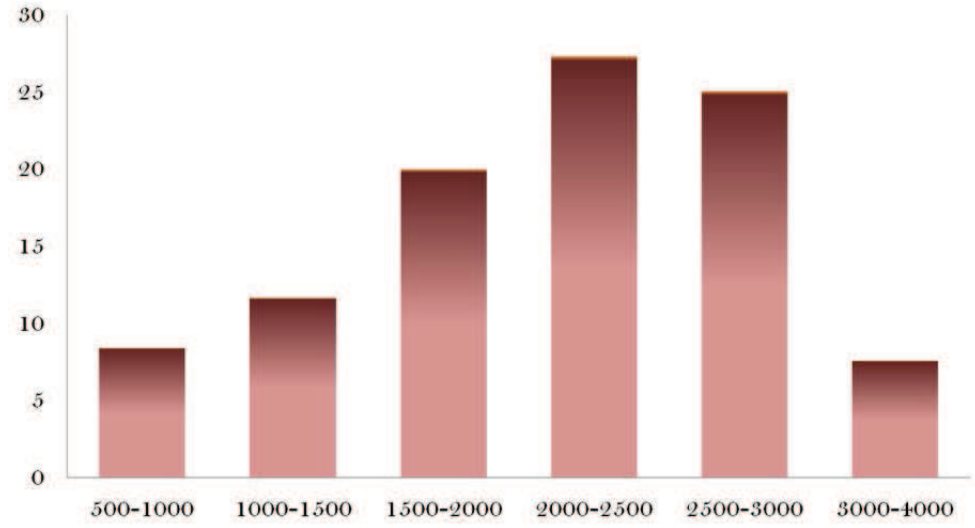

Figure 3. 2: Altitudinal distribution of Upper- and Middle-Venosta Valley.

The slope map (Fig. 3.3) highlights a homogeneous distribution of steep slopes in the southern and northern sections of Venosta Valley, with a flat area in correspondence of the flood plain.

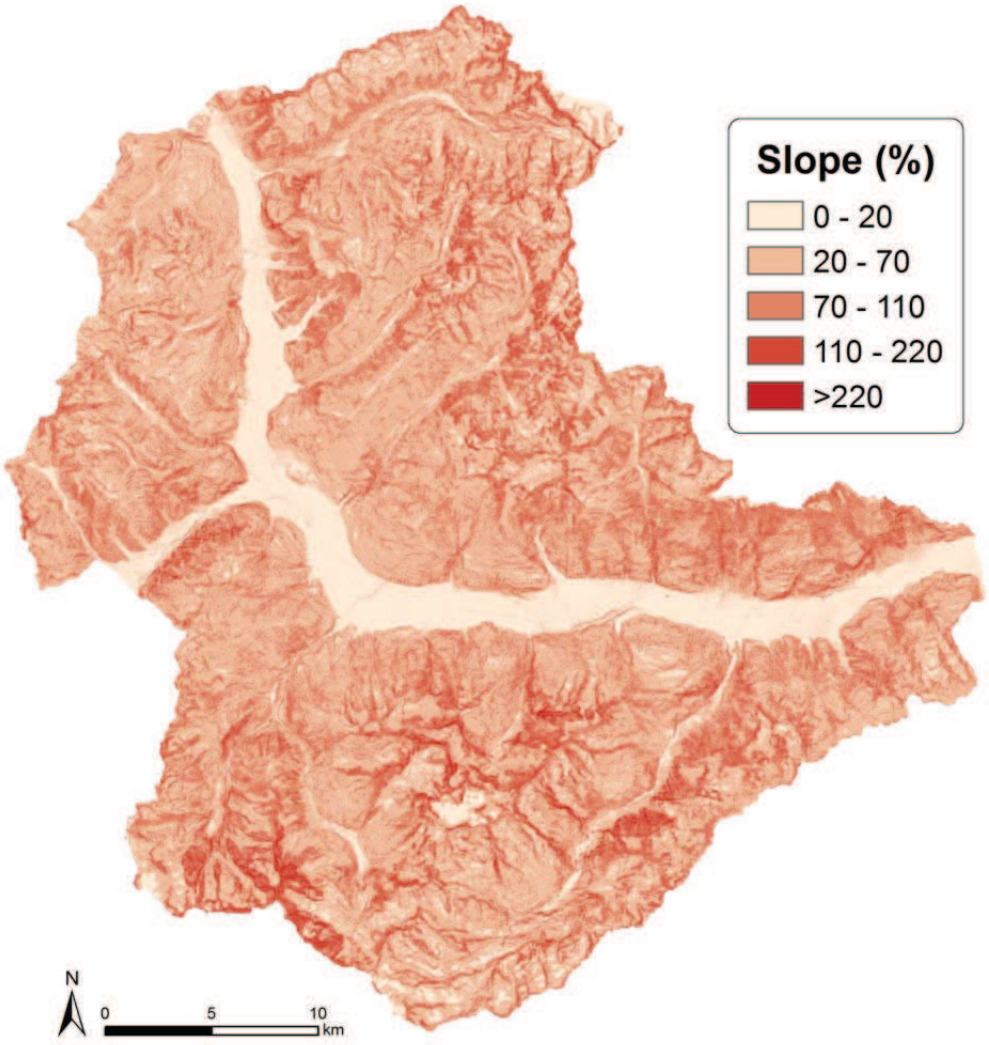

Figure 3. 3: Slope map of study area.

Bedrock geology of Venosta Valley belongs to Austroalpine domain and is dominated by metamorphic units: ortogneiss, paragneiss, phyllites, schists and micaschists. Sedimentary rocks such as sandstone, marls and carbonate rocks (mainly dolomite) are also present (Fig. 3.4).

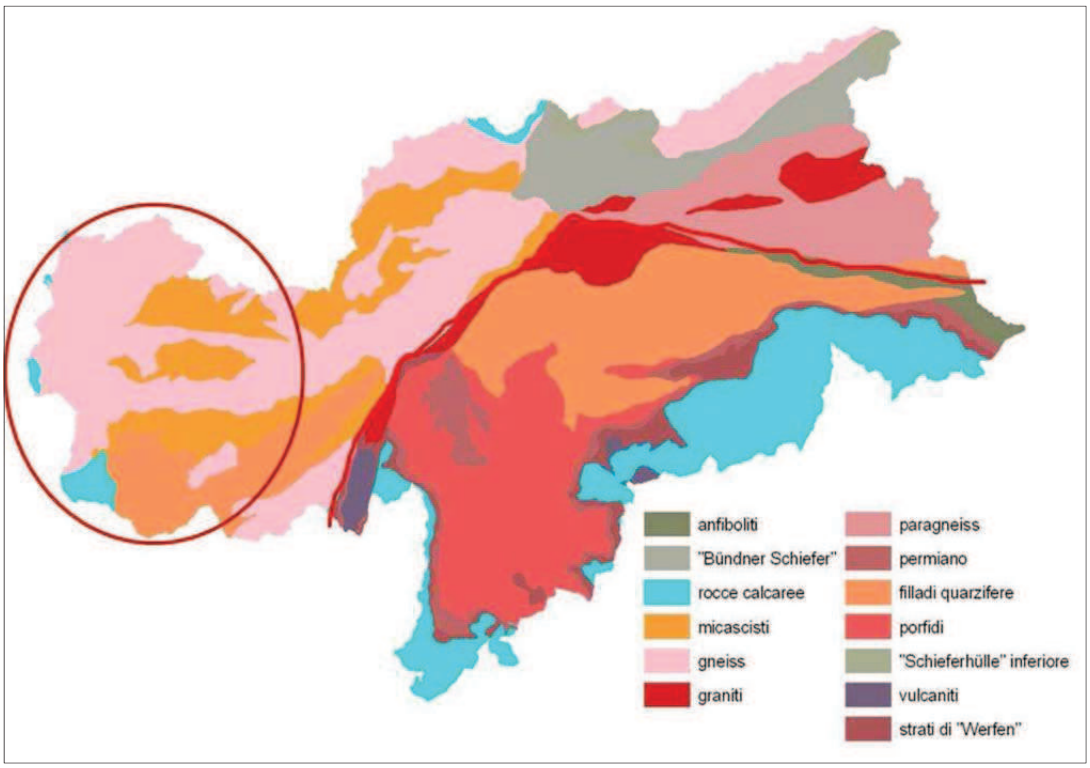

Figure 3. 4: Simplified geology map for the study area. The red circle identifies the upper and middle Venosta Valley (Provincia Autonoma di Bolzano, 2007).

The alluvial fans of Venosta Valley, amongst the largest ones of the Alpine region, represent an important morphological feature covering the 70% of the valley floor. These fans, deriving from both debris flow and bedload processes, play a fundamental role in the delineation of the longitudinal profile of the valley and its arrangement (Schenk, 1966). The largest cones of Venosta Valley are the Malser Heide covering an area of 13 km^2 and the debris flow fan of the Gadria and the Strimm creeks with a surface of 10 km^2. The origin of exceptionally large fans located in the Venosta valley is still uncertain: it can be interpreted as the result of giant catastrophic slope failures (Jarman et al., 2011) or of the paraglacial evacuation of glacial and glacio-fluvial deposits and downstream fan progradation due to debris-flow activity (Brardinoni et al., 2012).

Climatic characteristics of the Venosta Valley are typical of the inner part of the Alpine range. Thanks to the altitudinal distribution of the territory, the climatic regime is extremely variable, with marked daily and seasonal temperature fluctuations. According to Koppen classification, three different climate regions can be observed (Provincia Autonoma di Bolzano, 2007):

- Temperate climate (Cf) below 1200 m altitude, with mean temperature of the coldest and warmest month above -3° and above 10°C respectively;
- Boreal climate (Df) below 2000 m altitude, with mean temperature of the coldest and warmest month below -3° and above 10°C respectively;
- Polar climate (ET), above 2000 m, with mean temperature of the warmest month below 10° and at least one month per year has a mean temperature above 0°C.

The dominant climate pattern in the study area is continental: mean annual precipitations range between 500 and 600 mm, with maxima in summer and minimum during winter. Fig. 3.5 shows the rainfall map for the Upper Adige derived from the spatial interpolation of mean rainfall data sampled in a thirty years period from the meteorological monitoring system (Provincia Autonoma di Bolzano, 2007).

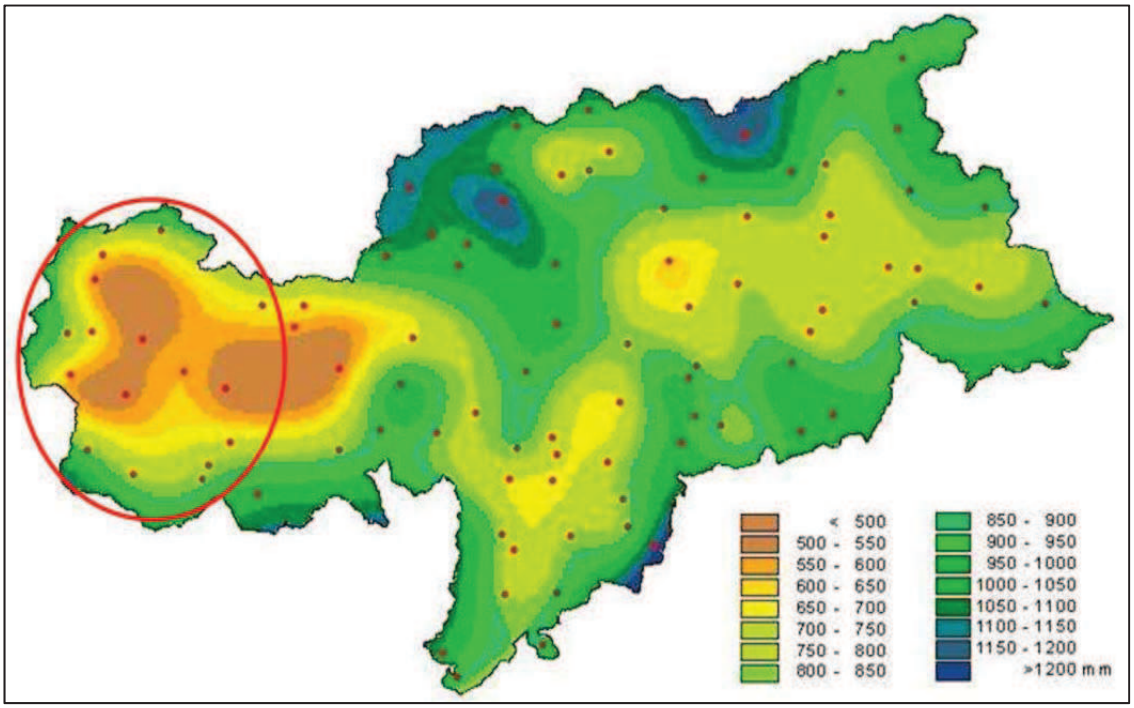

Figure 3. 5: Rainfall map based on mean annual data for the period 1961-2003. The red circle identifies the upper and middle Venosta Valley (Provincia Autonoma di Bolzano, 2007).

A strong altitude dependency can be observed for the mean annual precipitation: values ranges from about 660 mm in the band of 1700-2000 m a.s.l. to about 800-900 mm for the band of 2,000–2,500 m a.s.l. (Comiti et al., 2014).

Environmental and climatic characteristics define a wide variety of vegetation types typical of inner alpine environments. Vegetation and land use distribution follow elevation bands. Valley floors and alluvial fans are mainly characterized by agricultural settlements along with riparian vegetation; below 1000 m it is possible to find deciduous trees, beechs and pines. The greater part of woodlands is included in the 1000-2300 m belt, characterized by spruce and larch forests and some pine species (*Pinus sylvestris* and *Pinus cembra*) of high altitude. High elevation pastures and meadows can be found above 2300 m, whereas beyond this altitude mainly bare soil, debris and exposed rocks are present (Del Favero, 2004).

3.2 Subcatchments in Venosta valley

Several catchments of Venosta Valley, characterized by different size, morphology and sediment transport processes, were chosen for spatial sediment connectivity analysis (Fig. 3.6). Main morphological features of the 22 selected basins are reported in Table 3.2. The outlet of each basin has been identified, through ortophoto interpretation, at the fan apex.

Figure 3. 6: Selected catchments of Venosta valley for the characterization of sediment connectivity. Alluvial fans of each basin are also illustrated.

Table 3.2: Main morphometric parameters of the 22 chosen catchments.

Basin		Area ($km^{2)}$	Mean Slope (%)	Elevation (m)		
n	name			min	max	mean
1	Carlino	110	58	1487	3735	2545
2	Cengles	10.4	81	995	3372	2310
3	Ciardes	1.4	85	812	2543	1807
4	Colsano	6.1	78	676	2920	2101
5	Fossa dell'Alpe	6.2	66	1658	2908	2237
6	Frisio	8.1	53	662	2735	2049
7	Gadria	6.3	79	1373	2953	2148
8	Lasa	30.8	71	918	3543	2435
9	Maragno	3.3	66	769	2470	1630
10	Plazut	1.88	64	1051	2398	1716
11	Plima	160.2	65	760	3752	2434
12	Puni	40.8	56	1360	3392	2466
13	Reschen	1	83	1681	2973	2396
14	Saldura	95.7	63	946	3734	2435
15	Silandro	48.9	66	768	3364	2437
16	Solda	75.6	70	1194	3896	2567
17	Solume	5.2	68	672	2619	1798
18	Strimm	8.5	62	1394	3197	2484
19	Tanas	10.8	52	1013	3073	2094
20	Tarres	9.1	59	956	2727	1867
21	Trafoi	51.3	74	1194	3888	2442
22	Vezzano	5	86	864	3055	2019

3.2.1 Gadria and Strimm catchments

Gadria and Strimm are two small and adjacent catchments located in the upper Venosta valley (Autonomous Province of Bozen-Bolzano, Italy) (Fig. 3.7).

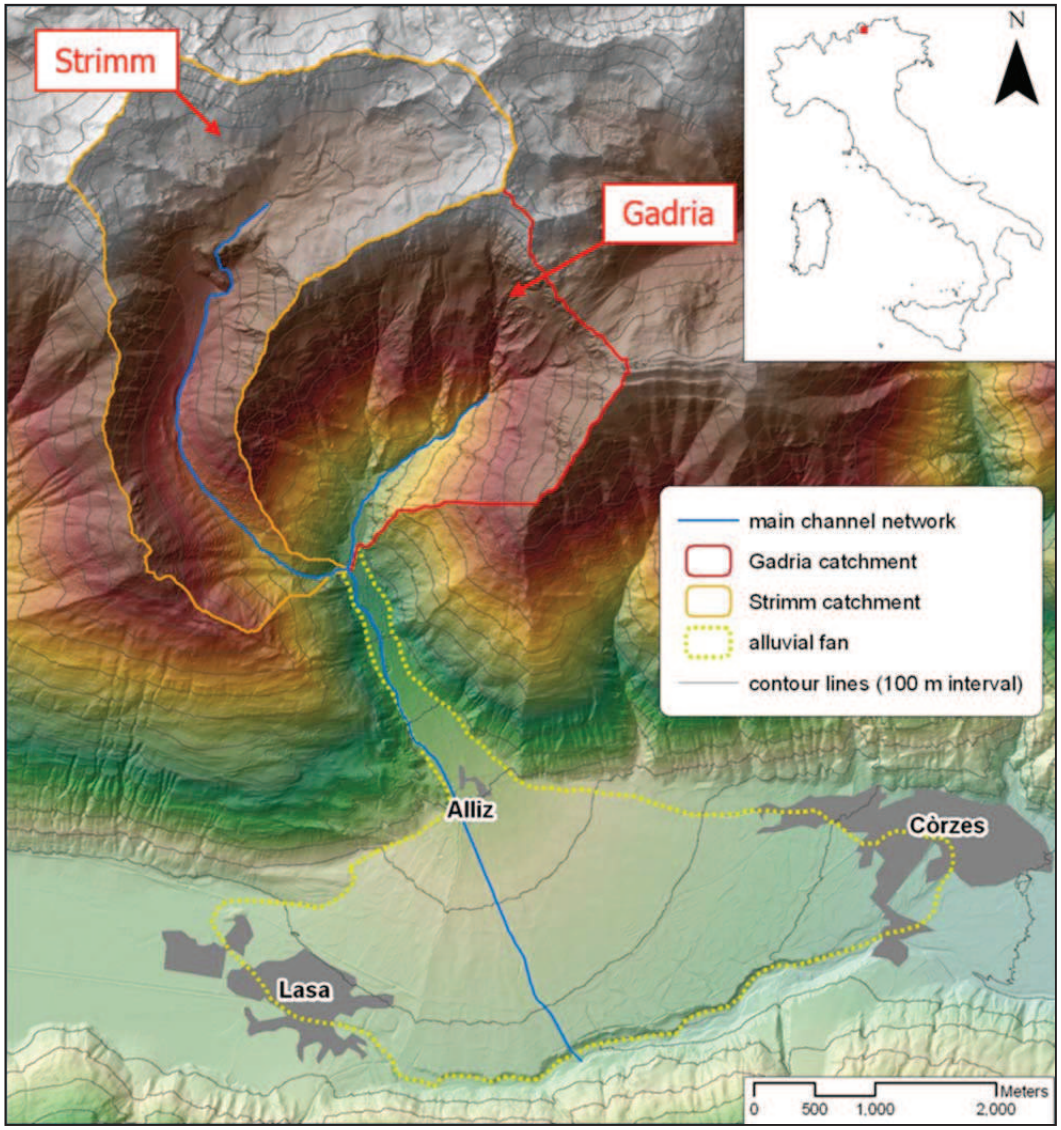

Figure 3. 7: Location of Gadria and Strimm basins.

The choice of these study areas for the DoD analysis was supported by the availability of LiDAR data derived from repeated surveys and by the different

characteristics of the basins. The Gadria catchment drains a smaller area (6.3 km^2 compared to Strimm basin (8.5 km^2) but presents a higher slope (79% compared to 62%). Hypsometric curve for Strimm basin (Fig. 3. 8b) shows that a very small area characterizes the lowest elevations, whereas almost 70% of the surface is above the median elevation. The upward concavity in the upper part of the hypsometric curve of the Gadria (Fig. 3.8a) corresponds to the cavity in the upper sector of the catchment, whereas the slight upward convexity of the remaining part of the curve indicates a more regular altitudinal distribution of catchment areas. This aspect is also reflected by the values of the hypsometric integral (0.47).

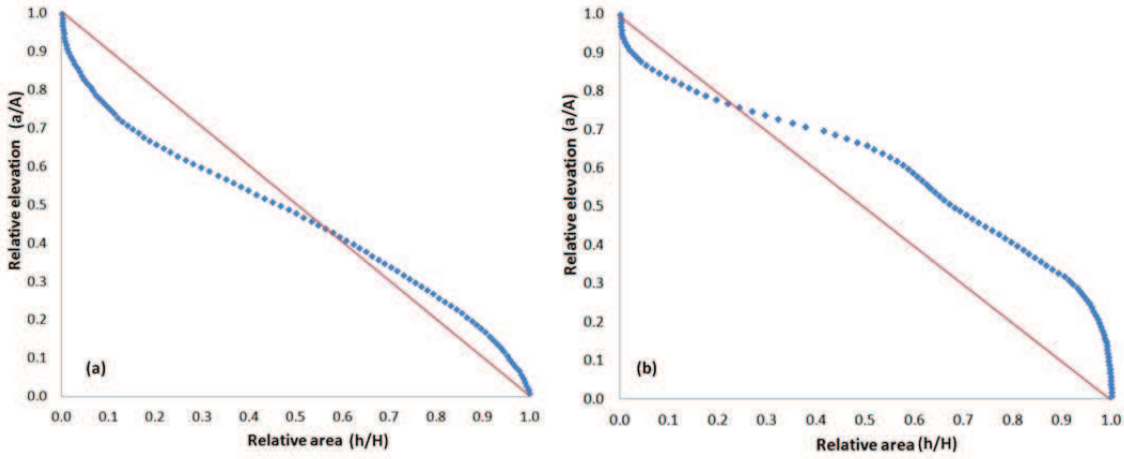

Figure 3. 8: Hypsometric curve as obtained for Gadria (a) and Strimm (b) rivers. Hypsometric curve as obtained for Gadria (a) and Strimm (b) rivers.

The Gadria stream is a debris-flow prone basin showing a relatively high frequency of events (approximately 1 per year) due to the combination of steep morphology, highly deformed metamorphic rocks and thick fluvio-glacial deposits. The Strimm is essentially a bedload stream even if some debris flows can occur in the steepest parts of the basin and in some sectors of the main channel. For example, an important debris flow event occurred in the lowest portion of the creek in July 2010 corresponding to a sudden increase of channel slope (Cavalli et al., 2013).

Geologically, both basins consist of highly fractured metamorphic rocks (mica-schist, gneiss, and quartz-phyllite). The Gadria-Strimm system is connected to the Adige river valley floor by a very large alluvial fan that is part of the cluster of anomalously large fans occupying the Venosta valley as described in previous section (Par. 3.1).

Low average annual precipitations (500 mm) is due to particular micro-climatic conditions; summer storms are the primary cause of debris-flow occurrence. The vegetation cover is mainly composed of coniferous forest (spruce and larch) and of alpine grassland above 2000 m a.s.l.. At highest elevation bare rocks and talus are widespread (Cavalli et al., 2013; D'Agostino and Bertoldi, 2014).

At the confluence of the Gadria and Strimm rivers (1394 m a.s.l.), an artificial debris retention basin was built in the 1970s (Fig. 3.9). The retention basin is equipped with a filter check dam and can store about 40,000–60,000 m^3 (for deposition angles in the range 2°–6°) (Comiti et al., 2014).

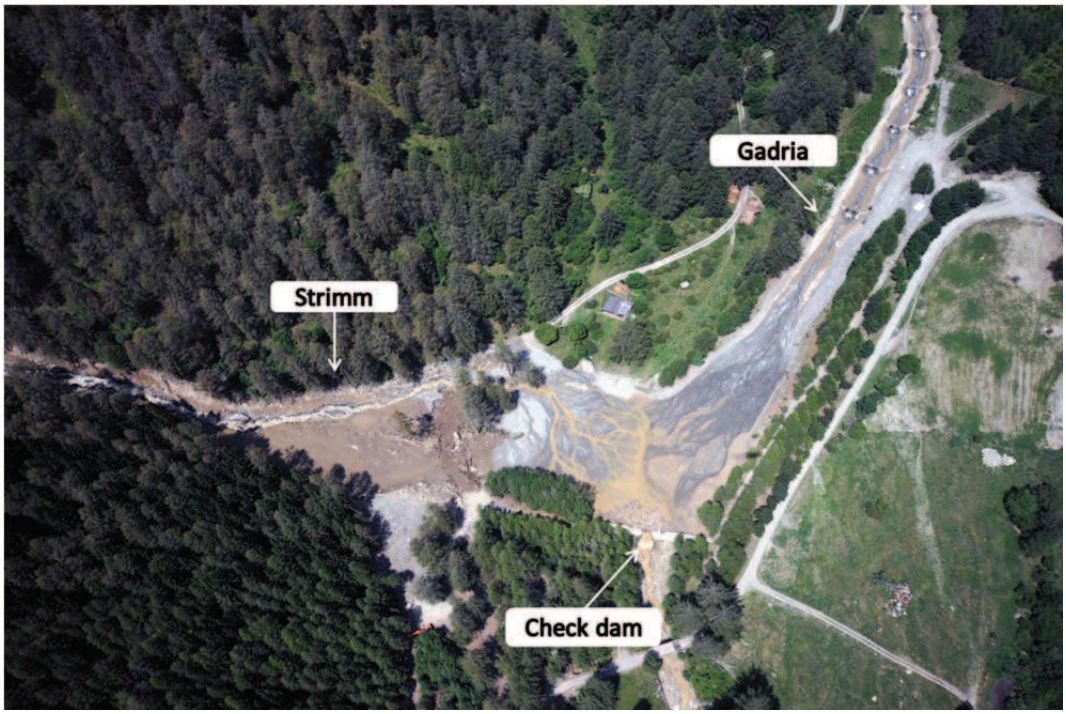

Figure 3. 9: Location of Gadria and Strimm outlet and of the retention basin (kindly provided by the Autonomous Province of Bozen-Bolzano).

In the Gadria catchment, a monitoring system for debris flows was installed in 2011 by the Department of Hydraulic Engineering of the Autonomous Province of Bozen-Bolzano just upstream the artificial debris retention basin. The monitoring system consists of raingauges, radar sensors, geophones, videocameras, piezometers and soil moisture probes. Most of these instruments have been installed on the channel. Further details of the debris-flow monitoring site can be found in Comiti et al. (2014).

3.3 Navizence catchment

The Navizence catchment (35.5 km^2) is located in the southern Walliser Alps, Valais, Switzerland (Fig. 3.10).

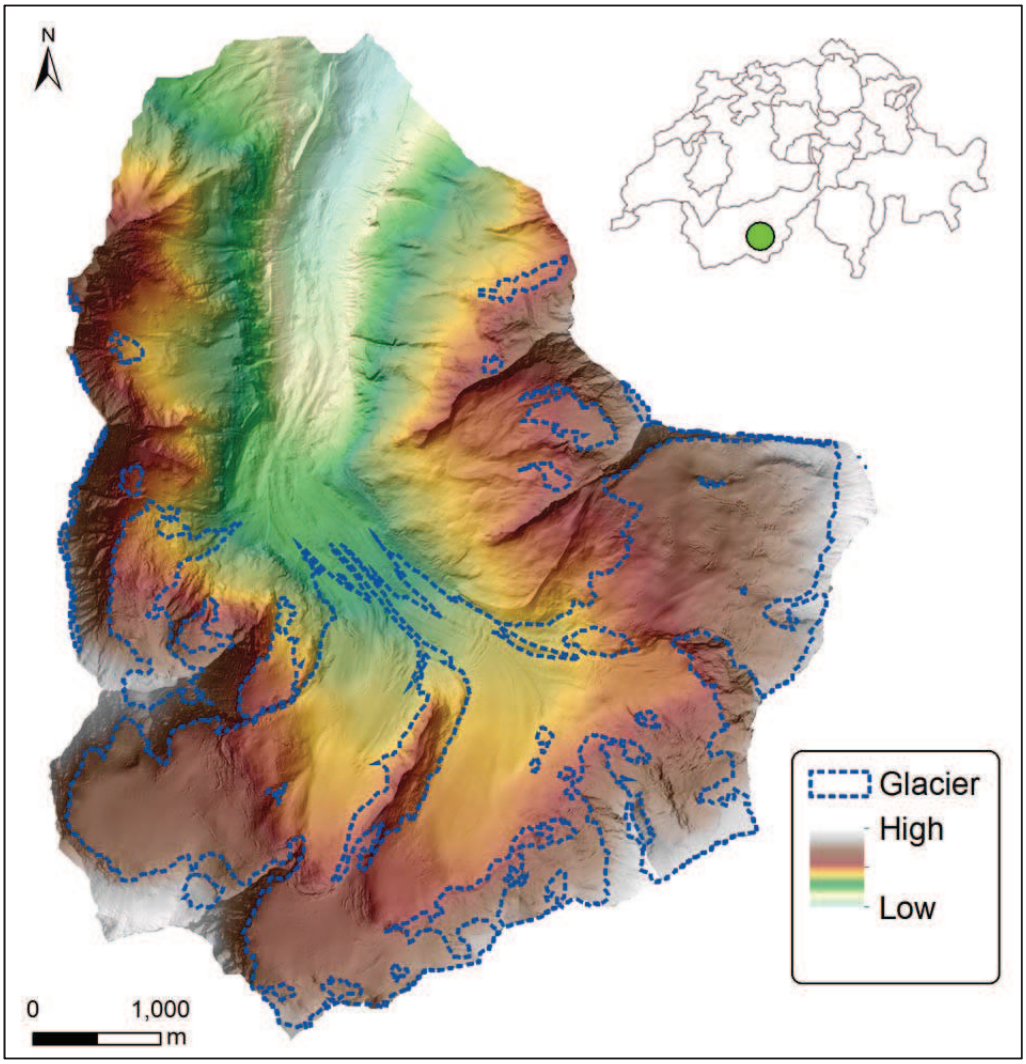

Figure 3. 10: Overview map of the study site.

The area of interest, characterized by several peaks reaching nearly 4350 m a.s.l., is occupied by a complex glacier system (Glacier de Zinal) with five main tributaries and a debris-covered glacier tongue (Huss et al., 2008). The main morphological features of the catchment and of the glacier are summarized in Table 3.3.

Table 3. 3: Characteristics of the investigated basin and of the ice-covered region within the catchment. The glacier area refers to the year 2006.

Area	Elevation (m)			Mean slope	Glacier area	Glacier elevation
(km^2)	Min	Max	Mean	(%)	(km^2)	(m)
33	1892	4354	2971	84.6	11.4	2483-3857

The Zinal glacier presents a significant sediment potential contribution in the context of the glacier retreat dynamic: well-developed lateral moraines, crossed by several channels, occur at toe slopes of Zinal glacier and distributed moraine bastions represent important sediment sources for channels.

Bedrock geology of the study area comprises Cretaceous-Jurassic calcshists of the Tsate Nappe and rocks of oceanic origin at high elevations, Cretaceous marbles and dolomites of the Frilihorn Nappe at middle elevations and Quaternary sediments at lower elevations (below 2200 m a.sl.) (Stampfly, 2001).

Meteorological conditions at the southern flank of the Alps determine the local climate that is relatively dry and characterized by mean annual precipitation of 728 mm per year (Fumeaux and Reynard, 2002).

Like almost all of the Swiss Alpine glaciers, Zinal glacier has been in regression since the end of the Little Ice Age (nearly 1550-1850), corresponding to the beginning of the global warming on Zinal valley (Fig. 3.11). Estimates on glacier retreat derived from systematic database of Swiss glaciers show for example that Zinal glacier lost about 1.6 km of its length in the period 1892-2000 (Fumeaux and Reynard, 2002).

Figure 3. 11: Evolution of the front of Zinal glacier between 1859 and 1967 where the retreat of the glacier is clearly visible. Dotted line represents the path used before the glacier retreat (Fumeaux and Reynard, 2002).

CHAPTER 4
MATERIALS AND METHODS

4.1 Input data

The database for the spatial and temporal analysis consists of LiDAR data acquired in different years for the study areas (Tab. 4.1).

Airborne laser scanner data for the entire Province of Bolzano were acquired during a four years period (2004-2006).

The surveyed area (7411 km^2) was split into three sections with different point density (Wack and Selzl, 2005):

- Section 1: urbanized areas and main valley floors (4 points/6.25 m^2);
- Section 2: all areas below 2000 m a.s.l. not belonging to the first section (8 points/25 m^2);
- Section 3: areas above 2000 m a.s.l. (3 points/25 m^2).

Gadria and Strimm basins were included within the second and the third section, while Venosta Valley encompasses all the different classes.

The 2011-LiDAR survey for Gadria and Strimm basins was acquired by the National Institute of Oceanography and Experimental Geophysics of Trieste (OGS) and sponsored by Free University of Bozen-Bolzano and Research Institute for Geo-Hydrological Protection of the Italian National Research Council (CNR-IRPI).

LiDAR data for the Navizence catchment were acquired by the Federal Department of Topography (Swisstopo) that regularly updates the elevation model of the whole territory of Switzerland.

Post-processing (i.e. filtering to remove non-ground points) and interpolation phases from the point clouds for different resolution DTM derivation are described in detail in the following sections.

Table 4. 1: Main characteristics of LiDAR surveys in the study areas. [1]: areas below 1500 m were surveyed in winter. For high elevation areas LiDAR data were acquired during the springtime and the summer of 2004 and after the springtime of 2005.

Study area	Acquisition Period	Sensor	Point density	
			points/m^2	area (%)
Venosta Valley	2004-2006[1]	ALTM 3033 (OPTECH) Falcon II	4 /6.25	35
			8 /25	29
			3 /25	36
Gadria	July 2005	ALTM 3033 (OPTECH) Falcon II	3 /25	88
			8 /25	12
	June 2011	RIEGL LMS Q560	> 8	-
Strimm	July 2005	ALTM 3033 (OPTECH) Falcon II	3 /25	37
			8 /25	63
	June 2011	RIEGL LMS Q560	> 8	-
Navizence	2010	Dual Leica Sensors ADS80-ALS60	1 /2	-

4.2. DTM quality assessment

Quality analysis of a LiDAR dataset represents an important step for morphological analysis since it is essential for the derivation of an appropriate DTM. The quality of morphometric information that can be derived from a digital model by applying terrain analysis techniques largely depends on the quality of the input dataset. DTM errors alter the representativeness of derived geomorphometric parameters since they are amplified when calculating first and second order derivatives of the studied surface, such as slope and curvature (Burrough and McDonnell, 1998). Furthermore, the results of quality assessment can be helpful for the choice of the interpolation method and the proper resolution (cell size) of the digital model (Cavalli, 2009).

In the process of geomorphic change detection based on high-resolution DTMs, the calculation and understanding of results rely in the accuracy of each multitemporal dataset. The analysis of accuracy can provide useful information on dataset uncertainty that can be propagated into the DoD. For instance, high noise levels can largely influence the sediment budget calculation at small scale preventing a correct identification of deposition and erosion patterns (Brasington et al., 2003). To this aim, LiDAR data quality assessment have been performed by analyzing two important parameters:

- LiDAR point density;
- DTM vertical accuracy.

High and spatially distributed point density, influenced by flight conditions, mission purpose, and required accuracy, is essential to accurately represent terrain and terrain features (FEMA, 2003). Point density map calculated on filtered data help in evaluating filtering process on raw data. Point density can also be considered as a proxy of the elevation uncertainty since surveyed areas where point density is low present high elevation uncertainties whereas surfaces that have high survey point density and are smooth have low elevation uncertainty (Wheaton et al., 2010). Density plots for both 2005 and 2011 point clouds were derived using the Point density tool of ArcGIS imposing a kernel of 1x1 m on the dataset.

In the assessment of vertical accuracy, reference values (Ground Control Point, GCP) are usually compared to DTM values. Quality control checkpoints should be randomly distributed, selected on flat terrain or uniformly sloping terrain, and derived from an independent source of higher accuracy than dataset values for identical points (Flood, 2004; Höle and Höle, 2009; Höle and Potuckova, 2011).

Vertical error (δz) are defined as (Hejmanowska and Kay, 2011):

$$\delta z = \delta z_{GCP} - \delta z_{DTM} \quad [2.1]$$

where δz_{GCP} and δz_{DTM} are respectively the reference height and the height derived from DTM corresponding to the same horizontal position. Statistical indices used to assess the accuracy of DTMs include the calculation of usual descriptors such as Mean Error, Root Mean Square Error (RMSE), Standard Deviation of Error (Tab. 4.2). The Mean Error is an indication of DTM shifting regarding to the reference value, whereas the standard deviation shows how much dispersion exists from the mean or expected value. As an indicator of random errors, the Root Mean Square Error is a widely used measure of accuracy between a set of estimates and actual values and has become a standard measure of map accuracy (Li, 1988; Fisher and Tate, 2006).

Table 4. 2: Accuracy measures for DTMs presenting normal distribution of errors; n is the number of sample points; δz_i denotes the differences from reference data for a point i.

Statistical descriptors	**Formula**
Mean Error ($\bar{\mu}$)	$\frac{1}{n}\sum_{i=1}^{1}\delta z_i$
Root Mean Square Error (RMSE)	$\sqrt{\frac{1}{n}\sum_{i=1}^{n}{\delta z_i}^2}$
Standard Deviation ($\hat{\sigma}$)	$\sqrt{\frac{1}{(n-1)}\sum_{i=1}^{n}(\delta z-\overline{\mu})^2}$

These accuracy measures can be applied if the distribution of vertical errors is normal and no outliers are present in the data (Höle and Höle, 2009). The normality of errors distribution can be checked by depicting a histogram of sample errors (Höle and Höle, 2009) and evaluating the absence of systematic errors (that

can be estimated based on the mean value distance from zero). Furthermore, the presence of outliers should be checked since it would lead to inaccurate and unreliable accuracy measures. Therefore, accuracy analysis can be performed on a dataset in which outliers have been discarded. One approach to deal with outliers is to remove them by applying a threshold. For instance, Hole and Potuckova (2006) classify errors as outliers if δz is greater than three times the RMSE, whereas Daniel and Tennant (2001) used a three times the standard deviation of original data.

If the errors distribution reveals non-normality, alternative approach should be applied. Höhle and Höhle (2009) propose some robust accuracy measures (Tab. 4.3):

- Median or 50% quantile ($Q_{\delta z}$), a robust estimator for a systematic shift of the DTM;
- Normalized Median Absolute Deviation (NMAD), an estimate for the standard deviation when no outliers exist;
- 68.3% quantile and 95% quantile, indicating values whose errors have a magnitude within the interval respectively $[0, \hat{\sigma}]$ and $[1.96\hat{\sigma}]$.

Table 4. 3: Accuracy measures for DTMs presenting normal distribution of errors; *n* is the number of sample points; δz_i denotes the differences from reference data for a point *i*.

Statistical descriptors	**Formula**
Median ($\bar{Q}_{\delta z}$)	$\bar{Q}_{\delta z}(0.5) = m_{\delta z}$
NMAD	$NMAD = 1.4826 \cdot median_j(\lvert \delta z_j - m_{\delta z)} \rvert)$
68.3% quantile	$\bar{Q}_{\lvert \delta z \rvert}(0.683)$
95% quantile	$\bar{Q}_{\lvert \delta z \rvert}(0.95)$

In this study GCPs were acquired both during topographic survey, using Total Station and GPS, led by CNR IRPI of Padova, TESAF Department (University of

Padova, Italy), CIRGEO (University of Padova, Italy) with the support of the Autonomous Province of Bolzano, and from official monographs of benchmarks of the Autonomous Province of Bolzano. To evaluate the accuracy of 2005- and 2011-DTM, surveyed GCPs were selected in stable and easily accessible areas (below 2000 m).

The accuracy assessment analysis aimed at providing information on DTMs uncertainty to be used in a Fuzzy Inference System (see Par 4.5) for estimating propagation of errors in the DoD.

4.3 DTMs derivation

LiDAR data filtering for Gadria and Strimm basins was carried out by using Terrasolid software. This procedure consisted of two steps:

- a semi-automated processing to remove false echoes (outliers);
- a semi-automated processing to classify different echoes by type, i.e. the first echo identifying top surfaces and the last echo including points belonging to the ground.

Due to the lack of information on flight-paths for the LiDAR survey of 2005, some overlapping points belonging to different flightlines remained. As a result, point cloud density is higher in areas characterized by two or more flightlines and smaller in areas covered by a unique flightline. Furthermore, overlapping can lead to generation of errors in the interpolation phase converting data from shapefile to ASCII since some adjacent flightlines are not perfectly aligned.

Filtering process for 2011-LiDAR survey has been carried out by OGS by using Terrasolid software.

Filtered points from both survey have been converted first to shapefile multipoint and then to Terrain dataset using ArcGIS 3D Analyst tools. Terrain dataset, a TIN-based surface built from measurements stored as features (points, lines, polygons) in a geodatabase, was chosen since it can help manage and process massive surface

data providing a high quality model. Each terrain dataset were used to create the DTM using natural neighbour interpolator which is an appropriate method for calculating a grid of values from data that can be a combination of regular, sparse, clustered or random distributions of points (Pirotti and Tarolli, 2010). Natural neighbor is a simple technique, requiring no input parameters, that is able to accurately reproduce the actual morphology (Abramov and McEwan, 2004; Yilmaz, 2007; Scheidl et al., 2008; Bater and Coops, 2009). Compared to other interpolation methods, such as Spline and Kriging, natural neighbor avoids the formation in the resulting DTM of other peaks and pits than those present in the original dataset (Höhle and Potuckova, 2011).

High point density values of 2011 LiDAR dataset permitted the derivation of a 1-m resolution DTM that was used for the analysis of sediment connectivity at basin scale. Geomorphic change detection was instead performed using a 2 m resolution DTM: the choice of the grid size is mainly due to the lower point density values of 2005-DTM and secondly to the computational effort required for analysis at basin scale.

Elevation data of Venosta Valley can be downloaded directly from the official website of the Autonomous Province of Bolzano[1] at the resolution of 2.5 m. Post-processing (i.e. filtering to remove non-ground points) and interpolation from the point cloud for DTM derivation were carried out by the Institute of Digital Image Processing/Johanneum Research of Austria (Wack and Selzl, 2005).

The elevation model of Navizence basin, the so called swissALTI3D, is available from the website of the Federal Office of Topography[2] and it has a 2m spatial resolution. The DTM used for the assessment of sediment connectivity after Zinal glacier melting simulation was derived from the application of the sloping local level (SLBL) techniques (Jaboyedoff and Derron, 2005) to the current DTM, describing the terrain after 40 years of glacier retreat.

[1] http://www.provincia.bz.it/aprov/amministrazione/default.asp
[2] http://www.swisstopo.admin.ch/internet/swisstopo/en/home.html

The SLBL concept allows the extrapolation of geomorphologic features beneath the surface. For the computation of the SLBL some fixed points (e.g. rivers, crests, landslide contours) need to be chosen in order to avoid a resulting flat topography. By applying an iterative procedure, the SLBL can be determined replacing the elevation of non-invariant points of a DEM by the mean value of the elevation of its neighbours ± a tolerance (Jaboyedoff et al., 2004; Jaboyedoff and Derron., 2005). The result of the procedure is a curved surface of second order.

To reconstruct the subglacial bedrock topography, the SLBL routine was applied to the Zinal glacier ice body, giving a typical U-shaped subglacial topography. The curvature of the new topography is adjusted to agree with the ice volume estimated by Huss et al. (2008) for the Zinal glacier (0.93 km^3) (Fig. 4.1).

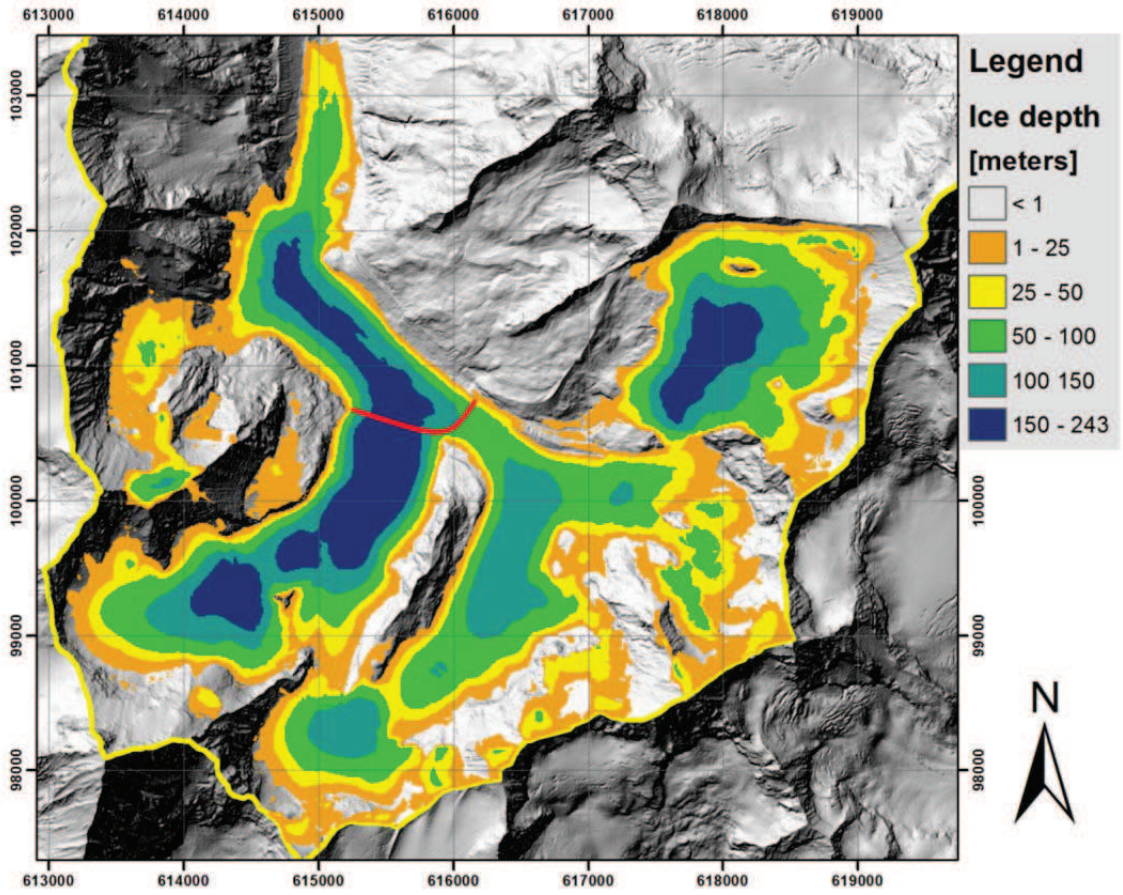

Figure 4. 1: Subglacial bedrock topography of Zinal glacier calculated by the SLBL model. The red line represents the estimated extension of the glacier in 2050.

4.4 Geomorphic change detection for Gadria and Strimm catchments

4.4.1 DoD and spatial uncertainty evaluation

The analysis of geomorphological changes based on multitemporal DTMs comparison required the understanding of model uncertainties that can lead to a misinterpretation of results. In fact, the evaluation of geomorphic changes largely depends on DTM quality which is basically function of sampling design, survey techniques, interpolation methods and topographic complexity (see Chapter 2). In

order to discriminate real changes from noise that arises from these errors, a probabilistic method based on a distributed measure of surface quality was used to quantify influence and propagation of DTM uncertainty into DoD.

In this work elevation changes occurred in the period 2005-2011 in Strimm and Gadria catchments were identified taking into account DoD uncertainty by applying a Fuzzy Inference System (FIS) to involved DTMs.

Predicted changes were then compared to post-event field observations and to geomorphometric indices, as described in the following paragraphs. The overall procedure applied for change detection analysis in Gadria and Strimm basins is illustrated in Fig. 4.2.

The method chosen for the DoD uncertainty assessment requires two main steps:

(i) Quantification of the surface representation uncertainty in the individual DEM surfaces,

(ii) Assessment of the significance of propagated uncertainty.

Quantification of the spatially variable uncertainty

This procedure is based on the estimate of the spatially structure of elevation uncertainty using a methodology introduced by Zadeh (1965) named Fuzzy Logic. The application of Fuzzy Logic to geomorphological interpretations deals with the need for a conceptual framework that can address the issue of uncertainty going beyond the limitations of probabilistic models that primarily describe random variability in parameters (Wheaton, 2008). Based on graded statements as opposed to Boolean crisp reasoning (i.e. true or false), Fuzzy Logic provides a robust and simple way to understand and represent vague, ambiguous or imprecise information within a system.

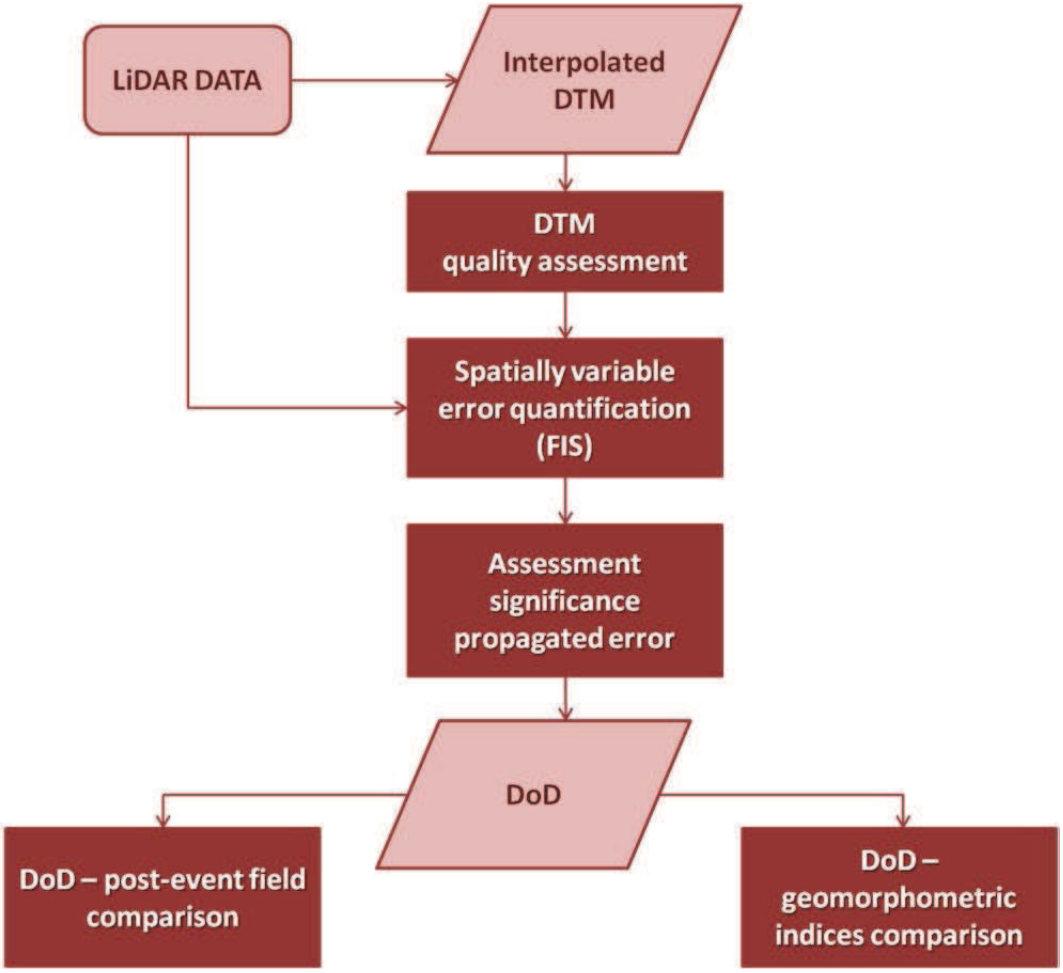

Figure 4. 2: Framework of methodology applied for change detection analysis.

Thanks to the implementation of Fuzzy Inference System (FIS) information related to morphology or survey techniques are combined to spatially evaluate the quantity of interest for geomorphological changes, i.e. elevation uncertainty (δz), for each DEM cell.

The most commonly used fuzzy inference technique, the so-called Mamandi method, require different steps (Fig 4.3) that can be summarized as (Klir and Yuan, 1995) :

- Fuzzification of the input variables;
- Rule evaluation (implication);

- Aggregation of the rule outputs;
- Defuzzification.

The first step requires the determination of Membership Functions (MFs), i.e. graphical representation of the degree to which inputs belong to each of appropriate fuzzy sets. MFs identify both linguistic adjectives (e.g. very high, extremely like) to characterize the variable to be described and the range of values covered by each adjective for inputs and output. The degree of membership of a value to a set is assigned using values ranging from 0 (no membership) to 1 (absolute membership). MF specification is more critical for the outputs than the inputs since values need to correspond to realistic values (Wheaton, 2008).

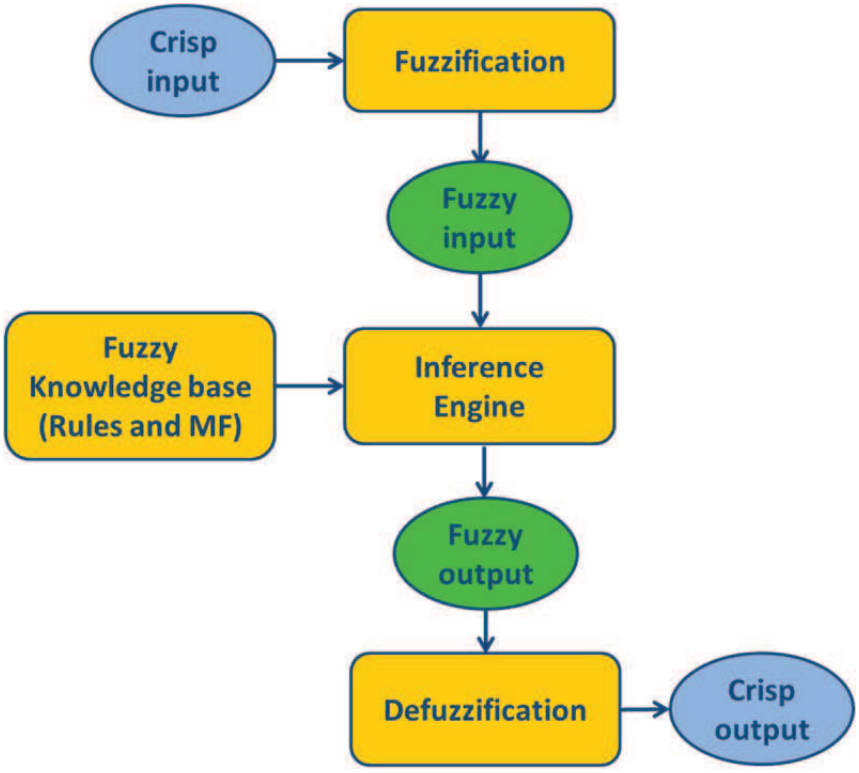

Figure 4. 3: Exemplification of Fuzzy Logic reasoning.

The second step represents the definition of fuzzy rules that is a linguistic process relating the inputs to an output defined by only one adjective. For instance,

vegetated areas featuring high slope and roughness and low point density are characterized by a high elevation uncertainty.

The aggregation phase implies the combination of fuzzy sets representing the outputs of each rule in order to obtain a single fuzzy set. The aim of this step is to obtain a fuzzy surface for both DTMs of input in which each cell is represented by a fuzzy number that expresses the range of uncertainty in the elevation values (Fig. 4.4)

The defuzzification is the process where the fuzzy output set is finally converted to crisp data , i.e. real numbers.

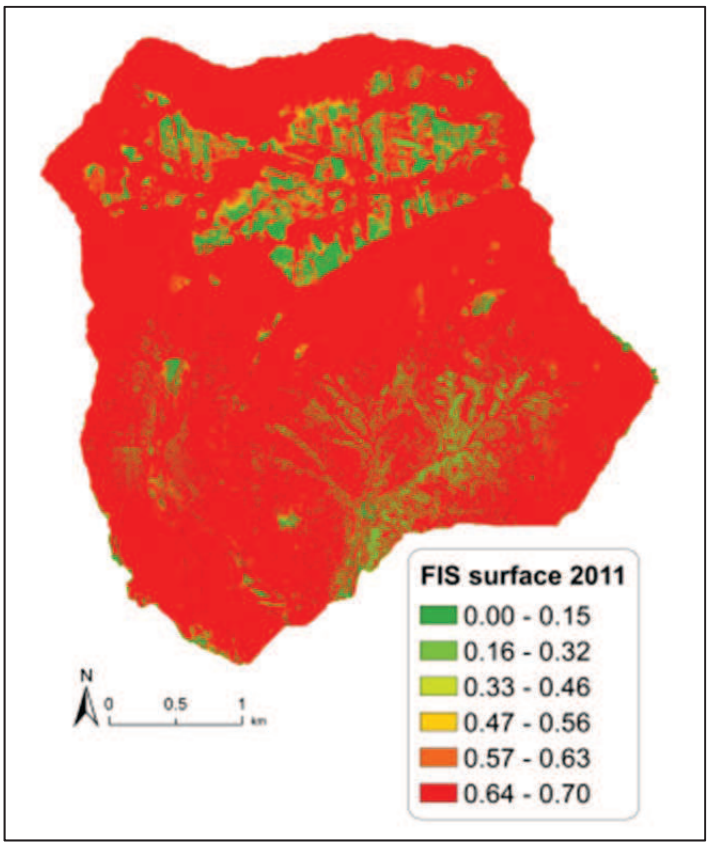

Figure 4. 4: Example of fuzzy surface derived for Gadria and Strimm basins DTM in which elevation uncertainty is represented with colours ranging from green (low uncertainty) to red (high uncertainty).

Assessing the significance of propagated errors

The significance of the DoD uncertainty can be expressed using probabilistic thresholding with a user-defined confidence interval. As defined by Taylor (1997), and later Brasington et al. (2003) and Lane et al. (2003), the threshold can be expressed as:

$$u_{Crit} = t\sqrt{(\delta z_{new})^2 + (\delta z_{old})^2} \quad [4.1]$$

where δz_{new} and δz_{old} are the individual errors in the new DTM and in the old one, respectively, and u_{crit} is the critical threshold error based on a critical student's t value at a given significance level:

$$t = \frac{(|Z_{DEM_{new}} - Z_{DEM_{old}}|)}{\delta u_{DoD}} \quad [4.2]$$

where $|Z_{DEM_{new}} - Z_{DEM_{old}}|$ is the absolute value of the DoD. The probability that an elevation difference is due to measurement errors can be calculated by relating the t-statistic to the cumulative distribution function. The DoD can be calculated by excluding all altitude variations that have lower probability than the threshold that is spatially variable based on a confidence interval (Wheaton, 2008).

In this work the fuzzy inference system approach and probabilistic thresholding has been applied at basin scale to identify elevation changes occurred in the period 2005-2011 in Strimm and Gadria catchments.

A two input FIS based on a parameter related to topography and one related to survey properties, respectively slope and point density, has been used (Fig. 4.5).

FIS characteristics have been specified as described by Wheaton (2008), using Mamdani as FIS type, maximum method for fuzzy operations, minimum method for the rule implication, maximum method for the aggregation and centroid method for the defuzzification.

Membership functions for each input parameter have been calibrated to the range of encountered values for each variable giving high point density a higher weight influencing uncertainty (Tab. 4.4) Taking into account the examined quality of the old and new surface (see Par. results), fuzzy surfaces were calculated by applying different interval values for the output values. Therefore, MF range from 0.14 to 1.2 for 2005- DTM and from 0.10 to 1.2 m for 2011-DTM. Maximum value (1.2 m) was chosen according to estimated elevation error on high slope and low point density area.

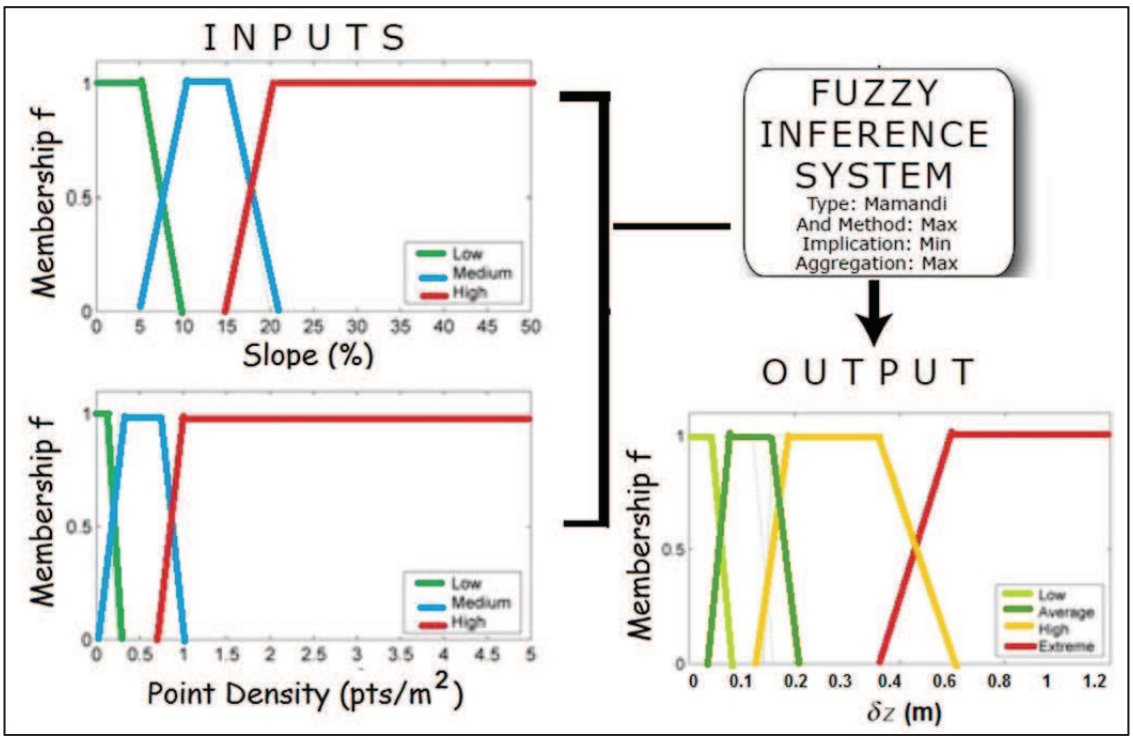

Figure 4. 5: The two inputs FIS used for the evaluation of geomorphic changes for Gadria and Strimm basins (Wheaton et al. (2010) modified).

The combined error was then calculated on a cell-by-cell basis considering spatial variability independently for both DTMs.

Concerning the assessment of significance of detected errors with DoD method, a confidence interval of 90% was used as a threshold. This means that all changes with probability values less than the chosen threshold are discarded.

Table 4. 4: Rules definition scheme for the 2 inputs FIS used to evaluate geomorphic changes in both Gadria and Strimm basin.

Inputs		**Output**
Slope	Point density	δz
Low	Low	Average
Low	Medium	Low
Low	High	Low
Medium	Low	High
Medium	Medium	Average
Medium	High	Average
High	Low	Extreme
High	Medium	Extreme
High	High	High

4.4.2 DoD and post-event field surveys

The Autonomous Province of Bolzano adopted an efficient and updated information system of natural hazard (ED30) aiming to document fluvial and torrential processes (e.g. debris flow, floods, erosion processes) occurring in the entire territory (Macconi et al., 2008). ED30 is a valid tool to support risk analysis assessment, landuse planning, future events management and more generally the understanding of sediment dynamic related processes that characterized alpine environments. Data stored in this database represent also a basis for the calibration

of simulation models (Mammoliti, 2011; Crema, 2014), which represent an essential instrument for process understanding and hazard assessment.

For a correct characterization of the occurred natural events, relevant information are detected by technicians of the Autonomous Province of Bolzano, in particular:

- date, type and magnitude of the process;
- geographical data and description of the area in which the event occurred (e.g. aspect, slope, landuse, roads, inhabitants);
- meteorological data derived from field observation or weather stations;
- damages to infrastructure, forests, agricultural areas and people;
- definition of presence and condition of protection structures.

Evidences of the event are detected along the process path (e.g. from the initiation point of a debris flow to the deposition area). Field documentation allows the reconstruction of the dynamics of the event and the identification of the main transport process. To this purpose, sediment volumes estimate is very helpful representing one of the more important and, at the same time, the more difficult step of the process documentation (Kienholz et al., 2006). Volume is calculated by multiplying the thickness by the area of the deposit measured in the field. Uncertainty factors in volume assessment are mainly linked to (Macconi et al., 2011):

- uneasy accessible sections;
- difficult recognition and quantification of mobilized volumes;
- overlapping of consecutive events;
- logistic problems (e.g. meteorological conditions).

Documentation of processes and volumes starts where channel clearing begins, usually in built-up area or near infrastructures. These works make the assessment of sediment volumes difficult in the entire basin due to the priority of areas subjected to emergency.

The documentation of the event, including also multimedia data (e.g. video, pictures), is stored in field reports and then into geodatabase that includes geometric features indicating the initiation point of the phenomenon (PIF), the location and volumes of deposits, the length of channel sections affected by the event, and other important elements describing the characteristics of the process. Therefore, the ED30 gives information that can be helpful for the analysis of catchments and their activity related to their morphometric and geomorphologic characterization. For instance, it is possible describe a debris flow characteristics by mapping deposits with areal elements, according to their different thickness, and by discriminating channel activity according to erosion, transport or deposition sectors (Mammoliti, 2011).

Figure 4. 6: Volume detection estimation in the field for a debris flow event occurred in Gadria stream in 2008 (A). Red lines in (B) show the location and the point of view from which volumes were estimated (kindly provided by the Autonomous Province of Bolzano).

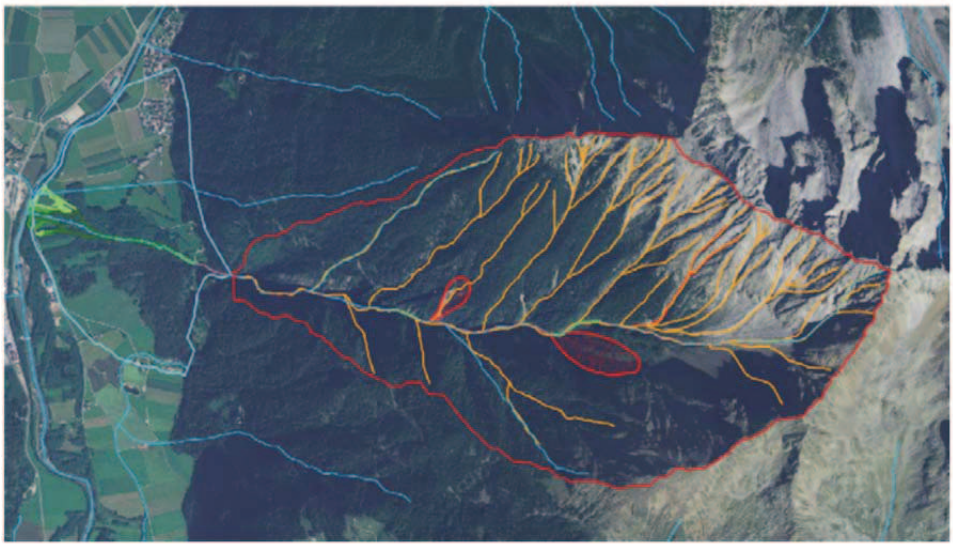

Figure 4. 7: Example of the representation of a debris flow process occurred in 2007 in Valburga basin (Venosta Valley). Deposits are depicted with different green intensities according to their various thickness, while channels are divided into erosion (red), transport (blue) and deposition (green) (Mammoliti, 2011).

In this study volumetric measurements of historical events stored in the ED30 database were used for the comparison with DoD results. To this purpose, only events occurred from June 2005 to June 2011, corresponding to the time interval separating the two LiDAR surveys, were considered. Therefore, geometric features such as PIF and corresponding deposition areas were extracted for Gadria and Strimm basins and managed in a GIS environment by means of geodatabase tools. Volume data were extracted both from the table attribute of deposition shapefile and from field reports.

Field estimate are essentially based on the sediment arriving to the retention basin, located at the confluence of the Strimm and Gadria rivers (see Par. 3.2.1). Since material is periodically removed from the retention basin, the latter was excluded from the DoD analysis. Sediment mapped and measured within the catchments in post-event surveys were compared with DoD-estimated deposits. Erosion computed by DoD was compared with gross erosion resulting from field surveys, i.e., the sum

of sediment volumes deposited within the catchment and sediment that attained the catchment outlet. This second component of field estimates was measured as sediment volumes accumulated in the debris basin and roughly corresponds to catchment sediment yield. Volumes detected in the field fall within the range of uncertainty of DoD estimates for both basins.

In order to focus the analysis on geomorphic changes occurred in areas connected to the channel network, volume computations were restricted to the areas delimited in Figure 4.8 by black boundaries where surface changes were clearly detectable from a preliminary raw DoD analysis and multi-temporal ortophoto interpretation.

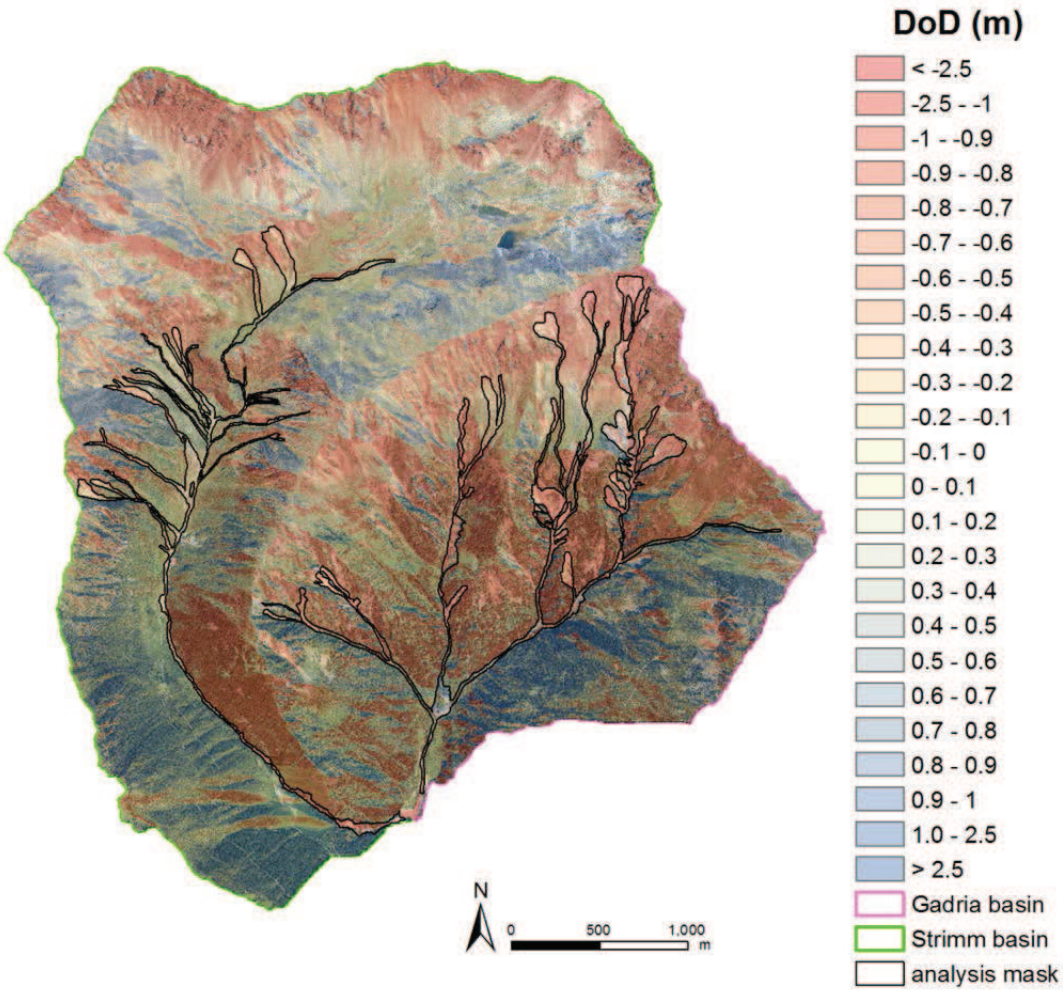

Figure 4. 8: Raw DoD map for Strimm and Gadria basins. Black borders represent areas for which the eroded and deposited volumes are calculated.

4.4.3 DoD and geomorphometric indices

Relationships between some geomorphometric parameters and DoD detected changes were investigated since they can offer a new perspective on the interpretation of multitemporal changes besides the estimate of erosion and deposition volumes.

A first analysis concerns surface curvature, one of the basic terrain parameters commonly used in geomorphometry, as explained in the Chapter 2. In this study plan and profile curvature were calculated within the same mask used for DoD analysis (see par.4.5.1) and then compared to DoD estimated changes. Curvature signs can vary according to different methods. In this study, curvature has been calculated using Landserf software that is based on Wood's algorithm (Wood, 1996) giving different signs as shown in Table 4.5.

Table 4. 5: The correspondence between the sign of the plan and profile curvature values and type of surface.

	Plan curvature		**Profile curvature**	
Sign values	(-)	(+)	(-)	(+)
Corresponding surface	convex	concave	concave	convex

Flat areas were then differentiated from convex and concave areas based on different values for planform and profile curvature: the interval of flat areas ranges from -0.2 to 0.2 for planform curvature and from -0.02 and 0.02 for profile curvature. These rules were chosen according to findings in literature that were suitable for the values of profile and plan curvature calculated in this study (Maggioni and Uber, 2003; Schmid and Sardemann, 2003; Aguilar et al., 2005; Mukherjee et al., 2013).

Both plan and profile curvature were calculated using a 5x5 moving window that, after several tests on different window sizes, proved to be a good compromise for a 2 m resolution DTM between the need for a good recognition of multiple surface features and the reduction of noise deriving from larger kernel that can lead to misinterpretation of analyzed morphology.

Relationship between DoD results, slope and drainage area was also investigated. Slope-area plots derived from digital elevation models were combined to DoD results for Gadria and Strimm basins, i.e. areas of erosion and deposition. Slope and contributing area were extracted from DTM using TauDEM ArcGIS extension. The contributing area was calculated using the D infinity flow algorithm (Tarboton, 1997) after filling local depression in the DTM using the pit remove tool. The described method was chosen since it avoids grid bias or unrealistic dispersion if compared to other algorithms (Tarolli and Dalla Fontana, 2009). Slope was computed as local slope, i.e. the steepest outwards slope on one of eight triangular facets centered at each grid cell, measured as drop/distance, i.e. tan of the slope angle (Tarboton, 1997).

4.5 Sediment connectivity: the quantitative approach

The assessment of sediment connectivity in Alpine catchments needs to consider both complex morphology and heterogeneity in type, extent and location of sediment sources since these factors affect the effectiveness and the variability of sediment transport processes.

In this study, sediment connectivity was characterized by using a distributed geomorphometric index, the Index of sediment Connectivity (*IC*), as developed by Cavalli et al. (2013) based on the work of Borselli et al. (2008). The index was chosen since it can be easily derived from a DEM and it is designed to model sediment connectivity in Alpine catchments related to the processes that this thesis intends to investigate, i.e. debris flow and channelized sediment transport. The

proposed index expresses the potential connection between hillslopes and features of interest (e.g. catchment outlet, roads, main channel network) or elements which act as storage areas (sinks) for transported sediment (e.g. lake, debris retention basin). In particular, *IC* aims to model two important characteristics of sediment connectivity, i.e. the sediment delivery across the drainage system (i.e. the potential connection of sediment between hillslopes and catchment outlets) and the sediment coupling-decoupling between hillslopes and selected targets or sinks. Therefore, the index allows the estimation of both the probability that the sediment from a sediment source will reach the catchment outlet and that the sediment eroded from hillslopes will attain the target of interest (Cavalli et al., 2013).

The IC is defined as:

$$IC = log_{10}\left(\frac{D_{up}}{D_{dn}}\right) \tag{4.3}$$

where D_{up} and D_{dn} are respectively the upslope and downslope components of connectivity. *IC* was defined in the range of [-∞, +∞], with connectivity increasing for larger *IC* values.

The upslope component D_{up} is the potential for downward routing of the sediment produced upslope and is estimated as follows:

$$D_{up} = \bar{W}\bar{S}\sqrt{A} \tag{4.4}$$

where $\bar{W}$ is the average weighting factor of the upslope contributing area, $\bar{S}$ is the average slope gradient of the upslope contributing area (m/m) and *A* is the upslope contributing area (m^2).

The downslope component D_{dn} takes into account the flow path length that a particle has to travel to arrive to the nearest target or sink. Therefore, D_{dn} can be expressed as:

$$D_{dn} = \sum_i \frac{d_i}{W_i S_i} \tag{4.5}$$

where d_i is the length of the flow path along the i^{th} cell according to the steepest downslope direction (m), W_i and S_i are the weighting factor and the slope gradient of the i^{th} cell, respectively.

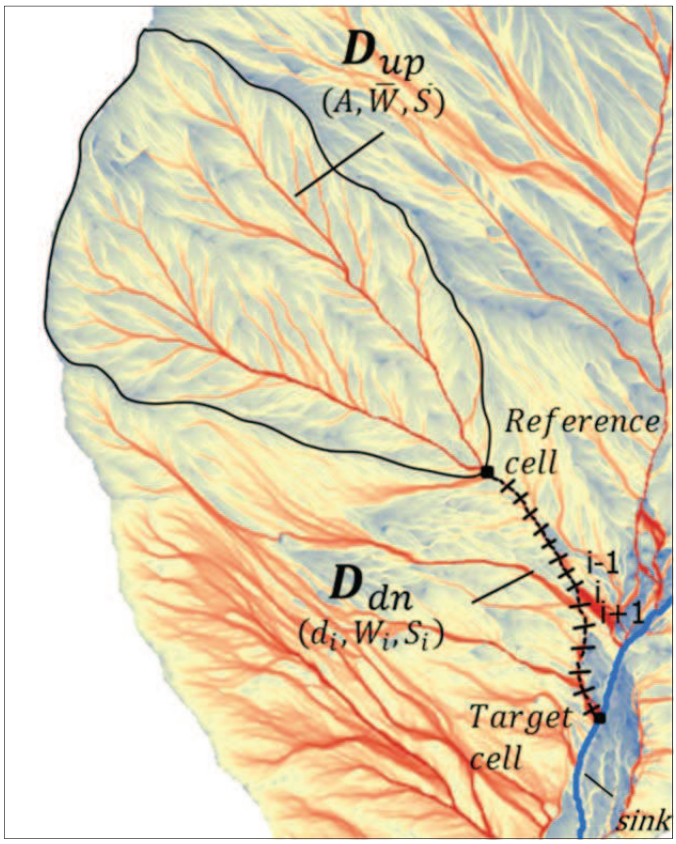

Figure 4. 9: Spatial representation of index of connectivity components.

Slope is calculated directly from the DTM and ranges from 0.005 to 1 m/m. The lower limit of the interval is set to avoid infinites in eq. [4], whereas the choice of the upper value has both a mathematical and a physical meaning. In fact, high slope

values can introduce bias in the *IC* calculation leading to very high index values on steep slopes; high slopes are also typical of near vertical rock cliffs or steep hillslopes and bedrock channels where sediment is mainly mobilized by rockfalls, a process excluded from those investigated by the *IC*.

The contributing area is calculated by applying the multiple flow D-infinity approach (Tarboton, 1997), a recursive method that split the flow coming from one grid into up to two downwards neighbours with the largest downslope. The choice of this method is linked to the need of finding a representative pattern of sediment connectivity through basins. In fact, D-infinity method correctly models sediment fluxes in mountain catchment since it allows the identification of real flow paths especially on hillslopes where divergent flow predominates (Fig. 4.10). Furthermore, the D-infinity algorithm avoids the problem of underestimating channel widths thanks to the partitioning of the flow over the entire cross section (Cavalli et al., 2013).

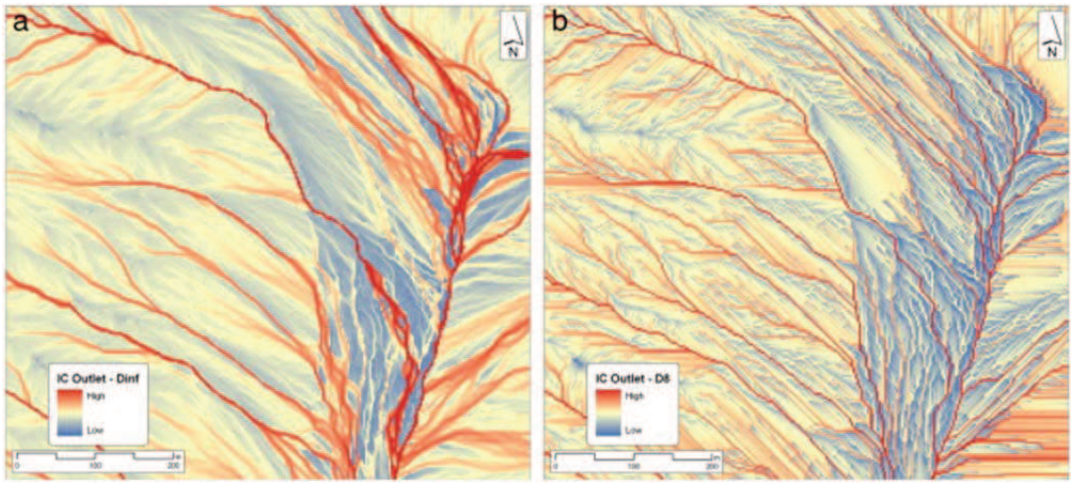

Figure 4. 10: Comparison between *IC* calculated with reference to the outlet of Gadria and Strimm catchments, using D-infinity (a) and single-flow direction (b) algorithms (from Cavalli et al., 2013).

The weighting factor *W*, which appears in upslope and downslope components of *IC*, represents the impedance to runoff and sediment fluxes due to properties of the local land use and soil surface. The weighting factor should meet some requirements: it must be derived from the surface characteristics that influence runoff process and sediment fluxes within a system, be related to measurable characteristics of land use and management and be applicable to the upslope and downslope side of any point along the slope (Borselli et al., 2008). A single parameter that fits all these prerequisites is hardly to define, so various alternatives have been implemented in the *IC* calculation according to objectives and study area characteristics.

Borselli *et al.*, (2008) used the C-factor derived from USLE and RUSLE models (Wischmeier and Smith, 1978; Renard et al., 1997) as weighting factor modelling the effects of vegetation cover and management practices on erosion rates. The C-factor varies from values approaching 0 (well protected soils) to 1 (high erosion risk soils); values greater than 1 can be found where site conditions are more erosive than the unit-plot conditions used to develop the C-factor (Toy et al., 1999).

Valuable information on surface roughness, suitable for the assessment of the impedance factor, can be derived from HR-DTMs by calculating geomorphometric indices representing fine-scale topographic variability. Cavalli et al. (2013) introduced a local measure of topographic surface roughness, i.e. the Roughness Index (*RI*), as weighting factor. *RI* is calculated as the standard deviation of the residual topography at a scale of few meters (Cavalli and Marchi, 2008; Cavalli *et al.*, 2008). The residual topography is calculated as the difference between the original DTM and a smoothed DTM created by averaging values within a nxn cells moving window. The standard deviations of residual topography values are computed in a nxn cells moving window over the residual topography grid. The roughness index is then defined as:

$$RI = \sqrt{\frac{\sum_{i=1}^{n^2}(x_i - x_n)}{n^2}} \quad (4.6)$$

where n^2 is the number of the processing cells within the nxn cells moving window, x_i is the value of one specific cell of the residual topography within the moving window, and x_m is the mean of the n^2 cells values.

The weighting factor, developed by Cavalli et al. (2013), was then defined as:

$$W = 1 - \frac{RI}{RI_{MAX}} \quad (4.7)$$

where R_{MAX} is the maximum value of *RI* in the study area. To avoid infinites in the Eq. (4.5) and Eq. (4.7), all values that fall in the interval of 0-0.001 are set to 0.001. Therefore, W values range from 0.001 to 1: this standardization is required in order to have the same range of variation as for S factor, to remove the bias due to high *RI* values and to provide comparable values with W as calculated by Borselli et al. (2008).

While the C-factor is specifically designed to describe impedance to runoff and sediment fluxes processes in agricultural and pasture lands, *RI* can be applied to Alpine catchments where bare areas are present. In these areas, characterized by different roughness according to the characteristics of outcropping rocks and debris cover, the C-factor would not provide differences in the impedance to sediment transport (Cavalli et al., 2013).

In areas with a great heterogeneity of land use or in the case of studies aiming at evaluating the role of different vegetation covers on sediment dynamic, an alternative approach to C-factor and *RI* is represented by a parameter related to hydraulic roughness, i.e. Manning's n roughness coefficient (*n*). Manning's n represents the resistance to flows in channels and flood plains, with values varying

according to different surface characteristics and factors affecting roughness. For example, Walling and Zhang (2004) derived a weighting factor by crossing *n* values with land use data to assess sediment connectivity between catchment and channel networks in England and Whales regions.

4.5.1 Sediment Connectivity Index applications

In this thesis, the connectivity index was applied to the study areas in order to evaluate the effect of spatial scale, in terms of spatial extent and resolution, on this geomorphometric parameter as described in the following sections. Relationship of IC with catchment shape factors, that represent areal properties expressing the overall planform and size of a basin, was also investigated. Time domain of sediment connectivity was analyzed by evaluating new potential connectivity pattern due to the retreat of the main glacial edifice in the Swiss basin. According to different objectives, two weighting factors were applied, i.e. Manning's n roughness coefficient and Roughness Index. In particular, the Roughness Index has been calculated to analyze the sediment connectivity at basin scale (i.e. 22 basins), whereas for the analysis at regional scale (i.e. Venosta valley) the Manning's roughness has been determined. For the evaluation of temporal and spatial sediment connectivity changes in the Zinal catchment a roughness proxy based on Manning's values has been applied.

The connectivity model was applied through the implemented Model Builder tool, running in ArcGIS 10.1 (ESRI), that uses functionalities and algorithms available in Spatial Analyst extension and Taudem 5.1.

4.5.1.1 Spatial scale analysis

In order to carry out the analysis on the effect of spatial extension on sediment connectivity, the *IC* was applied to regional and basin scale. *IC* was then computed considering two different management aspects:

- the sediment connectivity between hillslopes and catchment outlets (IC outlet);
- the sediment connectivity between hillslopes and main channels and lakes (IC channels).

For the analysis of sediment connectivity calculated with respect to the outlet, the only input required is represented by the DTM, whereas the evaluation of sediment connectivity to main channel network as final targets requires their identification.

To evaluate the sediment connectivity at regional scale, the *IC* outlet was analyzed on Venosta Valley using the 2.5 m DTM. Due to the large variability of land cover of the study area, the weighting factor chosen for the analysis was expressed by the Manning's n roughness coefficient. To this aim, Manning's n coefficients values, derived from literature (HEC, 1998; Engman, 1986; Downer et al., 2002), were assigned to corresponding land use or cover categories (Tab. 4.6) of the study area that were grouped into classes as defined by the CORINE Land Cover classification (Fig. 4.11).

Table 4. 6: Reference table for Manning's n values assigned to CORINE Land Cover classes for Venosta Valley.

CORINE Land Cover	Manning's n
Arable land	0.2
Artificial/non-agricultural vegetated area	0.02
Bare rock	0.05
Forest	0.4
Glacier	0.01
Grassland	0.1
Heterogeneous agricultural areas	0.2
Industrial or commercial units	0.02
Mine, dump, construction sites	0.01
Open space with little or no vegetation	0.15
Pasture	0.25
Permanent crops	0.2
Road and rail networks and associated land	0.01
Shrub/herabceous vegetation association	0.3
Urban fabric	0.02
Water body	0.001
Water courses	0.001
Wetlands	0.001

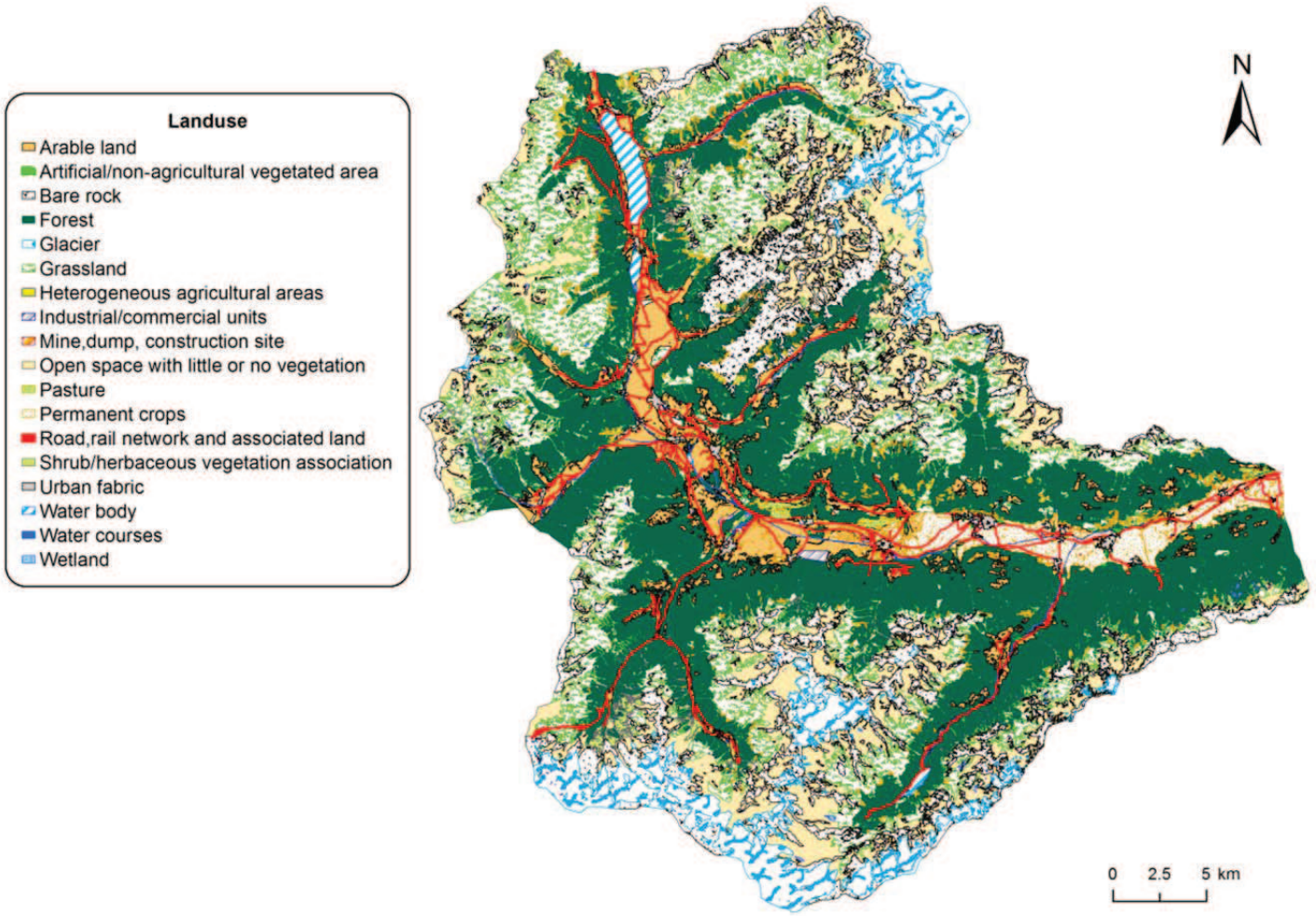

Figure 4. 11: Land use classification of Venosta Valley according to CORINE Land Cover nomenclature.

The Adige river and Resia and S. Valentino alla Muta lakes (Fig. 3.1) were chosen as target to compute the *IC* channels on Venosta valley.

Several catchments of Venosta Valley were selected for spatial sediment connectivity analysis at basin scale in order to explain the sediment connectivity model responses to different catchment size, slope and sediment transport dynamic. The input model is represented by the regional grid (2.5 m) from which the DTM for every basin was extracted at the same resolution. To analyze IC outlet, all basins outlets were calculated at the corresponding fan apex, identified through ortophoto and geological map interpretation, with the only exception of Trafoi and Solda catchments, whose outlets correspond to the convergence of their channel network (Fig. 4.12). For the computation of *IC* outlet, the Roughness Topographic index was applied to each basin on a 2.5x2.5 cells moving window.

For the calculation of IC channels, main stream lines were defined as valleys draining an area greater than 0.2 km^2. This threshold was chosen based on visual control of orthophoto and hillshade.

Resolution influence on sediment connectivity was investigated both at regional and catchment scale, respectively on Venosta Valley and Strimm catchment.

The effect of input data resolution was evaluated by running sediment connectivity scenarios, using both outlet and river channels as nearest sink, at increasing DTM grid size: for Venosta Valley, the 2.5 m input DTM was reduced to 5 and 10 meters resolution, whereas for Strimm catchment the 1–m input DTM was reduced to 2 and 5 meters.

Coarser DTMs resolution were achieved by using the Aggregate tool of ArcGIS 10.1 Spatial Analyst computing the mean of input cell values in a moving window equal to the new resolution.

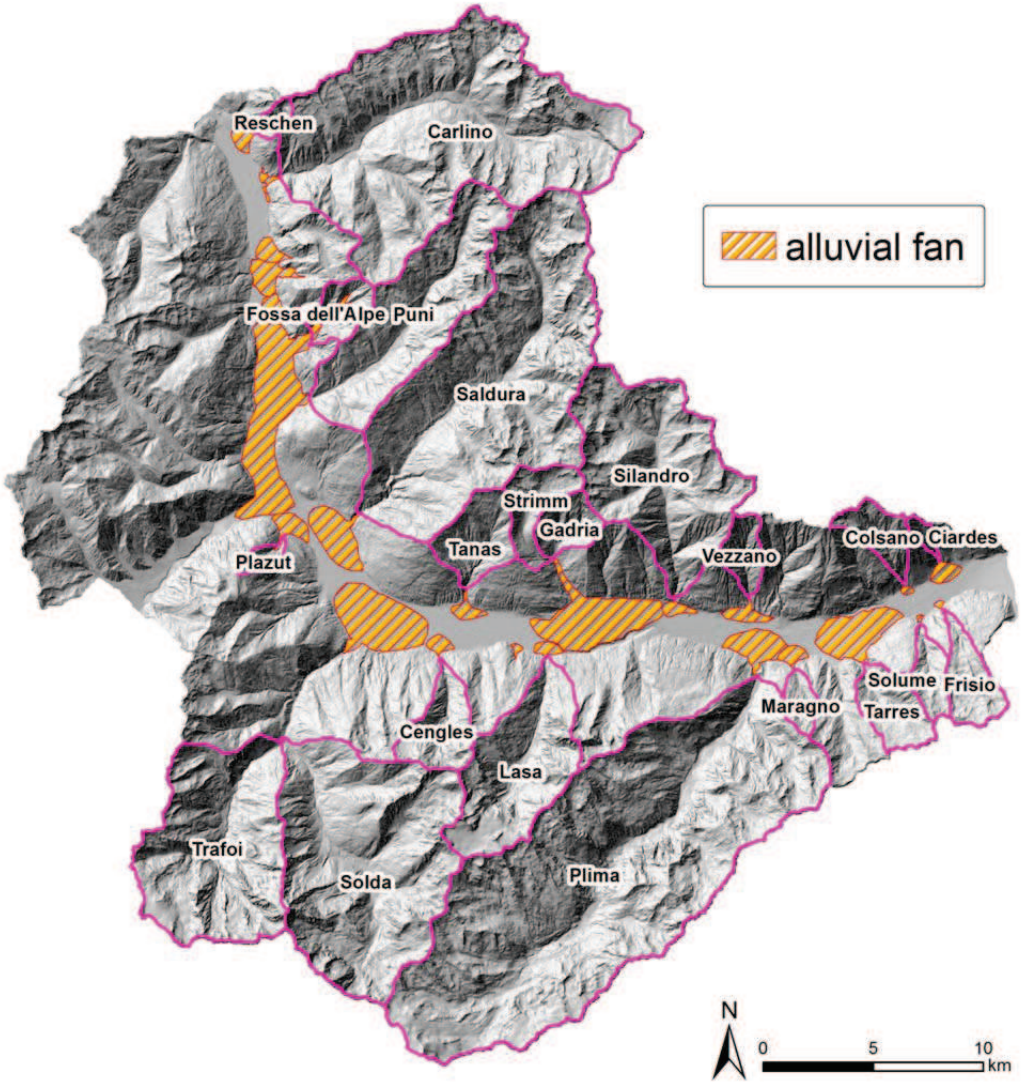

Figure 4. 12: Spatial representation of selected basins of Venosta Valley and related alluvial fans derived from ortophoto and geological map interpretation.

4.5.1.2 Morphometric analysis

Basin shape may play an important role in differentiating sediment connectivity patterns at the catchment scale (Baartman et al., 2013; Cavalli et al., 2013). In fact, elongated shape basins are characterized by a longer sediment transport path length to reach the outlet than circular ones, so leading to an increase of hillslope-outlet decoupling processes.

Elongation ratio (*Re*) and circularity ratio (*Rc*), as defined in Par. 2.1.1, have been calculated in order to investigate the relationship between the sediment connectivity index and the basin shape.

To investigate the relationship between sediment connectivity and relief, the basin relief ratio index (R_H), defined in Par. 2.1.1, was calculated.

Morphometric analysis was performed on the 22 selected basins of the Venosta Valley (Fig. 4.5) where the connectivity model was applied to analyze sediment delivery across the drainage system considering the alluvial fan apex as target. IC results where then compared to *Re* and *Rc* computed values.

Information related to the dominant sediment transport process (debris flow, bedload and mixed processes) characterizing the main channel of each basins was also derived from historical archive (ED 30) and field surveys carried out by the Autonomous Province of Bozen-Bolzano. For three catchments of Venosta valley such information was not available: hence, an indirect evaluation, based on the analysis of aerial photographs and on the computation of a morphometric parameter useful for distinguishing basins by process, i.e. the Melton index (*Me*) (see Par. 2.1.1), was applied.

4.5.1.3 Glacier connectivity

Sediment transport characteristics of glaciated alpine catchments can be modified by melting process affecting downstream channel network. In this study, the *IC* model was applied to Navizence catchment in the Southern Swiss Alps Glacier to analyze new potential connectivity pattern due to the retreat of the main glacial edifice.

To analyze sediment connectivity evolution two DTMs were used:

- the current DTM, obtained from high resolution photogrammetry (2 m) describing the terrain at the time of the survey (2010);
- the post-glacial DTM, derived from application of the SLBL techniques to the current DTM, as described in par. 4.3.

IC was calculated with reference to the outlet of the analyzed catchment and the channel network. In the latter case, the active hydrographic network for the actual scenario was identified by means of field observation and photo interpretation whereas for the future DTM main channel was extended to the glacier estimated base by applying a threshold value to the results of the D-infinity flow accumulation.

In the application of IC to Navizence catchment the impedance factors were derived from tabled values of Manning's n coefficients values for both the current and the future scenario. Hydraulic roughness values, derived from literature as in the case of Venosta Valley (HEC, 1985; Engman, 1986; Downer et al., 2002), were assigned to corresponding land uses (Tab 4.7) of the Navizence catchment (Fig. 4.13).

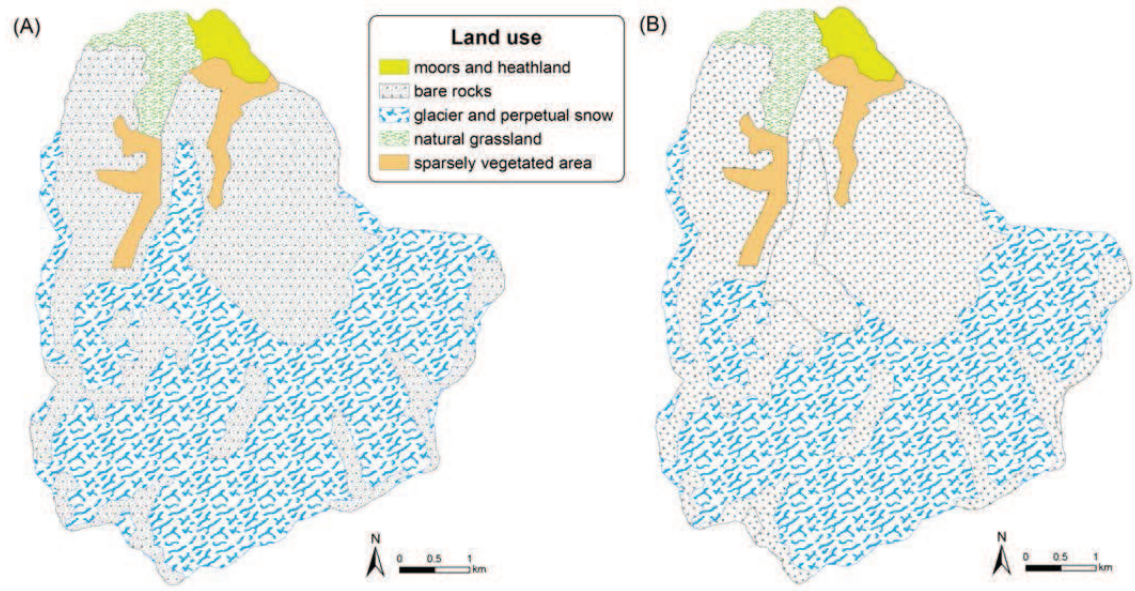

Figure 4. 13: Land use classification of Navizence catchment for the actual (A) and for the post-retreat situation (B). In the future scenario the bed glacier is assumed to be equal to a bare rock surface.

Table 4. 7: Reference table for Manning's n values assigned to land use classes for Navizence catchment.

Landuse	Manning's n
Bare rock	0.05
Glacier and perpetual snow	0.01
Moors and heathland	0.08
Natural grassland	0.1
Sparsely vegetated area	0.15

The choice of a proxy of sediment transport impedance linked to land cover is due to the fact that the future DTM is derived from a geometrically based model (SLBL method, see Par. 4.3); consequently the digital model could not properly represent the surface roughness.

In order to evaluate the potential evolution of sediment connectivity, future lateral moraines, that can be formed after glacial retreat, were mapped and insert into the DTM based on expert knowledge (Fig. 4.14).

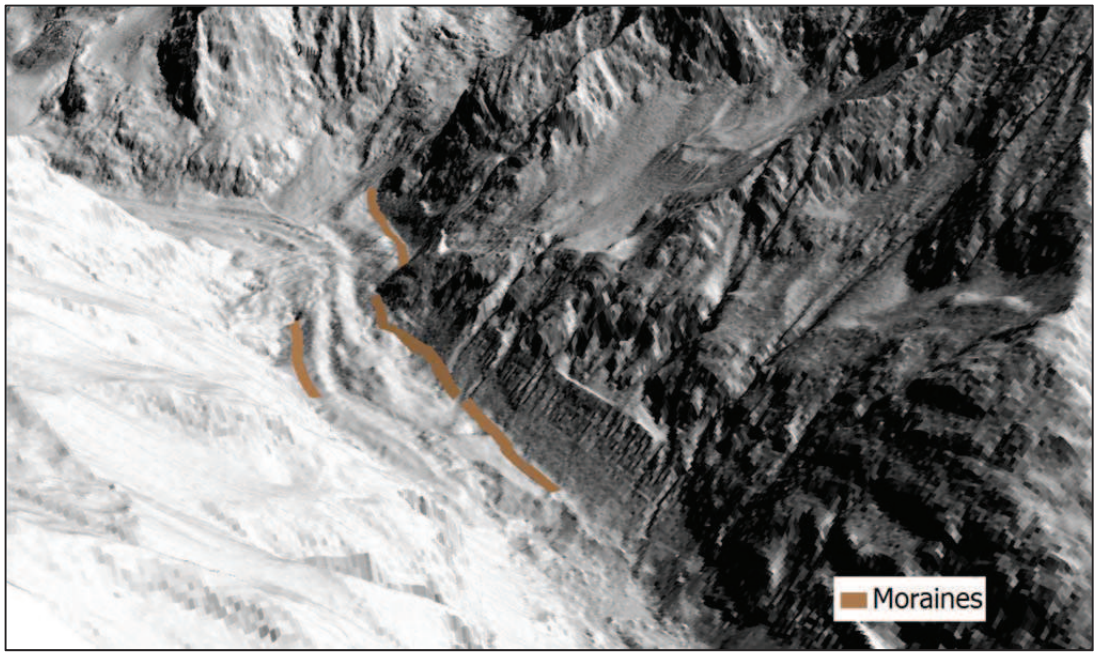

Figure 4. 14: Example of future moraines as estimated in a 40 years period after glaciation.

Since moraines can act as natural barrier to the downward sediment transport, they were treated as sink, i.e. upcoming sediment from these features not considered in the connectivity analysis on the future DTM since it will not likely propagate to investigated targets (outlet and channel network).

CHAPTER 5

RESULTS AND DISCUSSION

5.1 LiDAR data accuracy analysis

The accuracy analysis performed on 2005- and 2011- DTM represents the basis for the application of DoD to Gadria and Strimm basins. Maps of point density of bare ground points were used as a proxy of the quality of input DTM for the definition of the fuzzy system.

A summary of statistics for ground points density for the two surveys is displayed in Table 5.1.

Table 5. 1: Point density values calculated for 2005 and 2011 DTM.

Survey	Point density (pts/m^2)		
	Maximum	Minimum	Mean
2005	8.75	0	0.51
2011	77	0	2.23

In both surveys, lowest point density is associated with lakes and channel network as illustrated in Fig. 5.1. Maps of point density show that the 2011-DTM is characterized by a better spatially distributed point density than 2005-DTM. Higher point density values for 2011 survey (point density greater than 10 pts/m^2) are concentrated in the median-upper part of the study area, in correspondence of flightlines overlapping.

The 2005-map density highlights also some high density values in the lower part of Strimm catchment where vegetation filtering was less accurate than 2011 (Fig. 5.1 and 5.2).

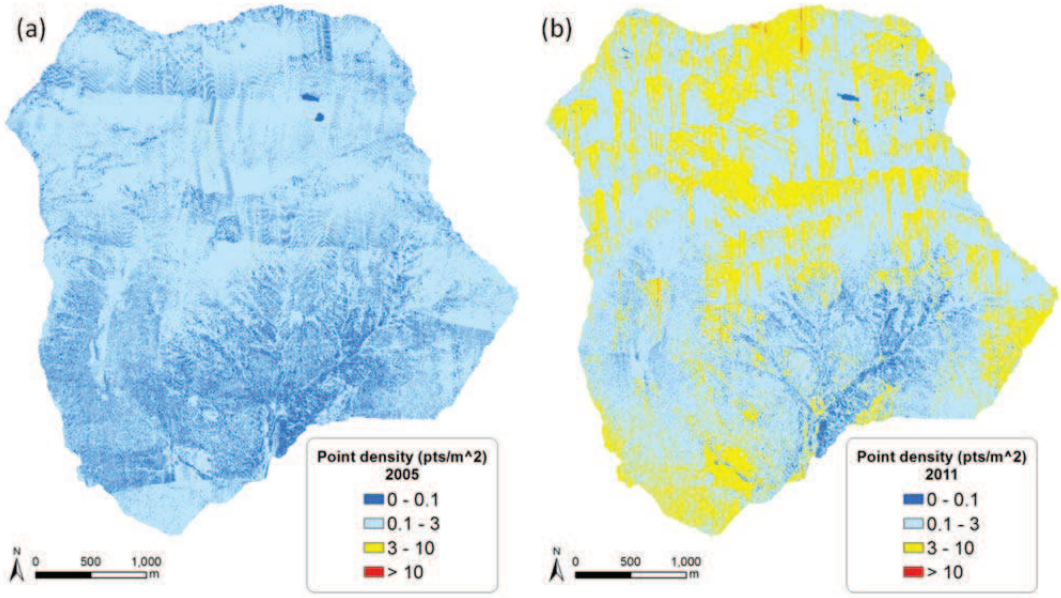

Figure 5. 1: Map of point density for bare ground point clouds related to 2005 (a) and 2011 (b) survey.

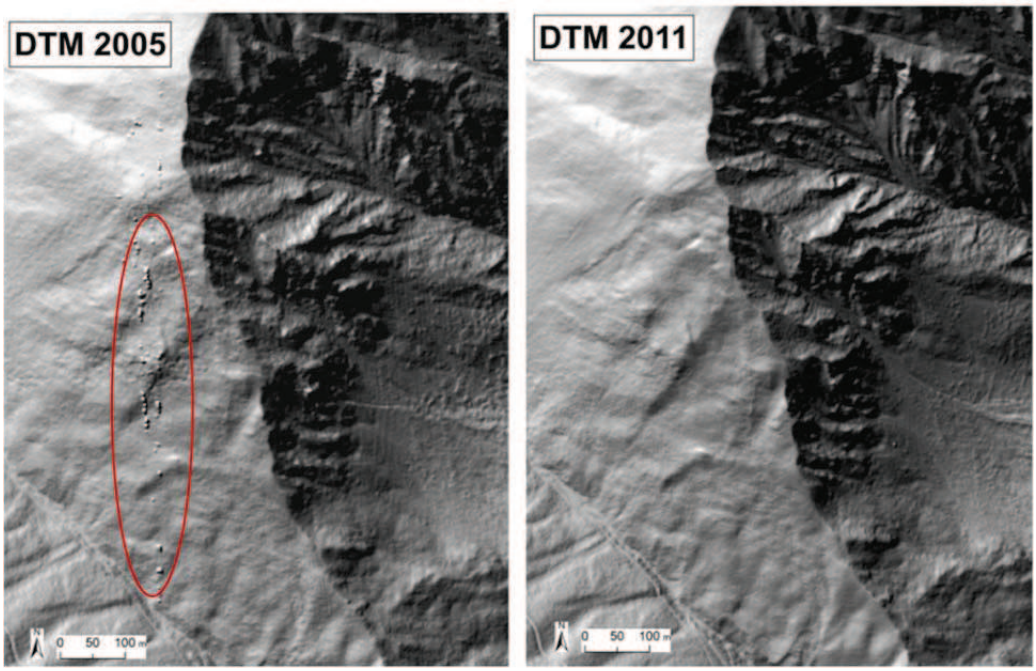

Figure 5. 2: Example of different vegetation filtering (red circle) between the two LiDAR derived DTMs.

Results on error analysis are summarized in Fig.5.3 (histograms of δz distribution) and Tab. 5.2 (statistical descriptors). Histograms on Fig. 5.3 show a different distribution: errors appears to be quite normally distributed for the 2011 DTM whereas a strong asymmetric distribution can be observed for the 2005 DTM. The asymmetric distribution of δz and the deviation of the mean from zero indicate the presence of systematic errors.

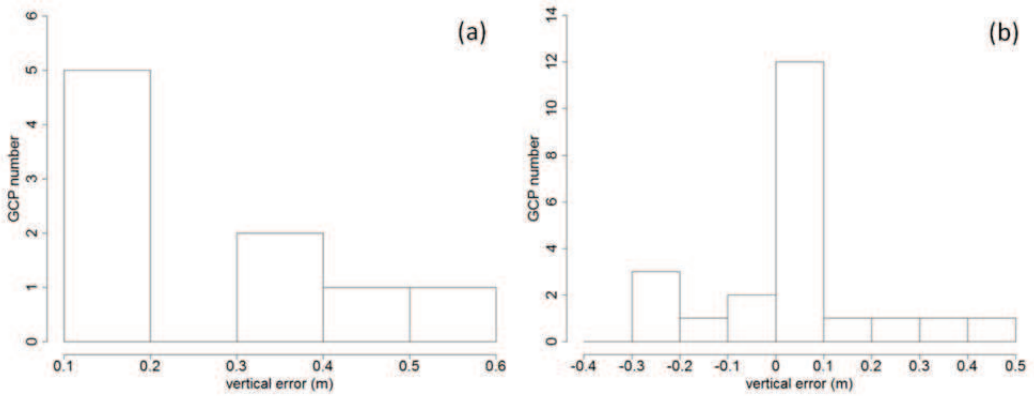

Figure 5. 3: Distribution of elevation differences (δz) between DTM and GCP used for the accuracy analysis of 2005- (a) and 2011- (b) DTM.

Table 5. 2: Accuracy analysis of DTM related to 2005 and 2011 surveys based on the difference between DTM and GCP elevations.

Accuracy measure	DTM 2005	DTM 2011
Mean	0.261	0.029
Standard Deviation	0.149	0.168
Median	0.195	0.028
RMSE (m)	0.296	0.167
NMAD (m)	0.118	0.061
MAD (m)	0.08	0.041
Quantile (68.3%) (m)	0.324	0.177
Quantile (95%) (m)	0.489	0.341
Checkpoints number	9	22

Higher overall LiDAR accuracy was achieved by the 2011-DTM (17 cm) while RMSE value of 2005-DTM (30 cm) is greater than the range of normally accepted values (15-20 cm). Even applying robust statistical descriptors useful for the analysis of a not normally distributed variable (i.e. NMAD, MAD, Quantiles) it is possible to notice that the 2011-DTM show lower values of errors than 2005 therefore confirming a higher overall accuracy.

5.2 DoD

As stated in previous chapters, the vertical uncertainty δz largely depends on morphological features of the study area and on the survey technique. Quality maps of DTMs were derived for the application of a spatially vertical uncertainty, implemented in the FIS method, for the DoD. Slope and point density maps are reported in Fig. 5.4 for different surveys (2005 and 2011), together with the DTM and the FIS error map derived as described in Chapter 4.

From Figure 5.4 and 5.5 it is possible to observe that δz is smaller in those areas where the combination of different indicators is favorable (e.g. areas featuring high point density and low slope). According to slope and point density values, the error ranges from 0.13 m to 0.87 m and from 0.15 m to 0.87 m respectively for the 2005 and 2011 DTM.

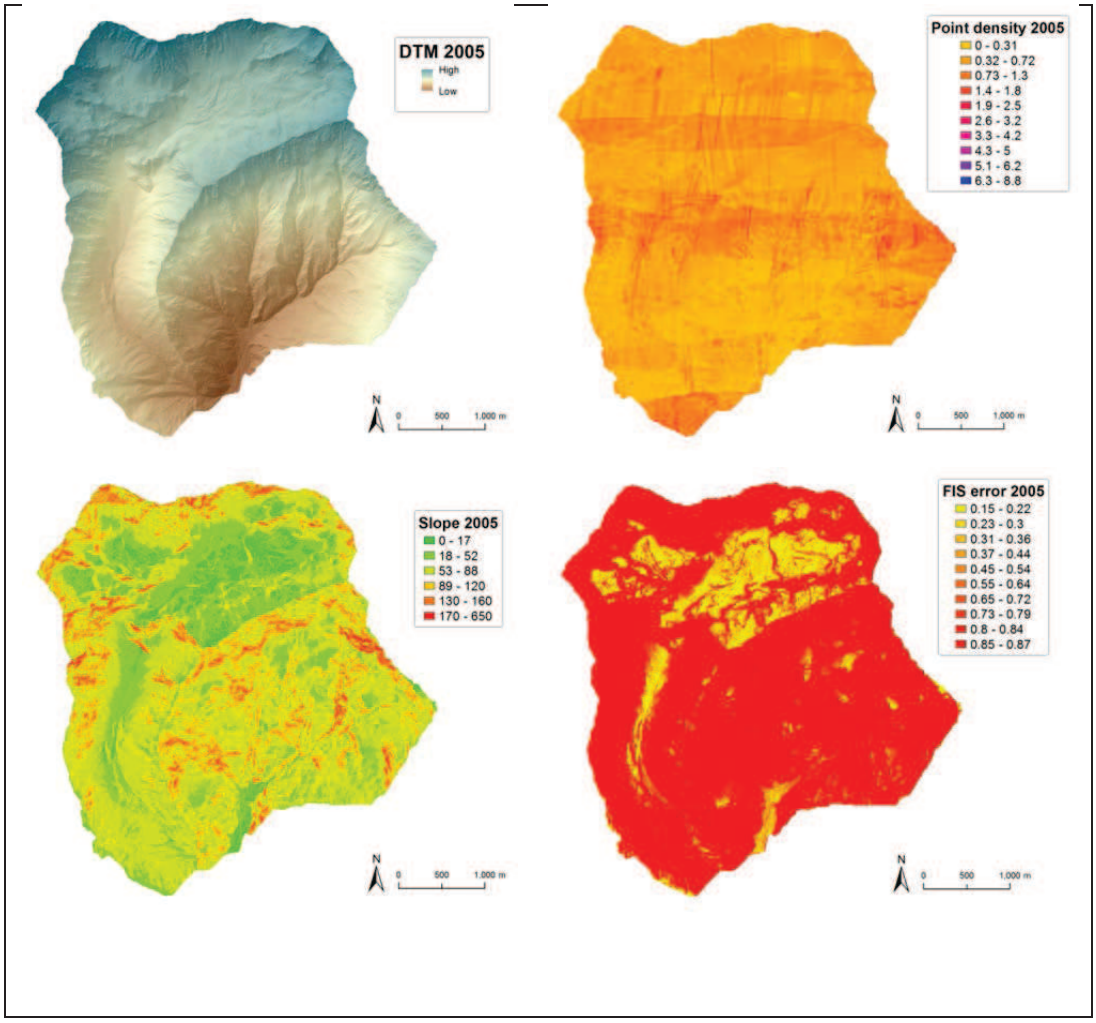

Figure 5. 4: Hillshade, point density, slope and FIS map derived for the 2005 DTM.

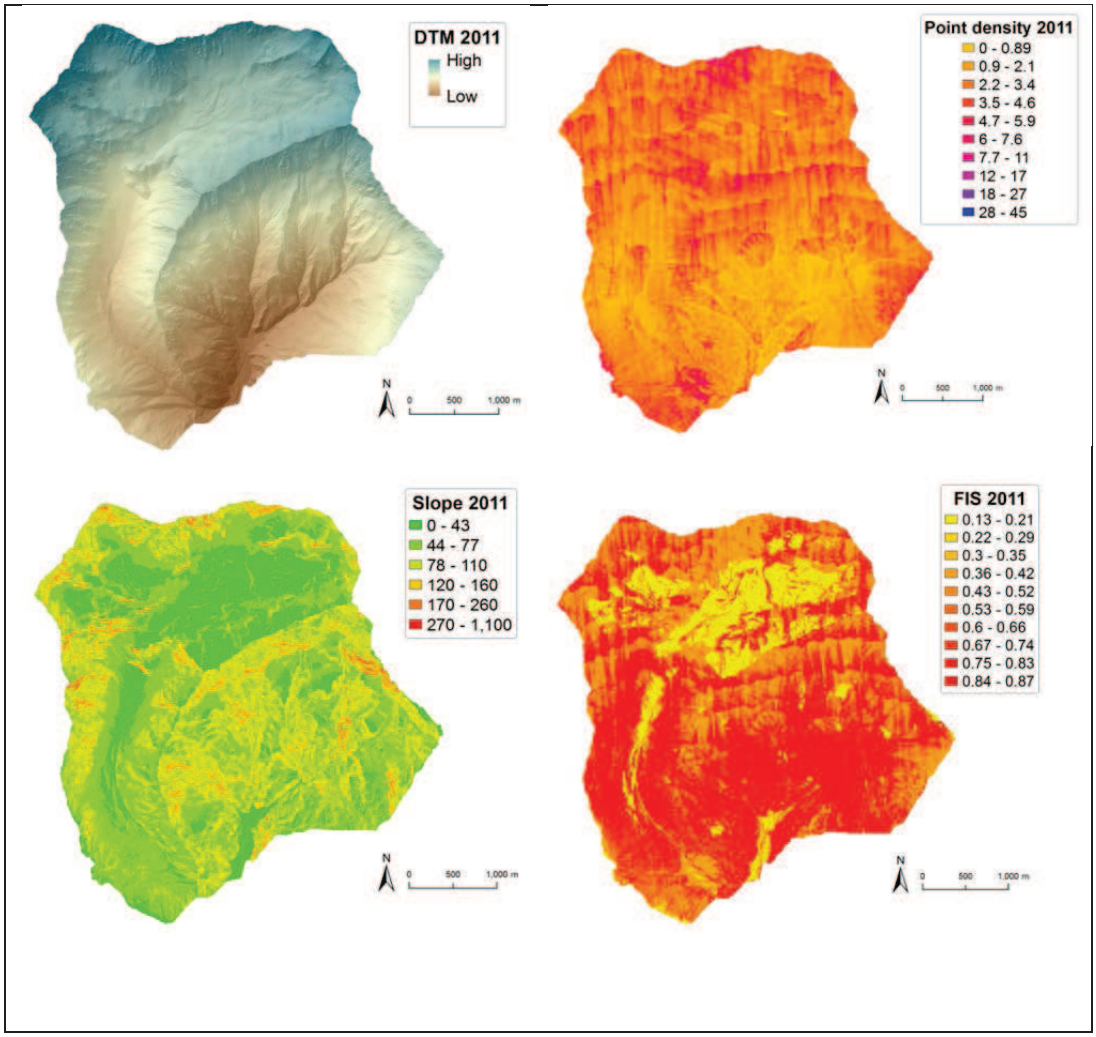

Figure 5. 5: Hillshade, point density, slope and FIS map derived for the 2011 DTM.

The uncertainty was then propagated on a cell by cell basis on both DTMs. The DoD map for consecutive DTMs of Gadria and Strimm catchment is presented in Figure 5.6 and 5.7. These maps are useful to highlight the spatial pattern of geomorphologic changes with colors scale ranging from blue (deposition) to red (erosion). Elevation differences analysis and erosion and deposition sediment budget are restricted to the surface defined by black mask in order to study geomorphological changes only in the channel network and on adjacent hillslopes.

This is motivated by the interest in sediment dynamics related to channelized processes and by the possibility of comparing DoD results with post-event field observations focusing on channel–related processes (typically debris flows).

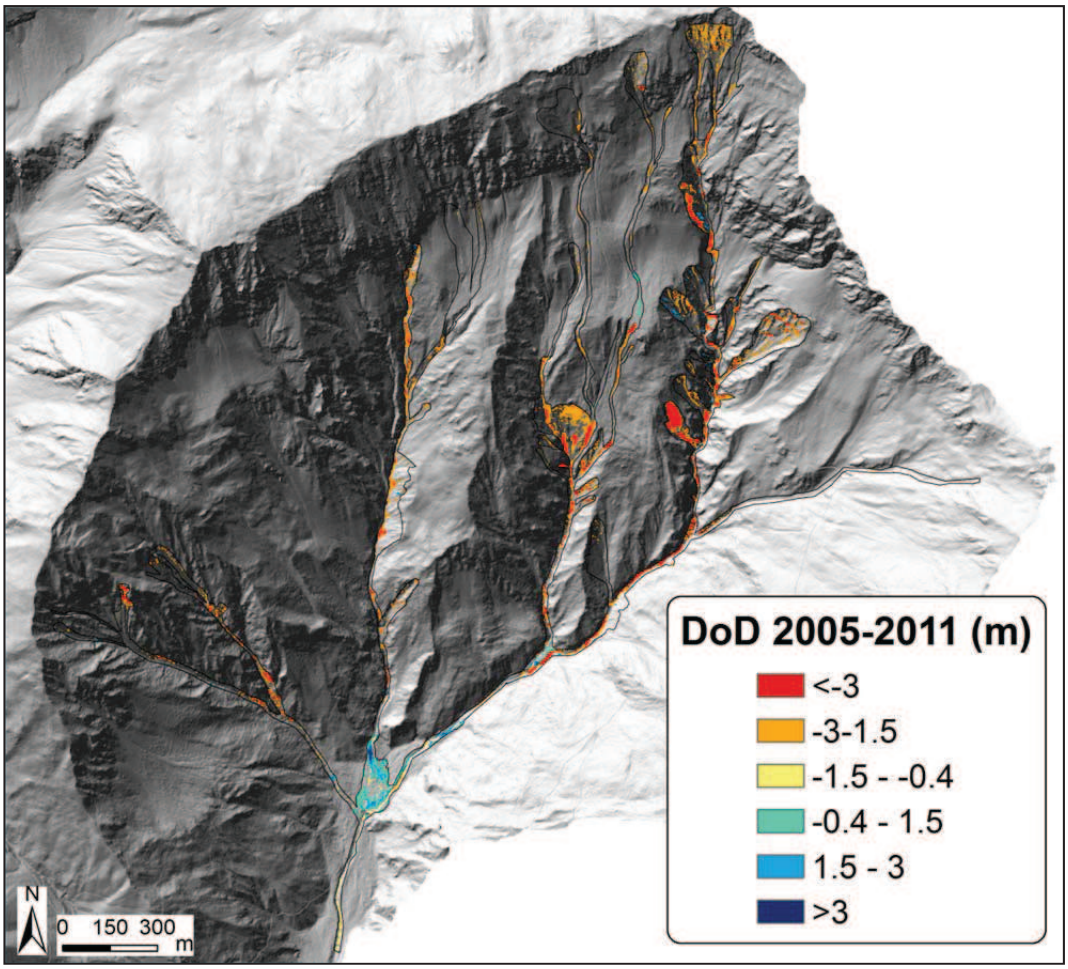

Figure 5. 6: DoD map for Gadria basin. Resulting DoD is calculated according to FIS implementation. Black boundaries define the area bordering the channel network where geomorphological changes have been analyzed.

Events occurred in the period 2005 and 2011 caused remarkable erosion in Gadria basin, especially in the upper part of the catchment. In sediment sources areas on hillslopes and minor channels, elevation differences range from –1.45 m to –9 m, whereas erosion in the main stream is characterized by a wider interval, i.e. from –

0.45 m to –13 m. Deposition is present only in the downstream part of Gadria creek and at its confluence with the last right bank tributary, with maximum thickness of 5.7 m.

Strimm basin features a spatial trend in geomorphological changes different from Gadria catchment since erosion process mainly occur in the downstream part of the basin. Concerning the main channel, major variations in erosion were detected in the downstream part, with values ranging from -0.45m to -10.8 m. This evidence is due to shallow landslides close to the channel that represent the main lateral sediment source activated during the debris flow event of July 12th 2010 that eroded the river bed in several places creating channel enlargement and deepening. The DoD map shows also the contribution of some lateral tributary to the erosion process including steep debris flow channels from the right side of the basin. Some deposit can be observed in the upper part of the basin on the left bank of Strimm river caused by debris flow events and in the final part of the river, near the retention basin, with values ranging in the intervals 0.66-2.4 m and 0.4-4.6 m respectively.

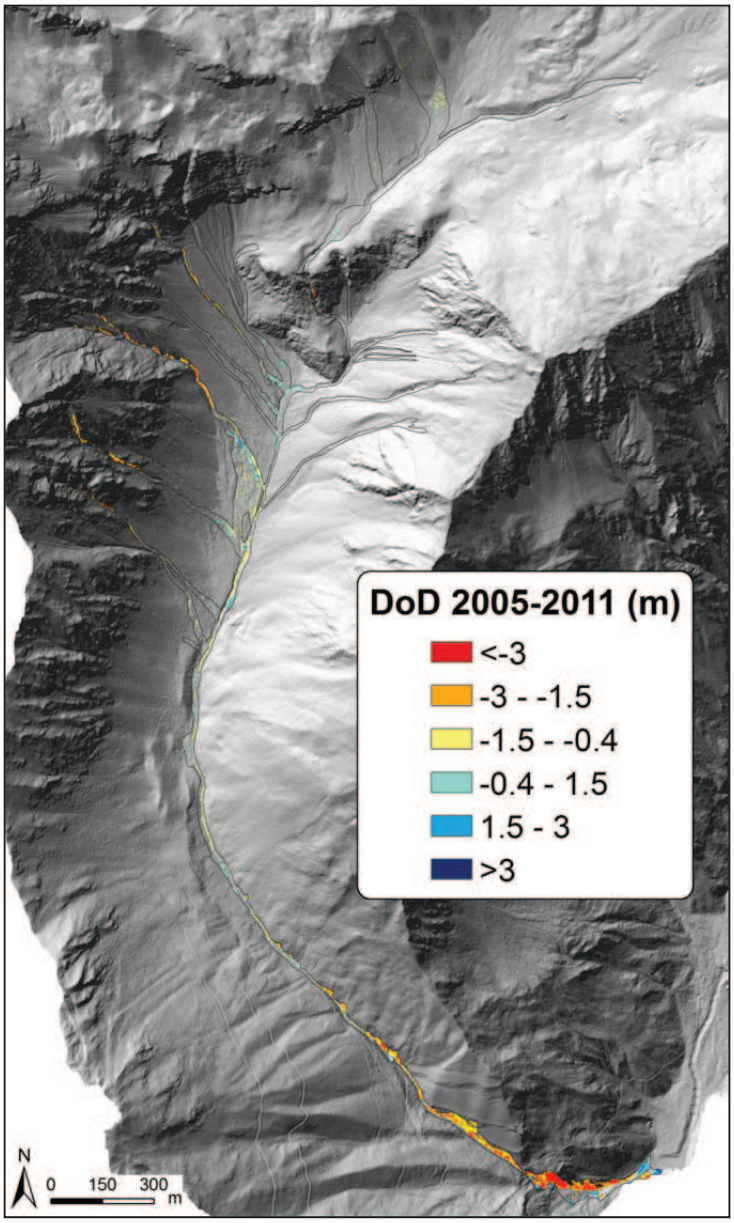

Figure 5. 7: DoD map for Strimm basin at 2 m resolution. Resulting DoD is calculated according to FIS implementation. Black boundaries define the area the area bordering the channel network where geomorphological changes have been detected.

Areal and volumetric budget derived from the DoD for Gadria and Strimm basin are summarized in Table 5.3 reported results are referred to the application of both the raw and the fuzzy method with a confidence interval of 90%.

Table 5. 3: Results of areal and volumetric budget for the raw and the fuzzy DoD. Surface extent of the analyzed masks are also indicated. CI: Confidence Interval.

Raw method					
Basin	Investigated area (km^2)	Areal change (m^2)		Volumetric change (m^3)	
		Erosion	Deposition	Erosion	Deposition
Gadria	0.45	364060	81888	416208	55685
Strimm	0.27	190724	84936	110264	37353
FIS method (90% CI)					
Basin	Investigated area (km^2)	Areal change (m^2)		Volumetric change (m^3)	
		Erosion	Deposition	Erosion ± Error	Deposition ± Error
Gadria	0.45	80320	12160	198000 ± 86690	20950 ± 6909
Strimm	0.27	26584	6420	49791 ± 18872	7539 ± 3406

Erosion areas cover the 80.5% and 86.8% of the analyzed surface of Strimm and Gadria basin respectively. Considering FIS method, high estimate of eroded volumes during the period 2005-2011 was calculated for Gadria (198000 m^3 ± 86690 m^3) and Strimm (49791 m^3 ± 18872 m^3) basins. Deposit volumes, concentrated in some areas as observed in the DoD maps, are obviously lower than eroded ones, with values attaining about 21000 m^3 in Gadria and 7500 m^3 in Strimm catchments.

The evaluation of geomorphological changes can also be performed on histograms of elevation change distribution (ECD). ECD represents the overall of both area and volume experiencing a given magnitude of elevation change in bin size classes. The ECD analysis allows the assessment of the representativeness of sediment mobility in studied areas and can be considered as discriminators of the different types of change between analyzed periods (Wheaton et al., 2010; Montreuil et al.,

2014). Since volumetric ECD are calculated from areal histograms by multiplying the area by the magnitude of elevation change, distributions are amplified going far from zero (i.e. no change) on x-axis.

The areal ECDs (Fig. 5.8 and Fig. 5.9) show a positively skewed distribution (2.9 for Strimm distribution and 4.6 for Gadria distribution) for both basins elevation changes. For the two basins, areal histograms appear to have a different distribution of erosion and deposition processes. The areal ECD across Gadria catchment produced a very peaked erosion distribution centered on an elevation change of -2.4 m, while histogram for Strimm basin show a bimodal distribution on erosion predicted changes with two peaks at -2.2 m and at -0.6 m. Mean deposition process, presenting a narrower range than the erosion peak, is approximately centered around 0.9 and 0.4 m respectively in Gadria and Strimm basin distribution.

Areal ECDs confirmed budget results shown in Table 5. 3 since erosion process dominates both basins occurring over 80% more surface area than deposition.

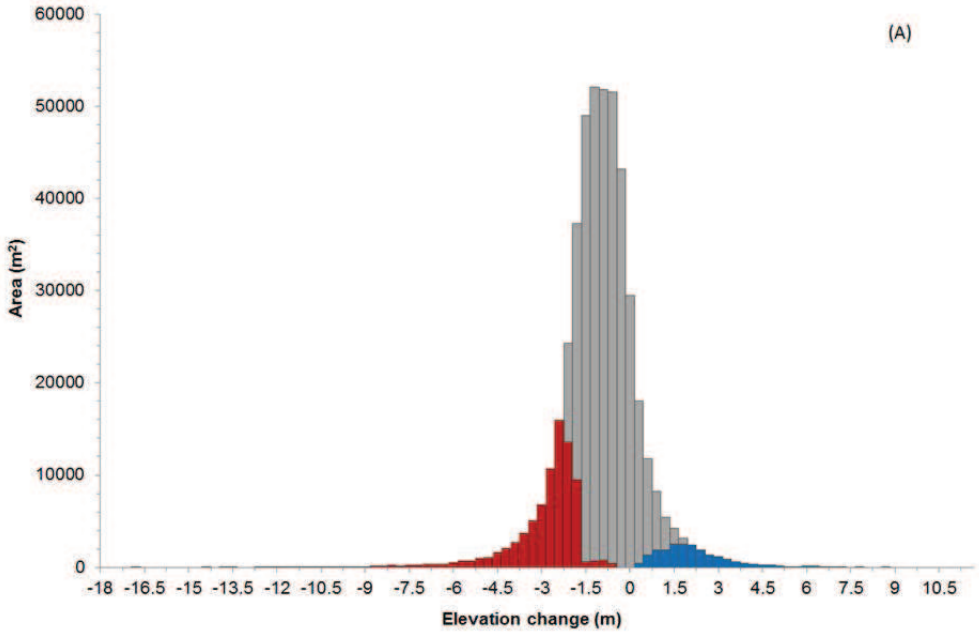

Figure 5. 8: Areal elevation change distribution (ECD) from the DoD for Gadria basin. The grey-shaded area represent excluded points from erosion and deposition estimate since they fall within the critical levels of detection as thresholded probabilistically at the 90% confidence interval.

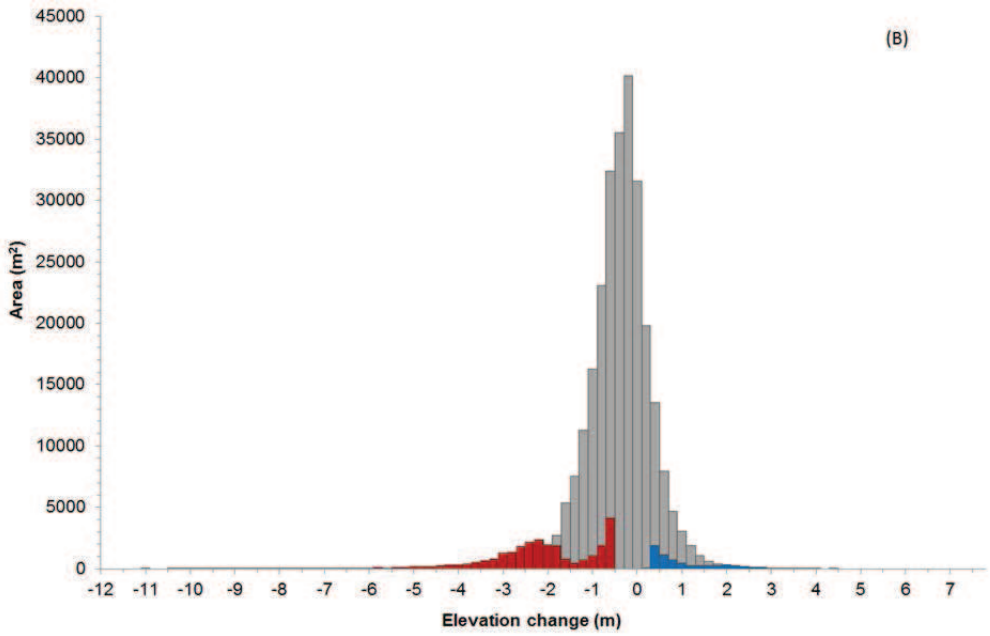

Figure 5. 9: Areal elevation change distribution (ECD) from the DoD for Strimm basin. The grey-shaded area represent excluded points from erosion and deposition estimate since they fall within the critical levels of detection as thresholded probabilistically at the 90% confidence interval.

Volumetric ECD of Gadria basin shows a shape similar to areal distribution (Fig. 5.10). The volumetric ECD confirms the dominance of erosion events on this basin with values ranging from −14.4 m to −0.6 m. The distribution is also very spiked containing a peak centered on medium-low magnitude elevation changes. On the contrary this area didn't experienced a very consistent accretion since deposit curve shows low magnitude change and a shorter range of values, i.e. from 0.3 to 8.6 m.
The volumetric ECD for Strimm (Fig. 5.10 B) is relatively similar to its areal distribution that is characterized by two peaks, one of low-magnitude and the other on high-magnitude elevation change centered on -2.4 and -0.6 m. The long negative tail, ranging from -0.4 to -10.4 m, indicates that Strimm creek and tributary are dominated by erosion. Even in this case, the ECD distribution doesn't show a balance between erosion and deposition which is confirmed by the low volumetric changes measured (Table 5. 3). The relative short tail of deposit distribution, with values ranging from 0.2 to 4.4 m, indicates that some areas featured deposition, but the analyzed surface (0.27 km^2) is anyway dominated by degradation.

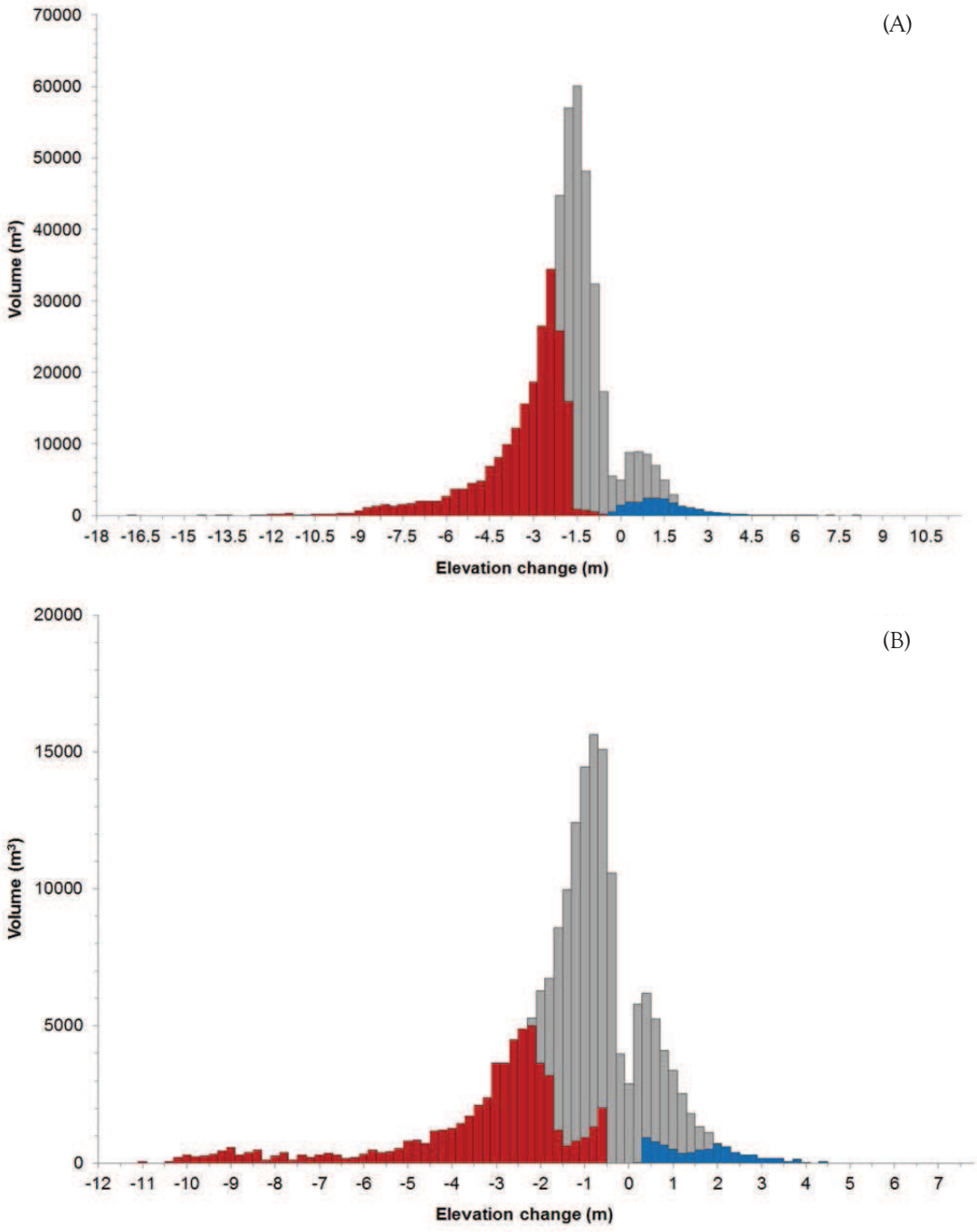

Figure 5. 10: Volumetric elevation change distribution (ECD) from the DoD for Gadria (A) and Strimm (B) basin. The grey-shaded area represent excluded points from erosion and deposition estimate since they fall within the critical levels of detection as thresholded probabilistically at the 90% confidence interval.

The low complexity of areal and volumetric elevation change distribution for Gadria and Strimm, consisting of one or two peaks, can also reveal the intensity of single events and reflect processes peculiarities.

The fuzzy method allowed the information retrieval linked to the variations of small entity that could be lost if a raw method or a LoD_{min} uniform threshold would be applied (Wheaton et al., 2010). From ECD histograms it is possible to observe that some information related to values closer to zero in the x-axis are lost as an inevitable consequence of the application of a threshold for the evaluation of uncertainty, even if spatially distributed. However, this uncertainty analysis represents an improvement in terms of geomorphic plausibility since it produces more meaningful results.

Some observations on geomorphometric analysis by means of DoD calculation is related to terrain data processing. Errors derived from survey techniques can heavily alter the quality of the resulting DoD. Although they should be recognized in a preliminary step, the DoD analysis can identify some inconsistencies due to the presence of errors that cannot be easily distinguished from DTM or points clouds. Through the application of a spatially uncertainty analysis some type of errors can be detected from the presence of anomalous variations.

In areas characterized by high slope, LiDAR data present high uncertainty that can be propagated in the DoD. This aspect can be very important where vertical elements are present (e.g. vertical cliffs, check dams) where errors can be of the same magnitude of the element itself (Blasone et al., 2014). The removal of these features from the DoD can represent a more rapid and effective system to manage errors than the manual correction of single cells of DTM, if they were not involved in morphological changes.

5.2.1 DoD and comparison with field surveys

Data of events occurred in Gadria and Strimm basins in the same period of LiDAR surveys (2005-2011) were selected from the ED30 database in order to compare field estimates of deposited volumes with DoD results (Tab. 5.3). Figure 5.11 reports the location of these events represented by the initiation point of the phenomenon (PIF).

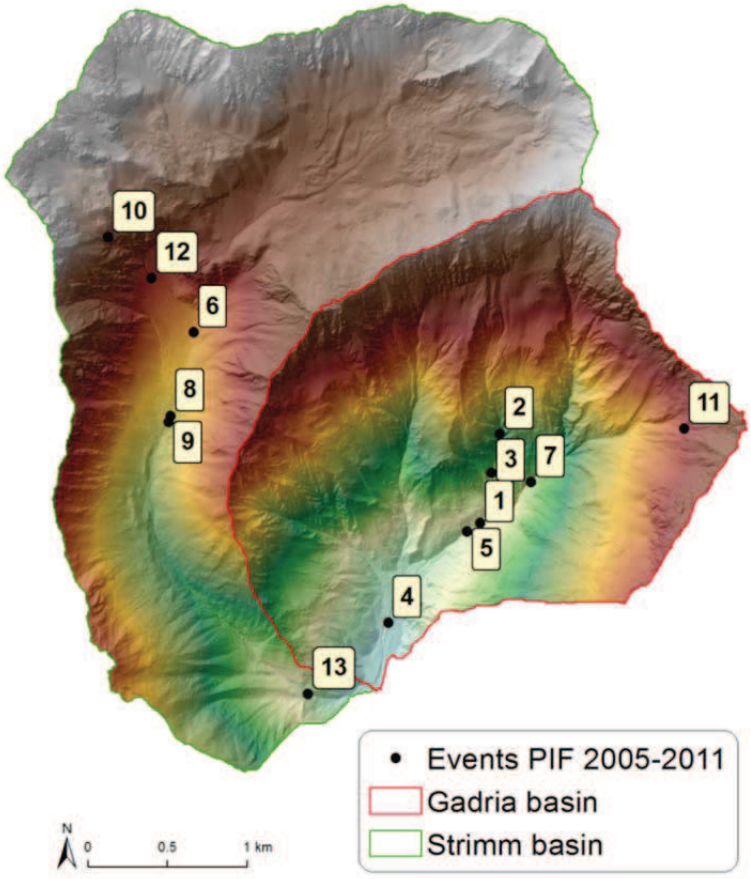

Figure 5. 11: Spatial distribution of debris flows and flood events in studied basins represented by the initiation point of the process.

Field volume estimates detected by the Autonomous Province of Bolzano and list of events occurred in Gadria and Strimm basin are reported in Tables 5.5 and 5. 6. As reported in the tables, sediment transport processes occurred in the period July

2005 – June 2011 are floods and debris flows. The seasonal distribution reflects the occurrence of debris flow in Alto Adige region, mostly concentrated in the summer period, between June and September (Nikolopoulos et al., 2014).

For each event data related to the mobilized sediment has been divided into two classes: the deposit that remained inside the basin (internal deposition) and the deposits in the retention basin at the outlet of Gadria and Strimm basins (sediment yield) (Fig. 5.12). The last one have been considered as the sediment that flows out from the system since the retention basin, where volumes derived from different events are detected, is periodically cleaned out. Therefore, as already pointed out in the Section 4.4.2, the retention basin was not considered in the DoD analysis.

Model results and field estimate are compared separately for erosion and deposition, in particular DoD deposition volumes are compared to internal deposition estimated by the ED30 whereas DoD erosion volumes are compared to total erosion i.e. the sum of the internal deposition and sediment yield as estimated in the field.

Table 5. 4: Volumes data derived from ED30 related to events occurred on Gadria basin within the period 2005-2011. Numbers of events (N) refer to Figure 5.11. *: Uncertain date; **: uncertainty about the typology of the event.

N	Type of process	Date	Volume (m^3)		
			Internal deposition	Sediment yield	Total erosion
1	Debris flow**	2006*		700	700
2	Debris flow	18/05/2006		10000	10000
3	Debris flow	25/07/2006		35000	35000
4	Debris flow	10/08/2007*		7000	7000
5	Debris flow	06/08/2008*	11900	27100	39000
6	Debris flow	24/07/2009	3200	35000	38200
7	Debris flow	12/07/2010	1000	20000	21000
			Total	Total	Total
			16100	134800	150900

Table 5. 5: volumes data derived from ED30 related to events occurred on Strimm basin within the period 2005-2011. Numbers of events (N) refer to Figure 5.11.*: Uncertain date.

N	Type of process	Date	Volume (m^3)		
			Internal deposition	Sediment yield	Total erosion
8	Debris flow	06/08/2008	1000		1000
9	Debris flow-Bedload	24/07/2009		3000	3000
10	Debris flood	13/06/2010	700		700
11	Debris flow	12/07/2010	10000	15000	25000
12	Debris flow-Bedload	01/10/2010*		3500	3500
13	Flood	27/05/2011		2500	2500
			Total	Total	Total
			11700	24000	35700

Compared to Strimm creek, Gadria creek produced a higher amount of sediment with a sediment yield of 3566 $m^3 km^{-1}y^{-1}$ compared to the sediment yield of Strimm creek, i.e. 470.6 $m^3 km^{-1}y^{-1}$. The magnitude of sediment yield in Gadria basin is relevant even for an active debris-flow catchment in the context of Upper Adige River basins (Brardinoni et al., 2012).

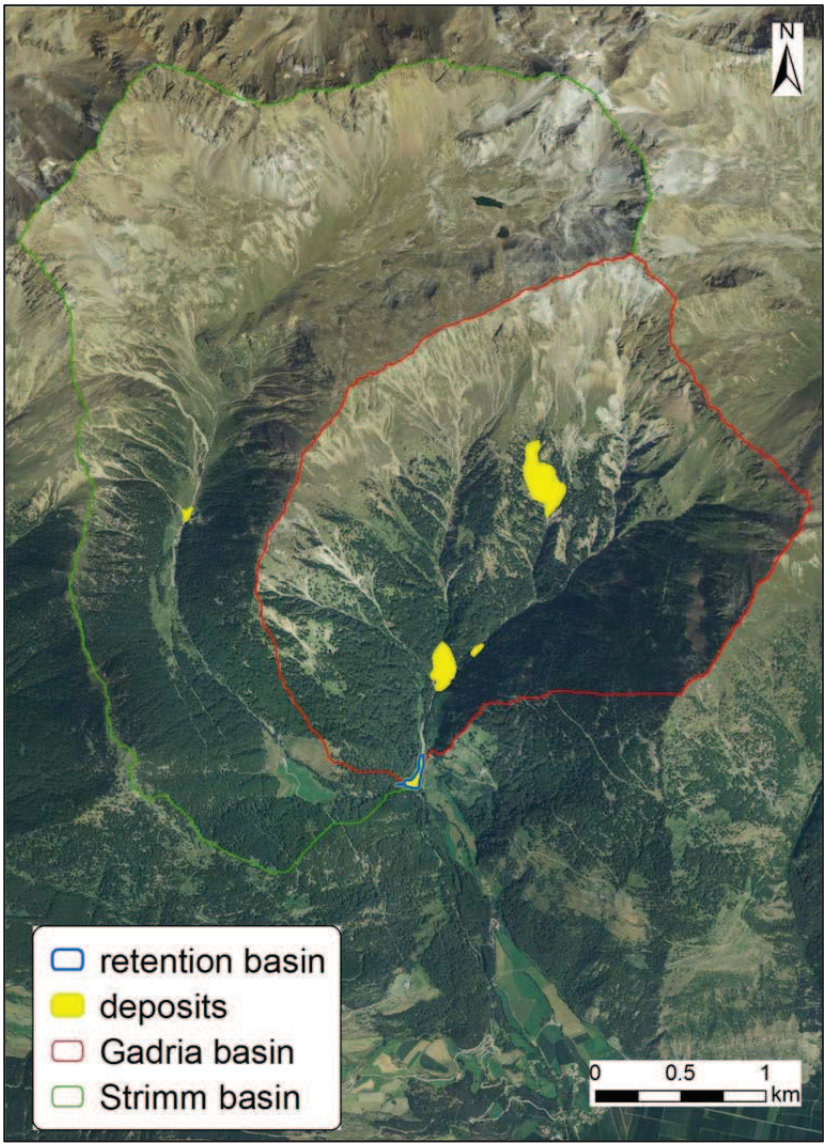

Figure 5. 12: Location of field detected deposit areas in both studied catchments and of the retention basin.

A particular event is represented by a storm occurred in July 12 2010 that triggered two different debris flows in both catchments (see Tab. 5.4 and 5.5). Events that occurred on the same day in the two catchments and caused the release of a high amount of sediment make the volumetric contribution of each stream difficult to estimate (Fig. 5.13).

Figure 5. 13: Water and sediment input from Strimm river into the retention basin. upstream point of view of the water and sediment input of Gadria creek into the open check dam. Large woods comes from Strimm creek.

The DoD was able to detect the effect of the above mentioned debris flow event occurred in July 2010, originated on the western slopes of Strimm basin, that lead to an increase of erosion in downstream sector of the main channel (Fig. 5.14).

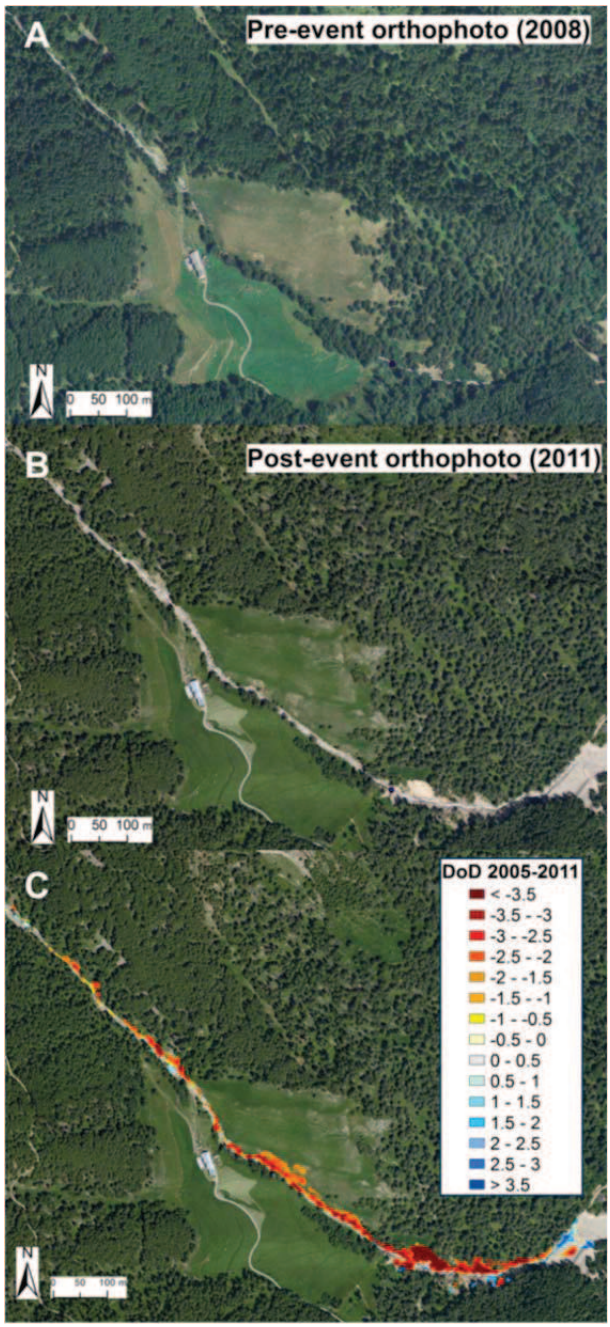

Figure 5. 14: Pre- (A) and post- (B) event orthophoto and DoD results (C) for the debris flow event of July 12th 2010.

Comparison between volumetric estimation derived from field surveys (Tab. 5.4. and 5.5) and that derived from DoD analysis (Tab. 5.3) highlights some interesting aspects concerning the magnitude of events. DoD derived values showed a net loss of sediment which is in accordance with the fact that both basins experienced output of sediment erosion.

For both studied areas, DoD estimated volumes (Table 5.3) are of the same order of magnitude as field estimated ones (Tables 5.4 and 5.5). The differences are moderate and will be discussed in the following pages.

Sediment volumes estimated by DoD are usually greater than post-event field estimates; only the field surveyed deposits in the Strimm catchment exceed the volume computed by DoD.

By applying a raw DoD, calculated volumes were largely overestimated if compared to field surveys, both for erosion (416208 m^3 from raw DoD compared to 150900 m^3 from ED30 for Gadria basin and 110264 m^3 from raw DoD compared to 35700 m^3 from ED30 for Strimm basin) and deposition (55685 m^3 from raw DoD compared to 16100 m^3 from ED30 for Gadria basin and 37353 m^3 from raw DoD compared to 11700 m^3 from ED30 for Strimm basin). The estimate of the magnitude of DoD variations in a spatially variable way by using fuzzy logic lead to more realistic results than unthresholded volumetric change, especially when DTMs present different quality.

In other cases, methods that do not consider the error uncertainty in the elevation differences led to the underestimate of deposited material. For instance Bull et al. (2010) found that estimates of material deposited by a debris flood occurred in a New Zealand catchment, calculated by applying a simple DoD, were of lower magnitude than volumes estimated by field observations. The application of a DoD on a landslide, where elevation errors are correlated with a slope inclination map, led to LiDAR based volumes overestimates with respect to field based estimates, moreover in steeper regions.

Other studies report some disagreement between volumes of eroded material estimated by field observations and those estimated by the LIDAR multitemporal data. Scheidl et al. (2008) for example, in the evaluation of volumetric sediment budget of debris flow events in a mountain catchment, found that the eroded material detected by DoD in the alluvial fan and in the main channel (Glyssibach and Glattbach rivers, Switzerland) was higher than the volumes derived from event documentation.

In this study, higher erosion values computed by DoD can be explained by the fact that DoD includes events that are not identified by field surveys. For example, events occurring in the upper part of the catchments are not usually detected by technicians of the Autonomous Province of Bozen-Bolzano unless they involved antrophic infrastructures (e.g. forest roads, bridges). Moreover, processes characterized by low intensity or not related to debris flows, such as floods with bedload and suspended loads, are not considered in the field volume estimates.

Another reason is linked to the fact that, during debris flow events, part of the sediment can pass through the check dam and is not retained in the debris basin. Nevertheless, comparison with field estimated volumes highlights the capability of DoD analysis in detecting morphological changes caused by debris flow and bedload transport at basin scale based on LiDAR surveys on complex and different morphological areas such as Gadria and Strimm basins.

A strength point of the applied method is based on the choice of the parameters for the building of the FIS system. It is well known that point density plays an important role in the analysis of mountain basins since it indicates whether there is enough information available for a sufficiently detailed representation of the analyzed topographic feature (Cavalli et al. 2008; James 2007). The density of scanned points over the surveyed surface is not homogeneous since the penetration rate of the laser beams depends on the surface typology. For instance some natural obstacles, such as the vegetation canopy, can alter the spatial density of the last echo

points (i.e. ground) (Scheidl et al., 2008). Although normally LiDAR is able to provide high density of ground point data, incorrect design of the surveys and the presence of some dense vegetation surfaces, as in the case of 2006-Lidar survey, can result in a inadequate density of ground pulse returns (Cavalli et al., 2008). Moreover, the interpolation of a DTM from ground points is subjected to uncertainty and the derived grid can be prone to misrepresent a surface characterized by both low point density and high topographic complexity. In this study, the use of a simple 2-input fuzzy system accounting for both the point density, as a proxy of the survey sampling errors, and the slope, a proxy of the surface morphology, proved to be effective for the qualitative and quantitative detection of morphological changes in a mountainous region. In particular, even if DTMs used for geomorphometric analysis can present different accuracy, it is possible to derive useful information on undetected events within the basin and identify erosional and deposition processes in uneasily accessible areas.

5.2.2 DoD and morphometric analysis

Morphometric analysis was performed on Gadria and Strimm basins on the same areas considered for the evaluation of geomorphic changes, i.e. within the mask shown in Figure 4.8, which encompasses the channel network and contiguous side slopes. To this aim, plan and profile curvature were derived from the 2005- and 2011-DTMs with a moving window size of 5x5 cells.

Curvature values have been then compared to DoD negative and positive values to evaluate the changing of convex, concave and flat surface where geomorphic variations occurred, according to curvature sign as described in Section 4.4.3.

Firstly, plan and profile curvature were derived from the 2011-DTM of both catchments to analyze the current morphology with the DoD predicted changes.

In the computation of erosion and deposition percentages, flat areas were not considered.

Plan curvature diagrams (Fig. 5.15) shows that erosion prevails on concave features, represented by positive values (67% and 72.6% for Gadria and Strimm mask respectively), while deposition mostly occur on convex features, characterized by negative curvature values (59.8% and 65.9% for Gadria and Strimm mask respectively).

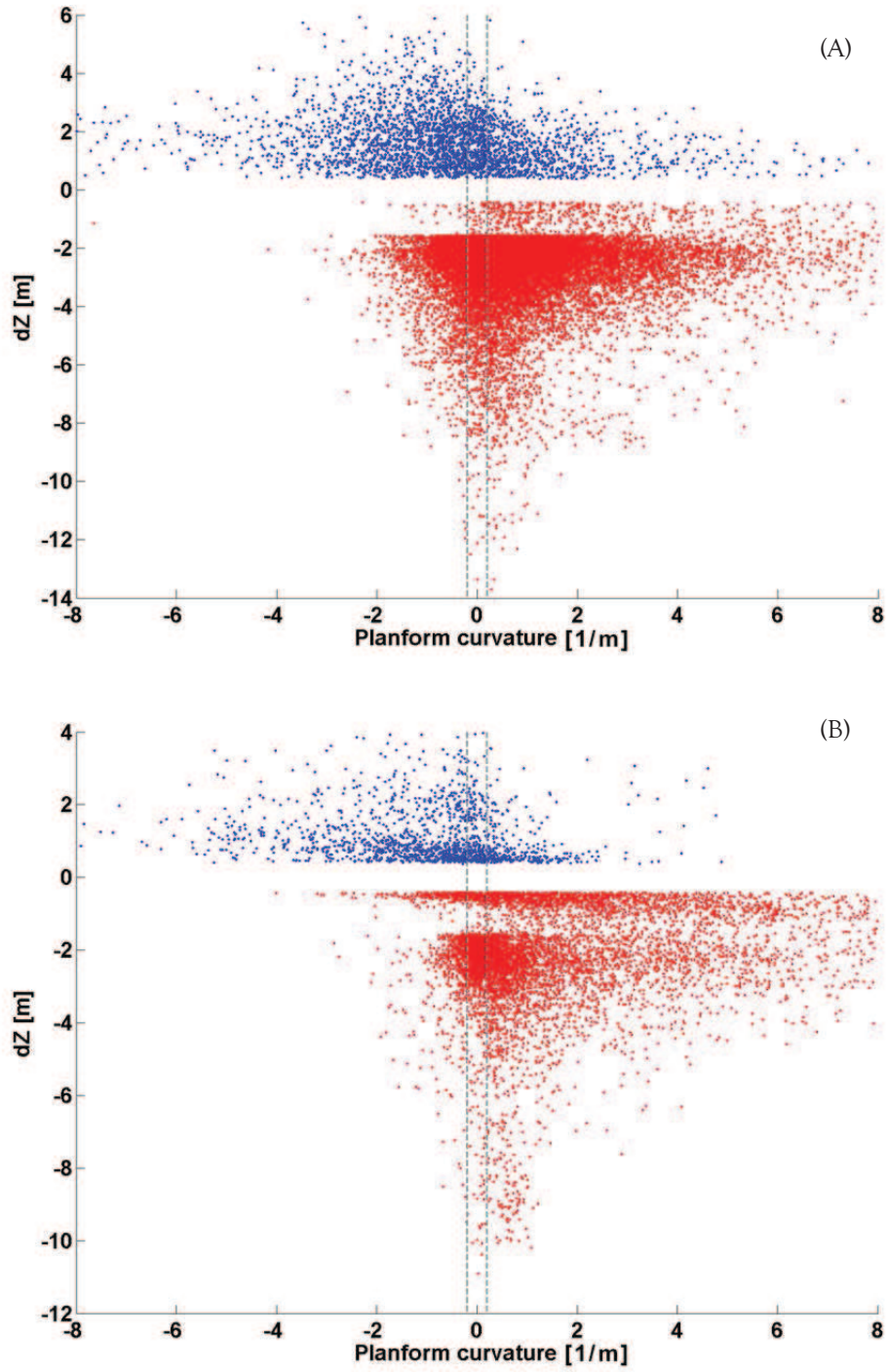

Figure 5. 15: Gadria (A) and Strimm (B) planform curvature derived from the 2011 DTM and compared to erosion (red) and deposition (blue) processes as predicted by the DoD. Points included in the range of flat values (-0.2-0.2), represented by the dotted lines, were not considered for the analysis.

A similar pattern is related to profile curvature (Figg. 5.16 and 5.17). Areas of concave curvature correspond to erosion predicted changes with a high proportion of negative DoD values (65.8% and 72.1% for Gadria and Strimm respectively) while areas of convex profile curvature indicate deposition areas, even if, compared to plan curvature, with lower percentages for Strimm basin (72.2% and 53.8% for Gadria and Strimm respectively).

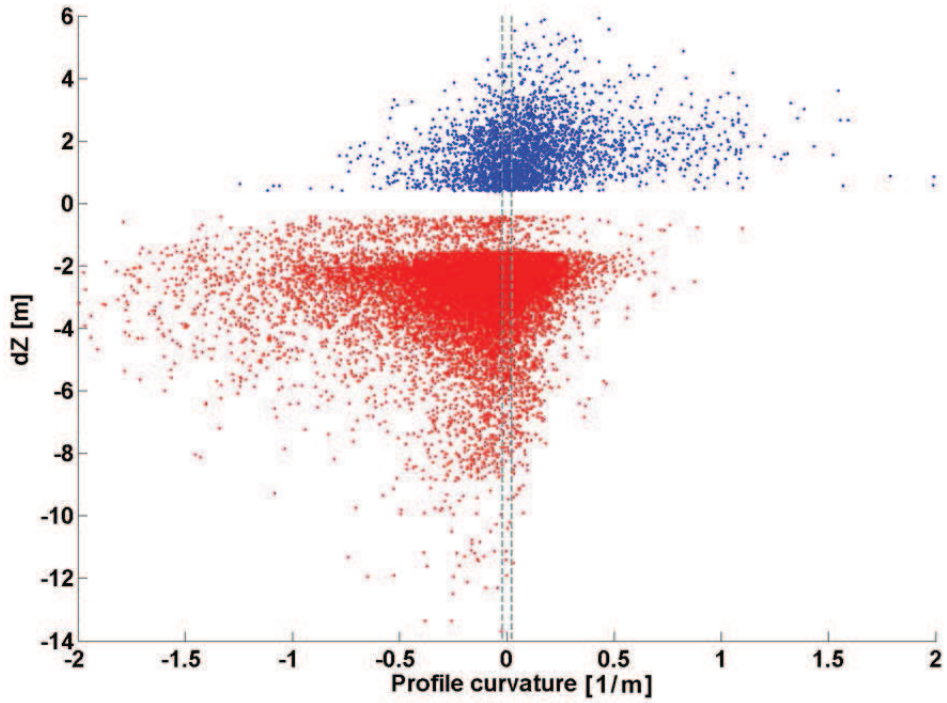

Figure 5. 16: Gadria profile curvature 2011 derived from the 2011 DTM and compared to erosion (red) and deposition (blue) processes as predicted by the DoD. Points included in the range of flat values (-0.02-0.02), represented by the dotted lines, were not considered for the analysis.

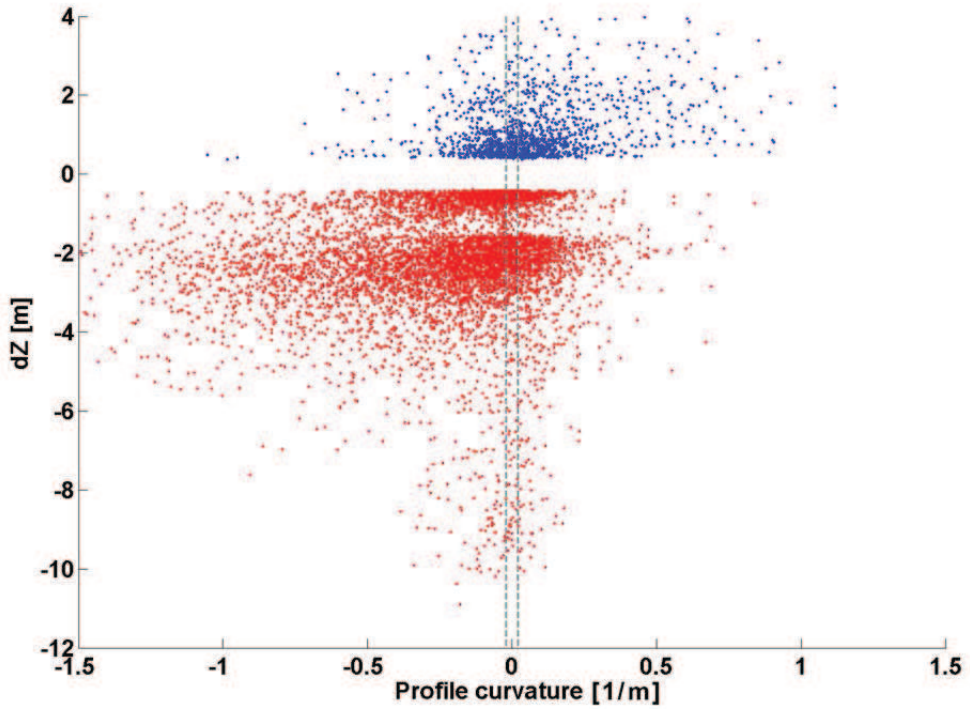

Figure 5. 17: Strimm profile curvature 2011 derived from the 2011 DTM and compared to erosion (red) and deposition (blue) processes as predicted by the DoD. Points included in the range of flat values (-0.02-0.02), represented by the dotted lines, were not considered for the analysis.

To improve the understanding of the relationship between topographic changes and curvature variations, planform and profile curvature were derived from 2005-DTMs at the same windows size (5x5 cells) chosen for curvature analysis of the 2011-DTMs.

Tables 5.6 and 5.7 report the percentage of planform curvature for Gadria and Strimm basins in areas where DoD showed both negative (i.e. erosion) and positive (i.e. deposition) elevation differences.

In Gadria catchment, erosion prevails in locations that experienced an increase in curvature morphology in concave surfaces (45%). Results for Strimm basin are similar to those derived for Gadria, with the highest percentage of erosion changes in concave areas (50.5%). For both catchments, the highest amount of deposition occurs in locations featuring a change from concavity to convexity (25.1% and

34.1% for Gadria and Strimm basins respectively) or an increase in convexity (23.7% for Gadria and 21 % for Strimm).

Table 5. 6: Planform curvature values calculated for Gadria catchment, divided into different classes of geomorphic changes related to DoD values of erosion and deposition.

Morphological variation	Erosion (%)	Deposition (%)
Convex to convex	13	23.7
Convex to concave	9.5	4.9
Convex to planar	7.6	2.9
Concave to concave	45	20.7
Concave to convex	0.9	25.1
Concave to planar	2.9	7.6
Planar to convex	2.2	11.0
Planar to concave	12.5	2.4
Planar to planar	6.4	1.7

Table 5. 7: Planform curvature values calculated for Strimm catchment, divided into different classes of geomorphic changes related to DoD values of erosion and deposition.

Morphological variation	Erosion (%)	Deposition (%)
Convex to convex	7.8	21
Convex to concave	9.9	0.8
Convex to planar	6.3	1.2
Concave to concave	50.5	18.5
Concave to convex	0.9	34.1
Concave to planar	2.8	11.1
Planar to convex	2.4	10.5
Planar to concave	12.2	0.8
Planar to planar	7.2	2.1

The same analysis was performed on profile curvature changes (Tab. 5.8 and 5.9).

Table 5. 8: Profile curvature values calculated for Gadria catchment, divided into different classes of geomorphic changes related to DoD values of erosion and deposition.

Morphological variation	Erosion	Deposition
Convex to convex	15.9	25.6
Convex to concave	19.8	8.1
Convex to planar	7.0	3
Concave to concave	38.5	6.3
Concave to convex	4.6	39.7
Concave to planar	2.8	7.5
Planar to convex	2.4	6.9
Planar to concave	7.5	2.1
Planar to planar	1.6	0.8

Table 5. 9: Profile curvature values calculated for Strimm catchment, divided into different classes of geomorphic changes related to DoD values of erosion and deposition.

Morphological variation	Erosion	Deposition
Convex to convex	11.1	17.1
Convex to concave	18.6	6.9
Convex to planar	3.8	3
Concave to concave	47.0	24.8
Concave to convex	6.3	31.4
Concave to planar	3.2	7.3
Planar to convex	2.5	5.3
Planar to concave	6.5	3.2
Planar to planar	1.1	0.9

In both study areas, erosion prevails on surfaces that experienced an increase of concave morphology (38.5 % and 47 % for Gadria and Strimm basins respectively) or where convex surfaces became concave (19.8 % and 18.6 % for Gadria and Strimm basins respectively). As expected, deposition mostly occurs on previously concave locations that became convex (39.7% for Gadria and 31.4% for Strimm basin).

Plan and profile curvature show a different capability in detecting erosion processes: plan curvature demonstrated a higher potential to detect erosion changes in areas evolving from flat to concave surface than profile curvature which, on the other hand, performed a better recognition of erosion processes on morphological features changing from convex to concave curvature. This can be probably due to the different functioning of the two type of curvatures. As described, for instance, in Sandric et al. (2010), the profile curvature proved to be useful for the classification of rotational landslide zones where convex curvature alternate with zone with concave curvature whereas the plan curvature identified better landslide boundaries occurring on areas with concave curvature.

Plan and profile curvature calculated from the 2005 DTM were plotted against those derived from the 2011-DTM, separating erosion and deposition values. This type of diagram helps in visualizing the temporal evolution of morphological features, as classified in Tables 5.6, 5.7, 5.8 and 5.9, due to occurred natural processes.

Concerning plan curvature (Fig. 5.18 and Fig. 5.19), it is possible to observe a general trend for erosion data (red color) going from areas where surface morphology evolves from convex (left lower quadrant) to concave shape (right upper quadrant). Deposition values (blue color) follow a different pattern since they are distributed in the left lower and right lower quadrants, indicating a change more concentrated on convex morphology. For both catchments, mean erosion (black circle) is centered on areas where an increase in concave topography occurred

whereas mean deposition (green circle) is centered on locations where morphology changes from concave to convex shapes.

In this case, as profile negative and positive values represent concave and convex morphology respectively, the main pattern for sediment erosion data goes from the right upper to the left lower quadrant indicating a temporal evolution to more concave areas.

Deposition trend is less evident than erosion one: data are centered on the left and right upper quadrant, i.e. on areas that experienced an increase in convex morphology or a change from concave to convex shape.

As for plan curvature, in both analyzed catchments mean erosion (black circle) is centered on areas where an increase in concave topography occurred whereas mean deposition (green circle) is centered on locations where morphology changes from concave to convex shapes.

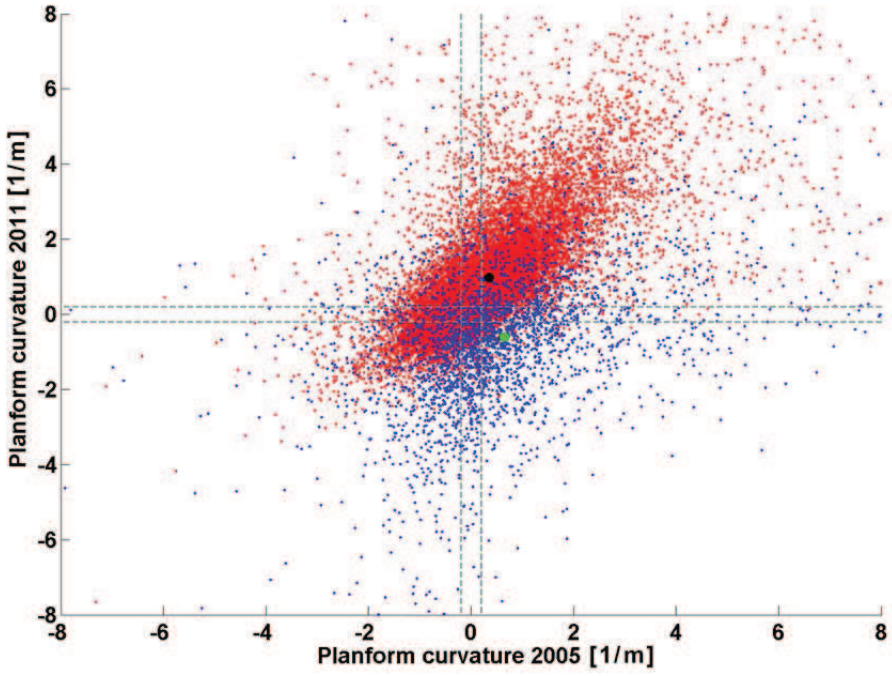

Figure 5. 18: Gadria planform curvature changes between 2005 and 2011 compared to erosion (red) and deposition (blue) values derived from the DoD. Grey dotted lines indicate the interval range of flat values (-0.2-0.2 m) where points were not considered for the analysis. Black and green circles indicate the centroid of the erosion and deposition values distribution respectively.

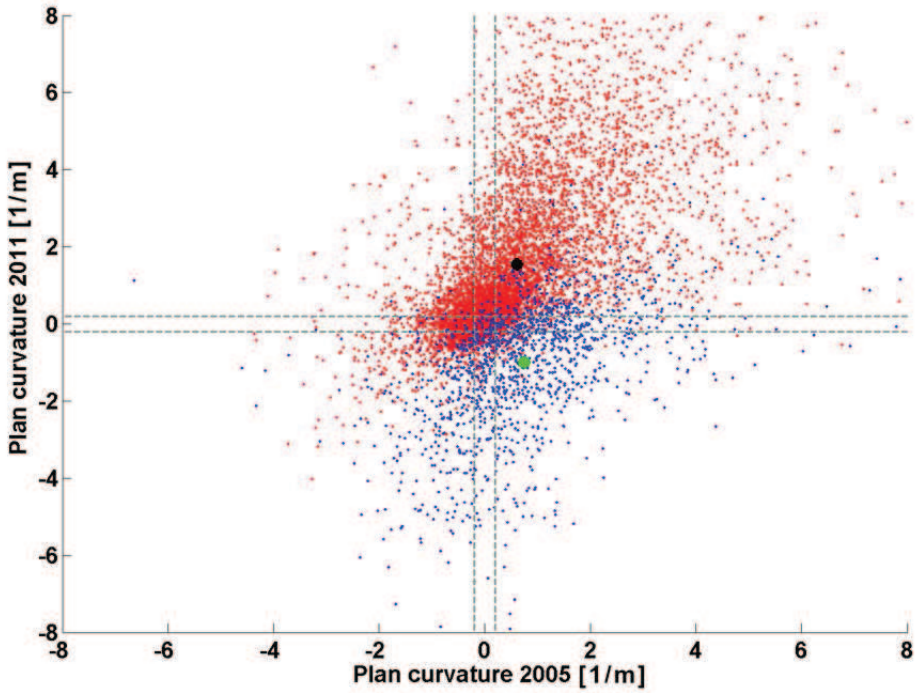

Figure 5. 19: Strimm planform curvature changes between 2005 and 2011 compared to erosion (red) and deposition (blue) values derived from the DoD. Grey dotted lines indicate the interval range of flat values (-0.2-0.2 m) where points were not considered for the analysis. Black and green circles indicate the centroid of the erosion and deposition values distribution respectively.

Similar results were obtained for profile curvature (Fig. 5.20).

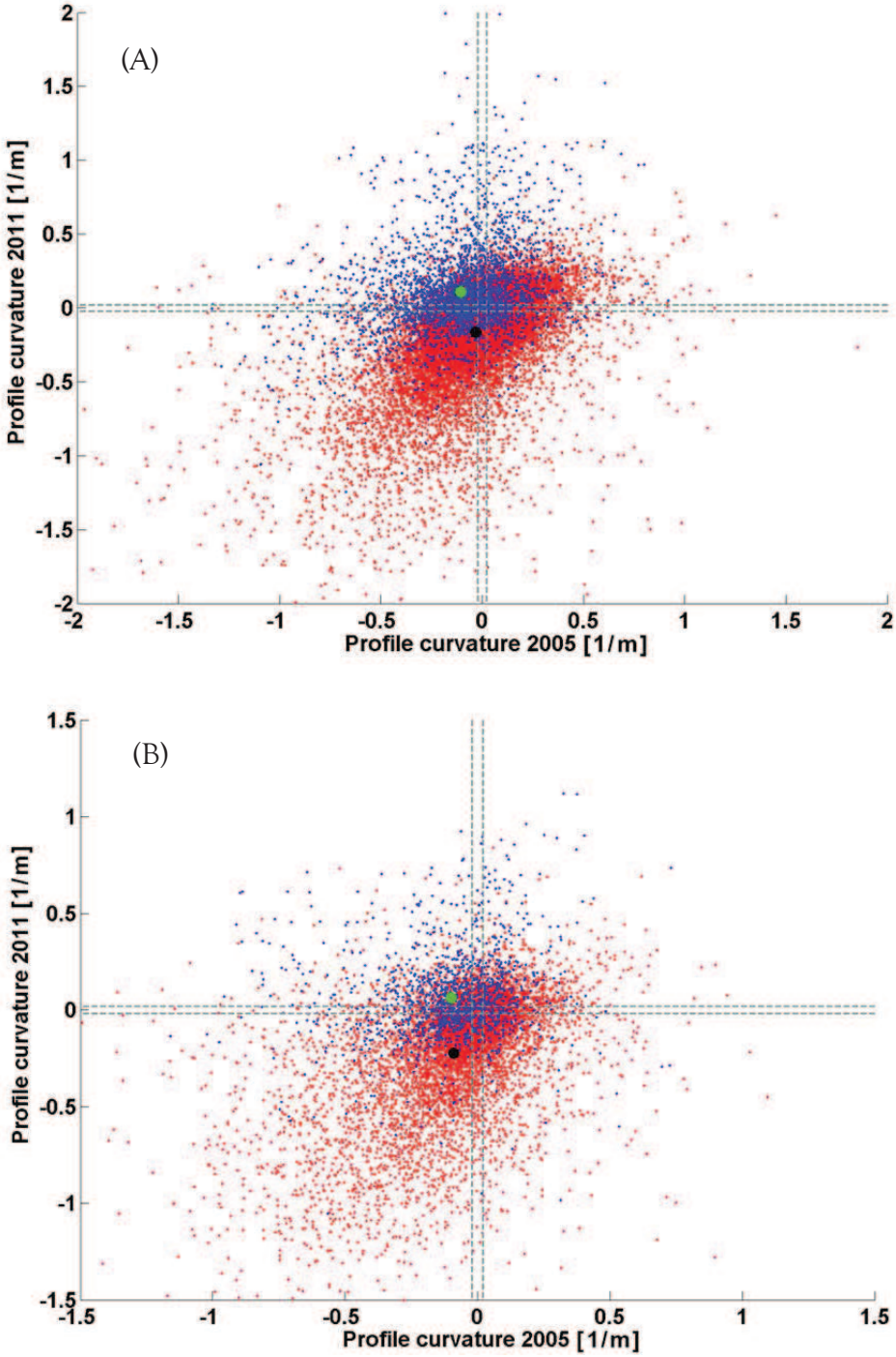

Figure 5. 20: Gadria (A) and Strimm (B) profile curvature changes between 2005 and 2011 compared to erosion (red) and deposition (blue) values derived from the DoD. Grey dotted lines indicate the interval range of flat values (-0.02-0.02 m) where points were not considered for the analysis. Black and green circles indicate the centroid of the erosion and deposition values distribution respectively.

Curvature variations from 2005 to 2011 associated to DoD-predicted changes are also exemplified by some figures showing erosion and deposition features in the two studied catchments. The classes of curvature changes that are more representative of erosion and deposition changes (see Tables 5.6, 5.7, 5.8, 5.9) are presented. Plan and profile curvature show a similar efficiency in detecting convex forms in a sediment deposit area in the Gadria catchment (Fig. 5.21 a, b) and a typical channel debris flow deposit in the Strimm creek (Figure 5.21 c, d).

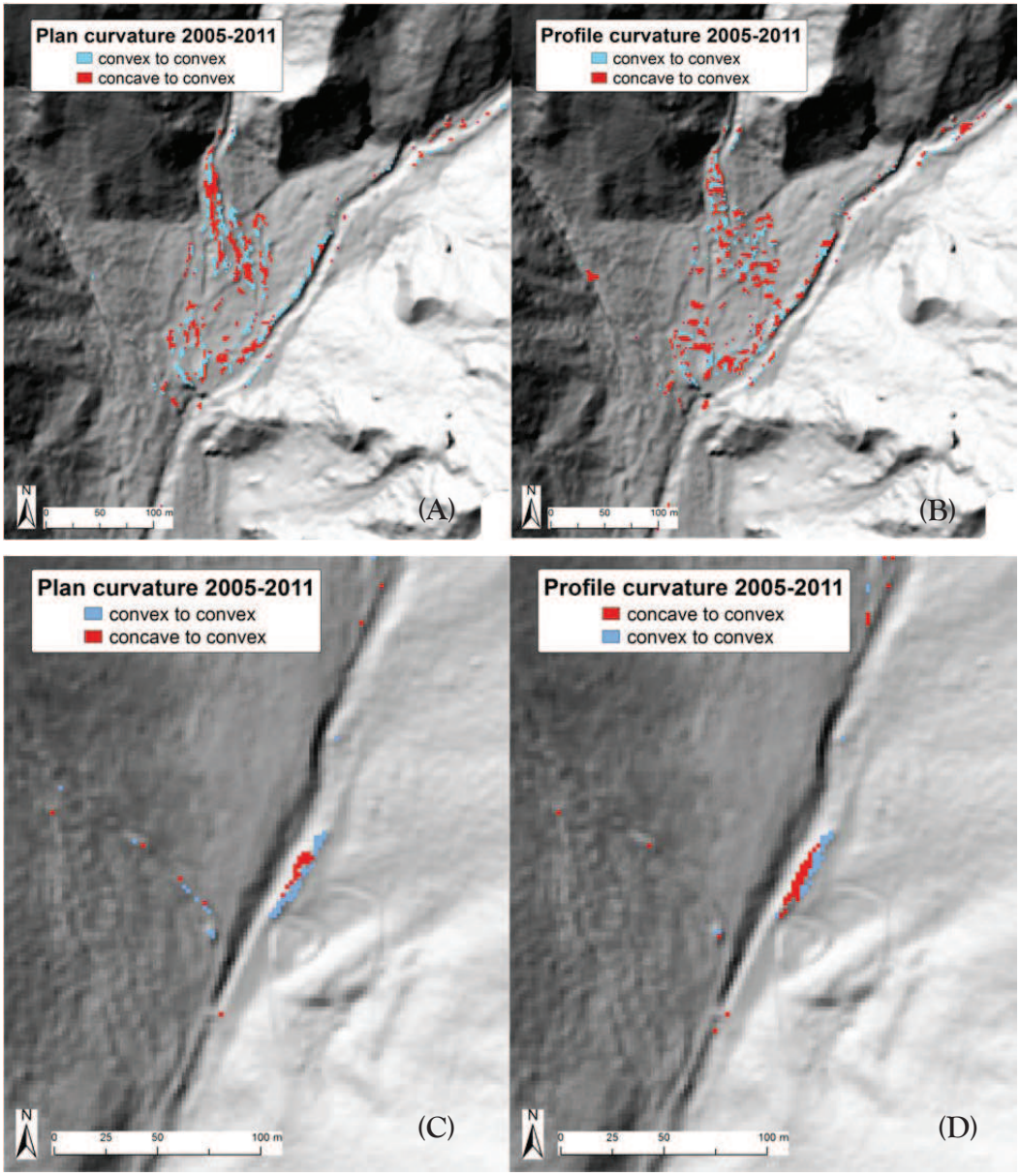

Figure 5. 21:Example of characterization of deposit processes in Gadria (A, B) and Strimm (C, D) basin using planform and profile curvature.

Planform and profile curvature seem to be suitable even for a good recognition of areas affected by erosion processes such as, for instance, landslides and erosion processes linked to debris flows channels in the upper part of Gadria basin and the erosion effects mainly due to debris flow event of 2010 12t^{h} July (Fig. 5.22).

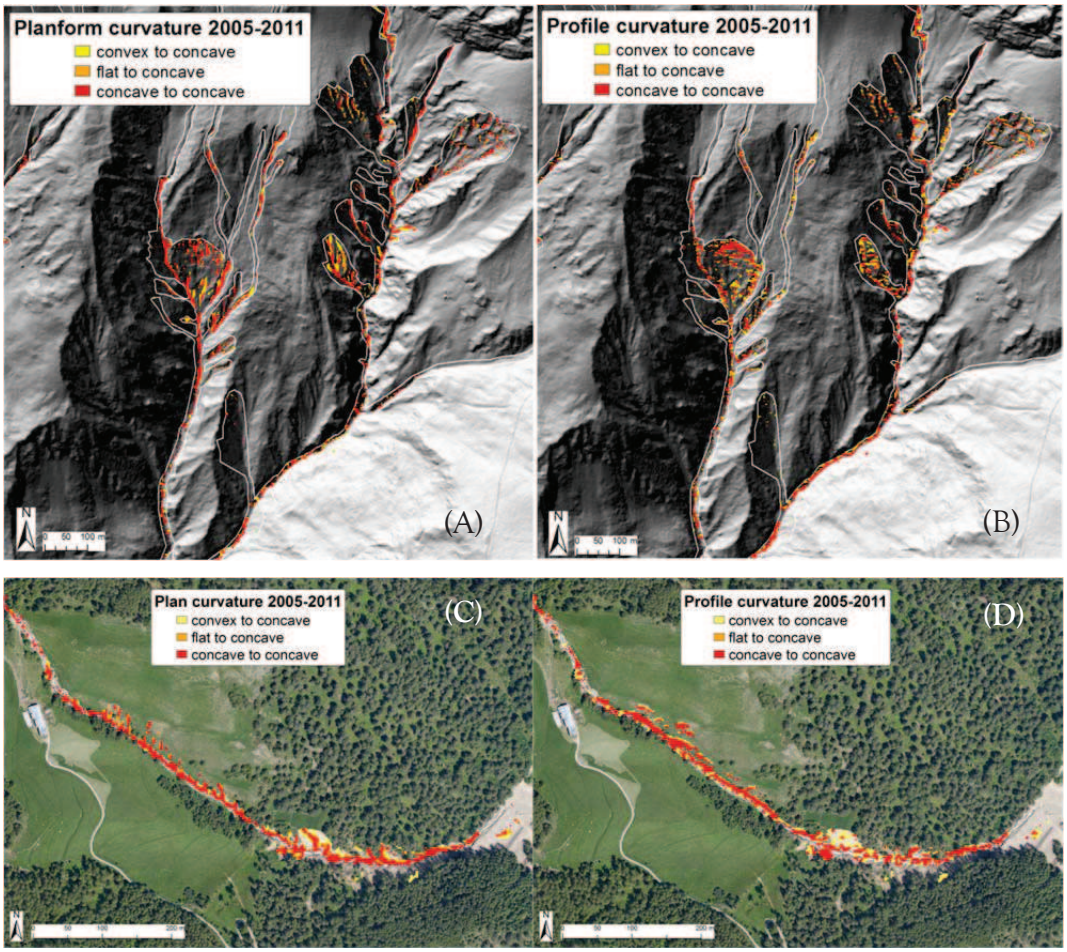

Figure 5. 22: Example of characterization of erosion processes in Gadria (A, B) and Strimm (C, D) basin using planform and profile curvature.

One of the limits of this type of analysis is linked to the difficulty in explaining the presence of deposit in areas characterized by changes from convex to concave forms. An example is given in Figure 5.23, representing deposits in areas of concave morphology identified by the DoD in the upper part of Gadria stream. In this case, the presence of deposition in the channel could be derived from the aggradation of the channel bed and that in the deposition area from a phase of rearrangement or from the effect of multiple events.

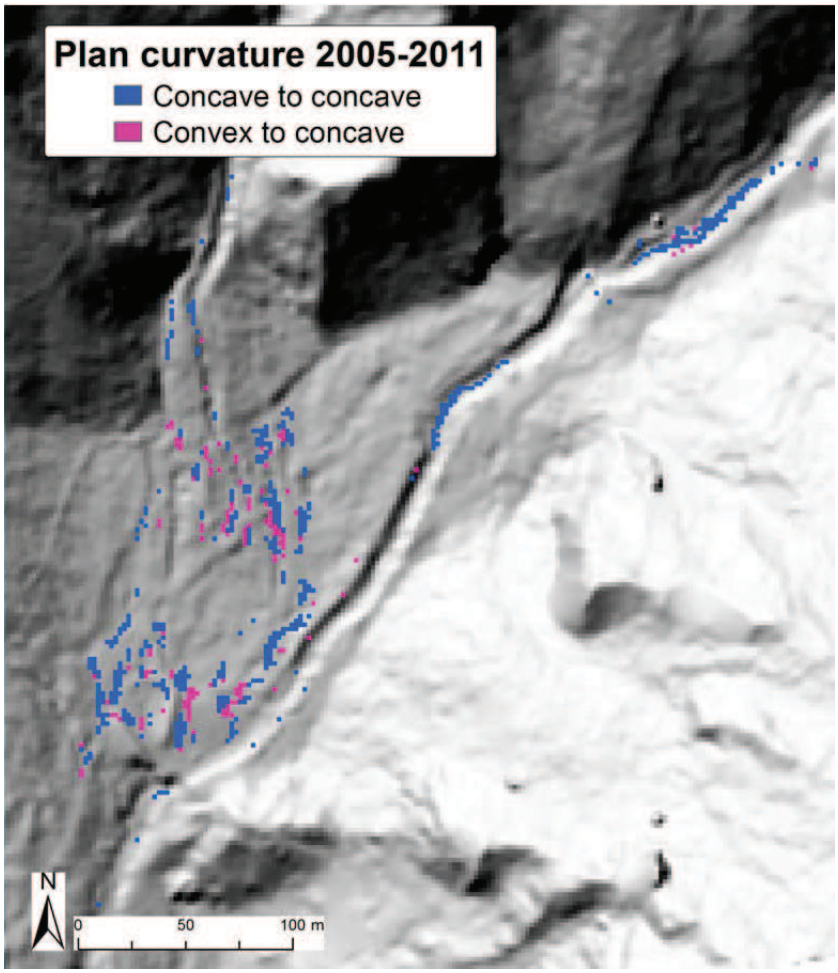

Figure 5. 23: Example of deposition predicted by the DoD in areas where actual concave morphology increases its concavity or derives from convex morphology.

Another possible explanation for deposition in areas that show curvature change from convex to concave is that multiple deposition events have resulted in an overall positive variation of the topographic surface, but the last event that occurred during the observation period was dominated by erosion and produced concavity in the aggraded surface. Conversely, erosion occurring with different intensity on contiguous areas may produce local convexities on terrain that experiences negative variation of elevation.

Less obvious changes in curvature may also be explained by the complex sediment transport processes in alpine headwaters, which often are characterized by alternation of prevailing erosion and deposition between different events and even within the same event.

Relation between slope-area and DoD changes was analyzed on the same spatial mask used for the volumes quantification and for plan and profile curvature analysis. Therefore, slope-area data are based on channel profiles and bordering areas rather than on catchment. Slope values were averaged for each 0.1 log interval of drainage area.

Results are given in Figure 5.24 and Figure 5.25. Diagrams slope-area-DoD show a different pattern for Strimm and Gadria suggesting a different hydrological control in the catchments. Gadria stream profile (Fig. 5.24) is more similar to the characteristic shape of log slope-area diagram (Montgomery and Foufoula-Georgiou, 1993). In Gadria basin erosion processes are evident along the whole profile with high concentrated zones for low drainage area values. Deposits occurs even on areas affected by landslide processes, in the hillslope pattern of the log area-slope diagram.

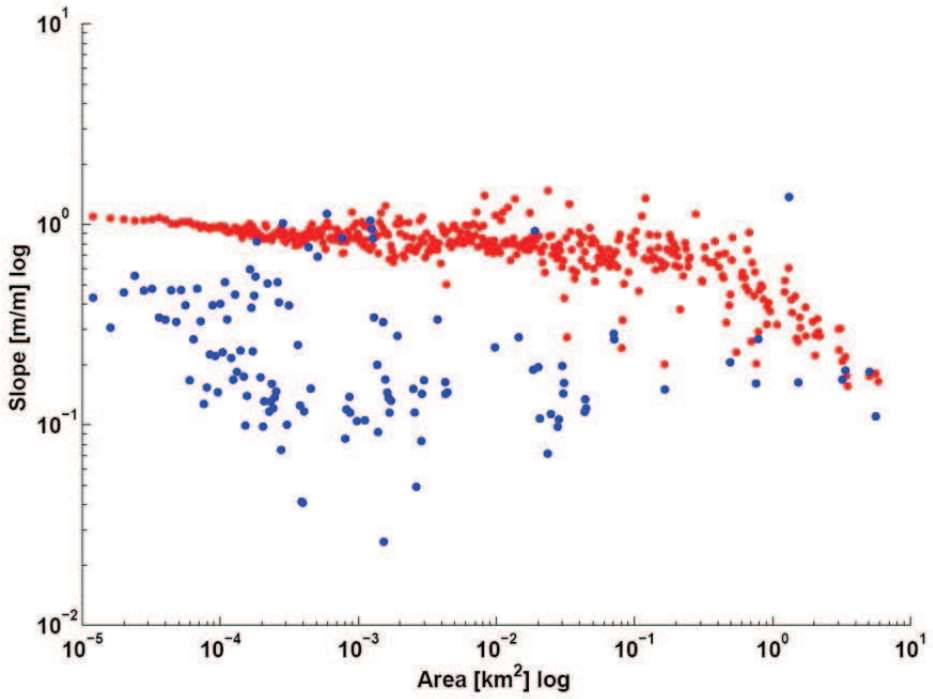

Figure 5. 24: Illustration of the relationship between drainage area and local slope and DoD predicted changes for Gadria river.

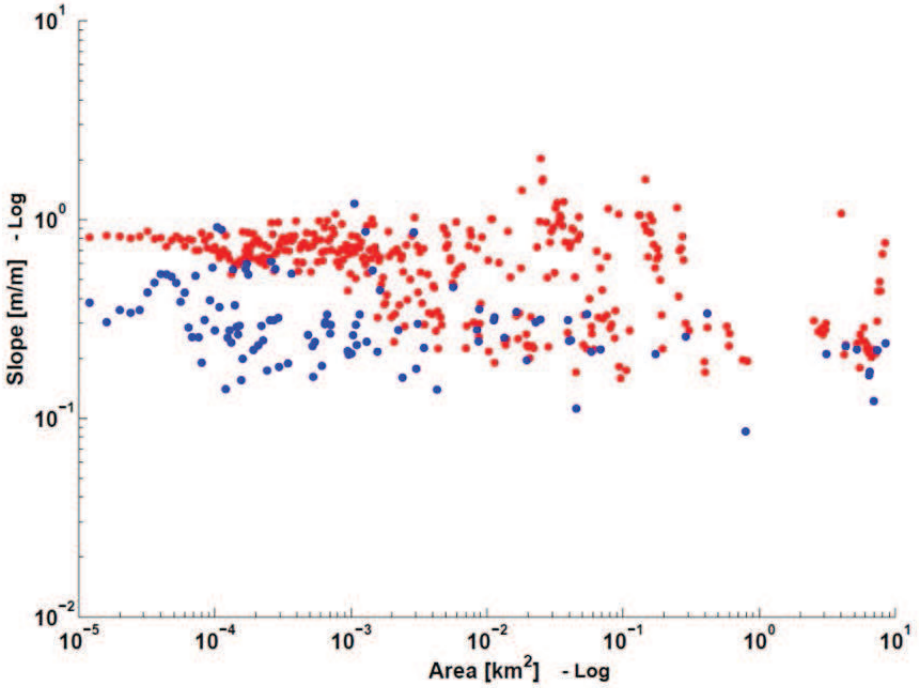

Figure 5. 25: Illustration of the relationship between drainage area and local slope and DoD predicted changes for Strimm river.

Strimm area-slope diagram (Fig. 5.25) shows instead a channelized pattern of sediment transport processes in which two main erosion trends can be observed: the first , in the upper part, refers to the main channel activity and the second one probably represents the main affluent of the Strimm that mostly contributed to sediment transport processes in the catchment. Pronounced erosion DoD predicted changes at high drainage area values correlate well with the effects of the event of 2010 12th that characterized the final section of the Strimm.

Results of curvature and slope-area analysis highlight the possibility to use relationship between these parameters and DoD to represent the interaction between the morphological evolution of the surface and the dynamic of the transport processes involved. In fact, these relationships can be used to evaluate morphological changes due to multiple and different types of process (e.g. debris flow, bedload transport, landslide) occurred in different periods. The limit of this relationship is linked to the difficulty in performing detailed analysis on morphologic features since the representation of the interaction could be problematic (e.g. few numbers of representing pixels).

5.3 Sediment connectivity applications

The spatial sediment connectivity analysis was carried out at regional and basin scales by applying the connectivity model described in chapter 4, considering the connectivity between hillslopes and catchment outlets (*IC* outlet) as well as between hillslopes and sinks of interest (*IC* channels, *IC* check dams).

5.3.1 Impedance in the *IC* model

As previously described, the choice of the impedance factor to model sediment connectivity by using the *IC* model depends on the aim of the analysis and on the

morphological characteristics of the study area. An analysis on the effect of different impact factors, i.e. the Roughness Index and Manning's n, was performed on the Strimm basin. This analysis helps in selecting the parameter suitable to model the impedance to sediment transport in different morphological areas at different scale.

Differences between the application of the topographic roughness (*RI*) and the hydraulic roughness (i.e. Manning's n) are reported in Figure 5.26. The main discrepancy can be observed in surfaces characterized by forest cover and bare rocks: Manning's n is able to best represent the role of the forest as impedance factor (0.4 compared to 0.12 of the *RI*), but in bare rocky areas the hydraulic roughness don't provide differences in the impedance to sediment transport, which can be better represented by the topographic roughness (0.22 of *RI* compared to 0.02 of the Manning's n). Furthermore, the Manning's n is suitable to describe the role of different vegetation types in their contribution to roughness and consequently to impedance to sediment transport, compared to *RI* whose values for arable land (0.082), pasture (0.086) and open space with little or no vegetation (0.089) are similar. It is also possible to observe that values range for *RI* (0-0.25) is lower than the range of Manning's n values (0-0.4): this can be due the normalization of both parameters as required by the *IC* model.

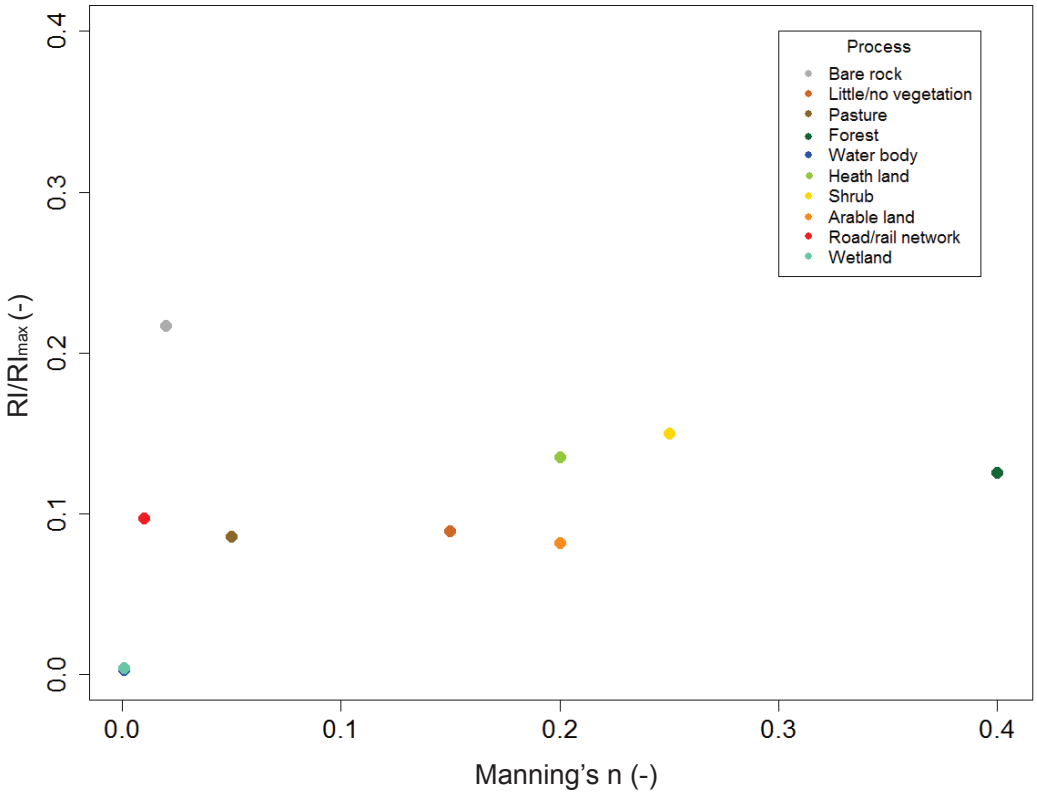

Figure 5. 26: Relation between topographic roughness, computed with the RI, and hydraulic roughness, as defined by the Manning's n values, for each classes of land use for the Strimm basin.

Result of the application if *IC* is shown in Figure 5.27. Different patterns can be observed depending on the selected impedance factors. In particular, when the Manning's n is applied, downstream areas with vegetation cover display lower *IC* values whereas higher values can be found in bare ground areas (e.g. rocky outcrop) in the upper part of the basin if compared with *IC* computed with *RI*.

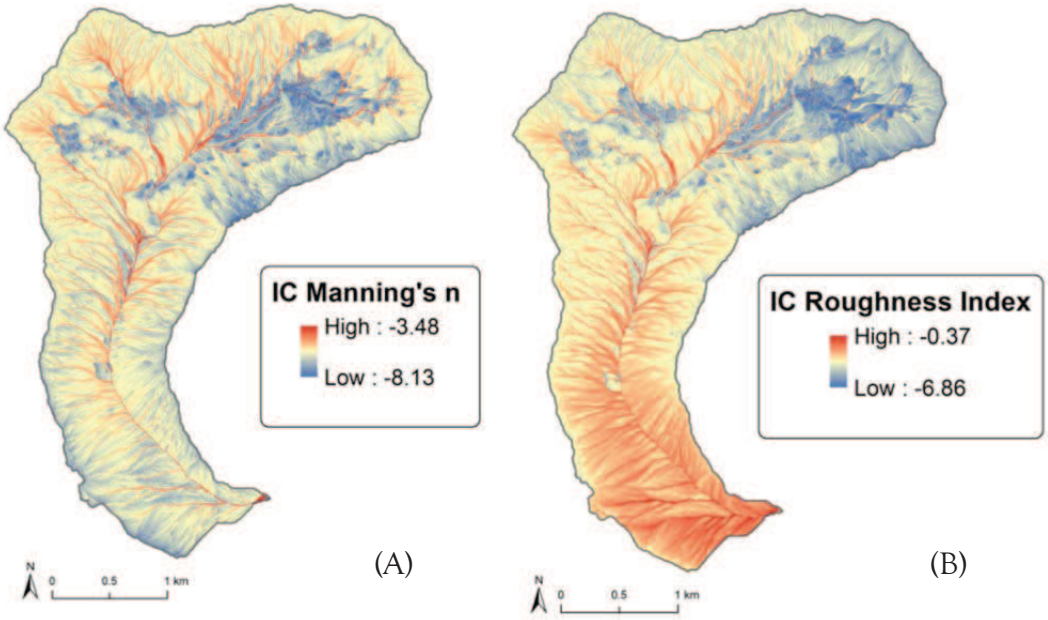

Figure 5. 27: Spatial distribution map of *IC* values derived from the application of the model to Strimm outlet by applying Manning's n (A) and Roughness Index (B).

Main statistics of *IC* computed with both weighting factors are reported in Table 5.11 and Figure 5.28. The application of Manning's n as weighting factor leads to lower average sediment potential connectivity (-5.76) when compared to *IC* modeled with the topographic roughness (-3.86). The application of the Roughness Index as impedance factor leads to larger variability of *IC* distribution, as described by the IQR: the 50% of values are included in a wider range (0.7) if compared to *IC* modeled with the hydraulic roughness (0.39).

Table 5. 10: main statistics for *IC* calculated with different weighting factor derived from Manning's n and the Roughness Index. 1Q: first quartile; 3Q: third quartile; IQR: Interquartile Range; StD: standard deviation.

Statistics	*IC* – Manning'	*IC* – Roughness Index
Minimum	-8.13	-6.86
Maximum	-3.47	-0.37
Mean	-5.76	-3.86
Median	-5.77	-3.87
1Q	-5.96	-4.20
3Q	-5.57	-3.50
StD	0.39	0.54
IQR	0.39	0.7

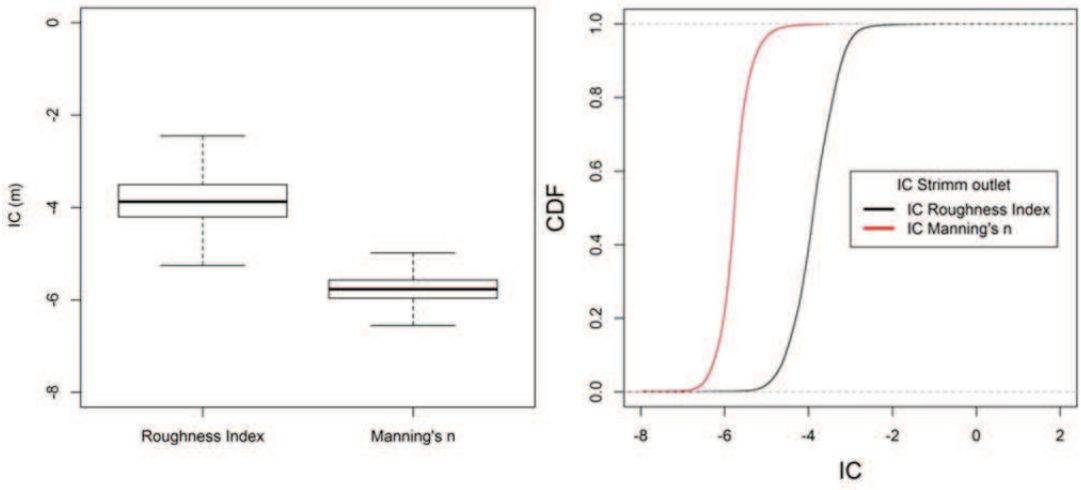

Figure 5. 28: Boxplot and cumulative distribution function of *IC* values derived from the application of topographic roughness and Manning's roughness to compute *IC* model in relation to the outlet of Strimm basin.

5.3.2 Effect of DTM resolution on *IC*

The effect of DTM resolution on *IC* was investigated at regional scale by applying the connectivity model to Venosta Valley at increasing DTM cell size, i.e. 2.5 m , 5 m and 10 m. Map of sediment connectivity for different DTM resolution are reported in Figures 5.29 and 5.30. The general pattern of sediment connectivity distribution is preserved across the range of resolutions.

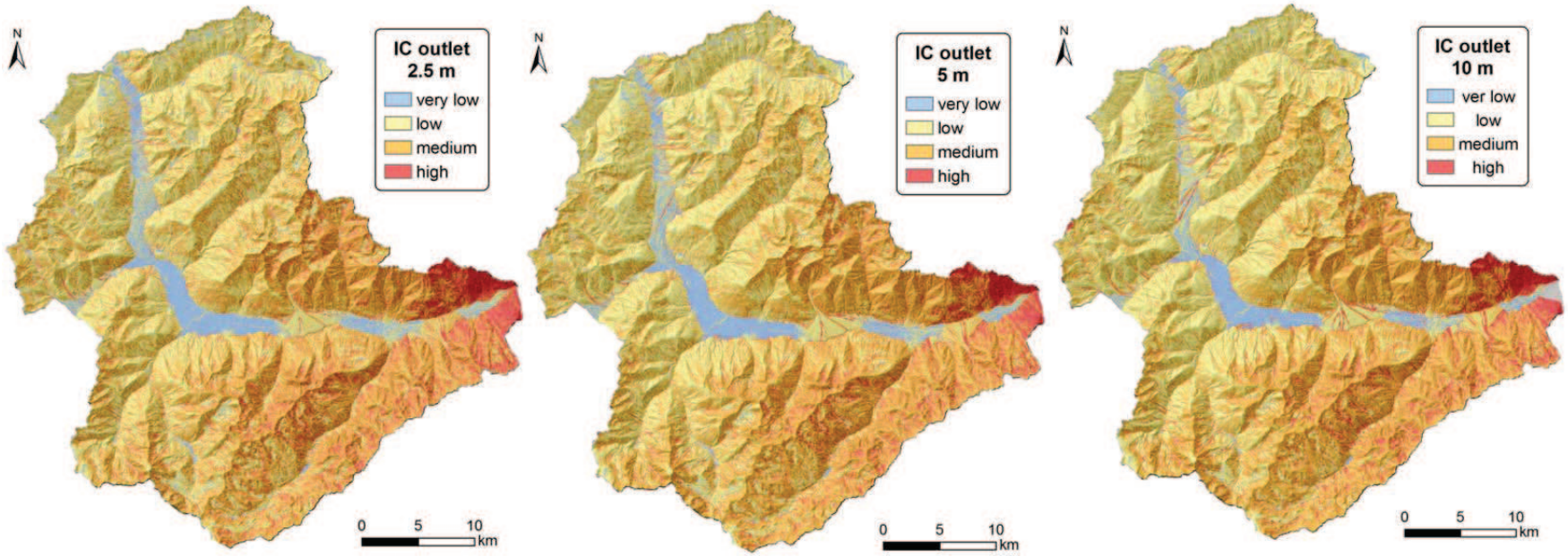

Figure 5. 29: Sediment connectivity maps computed with reference to Venosta Valley outlet at different DTM resolutions (2.5, 5 and 10 m).

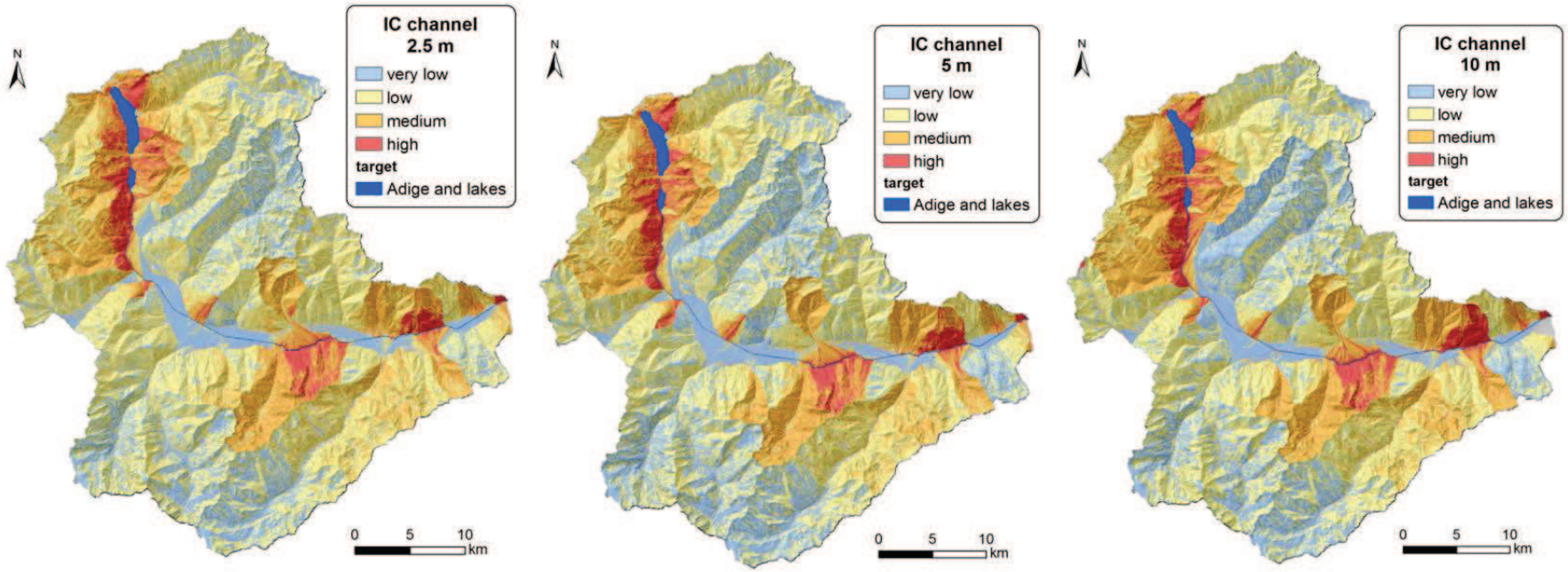

Figure 5. 30: Sediment connectivity maps computed with reference to Adige river and major lakes of Venosta Valley at different DTM resolutions (2.5, 5 and 10 m).

Summary statistics reported in Table 5.11 and boxplot in Figure 5.43 show that *IC* outlet and *IC* channel vary as a function of DEM resolution. Both mean and median values of *IC* increase slowly with the coarsening DEM resolution. This slight increase may be explained by shorter paths and consequent more effective transport as cell size increases that lead to higher *IC* values. The shortening of flow paths in the downstream component of *IC* prevails on the decrease of slope values at coarser resolutions.

Table 5. 11: main statistics for the *IC* referred both to the outlet and the main channel of Venosta Valley at different DTM cell sizes. 1Q: first quartile; 3Q: third quartile; IQR: Interquartile Range; StD: standard deviation.

Statistics	*IC* outlet			*IC* network		
	2.5 m	5 m	10 m	2.5 m	5 m	10 m
Minimum	-8.65	-8.3	-7.94	-7.95	-7.52	-7.17
Maximum	1.05	1.3	1.32	3.80	3.80	3.79
Mean	-5.96	-5.64	-5.36	-4.96	-4.58	-4.27
Median	- 5.96	-5.65	-5.37	-5.07	-4.72	-4.43
1 Q	-6.23	-5.9	-5.61	-5.40	-5.04	-4.74
3 Q	-5.66	-5.36	-5.09	-4.61	-4.21	-3.83
IQR	0.57	0.54	0.52	0.79	0.83	0.91
StD	0.51	0.53	0.53	0.72	0.73	0.76

As illustrated by the boxplots of Figure 5.31, *IC* increases with DTM coarsening regardless the index is computed with reference to basin outlet or Adige river and lakes, but the increase is more evident for the application of *IC* with regard to the main river.

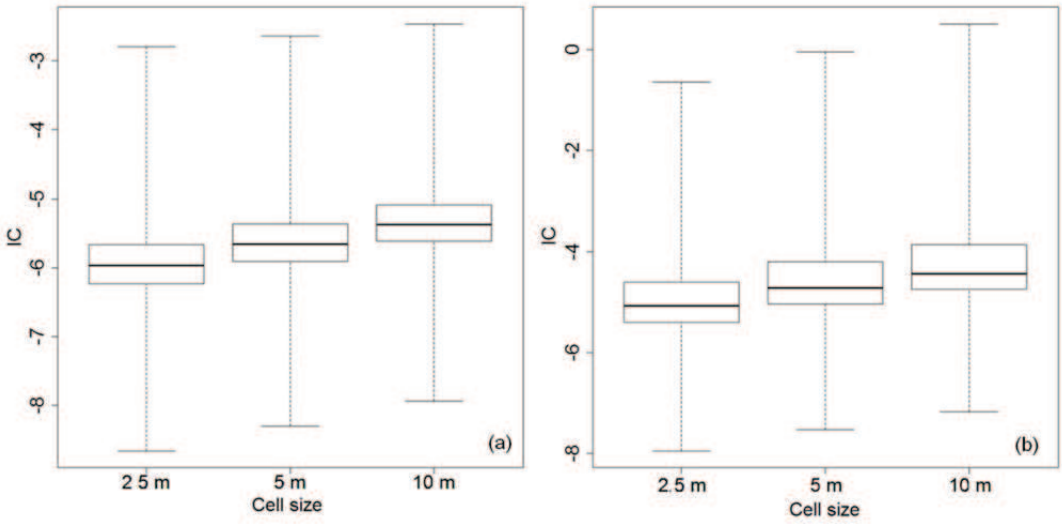

Figure 5. 31: DTM resolutions (2.5 m, 5 m and 10 m) and statistical variations of *IC* calculated at the outlet of Venosta Valley (a) and at the Adige river and lakes (b).

At local scale, however, variations in cell size may have a major influence on the representation of sediment connectivity. In Figure 5.32 an example of spatial pattern of sediment connectivity, derived from the regional *IC*, at increasing grid size at basin and fan scale is reported for Plazut catchment and its alluvial fan.

Although a decrease of *IC* mean values is observed for sediment connectivity calculated at the outlet of Venosta Valley, the overall distribution remain similar across different resolutions at catchment scale. Conversely, concerning the *IC* channel, while the coupling activity of alluvial fan with the Adige river is well represented at all resolutions, the modeled sediment connectivity for Plazut basin present different patterns with higher values calculated at 5 m and lower ones at 2.5 m.

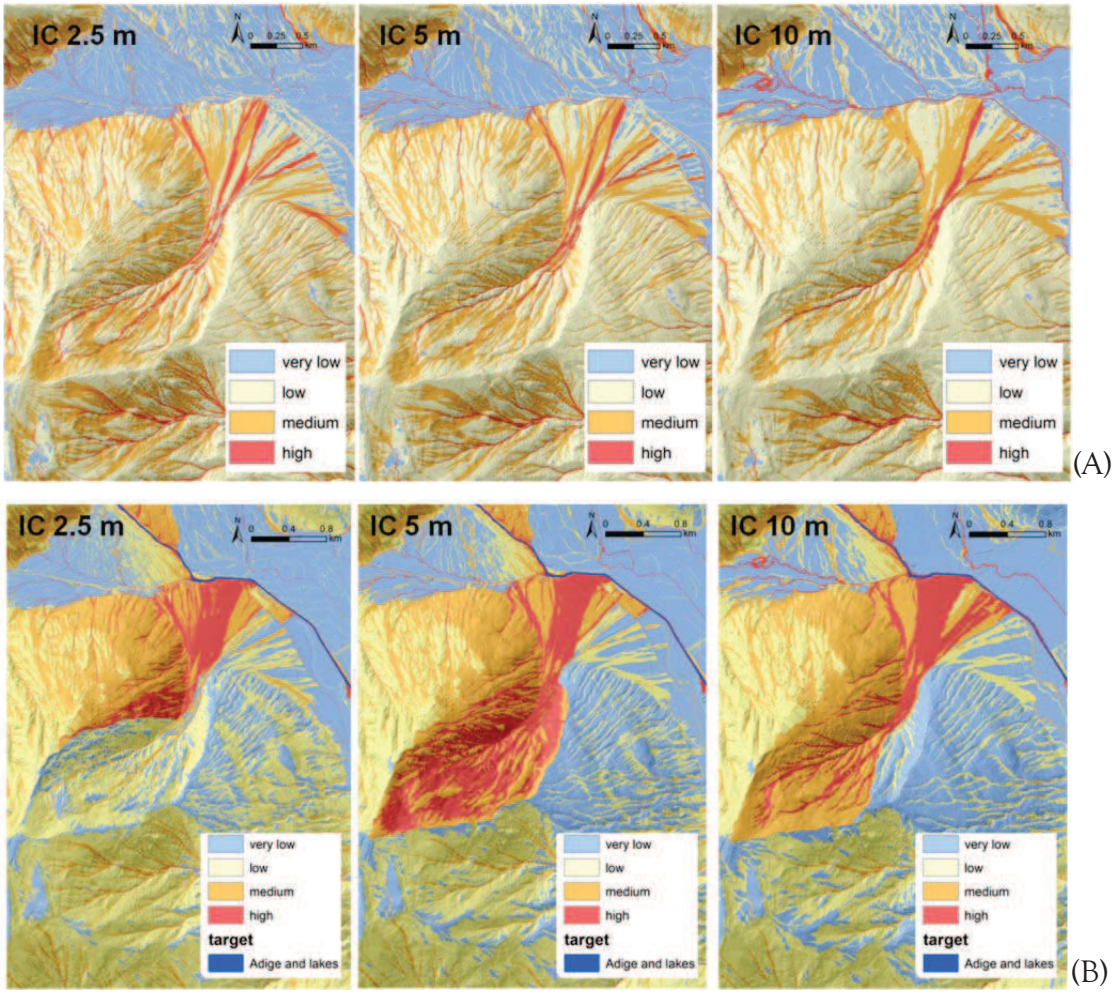

Figure 5. 32: Example of variation of modeled sediment connectivity in a prone to debris flow catchment (Plazut basin) and its alluvial fan derived from the application of the *IC* to the outlet (A) and to the Adige river (B).

To investigate how different DTM resolutions affect the sediment connectivity distribution at catchment scale, the behavior of *IC* for a sample area, i.e. Strimm basin, referred to both outlet and river network as target, derived from increasing DTM cell size (1, 2 and 5 m) was analyzed. Mean and median values of *IC* progressively increase as grid resolution decrease, whereas standard deviation is found to be an almost invariant property of different scale DTMs (Tab. 5.13).

Table 5. 12: Main statistics computed for *IC* calculated at the outlet (*IC* outlet) and at the main river network (*IC* channel) of Strimm basin. 1Q: first quartile; 3Q: third quartile; IQR: Interquartile Range; StD: standard deviation.

Statistics	*IC* outlet			*IC* channel		
	1 m	2 m	5 m	1 m	2 m	5 m
Minimum	-8.46	-6.89	-6.37	-6.84	-6.50	-5.99
Maximum	-0.49	-0.28	-0.12	2.76	2.76	2.745
Mean	-4.41	-3.82	-3.26	-3.16	-2.77	-2.33
Median	-4.46	-3.81	-3.22	-3.13	-2.67	-2.26
1 Q	-4.80	-4.21	-3.63	-3.93	-3.58	-3.11
3 Q	-4.01	-3.39	-2.84	-2.54	-2.12	-1.70
IQR	0.79	0.81	0.79	1.39	1.46	1.41
StD	0.61	0.60	0.59	0.94	0.96	0.94

Figure 5.33 shows the distribution of the *IC* for the chosen DTM resolution. For coarser resolution, larger *IC* values can be observed when sediment connectivity is calculated with reference to the outlet of the catchment.

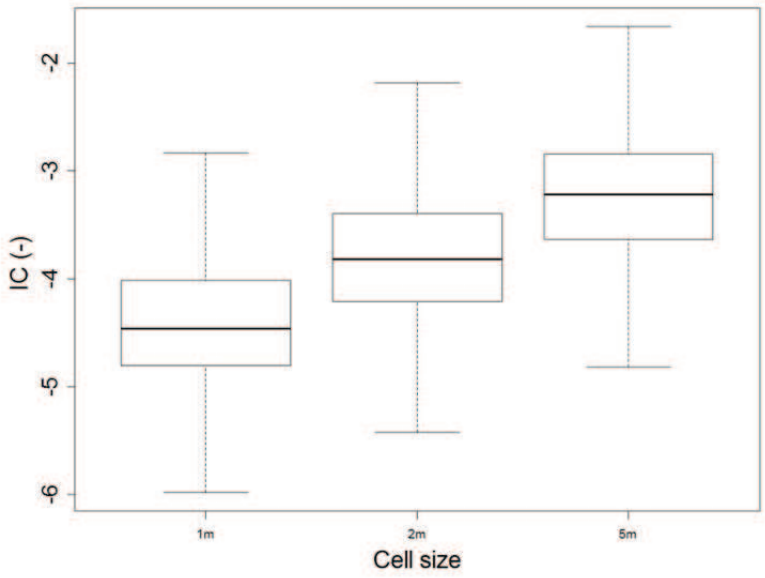

Figure 5. 33: Boxplot of *IC* referred to catchment outlet for three different DTM resolutions. The boxes show the 25th and 75th percentile, the whiskers extend to the 10th and 90th percentile, the horizontal line within the box indicates the median.

Results are similar to those obtained at regional scale: potential sediment connectivity increases across all resolutions (Fig. 5.34).

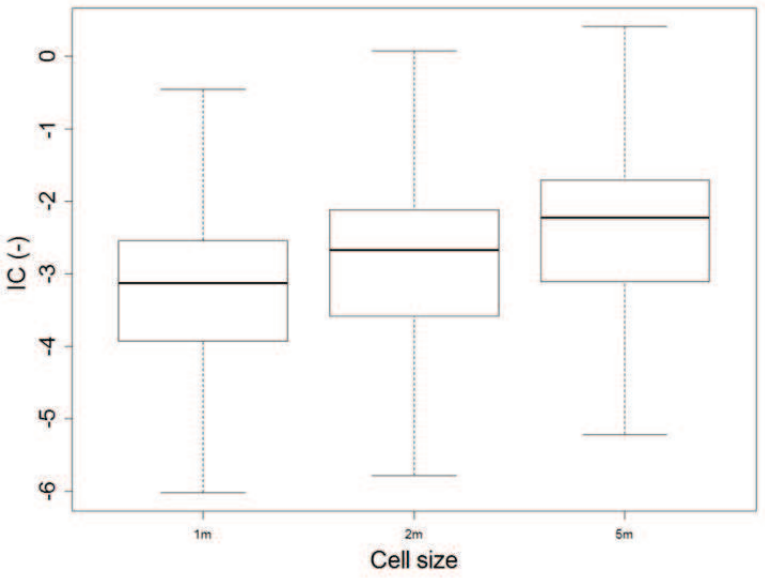

Figure 5. 34: Boxplot of *IC* referred to main channel for three different DTM resolutions. The boxes show the 25th and 75th percentile, the whiskers extend to the 10th and 90th percentile, the horizontal line within the box indicates the median.

The spatial representation of modeled *IC* show a simplification of the flow paths due to increased cell size that leads to an increase of sediment connectivity both in the lower part of the basin, characterized by vegetation, and on steep slopes (Fig. 5.35).

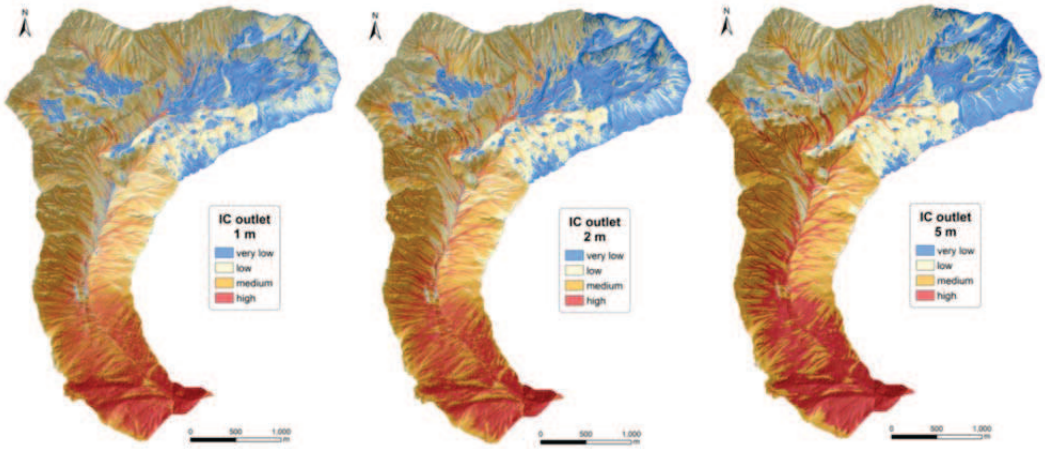

Figure 5. 35: Spatial characterization of sediment connectivity derived from the *IC* outlet at increasing DTM cell size (1, 2, 5m).

Map of *IC* related to Strimm river shows a pattern similar to *IC* referred to the outlet (Fig. 5.36). In this case main differences of *IC* can be observed for sediment connectivity values in steep slopes on the right hillslopes of Strimm basin that increase at lower cell sizes.

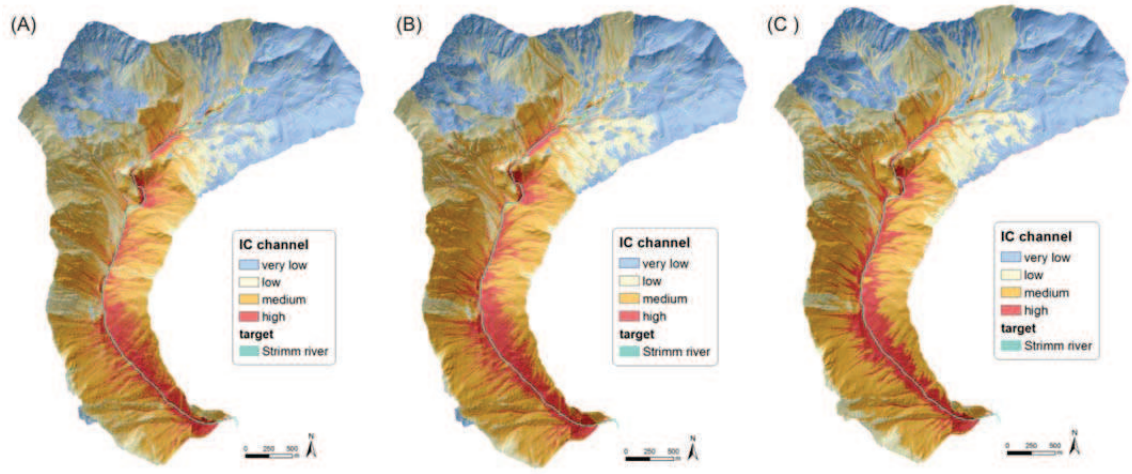

Figure 5. 36: Spatial characterization of sediment connectivity derived from the *IC* channel at increasing DTM cell size (1, 2, 5m).

This result reinforces the observation that the relation between DTM resolution and *IC* is independent from the size area (i.e. regional and catchment scale) and from the sink investigated (i.e. river network and outlet).

As previously stated for Venosta Valley, a possible explanation for the increase in predicted sediment connectivity as resolution become coarser is the change in flow path length values. Statistics reported in Table 5.13, referred to the flow path lengths derived from the application of the *IC* to the outlet of Strimm basin at 1 m, 2 m and 5 m resolution, show that the mean and median flow path lengths values decrease as grid cell size increase. Therefore, keeping roughness index and area constant, as the length required for the sediment particle to reach the outlet increases, the probability of the sediment to reach the outlet decrease.

Table 5. 13: Main statistics of flow path length calculated for Strimm basin at selected cell resolution (1 m, 2m, 5m). 1Q: first quartile; 3Q: third quartile; IQR: Interquartile Range; StD: standard deviation.

Statistics	Flow path length (m)		
	1 m - DTM	2 m - DTM	5 m - DTM
Minimum	167.6	111.7	1
Maximum	99.46 x10^4	25.16 x10^4	11.22 x10^4
Mean	48.53 x10^4	6.81 x10^4	1.86 x10^4
1 Q	40.51 x10^4	2.83 x10^4	0.17 x10^4
3 Q	56.58 x10^4	7.91 x10^4	2.89 x10^4
IQR	16.07 x10^4	5.08 x10^4	2.72 x10^4
Standard deviation	17.39 x10^4	6.22 x10^4	2.62 x10^4

The results of this study emphasize the question of the definition of an appropriate grid size for simulations of geomorphic processes using topographic parameters. Given that the cell size depends on the length scale of the feature of interest, the problem was examined taking into account two different aspect of the *IC* at two different scale (i.e. basin and regional): the potential sediment connectivity between sediment sources and the outlet and between hillslopes and main river network.

Concerning the *IC* outlet, observations for Strimm basin on the stability of standard deviations across DTM investigated resolutions and the detailed and representative spatial pattern at lower cell size suggest that a finer resolution (1 m) should be considered in order to investigate sediment connectivity at catchment scale. Even if similar considerations can be applied for Venosta Valley, it can be more practical to model *IC* at large scale using a coarse grid DTM without losing representativeness.

Results on *IC* channel show a different response to DTM resolution variability. The higher variability in spread measures (different IQR and Standard Deviation values) and the different *IC* pattern make difficult the identification of the best resolution

at regional scale, even if the 10 m resolution can offer the best trade-off between stable results and computation times, whereas at basin scale the lower grid size still allows a correct recognition of sediment connectivity for different processes and landforms.

5.3.3 *IC* at regional scale

In order to get a quantitative evaluation at regional scale of the potential connection between sediment sources and both the channel network and the outlet of the chosen area, the *IC* was applied in the whole Venosta Valley (about 1000 km^2). The impedance to sediment transport was expressed by the Manning's n roughness coefficient, whose values were assigned based on land use classes. Manning's n values range from 0.001 in areas characterized by a low roughness to 0.4 where surfaces present higher roughness (Fig. 5.37).

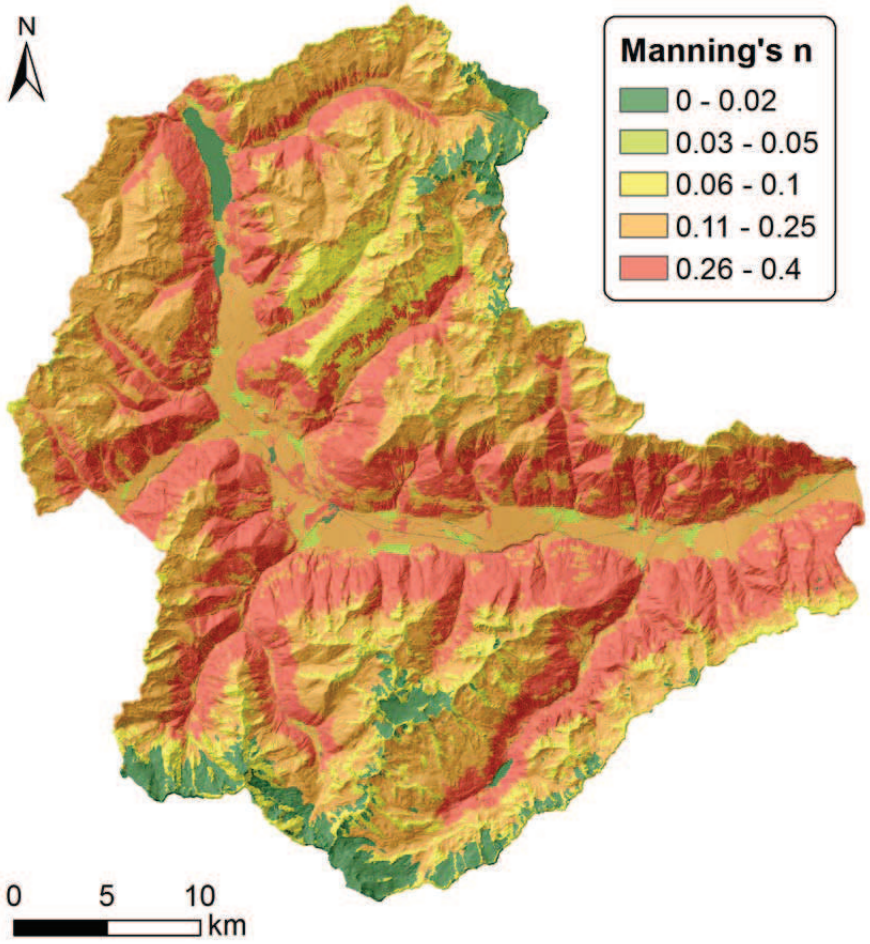

Figure 5. 37: Manning's n map calculated for Venosta Valley.

Result of the *IC* computation for Venosta Valley outlet and targets (i.e. Adige River and lakes and check dams) are presented in Figure 5.38 and Figure 5.39.

The connectivity values were classified into four classes (very low, low, medium, high) by analyzing the distribution of *IC* values within the study area with the Natural Breaks algorithm (Jenks, 1967), an approach that minimizes the variance within the class and maximizes the variance between classes.

As shown in Figure 5.38 and Figure 5.39, the applications of *IC* to the Venosta Valley depicts realistic connectivity patterns, showing very low values in the Adige floodplain.

Different patterns of sediment connectivity arise from the *IC* calculated at the outlet of the study area and at the Adige river and lakes. *IC* outlet map (Fig. 5.38) shows a distributed medium-high potential connectivity of the entire study area, with *IC* values increasing as approaching the outlet when this is chosen as target. This is in accordance to the fact that, considering Venosta Valley outlet as the target for *IC* calculation, downslope component influence on sediment connectivity is higher than that of the upslope component.

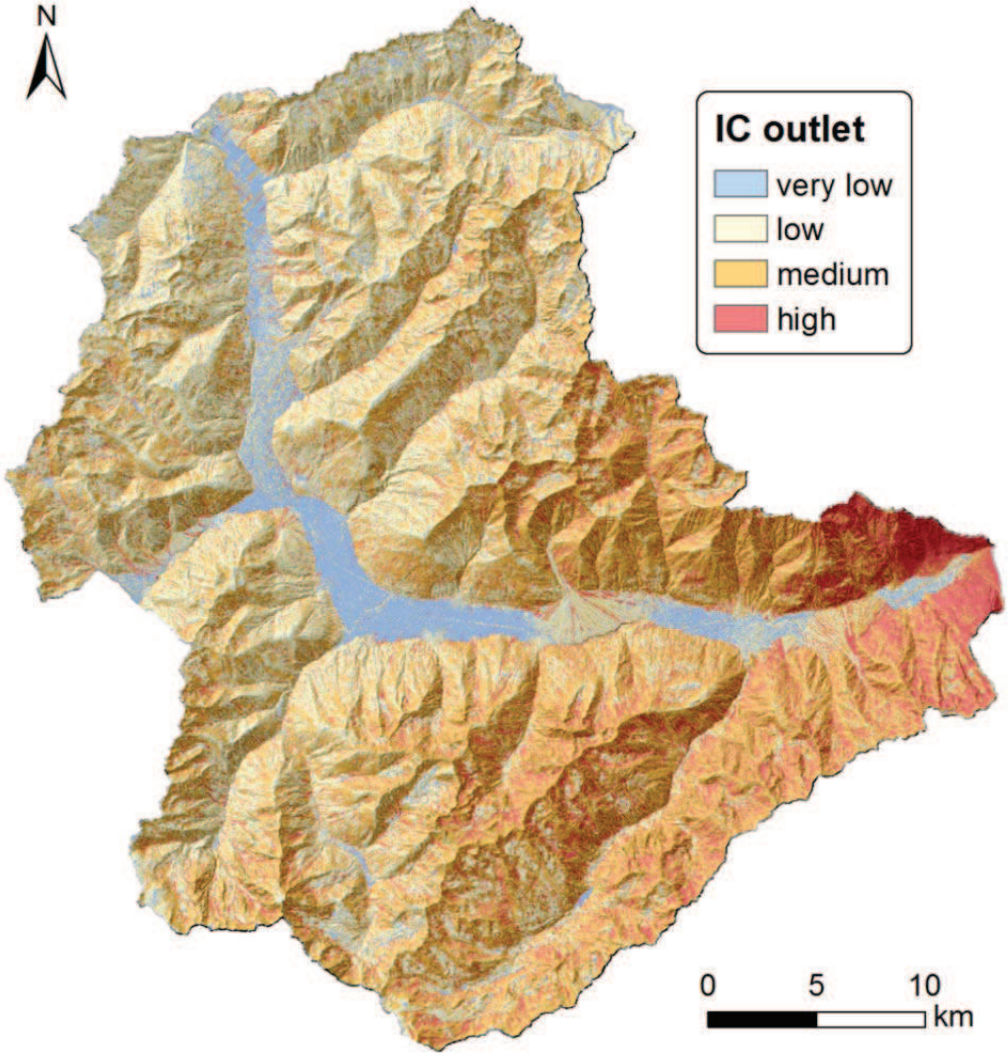

Figure 5. 38: *IC* outlet map for Venosta Valley computed by applying the Manning's n map as weighting factor to model impedance to sediment transport.

IC map related to main channel and lakes (Fig. 5.39) indicates a major contribution to sediment transfer from basins located in the upper part and near the outlet of Venosta Valley and characterized by medium-low catchment size. Moreover, results of *IC* related to channels highlight the role of alluvial fans in favoring the coupling of the upstream catchments and of the opposite hillslopes with the Adige River. In fact, steep and large alluvial fans (8-12°) that occupy the valley floor favor the coupling of the upstream catchments and of the opposite hillslopes with the Adige

river, such as for example the debris cone of Gadria, Strimm, Reschen and Tarres basins. This is in accordance with the fact that alluvial fans and debris cones can act not only as buffering elements but also as coupling systems since they link different zones of the fluvial system (e.g. mountain catchment sediment source areas to main river systems) (Harvey, 2011). In this study, alluvial and debris fans occupying the valley floor allow the coupling of the upstream catchments and of the opposite hillslopes with the Adige River. A high variability of *IC* between different sectors of the alluvial fans body can also be observed.

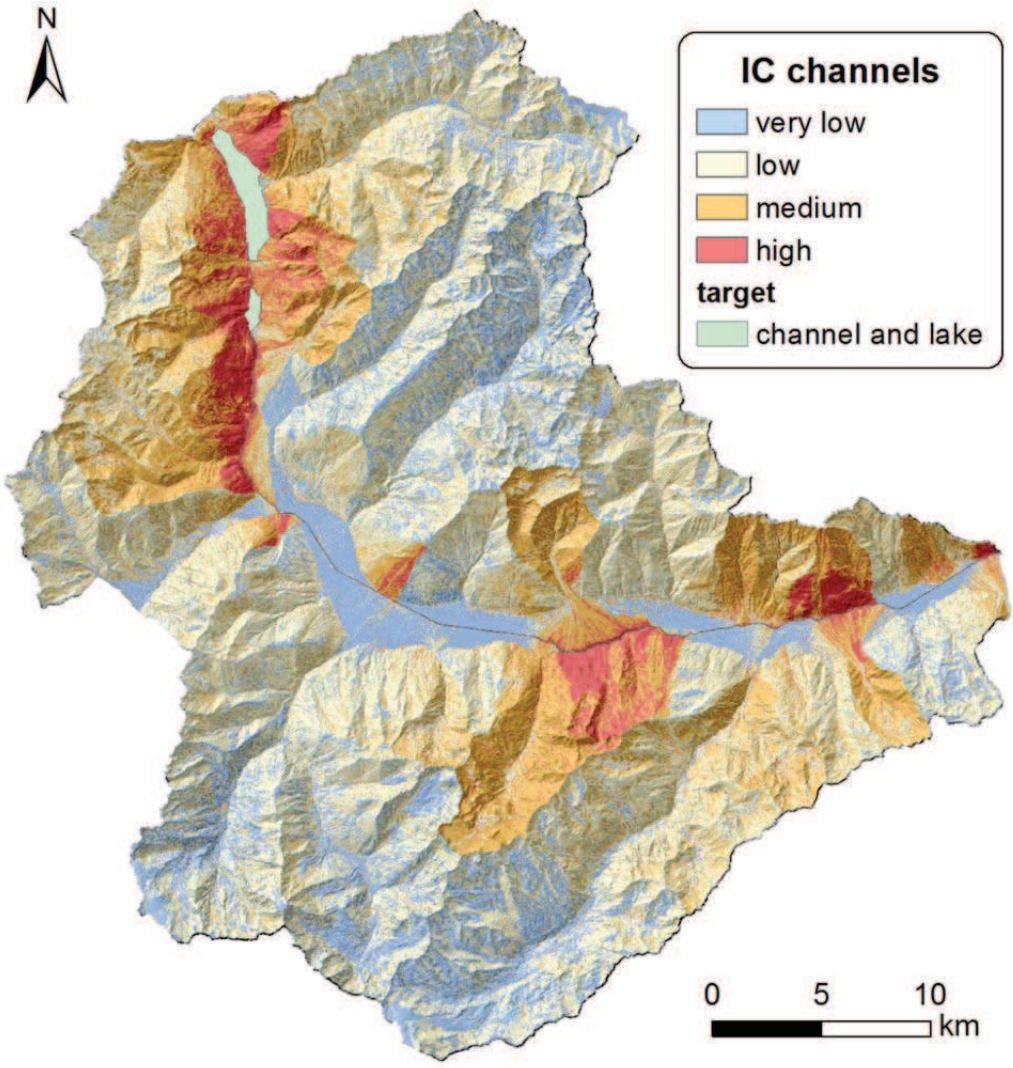

Figure 5. 39: sediment connectivity map depicting coupling and decoupling processes between sediment sources and main channel network (i.e. Adige river) and major lakes. The *IC* channel map was derived from the application of the Manning'n map as impedance factor to sediment fluxes.

The interpretation of results needs to consider that the connectivity map of Venosta Valley do not include the temporal variability of the analyzed systems. In fact, the connectivity map does not capture the geomorphic changes of the landforms, for instance the enlargement of some alluvial fans or the dynamic of ephemeral channels.

Likewise, the vegetation cover is characterized by a high degree of spatial and temporal variation depending on seasonal changes and land use. Therefore, the representativeness of the potential sediment connectivity on Venosta Valley based on the computation of a weighting factor derived from the land use classification is temporally limited.

Nonetheless, using the land cover to derive the Manning's n for the computation of *IC* map for Venosta Valley, allow to consider the effect of the different type of vegetation on sediment connectivity (see Fig. 5.26). The type of vegetation, in fact, can impact in different way on the coupling system since for example bushes and trees are characterized by different root depths and can lead to stabilization or loading of sediment on the slopes (Meßenzehl, 2014).

Furthermore, the *IC* model, requiring a reduced amount of input data, allows a spatially distributed interpretation of sediment connectivity at large spatial scale. The application of the *IC* over Venosta Valley gives a realistic spatial characterization of sediment connectivity in a complex and large mountain watersheds. In particular, *IC* channel highlights the role of the alluvial fans in conditioning connectivity of upstream catchments.

The model has thus proved very promising for a rapid spatial characterization of sediment dynamics at large scale combining both process responses, spatial heterogeneity and landscape characteristics.

5.3.4 *IC* at basin scale and relations with morphometric parameters

Several catchments of Venosta Valley, characterized by different size and sediment transport processes, were selected for spatial sediment connectivity analysis.

Table 5.14 summarize main statistics for *IC* calculated both in relation to the outlet of the basin and to the main channel of every catchment, along with morphometric parameters used in this section and described in Section 2.1.1, i.e. drainage area,

mean slope, basin relief ratio (R_H), and parameters describing the shape of the basin such as the Elongation Ratio (*Re*) and the Circularity Ratio (R_C). Catchments cover a wide range of drainage areas, with values varying from 1 km^2 (Reschen basin) to 160 km^2 (Plima basin). Mean slope values, from 0.5 to 0.86 m/m, indicate that basins are characterized by steep slopes. According to historical data, different flow processes affected selected basins. Considering the events occurring in the main stream, they were classified into three categories i.e. debris flow, bed-load transport or mixed when the basin was subjected to both debris flows and floods with sediment transport. As reported in Table 5.14, debris flows and bed-load transport are the dominant processes for the majority of catchments (10 basins prone to debris flow and 9 to bedload transport), whereas only 3 basins are characterized by mixed transport processes.

To investigate the impact of these factors on the sediment connectivity pattern of each considered catchment, the *IC* mean values were considered. The choice between using the mean or the median is arbitrary since the index, expressed as logarithmic scale, follow a normal distribution where mean and median values coincide.

Table 5. 14: main statistics for the 22 selected basins for the analysis of *IC* at catchment scale.

Basin		Area ($km^{2)}$	Mean slope (m/m)	Rc	Re	R_H	IC outlet				IC channel				Process
n	name						Mean	Min	Max	StD	Mean	Min	Max	StD	
1	Carlino	110	0.58	0.3	0.5	0.1	-5.01	-8.09	-1.34	0.5	-3.48	-6.89	3.33	0.8	Bedload
2	Cengles	10.4	0.81	0.3	0.5	0.4	-3.9	-6.59	-0.81	0.4	-2.59	-6.28	2.85	0.7	Debris Flow
3	Ciardes	1.4	0.85	0.3	0.4	0.5	-2.53	-5.63	0.14	0.4	-2.15	-5.52	2.6	0.6	Debris Flow
4	Colsano	6.15	0.78	0.3	0.5	0.4	-3.41	-6.26	0.64	0.5	-2.32	-5.83	2.76	0.7	Debris Flow
5	Fossa dell'Alpe	6.19	0.66	0.4	0.6	0.3	-3.78	-6.53	0.34	0.5	-2.98	-6.32	2.73	0.7	Mixed
6	Frisio	8.14	0.53	0.3	0.4	0.3	-3.91	-6.93	0.6	0.7	-3.74	-6.95	2.74	1	Bedload
7	Gadria	6.26	0.76	0.4	0.9	0.5	-3.45	-6.18	-0.17	0.4	-2.66	-5.66	2.89	0.7	Debris Flow
8	Lasa	30.8	0.75	0.3	0.5	0.2	-4.04	-7.21	-0.35	0.4	-2.84	-6.24	3	0.6	Mixed
9	Maragno	3.3	0.65	0.4	0.6	0.5	-3.18	-6.04	-0.37	0.4	-2.53	-5.99	2.3	0.7	Debris Flow
10	Plazut	1.88	0.65	0.3	0.5	0.4	-2.95	-5.46	-0.23	0.4	-2.54	-5.88	2.31	0.7	Debris Flow
11	Plima	160.2	0.64	0.3	0.5	0.1	-4.93	-7.9	0.85	0.6	-3.73	-7.05	3.21	0.7	Bedload
12	Puni	40.8	0.62	0.2	0.4	0.1	-4.54	-7.36	-0.57	0.5	-2.85	-6.56	2.82	0.8	Bedload
13	Reschen	1	0.82	0.2	0.4	0.5	-2.68	-5.98	-0.11	0.6	-2.44	-6	2.47	0.8	Debris Flow
14	Saldura	95.7	0.63	0.3	0.5	0.1	-4.86	-7.73	0.88	0.5	-3.21	-6.97	3.03	0.8	Bedload
15	Silandro	48.9	0.66	0.3	0.6	0.2	-4.37	-7.22	0.3	0.5	-3.24	-6.94	3.03	0.9	Bedload
16	Solda	75.6	0.7	0.4	0.5	0.2	-4.55	-7.39	-1.77	0.6	-3.39	-7.11	3.21	0.8	Bedload
17	Solume	5.16	0.68	0.3	0.5	0.4	-3.2	-6.31	0.09	0.5	-2.47	-6.19	2.57	0.8	Debris Flow
18	Strimm	8.5	0.64	0.3	0.4	0.2	-3.87	-6.86	-0.37	0.5	-2.75	-6.43	2.64	0.9	Mixed
19	Tanas	10.8	0.62	0.4	0.7	0.4	-3.73	-6.36	-0.08	0.4	-2.89	-6.12	2.78	0.8	Debris Flow
20	Tarres	9.1	0.59	0.3	0.6	0.3	-3.74	-6.7	-0.21	0.5	-3.19	-6.56	2.59	0.8	Bedload
21	Trafoi	51.3	0.74	0.3	0.6	0.2	-4.63	-7.34	1.07	0.4	-3.31	-6.76	3.17	0.8	Bedload
22	Vezzano	5	0.86	0.4	0.5	0.5	-3.37	-5.9	0.4	0.4	-2.14	-5.65	2.61	0.7	Debris Flow

A significant relationship (R^2 = 0.57 at 0.001 significance level) between *IC* mean values and catchment area, expressed as a logarithmic function, can be observed in Figure 5.40: *IC* mean values tend to decrease for higher catchment sizes. This is due to the fact that the probability of sediment particle to reach the outlet depends on path flow length required for sediment transport.

Results similar to the inverse relationship between sediment connectivity and basin area are widely documented in the literature for the Sediment Delivery Ratio (SDR), an index of sediment transport efficiency. General observations that sediment delivery ratio decline with increasing basin size, verified by many authors in different geographic and geomorphologic settings (Roehl, 1962; Williams, 1977; Walling, 1983; Ichim and Radoane, 1987; Ferro and Minacapilli, 1995; Lane et al., 1997; Verstraeten and Poesen, 2001; Alatorre et al., 2010), is in accordance to Boyce (1975): large basins are characterized by a lower average slope and a higher amount of sediment storages between sediment sources areas and the outlet than small catchments.

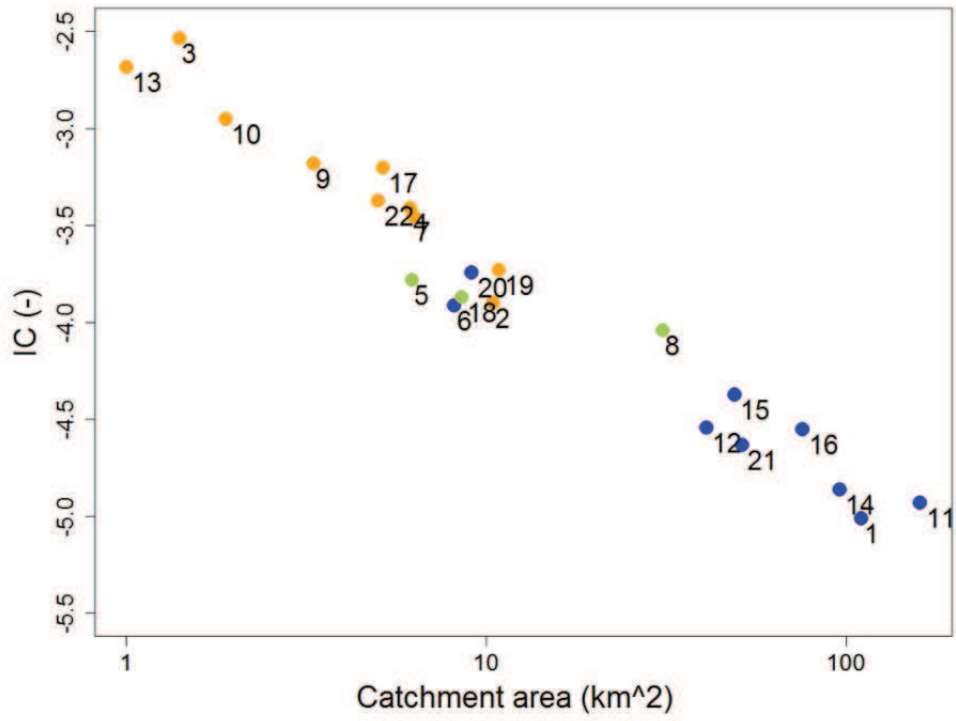

Figure 5. 40: Relationship between connectivity index calculated with reference to the fan apex of the basin and drainage area proposed for selected study areas. Selected catchments, represented by numbers (see Tab. 5.14), are grouped into processes characterizing the main channel.

From the same diagram of the relationship between area and *IC* it is also possible to notice an interesting aspect of sediment connectivity related to investigated processes. *IC* values are higher for those basins, from 1 up to about 10 km^2 of drainage area, where sediment transport is mainly characterized by debris flow events whereas lower *IC* values are present on basins of larger size whose main channel is mostly affected by bedload sediment transport. Medium size basins (from 6 km^2 to 30 km^2 of drainage area) represent the central part of the relationship where different type of processes occurred.

As for the examined relationship between *IC* calculated with reference to the outlet and drainage area, *IC* referred to the main channel shows a similar dependency to

basin size (Fig. 5.41) but with a lower correlation coefficient (R^2 = 0.47 at 0.001 significance level).

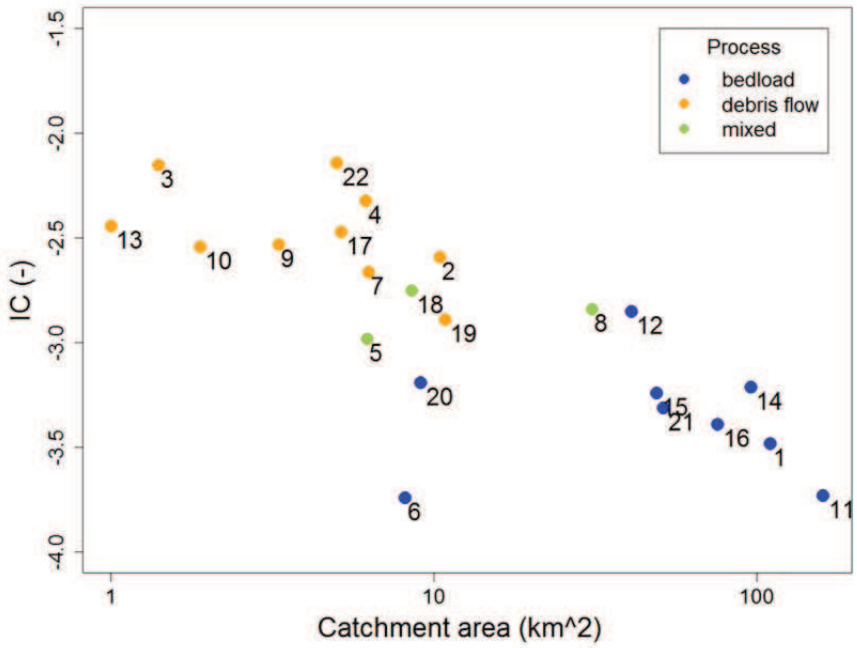

Figure 5. 41: Relationship between mean values of connectivity index calculated with reference to channel network of each basin and drainage area proposed for selected study areas. Selected catchments, represented by numbers (see Tab. 5.14), are grouped into processes characterizing the main channel.

IC referred to the main channel on medium and small basin size follow the same pattern related to processes as for *IC* calculated at the outlet of each catchment.

IC determines the potential connectivity taking into account both the distance to the nearest sink and the properties of the upslope contributing areas. Therefore, the analysis of the relationship between the connectivity index and the drainage area need to consider both components. Figure 5.42 shows that the downslope component is more correlated (R^2 = 0.71 at 0.001 significance level) to basin size than the upslope one whose influence on *IC* is not significant (R^2=0.1).

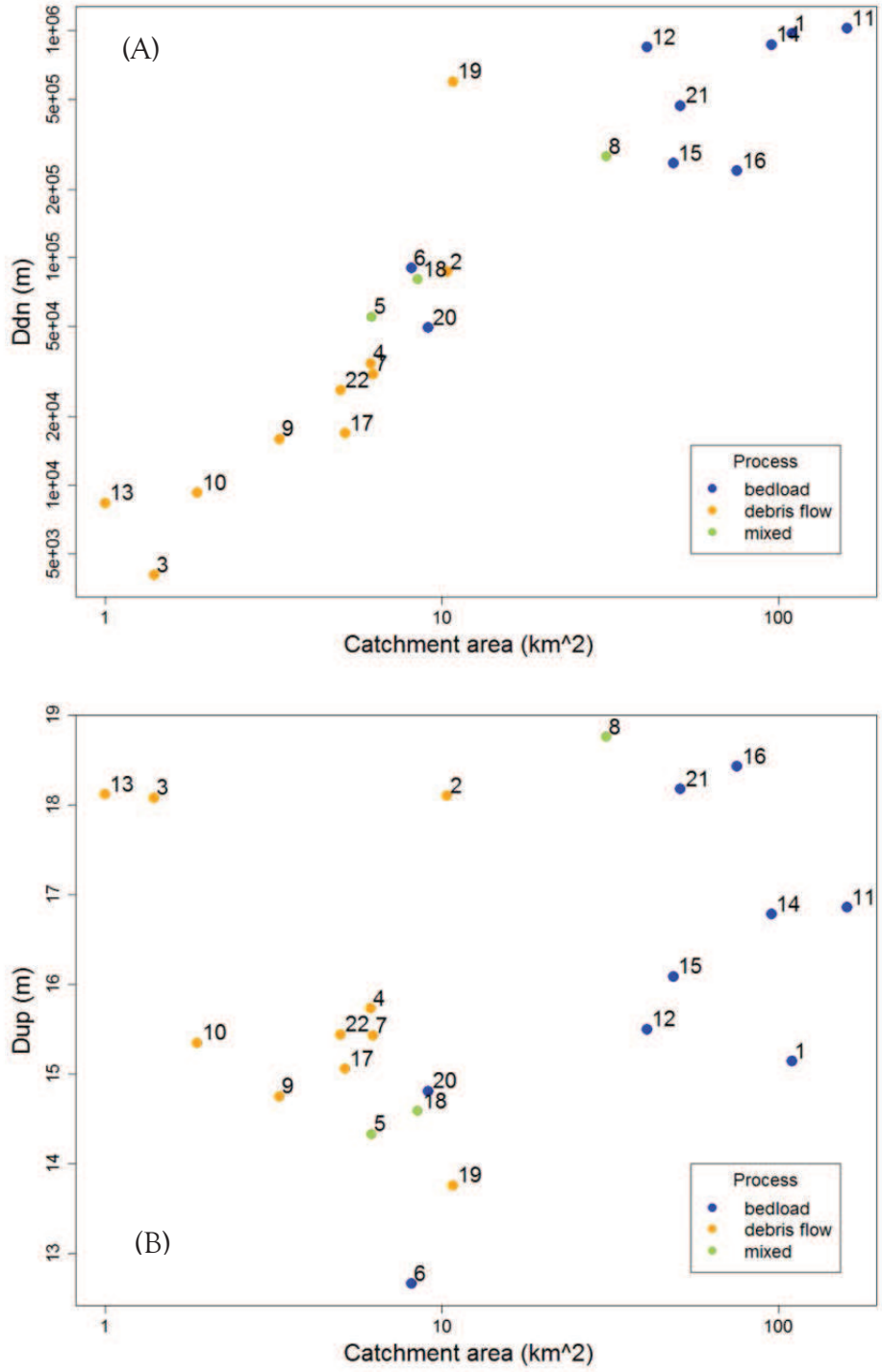

Figure 5. 42: Relation between the upslope (A) and downslope (B) components of the connectivity index, calculated with reference to the outlet, and the drainage area. In each figure, even main process characterizing main channel is reported.

A different pattern can be observed for the downslope and upslope components of *IC* calculated with reference to the channel network (Fig. 5.43). Downslope component is less correlated (R^2=0.15) than the upslope component with drainage area (R^2=0.37).

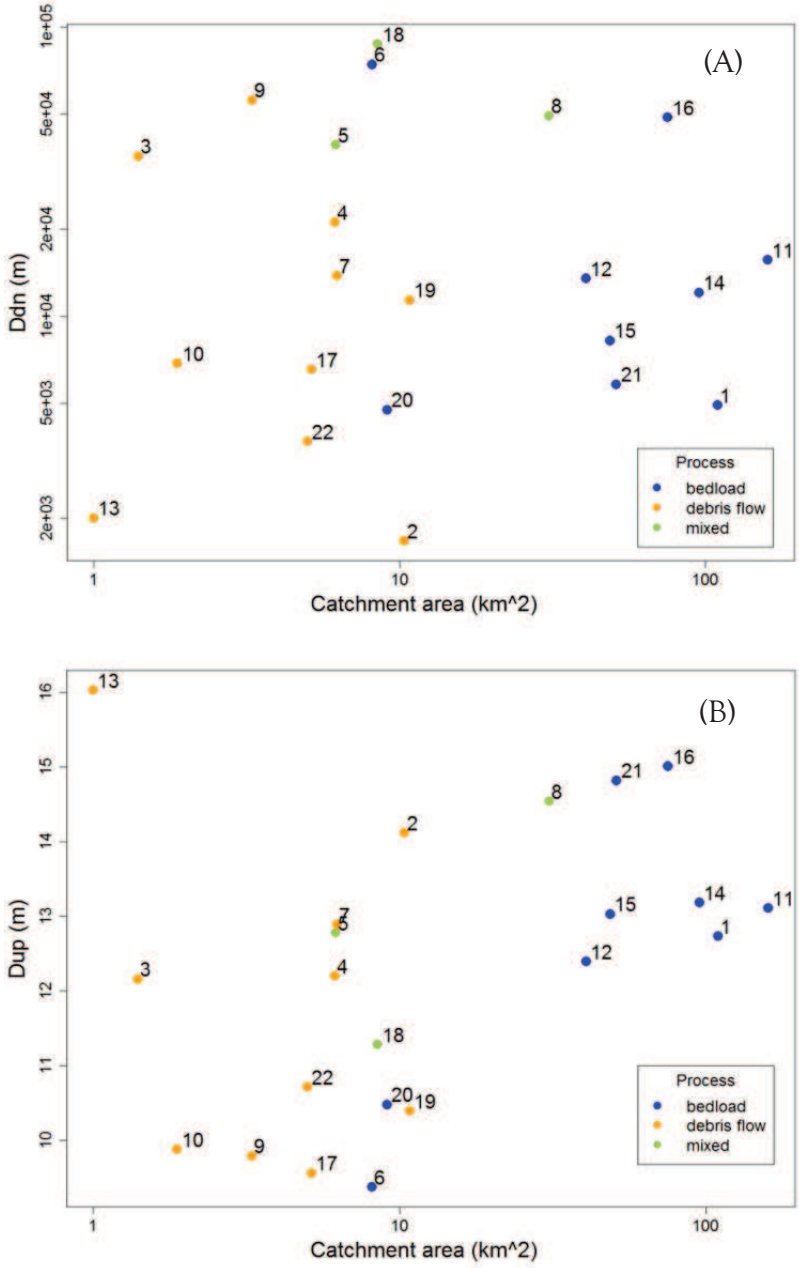

Figure 5. 43: Relation between the downslope (A) and upslope (B) components of the connectivity index, calculated with reference to the main channel, and the drainage area. In each figure, also main process characterizing main channel is reported.

IC mean values calculated at the outlet don't show a clearly defined relation with average slope for each basin (Fig. 5.44). Basins with high slope, and presenting different catchment size, can be characterized by both low or high sediment connectivity, for example Ciardes (number 3) and Vezzano basins (number 22). This result suggests that the *IC* is not a mere index of the mean slope.

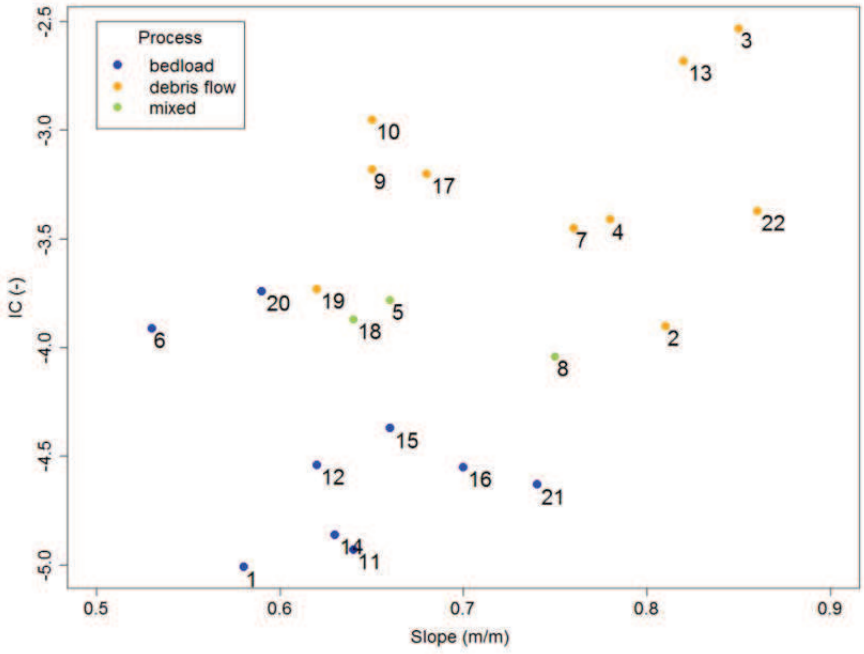

Figure 5. 44: Relation between *IC* mean values calculated with reference to the outlet of each basin and the mean slope of the basin. In each figure, even main process characterizing main channel is reported.

Scatterplot of *IC channels* values and slope (Fig. 5.45) presents a moderate relationship (R^2=0.51 at 0.001 significance level), with the sediment connectivity rising as mean slope increases.

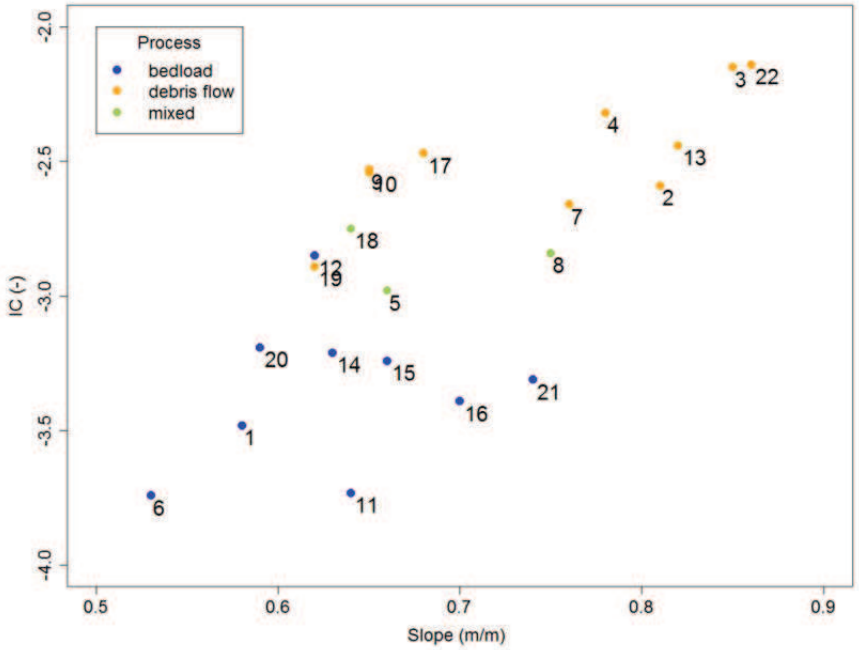

Figure 5. 45: Relation between *IC* mean values calculated with reference to the main channel network of each basin and the mean slope of the basin. In each figure, even main process characterizing main channel is reported.

The connectivity index shows a strong dependency (R^2 = 0.71 and R^2 = 0.65, at the 0.001 significance level for *IC* calculated at the outlet of the basin and at the hydrographic network respectively) on relative relief ratio (Fig. 5.46) in basins characterized by different size and geomorphic processes.

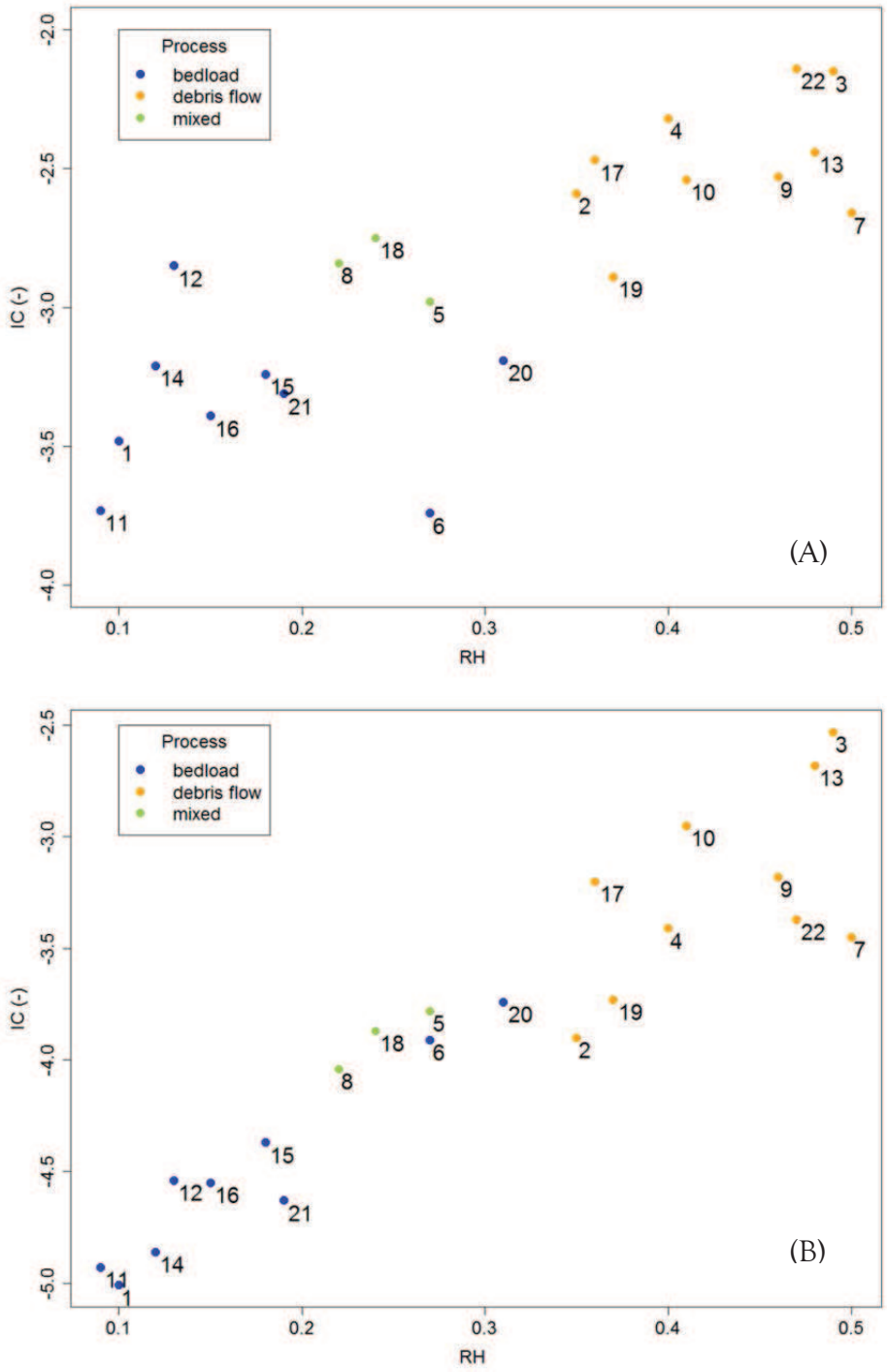

Figure 5. 46: Relation between the mean connectivity index, calculated with reference to the outlet (A) and the main channel of each basin (B), and R_H. In each figure, even main process characterizing main channel is reported.

These results are in good agreement with findings from literature for sediment delivery ratio. For example, Maner (1958), Roehl (1962) and Schumm (1955) found sediment delivery ratio to be highly correlated with relief ratio in morphologically different physiographic areas. Results obtained for a hill region (Red Hills, USA) suggest also that R_H can discriminate sediment delivery ratio in drainage basins presenting different lithologic, structural and dimensional characteristics (Maner, 1963).

IC proved to be independent from the basin shape (Fig. 5.47). Elongation Ratio (*Re*) and Circularity Ratio (*Rc*) calculated for selected basin, according to equations (2.3) and (2.4), are given in Table 5.14.

Re index is found to range from 0.38 to 0.9 indicating a wide variety of morphological characteristics for studied catchments. Basins with elongated shape, such as Carlino (1), Plima (11), Saldura (14), show the lowest *IC* mean values (Fig. 5.47) while circular shape are typical of basins characterized by higher mean connectivity (e.g. Gadria (7), Tanas (19)).

Even though Ciardes (3) and Reschen (13) catchments present low Re values, the high potential of sediment transport can be due to their small drainage area (1 km^2 and 1.4 km^2) and high mean slope values (0.82 m/m and 0.85 m/m) that make runoff discharge more efficient. Basins featuring similar shape (i.e. similar *Re* values) can present different potential of sediment transfer suggesting that connectivity is controlled by other structural and geological factors.

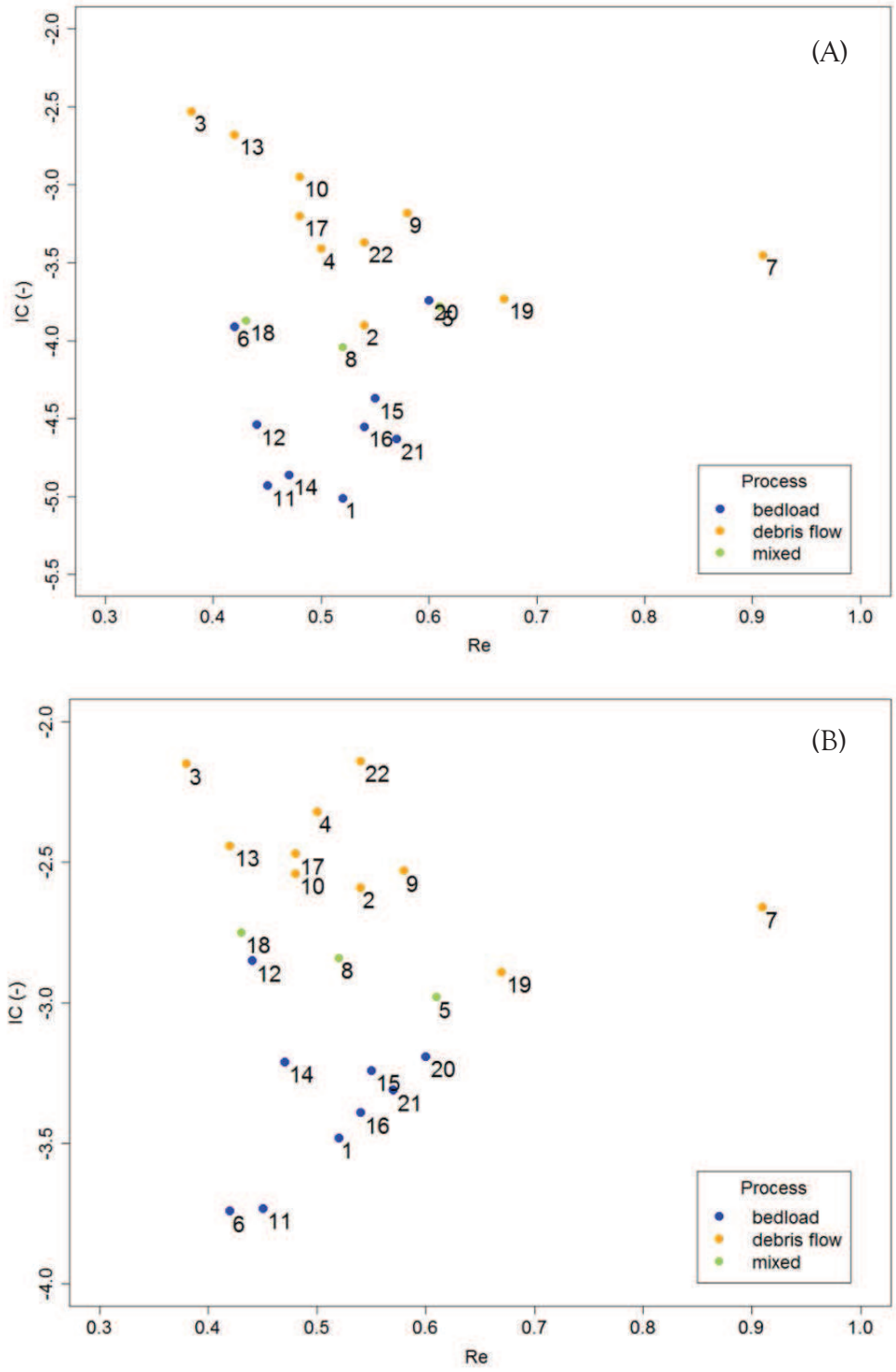

Figure 5. 47: Relation between the mean connectivity index, calculated with reference to the outlet (A) and to the main channel network of each basin (B), and *Re*. In each figure, even main process characterizing main channel is reported.

These observations are also corroborated by scatterplot of *Rc* values versus *IC* outlet and *IC* channel, even if in this case a lower variability of the basin shape index, with values ranging from 0.2 to 0.4, is observed (Fig. 5.48). Basins featuring similar shape show more similar *IC* mean values (e.g. Gadria and Maragno basins) than Re results.

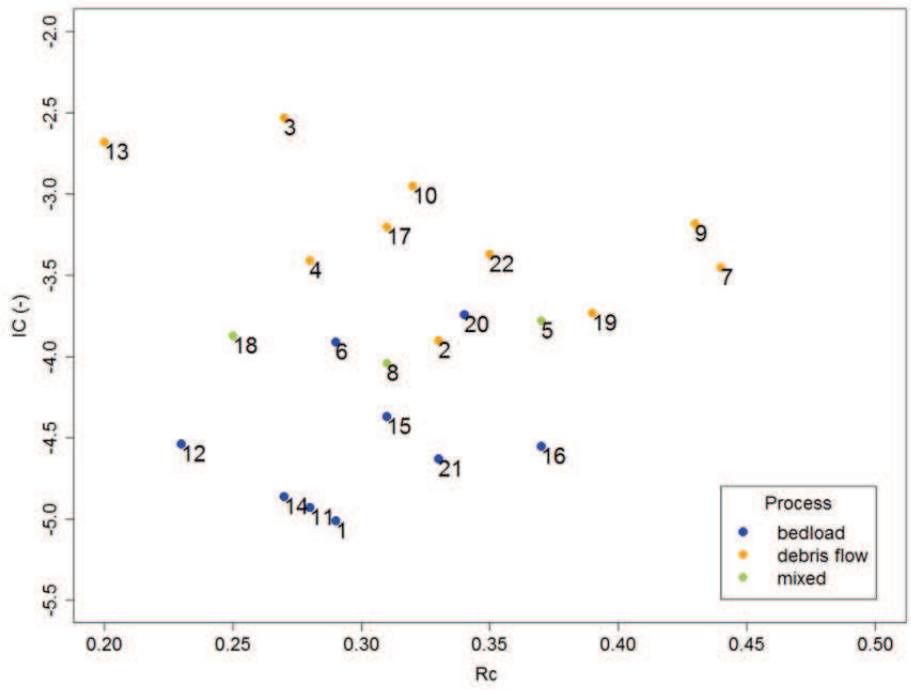

Figure 5. 48: Relation between the mean connectivity index, calculated with reference to the outlet, and *Re*. In each figure, even main process characterizing main channel is reported.

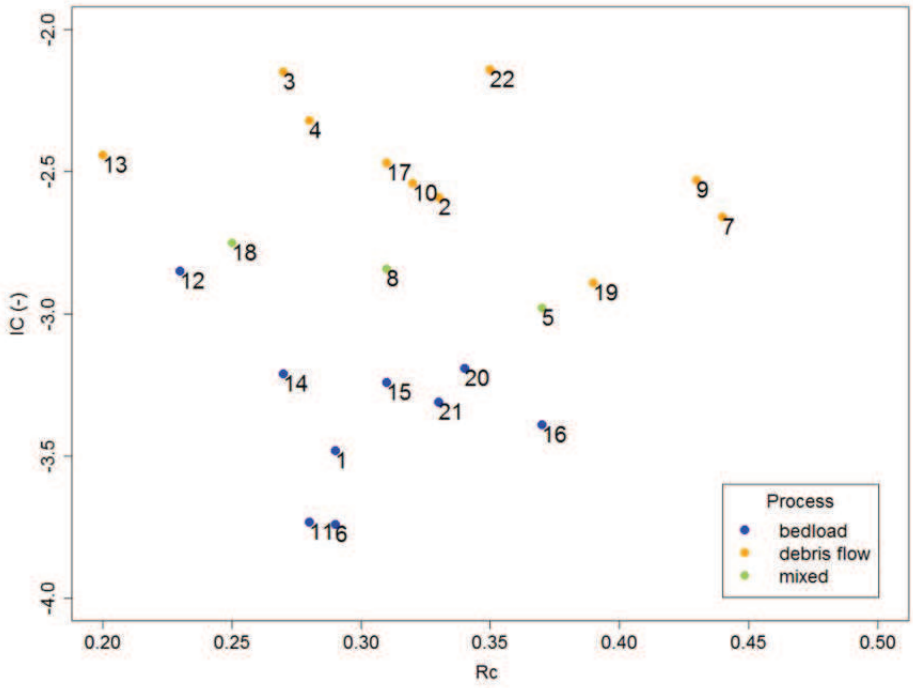

Figure 5. 49: Relation between the mean connectivity index, calculated with reference to the main channel network of each basin, and *Re*. In each figure, even main process characterizing main channel is reported.

Brierley et al. (2006) indicate that the shape of the catchment is a controlling factor of the supply, transfer and storage of sediments through a system when the connectivity is studied in a longitudinal linkage (i.e. from tributary to trunk stream). As suggested by this study, the elongation ratio and circularity ratio cannot sufficiently explain the sediment connectivity as modeled by the *IC* for selected catchments.

The discussion of these results needs to consider the assumption done for the analysis of the relation between the connectivity modeling and both sediment related processes and geomorphometric parameters. In fact, the relationship between the sediment transport capability, both with regard to the outlet and the main channel, of different catchments and geomorphometric parameters, such as area, slope and shape indices, was coupled with the frequency of main sediment

dynamic processes in the main channel rather than the magnitude of events. This aspect can be crucial when analyzing the connectivity. In fact, high-magnitude but infrequent events can lead to a decrease of sediment connectivity by disconnecting some parts of the system: for instance, coarse debris deriving from tributaries can disconnect downstream channels from upstream reaches (Bracken et al., 2014). Alternatively, these type of events can cause an increase of sediment connectivity due to the transport and mobilization of sediment or to the removal of an impedance element, such as a floodplain that before the event disrupted hillslope-channel coupling. On the contrary, higher frequency and smaller magnitude events can continue to release sediments from hillslopes or channel banks, leading to an increase in sediment connectivity (Bracken et al., 2014).

Nonetheless, since time component is not considered in the analysis of sediment connectivity with the quantitative model applied in this study, the definition of the dominant process based on the frequency of events in the main channel can be considered an appropriate compromise between the investigated spatial scale and the possibility to compare different catchment on a unique and simple criterion. Furthermore, the application of the D-infinity approach and the definition of the channel formation threshold value, has proved to be an objective method in good agreement with the goal of the analysis and the best way to compare connectivity in a systematic way between several catchments presenting different characteristics (e.g. morphology, catchment area and shape).

Some important considerations can be derived from the analysis of the relationship between *IC* and geomorphometric parameters. First, the proposed sediment connectivity appears dependent from the catchment size, mainly due to the downslope component of the index or to the slope catchment depending on the chosen target, i.e. the outlet or the main channel of the catchment. This result suggests that the model can be used to compare quantitatively only catchments of similar size.

The *IC* has proved to discriminate between bedload transport and debris flow processes when analyzing the potential sediment connectivity in relation to the area and the relief ratio of the basins. In fact, *IC* is high for basins characterized by small drainage area (up to 10 km^2) and almost circular or round-shaped (RH greater than 0.4) in which debris flow occurred more frequently. This aspect highlights the practical application of the model in relation to the analyzed sediment dynamics in catchment characterized by different process type. Therefore, the *IC* model can be useful when the aim is to analyze the interaction between the dynamic evolution of transport processes and the morphological structure represented by both catchment area and basin concavity and cross sectional slope characteristics (as defined by the RH index) of a drainage basin.

On the contrary, *IC* is not correlated to neither the elongation ratio or the circularity ratio. The shape of the basin is generally linked to the drainage density that influences the connectivity within the system. Therefore further analysis that consider the relation of the order of the tributary streams and the *IC* model could help in the understanding of the relation between sediment connectivity calculated to the main channel and the shape of a catchment. Moreover, the interpretation of sediment connectivity behavior could be better enclosed in the framework of subcatchment scale by analyzing specific subcatchment attributes (e.g. slope of the longitudinal profiles) since within any catchment, different sub-catchments can present different type of landscape units and variability in geomorphic process zones (Brierley and Fryirs, 2005).

5.3.5 Effect of glacier retreat on sediment connectivity

In order to assess the potential connectivity evolution due to glacier melting, the *IC* was applied in the Navizence basin. The input digital elevation model was a 2-m resolution LiDAR derived DTM representing actual morphology (current DTM)

and the DTM, at the same resolution, derived from the application of the sloping local base level (SLBL) technique (Jaboyedoff et al., 2004) to current DTM (post-glacial DTM). The weighting factor expressing the resistance to sediment fluxes was derived from tabled values of hydraulic roughness (Manning's n) for both scenario (Par. 4.5.1.3). Impedance factor values (Fig. 5.49) range from 0.01, corresponding to glacial zone, to 0.15 for vegetated area.

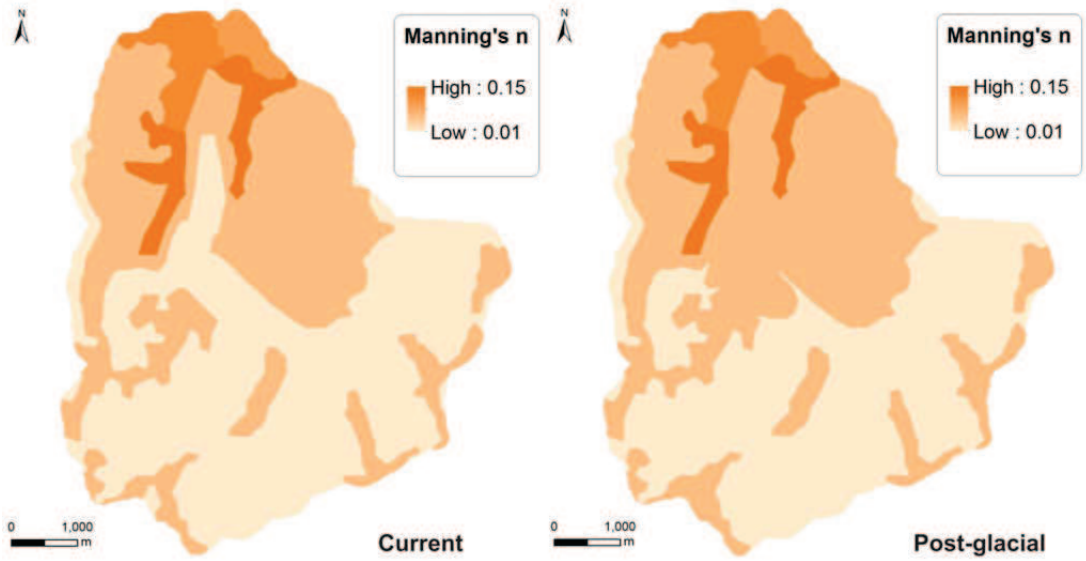

Figure 5. 50: Impedance factor derived for the current and post glacial scenario from the application of Manning's n roughness to land use classification of Zinal catchment.

The difference in the resulting weighting factor is evident in the area where glacier is expected to retreat within a 50 years period. This is due to the fact that, after melting process, the surface is supposed to be composed of debris and bare rocks as the surrounding surface.

The computation of *IC* for the Zinal catchment was carried considering both the catchment outlet and the main channel network as target. In assessing the probability that eroded sediment coming from hillslopes will attain the river network, both actual and future structure of channel system were delineated. In

particular, the actual river network was identified by means of field observations conducted in the lower part of the basin (up to the terminal part of the glacier). The channel pattern in the future scenario reflects the possible variation due to glacier retreat during deglaciation, in response to changing water and sediment.

Spatial maps of modeled *IC* at the outlet for current and post glacial scenario are shown in Figures 5.50 and 5.51. As for Venosta Valley, connectivity values were classified into four classes with the Jenks Natural Breaks algorithm according to *IC* distribution values.

Sediment connectivity calculated for the actual DTM shows a homogeneous pattern, presenting high values of the index also in the upper part of the catchment suggesting that maybe some gullies can play an important role too in delivering sediment to the outlet.

Lower values of the index are found mainly in correspondence with glacier along the basin and with moraine and periglacial deposits that contribute, together with low slope, to sediment decoupling.

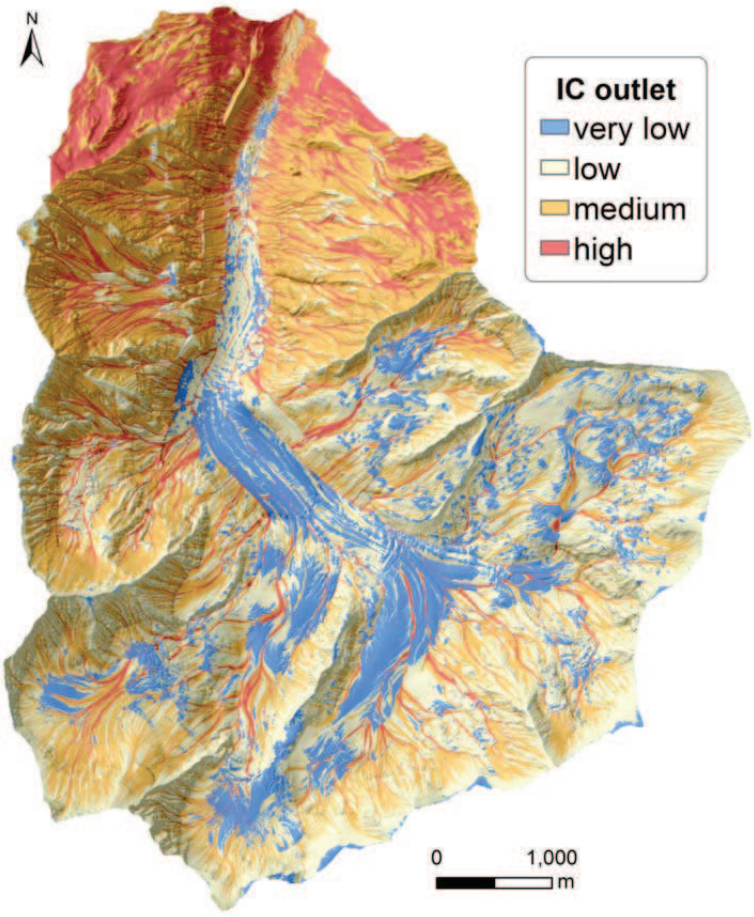

Figure 5. 51: *IC outlet* map for the characterization of sediment connectivity in a pre-glacial scenario.

When excluding decoupled areas, a significant variation can be observed for *IC* modeled in a glacier melting process system (Fig 5.51). The downstream area shows a lower potential connectivity along with the upper part of the basin. On the contrary, the disappearing of the main edifice of the glacier lead to an increase in sediment potential connectivity with higher values on the left bank side than the right side where the future moraine deposits interrupt sediment fluxes.

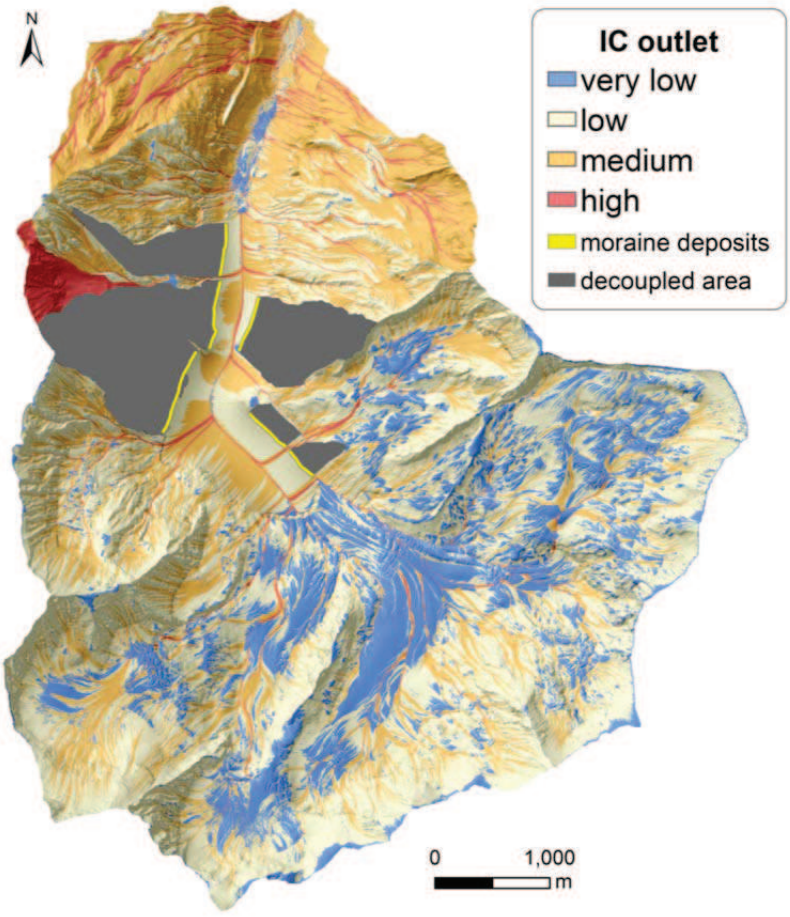

Figure 5. 52: *IC outlet* map for the characterization of sediment connectivity in a post-glacier melting scenario. Grey areas represent area disconnected by moraine deposits that will probably arise after the glacier retreat process.

Analysis of *IC* predictive maps highlight a limited contribute of sediment transport from hillslope during the post glacier retreat scenario.

IC calculated in relation to hydrographic network (Fig 5.52) shows a different pattern of sediment connectivity. Higher values in the *IC* channels map are related to areas and hillslopes adjacent to the main channels in the lower part of the basin, moreover in those channels characterized by steep slopes and very close to the

hydrographic network. The potential sediment transport in the rest of the basin is lower mainly due to simple main channel network and for moderate slope.

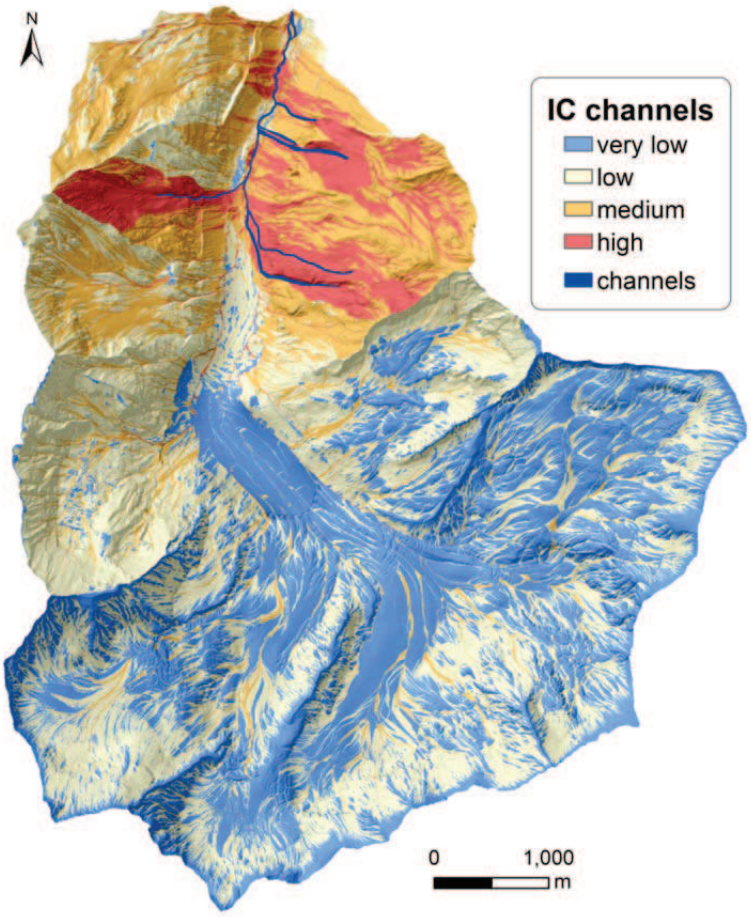

Figure 5. 53: *IC channel* map for the characterization of sediment connectivity in a pre-glacial scenario.

Analysis of *IC* modeling sediment coupling between sediment sources and the hydrographic network reveals a different spatial pattern since potential sediment connectivity changes due to glacier retreating process. In fact, in the map of *IC* related to the outlet the main change is represented by a decrease of connectivity in the downstream part of the catchment, while in the map of *IC* related to channels

the presence of new decoupled areas and an increase in connectivity to other sectors of the Navizence river can be observed (Fig. 5.53).

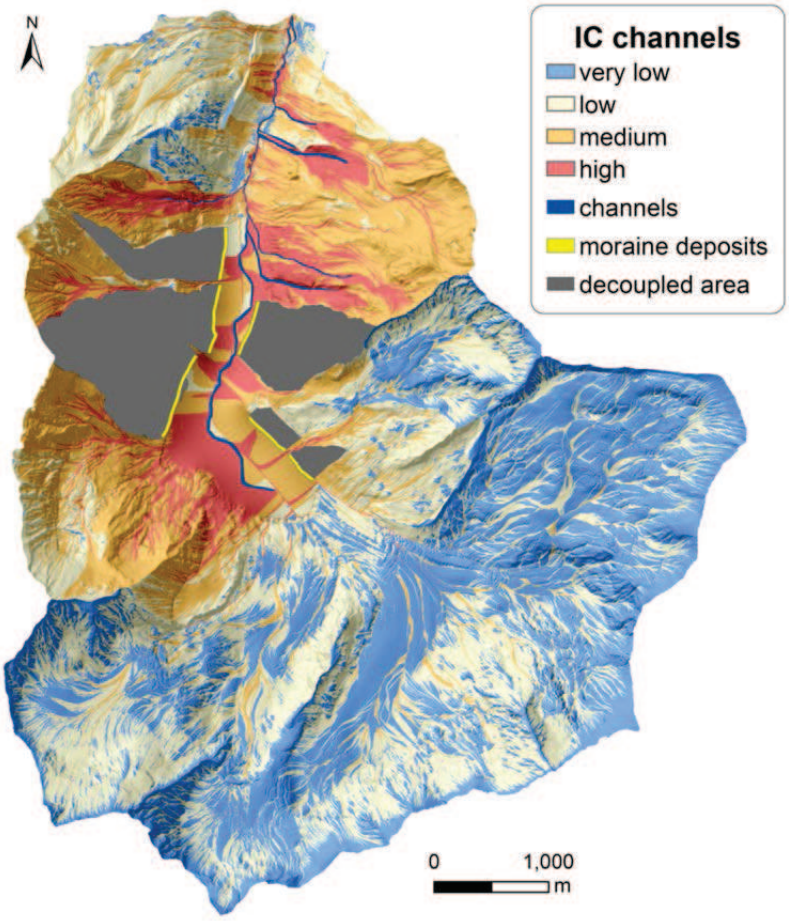

Figure 5. 54: *IC channel* map for the characterization of sediment connectivity in a post-glacier melting scenario. Grey areas represent area disconnected by moraine deposits that will probably arise after the glacier retreat process.

From statistics reported in Table 5.15, it is possible to see that the presence of natural buffers, i.e. lateral moraines, lead to an increase of *IC* values in the unbuffered areas when calculated in relation to channels, whereas no major variation is observed for *IC* related to the outlet.

The analysis of *IC* values need to consider also that post-glacial decoupled areas, buffered by lateral moraines (grey color in Fig. 5.51 and Fig. 5.53), cover 7.5% of the total catchment area.

Table 5. 15: statistical measures for *IC* computed both at the outlet of Navizence catchment (*IC outlet*) and in relation to its actual and future main channel (*IC channel*) in a pre- and post- glacier melting scenario.

Statistics	*IC outlet*		*IC channel*	
	PRE	POST	PRE	POST
Minimum	-7.15	-7.13	-6.99	-6.78
Maximum	-0.015	2.35	3.31	3.19
Mean	-4.41	-4.36	-3.95	-3.43
Median	-4.45	-4.40	-4.18	-3.66
First quartile	-4.75	-4.68	-4.53	-4.09
Third quartile	-4.09	-4.07	-3.61	-2.85

The application of *IC* to the Navizence catchment has enabled assessing of the evolution of the sediment potential connectivity of the studied landform taking into account the temporal dynamic of the glacier system. Based on the assumption that moraine deposits act as buffering elements for sediment transport, the changes of the coupling system in a catchment featuring glacier retreat can be analyzed.

The computation of *IC* model to Navizence catchment allows a qualitative estimation of the future behavior of sediment connectivity in relation to the glacier fluctuation. In fact, the degree of connectivity in Zinal glacier is a key control on sediment delivery affecting hillslope and meltwater sediment delivery.

Scenarios of future sediment fluxes from glacial zone would depend critically on the development of lateral moraines.

It is important to stress the fact that the applied SLBL to derive the melt surface of the glacier is a geometric procedure that excavates iteratively the topography.

Therefore it doesn't take into account the real glacier bed structure, providing only a proxy of the future morphological feature. Although a more accurate knowledge of the glacier bed topography evolution would be required in order to improve the model and predict its future influence on the (de)coupling system, the proposed approach can contribute to the development of a rapid forecast tool helping the understanding of hillslope to channel sediment connectivity changes.

CHAPTER 6

CONCLUSIONS

In this study, geomorphometric methods for the analysis of sediment dynamics related to debris flows and bedload transport at different spatial and temporal scale have been developed and tested. The analyses were conducted in different study areas located in the oriental Alps of northern Italy and in the Swiss Alps.

Geomorphic changes in two small catchments (Gadria and Strimm) were analyzed from LiDAR repeated surveys by applying a method based on the fuzzy logic (FIS) that considers a spatially distribution of elevation errors. The resulting DTM of Difference (DoD) permitted to characterize the elevation differences deriving from multiple events (debris flows, flood, bedload), occurred in a six years period, recovering variations of small magnitude that could be lost, especially in low slope areas, if a raw method or a spatially uniform threshold would be applied. Moreover, meaningful results on erosion and deposition processes were derived even if input DTMs present a different accuracy, highlighting the possibility to use the DoD for different research and practical aims. The application of a two-input FIS based on survey quality (i.e., ground point density) and on the surface morphology (i.e., slope) allowed the interpretation of geomorphic changes and the estimate of erosion and deposition volumes from data presenting both high and low accuracy, highlighting the possibility to use the DoD in complex morphologic surfaces and at basin scale.

The availability of data from field observations on events occurred in analyzed basins in the same period of LiDAR surveys (2005-2011) permitted the comparison between post-event field surveys and calculated geomorphic changes. The analysis proved the consistency of the volume quantification derived from DoD with field estimates and it

encourages the integration of these two approaches. This integrated approach may permit overcoming limitations of both methods. In fact, some restrictions of DoD are associated to the approximations of input data, especially when data derived from aerial LiDAR surveys present different accuracy, like in the case considered in this study. Moreover, DoD estimation of erosion and sediment depositions usually encompasses several events since topographic surveys at very short time intervals are hardly to apply on large areas due to economic and time constraints. Concerning field surveys, usually no quantitative measurements of erosion are performed and the assessment of deposits is limited to the sites where large deposits occur, thus disregarding smaller deposits whose total volume can be relevant at catchment scale.

Therefore, the analysis of the comparison of field and remote sensing surveys suggests the integration of both approaches that can lead to some advantages:

- DoD may put on evidence erosion and deposition areas that were remained unsurveyed during post-event observations because they were located far away from element at risk for floods, erosion and debris flows;
- Post-event surveys enable expert evaluation of phenomena that may increase the informative content of DoD estimates of erosion and deposition, thus permitting of linking topographic variations to local features observed in the field just after floods and debris flows.

Furthermore, the relation between DoD results and morphometric parameters such as plan and profile curvature, slope and area was investigated. A correspondence between eroded area as computed by the DoD and the change from convex to concave areas as represented by the plan and profile curvature, as well as between deposition areas and change from flat and concave to convex curvature, was observed. Types of erosion and deposition pattern can be detected for channel network and adjacent areas by the slope-area diagram which also highlights areas of concentrated erosion and deposition.

Results highlight the possibility to use geomorphometric parameters in an innovative way since the analyzed relationships offer a new perspective on the interpretation of temporal changes besides the estimate of erosion and deposition volumes. In fact, these relationships allow the analysis of the interactions between the landscape evolution and the dynamic of sediment transport processes involved, especially when morphological changes are due to effect of multiple events. Furthermore, they could be helpful as preliminary analysis for hazard mapping and for the recognition of stable or susceptible areas.

The analysis of spatial scale, including geographic and computational scales, was performed by applying a distributed geomorphometric index of sediment connectivity (*IC*) on selected study areas.

The effect of the grid size on the connectivity index was analyzed at both basin and regional scale. This issue was addressed by looking at the dependence of the main statistics (e.g. mean, median, standard deviations) of the *IC* and of its spatial distribution from cell size at different scales.

At basin scale, statistical values of the topographic based index slightly depend on the DTM resolution, tending to increase as resolution decreases, mainly due to the effect of the downslope component on *IC*. Regardless the chosen target (i.e. the outlet of the basin or the main channel), reliable results in terms of spatial pattern representation of sediment connectivity have been obtained when using a more detailed description of the topography. At regional scale, *IC* exhibits a different sensitivity on the grid resolution according to the chosen target since the downslope component influence is more evident when *IC* is calculated with reference to the channel network: as resolution decreases, calculated statistics for *IC* tend to increase and the spatial representativeness at local scale of sediment connectivity varies differently according to different cell sizes.

Therefore, results on DTM resolution analysis suggest that a fine resolution (1 m) should be applied when analyzing sediment connectivity at basin scale whereas at regional scale the choice of the cell size depends on the aim of the research (i.e. the chosen sink for the analysis of sediment connectivity) and the interpretation of local patterns variability should be combined with specific field survey.

Relations between size, slope, shape of basins, main sediment transport process, and IC were investigated at basin scale, considering both the channel network and the catchment outlet as target of the analysis. Results on such analysis entail important implications:

- strong dependence of *IC* on drainage area suggests that the sediment connectivity index as lumped parameter is suitable only for comparison between catchments of similar size;
- the absence of a correlation between *IC* and mean slope of the basin points out that the *IC* is not merely an indicator of the slope but it considers other important factors linked to sediment transport dynamics and morphology;
- the *IC* channels is able to discriminate between sediment transport processes (debris flows, floods with bedload) for different basins, moreover when the computation is performed in relation to main channel network;
- the lack of correlation between catchment shape and *IC* reveals that the shape is not a good indicator in differentiating sediment connectivity patterns at catchment scale.

To date, the assessment of spatial connectivity by means of *IC* was mainly performed on rather small areas. In this study, the application of the connectivity index *IC* to the Venosta valley (1210 km^2) represents one of the first attempts to study the sediment connectivity at larger scale. Predictive maps of sediment connectivity, related to both the outlet of the Venosta valley and to the main channel (Adige river), depict realistic

sediment patterns, highlighting potential coupled and decoupled areas. In particular, the model permitted to evaluate the role of alluvial fans in the overall framework of sediment connectivity. In fact, these geomorphologic features favor the coupling of the upstream catchments and of the opposite hillslopes with the main river but they also show a great variability between sectors of high and low connectivity in the fan body. The modeling approach could help so in the interpretation of the dual role of alluvial fans, as coupling and decoupling features, at large scale and when complex morphologies are involved.

The connectivity index focused on the influence of topography and vegetation cover and type on sediment connectivity, since two different impedance factors are taken into account, based on the topographic roughness index (*RI*) and the Manning's n values. Realistic patterns of sediment connectivity are obtained for both regional and basin scale by applying the two mentioned weighting factors accordingly to chosen scale, respectively Manning's n for regional areas and *RI* for basin scale. This lead to the possibility of applying the proposed index in mountain basins where a wide variety of morphological characteristics and land uses occur. A limit of such approach is that values range for topographic roughness is lower than the range of Manning's n values, maybe due the normalization of both parameters as required by the connectivity model. Future research on this topic would suggest an improvement of the characterization and standardization of weighting factors values.

A valuable feature of IC application at large scale is that it allows a preliminary exploration of potential sediment connectivity over large areas, overcoming field mapping limits since they could be time consuming and hardly feasible due to the presence of steep reliefs and of dense vegetation cover areas (van Asselen and Seijmonsbergen, 2006). Moreover, the advantage of such an automated mapping is that it can be easily updated and combined with other thematic layers in geographic

information system (GIS) for different applications, including the exploration of landscape change scenarios. The study case of Navizence catchment (Switzerland) represents an example of these applications. The time domain was integrated with the spatial scale by investigating the sediment connectivity evolution due to glacier retreat in the Swiss alpine basin. The connectivity index was computed on two successive high-resolution DTMs representing respectively the present morphology (2010) and the future surface, derived from the application of the slope local base level (SLBL) to the actual DTM, describing the terrain after fourty years of glacier retreat.

Although a more accurate knowledge of the glacier bed topography evolution is required in order to improve the model and predict its future influence on the (de)coupling system, the applied procedure allowed a qualitative estimation of the future behavior of sediment connectivity in relation to the glacier fluctuation. It also emphasizes the role of lateral moraines development in influencing the future sediment fluxes from the glacial zone, acting as barriers for the downward sediment transport.

The flexibility of *IC* lays on its applicability to a wide variety of planning scenarios. For instance, by applying Manning's n to subsequent land use maps, qualitative information on consequences of land use changes on sediment connectivity dynamic can be provided. The impact of open check dams building on sediment coupling and decoupling processes can be also investigated by incorporating these targets in the connectivity model.

Qualitative information derived from *IC* maps would allow a rapid characterization of sediment connectivity changes at large scale that could address stakeholders and decision makers to make choices regarding land management in mountainous areas encompassing different morphologies and sediment transport processes.

BIBLIOGRAPHY

Abermann J, Fischer A, Lambrecht A, Geist T. 2010. On the potential of very high-resolution repeat DEMs in glacial and periglacial environments. *Cryosphere*, **4**: 53-65. DOI: doi:10.5194/tc-4-53-2010.

Abramov, O., McEwen, A., 2004. Technical note: An evaluation of interpolation methods for Mars Orbiter Laser Altimeter (MOLA) data. International Journal of Remote Sensing 25, 669-676.

Adams, J.D., Visser R.J.M., Prisley S.P., 2003. Modeling steep terrain harvesting risks using GIS: High Tech Forest Operations for Mountainous Terrain, Stift Schlaegl, Austria.

Aguilar F.J., Agüera F., Aguilar M.A., Carvajal F., 2005. Effects of terrain morphology, sampling density, and interpolation methods on grid DEM accuracy. Photogrammetric Engineering and Remote Sensing, 71: 805-816.

Alatorre L.C., Begueria S., Garcìa-Ruiz J.M., 2010. Regional scale modeling of hillslope sediment delivery: A case study in the Barasona Reservoir watershed (Spain) using WATEM/SEDEM, Journal of hydrology, Volume 391, Issues 1-2, pp. 109-123.

Axelsson P., 1999. Processing of laser scanner data – algorithms and applications. ISPRS Journal of Photogrammetry & Remote Sensing, 54(1999): 138-147.

Baartman, J.E.M., Masselink, R., Keesstra, S.D., Temme, A.J.A.M., 2013. Linking landscape morphological complexity and sediment connectivity. Earth Surface Processes and Landforms, 38(12), 1457-1471.

Baldo M., Bicocchi C., Ciocchini U., Giordan D., Lollino G., 2009. LIDAR monitoring of mass wasting processes: The Radicofani landslide, Province of Siena, Central Italy, Geomorphology 105, pp. 193–201.

Band L.E., 1986.Topographic partition of watersheds with digital elevation models Water Resource Research, 22 ,pp. 15–24

Bangen S. G., Wheaton J.M., Bouwes N., Bouwes B., Jordan C., 2014. Amethodological intercomparison of topographic survey techniques for characterizing wadeable streams and rivers, Geomorphology 206, pp. 343-361.

Barrand NE, Murray T, James TD, Barr SL, Mills JP. 2009. Optimizing photogrammetric DEMs for glacier volume change assessment using laser-scanning derived ground-control points. *Journal of Glaciology,* **55**: 106-116. DOI: 10.3189/002214309788609001.

Bater, C.W., Coops, N.C., 2009. Evaluating error associated with lidar-derived DEM interpolation. Computers & Geosciences 35, 289-300.

Beel C.R., Orwin J.F., Holland P.G., 2011. Controls on slope-to-channel fine sediment connectivity in a largely ice-free valley, Hoophorn Stream, Southern Alps, New Zealand. Earth Surface Processes and Landforms 36, 981-994.

Bennett, G.L., Molnar, P., Eisenbeiss, H., McArdell, B.W., 2012. Erosional power in the Swiss Alps: characterization of slope failure in the Illgraben. Earth Surf. Proc. Land.,37,1627–1640.

Bishop M.P., 2013. Remote sensing and GIScience in geomorphology: Introduction and overview. In: J. Shroder (editor in chief), M.P. Bishop (ed.), Treatise on Geomorphology. Vol. 3. Remote Sensing and GIScience in Geomorphology. Academic Press, San Diego: 1–24.

Blasone G., Cavalli M., Marchi L., Cazorzi F., 2014. Monitoring sediment source areas in a debris-flow catchment using terrestrial laser scanning, Catena, 123, pp. 23-36.

Blaszczynski, J.S., 1997. Landform characterization with geographic information systems, Photogrammetric Engineering 6. Remote Sensing, 63:183-191.

Booth, A.M., Roering, J.J., Perron, J.T., 2009. Automated landslide mapping using spectral analysis and high-resolution topographic data: Puget Sound lowlands, Washington, and Portland Hills, Oregon. Geomorphology 109, 132–147.

Borselli, L., Cassi, P., Torri, D., 2008. Prolegomena to sediment and flow connectivity in the landscape: A GIS and field numerical assessment. Catena, 75(3), 268-277.

Boyce R.C., 1975. Sediment routing with sediment delivery ratios. Present and Prospective Technology for Predicting Sediment Yield and Sources, Publ. ARS-S-40, U.S. Department of Agriculture, Washington, D.C. (1975), pp. 61–65.

Bracken L. J., Croke J., 2007. The concept of hydrological connectivity and its contribution to understanding runoff-dominated geomorphic systems. Hydrological Processes 21: 1749-1763.

Brardinoni F, Church M, Simoni A, Macconi P., 2012. Lithologic and glacially conditioned controls on regional debris-flow sediment dynamics. Geology 40(5):455–458.

Brasington J., Rumsby B.T., McVey R.A., 2000. Monitoring and modelling morphological change in a braided gravel-bed river using high resolution GPS-based survey. Earth Surface Processes and Landforms, 25, 9, pp. 973-990.

Brasington J., Langham J., Rumsby B., 2003. Methodological sensitivity of morphometric estimates of coarse fluvial sediment transport. Geomorphology, 53 (3-4) , pp. 299-316.

Brasington J, Wheaton J., Williams RD, 2004. Sub-Reach Scale Morphological Interpretations from DEM Differencing: Accounting for DEM Uncertainty, Eos Trans. AGU, 85(47): Fall Meeting Supplement, Abstract H43A-0352.

Brewer PA., Passmore DG, 2002. Sediment budgeting techniques in gravel bed rivers, in: In Sediment Flux to Basins:Causes, Controls and Consequences, Special Publication 191 (Edited by S J & Frostick L), Geological Society,London, pp. 97-113.

Bremer M., Sass O., 2012. Combining airborne and terrestrial laser scanning for quantifying erosion and deposition by a debris flow event Geomorphology, 138 (1) , pp. 49-60.

Brierley G., Fryirs K., 2005. Geomorphology and River Management: Applications of the River Styles Framework. Blackwell Publishing, Oxford, UK, 398 pp.

Brierley, G., Fryirs, K., Jain, V., 2006. Landscape connectivity: the geographic basis of geomorphic applications. Area, 38(2), 165-174.

Brunsden D., Thornes, J.B., 1979. Landscape sensitivity and change. Transactions of the Institute of British Geographers 4, 463-484.

Brunsden D., 1993. Barriers to geomorphological change. In: Thomas, D. S. G., Allison, R. J. (Eds.), Landscape Sensitivity. Wiley, Chichester, U.K., pp 7 – 12.

Brunsden, D., 2001. A critical assessment of the sensitivity concept in geomorphology. Catena 42, 99-123.

Bubenzer O., Bolten A., 2008. The use of new elevation data (SRTM/ASTER) for the detection and morphometric quantification of Pleistocene megadunes (draa) in the eastern Sahara and the southern Namib, Geomorphology, 102, 221-231.

Bull JM, Miller H, Gravley DM, Costello D, Hikuroa DCH, Dix JK. 2010. Assessing debris flows using LIDAR differencing: 18 May 2005 Matata event, New Zealand. *Geomorphology*, **124**: 75-84. DOI: 10.1016/j.geomorph.2010.08.011.

Burrough, P., McDonnell, R., 1998. Principles of Geographic Information Systems. Oxford University Press, New York, NY. 333 pp.

Caine N., Swanson, F.J., 1989. Geomorphic coupling of hillslope and channel systems in two small mountain basins. Zeitschrift Fur Geomorphologie 33, 189-203.

Carley J.K., Pasternakc G.B., Wyrick J.R., Barker J., Bratovich P. M., Massa D. A., Reedy G.D., Johnson T.R., 2012. Significant decadal channel change 58–67 years post-dam accounting for uncertainty in topographic change detection between contour maps and point cloud models, Geomorphology 179, pp. 71–88.

Cavalli M., 2009. Caratterizzazione idrologica e morfologica dei bacini montani mediante scansione laser da aeromobile. Tesi di dottorato di ricerca, Dipartimento Territorio e Sistemi Agro-Forestali, Università degli Studi, Padova, 186 pp.

Cavalli M., Grisotto S., 2006. Individuazione con metodi GIS delle aste torrentizie soggette a colate detritiche: applicazione al bacino dell'alto Avisio (Trento). In: Le sistemazioni idraulico-forestali per la difesa del territorio, Quaderni di Idronomia Montana, 26, 83-94.

Cavalli M., Marchi L., 2008. Characterisation of the surface morphology of an alpine alluvial fan using airborne LiDAR. Nat. Hazards Earth Syst. Sci., 8, 323–333.

Cavalli M., Tarolli P., Marchi L., Dalla Fontana G., 2008. The effectiveness of airborne lidar data in the recognition of channel-bed morphology, Catena, 73(3): 249-260.

Cavalli M., Trevisani S., Comiti F., Marchi L. 2013. Geomorphometric assessment of spatial sediment connectivity in small Alpine catchments, Geomorphology, Volume 188, 15 April 2013, pp. 31-41.

Carley, J. K., Pasternack, G. B., Wyrick, J. R., Barker, J. R., Bratovich, P. M., Massa, D. A., Reedy, G. D., Johnson, T. R. 2012. Significant decadal channel change 58-67 years post-dam accounting for uncertainty in topographic change detection between contour maps and point cloud models. Geomorphology, doi:10.1016/j.geomorph.2012.08.001.

Carrivick JL, Geilhausen M, Warburton J, Dickson NE, Carver SJ, Evans AJ, Brown LE. 2013. Contemporary geomorphological activity throughout the proglacial area of an alpine catchment. *Geomorphology* 188, pp. 83-95.

Coe J. A., Glancy P. A., Whitney J.W., 1997. Volumetric analysis and hydrologic characterization of a modern debris flow near Yucca Mountain, Nevada, Geomorphology, , Volume 20, Issues 1–2, pp. 11-28.

Comiti F., Marchi L., Macconi P., Arattano M., Bertoldi G., Borga M., Brardinoni F., Cavalli M., D'Agostino V., Penna D., Theule J., 2014. A new monitoring system for debris flows in the European Alps: first observations in the Gadria basin, Natural Hazards, DOI 10.1007/s11069-014-1088-5.

Corsini A., Borgatti L., Cervi F., Dahne, A., Ronchetti F., Sterzai P, 2009 a. Estimating mass-wasting processes in active earth slides – earth flows with time-series of High-Resolution DEMs from photogrammetry and airborne LiDAR, Nat. Hazards Earth Syst. Sci., 9, pp. 433-439.

Corsini A, Cervi F, Daehne A, Ronchetti F. 2009 b. Coupling geomorphic field observation and LiDAR derivatives to map complex landslides. In *Landslide Processes from Geomorphologic Mapping to Dynamic Modelling*, Malet JP, Remaitre A, Bogaard T (eds) CERG Editions: Strasbourg, France; 15–18. ISBN 2-9518317-1-4.

Crema S., 2014. Hydrologic control on the triggering and magnitude of debris flows in alpine catchments, PhD Thesis, University of Padova, Padova, pp. 194.

Croke, J., Todd P., Thompson C., Watson F., Denham R., Khanal G., 2013. The use of multitemporal LiDAR to assess basin-scale erosion and deposition following the catastrophic January 2011 Lockyer flood, SE Queensland, Australia. Geomorphology, 184,(0): 111-126.

D'Agostino V., Bertoldi G., 2014. On the assessment of the management priority of sediment source areas in a debris-flow catchment, Earth Surface Processes and Landforms Volume 39, Issue 5, pp. 656–668.

Daniel, C., Tennant, K., 2001. DEM quality assessment. In: Maune, D.F. (Ed.), Digital Elevation Model Technologies and Applications: The DEM User Manual, 1st ed.ISBN: 1-57083-064-9, pp. 395–440.

Del Favero, R., 2004. I Boschi delle Regioni Alpine Italiane. Tipologia, funzionamento, selvicoltura. Coop. Libraria Editrice Università di Padova (PD), pp. 599 (con CDROM).

Delong SB, Prentice CS, Hilley GE, Ebert Y. 2012. Multitemporal ALSM change detection, sediment delivery, and process mapping at an active earthflow. *Earth Surface Processes and Landforms,* **37**: 262-272.

De Rose RC, Basher LR 2011. Measurement of river bank and cliff erosion from sequential LIDAR and historical aerial photography. Geomorphology 126(1-2): 132-147.

Dewitte O., Jasselette JC, Cornet Y, Van Den Eeckhaut M, Collignon A, Poesen J, Demoulin A. 2008. Tracking landslide displacements by multi-temporal DTMs: A combined aerial stereophotogrammetric and LIDAR approach in western Belgium. Engineering Geology, 99: 11-22.

Dietrich,W.E., C.J. Wilson, D.R. Montgomery, J. McKean, 1993. Analysis of erosion thresholds, channel networks, and landscape morphology using a digital terrain model, J. of Geol., 101, pp.259-278.

Dikau, R, 1989. The application of a digital relief model to landform analysis in geomorphology. In: RAPER, J. (ed): Three dimensional applications, in Geographical Information Systems, pp.51-77.

Downer, C. W., W. James, A. Byrd, and G. Eggers. 2002. Gridded surface subsurface hydrologic analysis (GSSHA) simulation of hydrologic conditions and restoration scenarios for the Judicial Ditch 31 Watershed. MN, ERDC WQTN AM-12.

Engman, E. T. 1986. Roughness coefficients for routing surface runoff. J. Irr. and Drain. Engr. 112(1): 39-53.

Evans, L S., 1972. General geomorphometry, derivation of altitude and descriptive statistics. In Chorley, R. J. (Ed) Spatial Analysis in Geomorphology.Methuen.London

FEMA, 2003. Guidelines and Specifications for flood hazard mapping partners, Appendix A: Guidance for aerial mapping and surveying, www.fema.gov.

Ferro V., Minacapilli M., 1995. Sediment delivery processes at basin scale, Hydrological Sciences Journal, 40:6, 703-717.

Fisher P. F., Tate N. F., 2006. Causes and consequences of error in digital elevation models. Progress in Physical Geography, 30, pp. 467-489.

Fleming, M. D. and Hoffer, R. M., 1979. Machine processing of landsat MSS data and DMA topographic data for forest cover type mapping. LARS Technical Report 062879. Laboratory for Applications of Remote Sensing, Purdue University, West Lafayette, Indiana.

Flood, M., 2004. ASPRS Guidelines Vertical Accuracy Reporting for Lidar. Available online: http://www.asprs.org/a/society/committees/lidar/Downloads/Vertical_Accuracy_Reporting_for_Lidar_Data.pdf

Fourniadis I.G., Liu J.G. , Mason P. J., 2007. Landslide hazard assessment in the Three Gorges area, China, using ASTER imagery: Wushan-Badong. Geomorphology, 84 (1-2): 126-144.

Frankel K.L., Dolan, J.F., 2007. Characterizing arid-region alluvial fans with airborne laser swath mapping digital topographic data. Journal of Geophysical Research — Earth Surface 112, F02025. http://dx.doi.org/10.1029/2006JF000644.

Fryirs, K., Brierley, G. J., Preston, N. J. and Kasai, M. 2007 (a). Buffers, barriers and blankets: The (dis)connectivity of catchment-scale sediment cascades. Catena, 70, 49-67.

Fryirs K., Brierley, G. J., Preston, N. J. and Spencer, J. 2007 (b). Catchment-scale (dis)connectivity in sediment flux in the upper Hunter catchment, New South Wales, Australia. Geomorphology, 84, 297-316.

Fryirs K., 2013. (Dis)Connectivity in catchment sediment cascades: a fresh look at the sediment delivery problem. Earth Surface Processes and Landforms 38, 30-46.

Fuller I.C., Large A.R.G., Charlton M.E., Heritage G.L., Milan D.J., 2003. Reach-scale sediment transfers: an evaluation of two morphological budgeting approaches Earth Surf. Process. Landf., 28 (8), pp. 889–903.

Fuller IC, Marden M. 2010. Rapid channel response to variability in sediment supply: Cutting and filling of the Tarndale Fan, Waipaoa catchment, New Zealand. *Marine Geology*, **270**: 45-54. DOI: 10.1016/j.margeo.2009.10.004.

Fuller I.C., Marden M., 2011. Slope–channel coupling in steepland terrain: a fieldbased conceptual model from the Tarndale gully and fan, Waipaoa catchment, New Zealand. Geomorphology 128, 105–115.

Fumeaux D., Reynard E., 2002. Les fluctuations récentes des glaciers du val de Zinal (Ayer, Valais) selon les sources historiques, in Bulletin de la Maurithienne, 120, p.7-18.

Gallant, J. C., and J. P. Wilson, 2000, Primary topographic attributes, in Terrain Analysis: Principles and Applications, edited by J. P. Wilson and J. C. Gallant pp. 51-86, John Wiley, Hoboken, N.J.

Ghoshal S., james L.A., Singer M.B., Aalto R., 2010. Channel and Floodplain Change Analysis over a 100-Year Period: Lower Yuba River, California, *Remote Sensing* 2010, *2*, 1797-1825; doi:10.3390/rs2071797.

Gianinetto M., Villa P., 2006. Monsoon flooding response: a multi-scale approach to water-extent change detection, International Archive of the Photogrammetry, Remote Sensing and Spatial Information Sciences.

Glenn, N.F., Streutker, D.R., Chadwick, D.J., Thackray, G.D., Dorsch, S.J., 2006. Analysis of LiDAR-derived topographic information for characterizing and differentiating landslide morphology and activity. Geomorphology 73, 131–148.

Gomez B. 1991. Bedload transport. EarthScience Reviews, 31: 89-132.

Gough A., Clarke S.M., Milodowski A. E., 2012. Controls upon Depositional Architecture and Cyclicity of Alluvial Fan Systems and Associated Environments: Implications for Hydrocarbon Potential, Search and Discovery Article #50589

Gruber, S., Peckham, S., 2009. Land-surface parameters and objects in hydrology, 2009. In:Hengl, T., and Reuter, H.I. (Eds.): Geomorphometry: Concepts, Software, Applications.Elsevier, Amsterdam, pp. 171-194.

Gumiero, B.,B. Maiolini,N. Surian,M. Rinaldi,B. Boz;F. Moroni, 2009. The Italian Rivers, In K. Tockner;U. Uehlinger;C.T. Robinson (Ed.).Rivers of Europe. (pp. Pp 467-495) London, UK: Academic Press.

Hack, J.T., 1957.Studies of longitudinal stream profiles in Virginia and Maryland U. S. Geol. Surv. Prof. Pap., 294B, 97 pp.

Ham DG, Church M. 2000. Bed-material transport estimated from channel morphodynamics: Chilliwack River, British Columbia. Earth Surface Processes and Landforms, 25: 1123-1142.

Hani, A.F.M., Sathyamoorthy, D., Asirvadam, V.S., 2011. A method for computation of surface roughness of digital elevation model terrains via multiscale analysis. Computers & Geosciences 37, 177–192.

Harvey A.M., 2001. Coupling between hillslopes and channels in upland fluvial systems: implications for landscape sensitivity, illustrated from the Howgill Fells, northwest England. Catena 42, pp. 225-250.

Harvey A.M., 2002. The Relationships Between Alluvial Fans And Fan Channels within Mediterranean Mountain Fluvial System. In: Dryland Rivers: Hydrology and Geomorphology of Semi-Arid Channels, Edited by L.J. Bull and M.J. Kirkby, Wiley, pp. 205-227.

Harvey A.M., 2011. The coupling status of alluvial fans and debris cones: a review and synthesis, Earth Surf. Process. Landforms 37, 64–76.

Headquarters, U.S. Army Corps of Engineers. 1985. HEC-1 flood Hydrograph Package, User's manual. Davis, CA: Hydrologic Engineering Center.

Hebeler, F.; Purves, R.S., 2009. The influence of elevation uncertainty on derivation of topographic indices. In Geomorphology 111 (1), pp. 4–16.

Heckmann, T., Schwanghart, W., 2013. Geomorphic coupling and sediment connectivity in an alpine catchment - exploring sediment cascades using graph theory. Geomorphology. Bd. 182,- S. 89-103.

Hejmanowska B., Kay S., 2011. A new approach to DTM error estimation basing on laplacian probability distribution function, Archives of Photogrammetry, Cartography and Remote Sensing, Vol. 22, 2011, pp. 201-213.

Hengl T., Evans I.S., 2009. Mathematical and Digital Models of the Land Surface. In: Geomorphometry. Concepts, Software, Applications. T. Hengl and H. I. Reuter Eds, 31-63.

Heritage GL, Milan DJ, Large ARG, Fuller IC. 2009. Influence of survey strategy and interpolation model on DEM quality. *Geomorphology,* **112**: 334-344.

Hooke J., 2003. Coarse sediment connectivity in river channel systems: a conceptual framework and methodology. Geomorphology, 56 (1-2). pp. 79-94.

Höhle, J., Potuckova, M., 2006. The EuroSDR test checking and improving of digital terrain models. In: EuroSDR Official Publication no. 51. pp. 10–55.

Höhle, J., Potuckova, M., 2011. Assessment of the Quality of Digital Terrain Models. European Spatial Data Research, Official Publication n. 60.

Höhle J., Höhle M., 2009. Accuracy assessment of digital elevation models by means of robust statistical methods, ISPRS Journal of Photogrammetry and Remote Sensing 64, 398–406.

Horn B.K.P, 1981. Hill shading and the reflectance map Proceedings of the IEEE, 69 (1), pp. 14–47.

Hubbard A, Willis I, Sharp M, Mair D, Nienow P, Hubbard B, Blatter H. 2000. Glacier mass-balance determination by remote sensing and high-resolution modelling. *Journal of Glaciology,* **46**: 491-498. DOI: 10.3189/172756500781833016.

Hughes M.L., McDowell P.F., Marcus W.A., 2006. Accuracy assessment of georectified aerial photographs: Implications for measuring lateral channel movement in a GIS, Geomorphology, Volume 74, Issues 1–4, pp. 1-16.

Huss M., Farinotti D., Bauder A., Funk M., 2008. Modelling runoff from highly glacierized alpine drainage basins in a changing climate, Hydrological Processes, 22, 3888-3902.

Hydrologic Engineering Center, 1998. HEC-1 Flood Hydrograph Package User's Manual. Hydrologic Engineering Center, US Army Corps of Engineer, Davis, California.

Ichim, I., Rădoane, Maria, 1987. A multivariate statistical analysis of sediment yield and prediction in Romania. Geomorphological Models, ed. Fr.Ahnert, Catena Suppl.10,137 - 146. ISBN 3-923381-10-7.

Li, Z., 1988. On the measure of digital terrain model accuracy, The Photogrammetric Record, 12(72):873–877.

Jaboyedoff, M., Baillifard, F., Couture, R., Locat, J., and Locat, P., 2004. Toward preliminary hazard assessment using DEM topographic analysis and simple mechanic modeling, in: Landslides Evaluation and stabilization.

Jaboyedoff M., Derron M.-H., 2005. A new method to estimate the infilling of alluvial sediment of glacial valleys using a sloping local base level, Geografia Fisica e Dinamica Quaternaria 28, 37-46.

James, L. A.,Watson, D. G., and Hansen,W. F. , 2007. Using LiDAR data to map gullies and headwater streams under forest canopy: South Carolina, USA, Catena, 71, pp. 132–144.

James L.A., Hodgson M E., Ghoshal S., Latiolais M. M., 2012. Geomorphic change detection using historic maps and DEM differencing: The temporal dimension of geospatial analysis, Geomorphology 137 (2012) 181–198.

Jain, V., Tandon, S.K.., 2010. Conceptual assessment of (dis)connectivity and its application to the Ganga river dispersal system. Geomorphology, 118, 349-358.

Jarman D, Agliardi F, Crosta GB., 2011. Megafans and outsize fans from catastrophic slope failures in Alpine glacial troughs: the Malser Haide and the Val Venosta cluster, Italy. Geol Soc Lond Spec Publ. 351:253–277.

Jenks, G. F. 1967. The Data Model Concept in Statistical Mapping, International Yearbook of Cartography 7: 186-190.

Karimi, N., Farokhnia, A., Shishangosht, S., Elmi, M., Eftekhari, M., & Ghalkhani, H. 2012.. Elevation changes of Alamkouh glacier in Iran since 1955, based on remote sensing data. *International Journal of Applied Earth Observation and Geoinformation, 19*, 45–58. doi:10.1016/j.jag.2012.04.009.

Kienholz, H., Perret, S., Schmid, F., Naturgefahren, A.P., Alpenkonvention, 2006. Documentazione degli eventi naturali: guida per la documentazione sul terreno. Segretariato permanente della Convenzione delle Alpi.

Klir G ., Yuan B., (1995). Fuzzy Sets and Fuzzy Logic: Theory and Applications, Prentice Hall, Upper Saddle River, NewJersey, 574 pp.

Korup O. 2013. Landslides in the fluvial system. In: Orme A.R. and Sack D. (Eds), Treatise on Geomorphology, Academic Press, San Diego, pp. 244-259.

Lague D., Davy P., Crave A., 2000. Estimating uplift rate and erodibility from the area-slope relationship: examples from Brittany (France) and numerical modeling, Phys. Chem. Earth (A), 25. n.6-7, pp- 543-548.

Lane L., J., Hernandez M., Nichols M., 1997. Processes controlling sediment yield from watershed as functions of spatial scale, Environemntal Modelling & Software, Vol. 12, No. 4, pp. 355-369.

Lane SN, Westaway RM, Hicks DM. 2003. Estimation of erosion and deposition volumes in a large, gravel-bed, braided river using synoptic remote sensing. *Earth Surface Processes and Landforms,* **28**: 249-271. DOI: 10.1002/esp.483.

Lashermes B, Foufoula-Georgiou E, Dietrich WE. 2007. Channel network extraction from high resolution topography using wavelets. Geophysical Research Letters 34: L23S04. DOI:10.1029/2007GL031140.

Li, Z. 1988: On the measure of digital terrain model accuracy. Photogrammetric Record 12, 873–77.

MacMillan R.A., Shary P.A., 2009. Landforms and landform elements in geomorphometry. In: Geomorphometry - Concepts, Software, Applications, Hengl, T. and Hannes I. Reuter (eds.), Series Developments in Soil Science, pp. 227-254.

Macconi P., Zischg A., Mazzorana B., Sperling M., Marangoni N., Pollinger R., 2008. A standardized procedure for the compilation and documentation of

historical flood and debris flow events in south tyrol within the framework of the event documentation system ED30, in Tagungsband der Fachtagung der Internationalen Forschungsgemeinschaft, INTERPRAEVENT 2008.

Macconi P., Formaggioni O., Sperling M., 2011. Report Annuale ED30 2011, Provincia Autonoma di Bolzano.

Maggioni M., Gruber U., 2003. The influence of topographic parameters on avalanche release dimension and frequency, Cold Regions Science and Technology 37, 407– 419.

Mammoliti M, 2011. Studio dei metodi di Valutazione della Pericolosità associata ai Debris Flow in Ambiente Alpino, Tesi di dottorato di ricerca, Dipartimento di Scienze della Terra e Geologico-Ambientali, Università degli Studi, Bologna, 204 pp.

Maner S.B., 1958. Factors influencing sediment delivery rates in the red Hills physiographic area. Trans.Am. Geophys.Union, 39: 669-675.

Maner S.B., 1963. Geology in sediment delivery ratios, in Proceedings of the Federal Inter-Agency Sedimentation Conference, [January 28-February 1] 1963.

Mark D.M., 1975. Geomorphometric Parameters: A Review and Evaluation, Geografiska Annaler. Series A, Physical Geography, Vol. 57, No. 3/4, 165-177.

Mark D.M., 1988. Network models in geomorphology M.G. Anderson (Ed.), Modelling Geomorphological Systems, John Wiley and Sons, Chichester, pp. 73–97

Martin Y , Church M, 1995. Bed-Material Transport Estimated from Channel Surveys - Vedder River, British-Columbia, Earth Surface Processes and Landforms, 20(4): 347{361.

McKean J., Roering, J., 2004. Objective landslide detection and surface morphology mapping using high-resolution airborne laser altimetry. Geomorphology 57, 331–351.

Melton M.A., 1965. The geomorphic and paleoclimatic significance of alluvial deposits in Southern Arizona Journal of Geology, 73, pp. 1-38.

Meßenzehl, K., Hoffmann, T., Dikau, R., 2014. Sediment connectivity in the high-alpine valley of Val M¨uschauns, Swiss National Park linking geomorphic field mapping with geomorphometric modelling, Geomorphology, DOI: 10.1016/j.geomorph.2014.05.033.

Milan, D. J., Heritage, G. L. and Hetherington, D., 2007. Application of a 3D laser scanner in the assessment of erosion and deposition volumes and channel change in a proglacial river. Earth Surf. Process. Landforms, 32, pp. 1657–1674.

Milan D.J., Heritage G.L., Large A.R.G., Fuller I.C., 2011. Filtering spatial error from DEMs: Implications for morphological change estimation, *Geomorphology*, 125 (1) , pp. 160-171.

Miller VC., 1953. A quantitative geomorphologic study of drainage basin characteristics in the Clinch Mountain area, Virginia and Tennessee, Project NR 389042, Tech Report 3. Columbia University Department of Geology, ONR Geography Branch, New York

Miller, P.E., Kunz, M., Mills, J.P., King, M.A., Murray, T., James, T.D., Marsh, S.H., 2009. Assessment of Glacier Volume Change Using ASTER-Based Surface Matching of Historical Photography. Ieee T Geosci Remote, 47(7), 1971-1979.

Molloy B. I., Stepinski T.F, 2007. Automated Mapping of Valley Networks on Mars. Computers and Geoscience, 33, p728-738

Montgomery D.R., 2001. Slope distributions, threshold hillslopes, and steady-state topography Am. J. Sci., 301, pp. 432–454.

Montgomery, D.R. , Dietrich, W.E., 1992. Channel initiation and the problem of landscape scale Science, 255 , pp. 826–830.

Montgomery, D.R., Foufoula-Georgiou E., 1993. Channel network source representation using digital elevation models Water Resour. Res., 29, pp. 3925–3934.

Montreuil A.L., Levoy F., Bretel P., Anthony E.J., 2014. Morphological diversity and complex sediment recirculation on the ebb delta of a macrotidal inlet (Normandy, France): A multiple LiDAR dataset approach, Geomorphology, Volume 219, 15 August 2014, pp. 114-125, ISSN 0169-555.

Moretto, J., Rigon, E., Mao, L., Picco, L., Delai, F. & Lenzi, M.A., Medium- and shortterm channel and island evolution in a disturbed gravel bed river (Brenta River, Italy). Journal of Agricultural Engineering, 43(4), pp. 176–188, 2012.

Mukherjee, S., Mukherjee, S., Garg, R. D., Bhardwaj, A., and Raju, P. L. N., 2013. Evaluation of topographic index in relation to terrain roughness and DEM grid spacing, J. Earth Syst. Sci., 122-3, 869– 886.

Nikolopoulos E.I., Borga M., Marra F., Crema S., Marchi L., 2014. Debris flow in the Eastern Italian Alps: seasonality and atmospheric circulation patterns. Submitted to Natural Hazards and earth System Sciences.

O'Callaghan, J.F., Mark, D.M., 1984, The extraction of drainage networks from digital elevation data,*Computer Vision, Graphics, and Image Process.* , 28(3), 323-344.

Olaya, V., 2009. "Basic land-surface parameters." In: T. Hengl and H.I. Reuter, eds. Geomorphometry: concepts, software, applications. Developments in Soil Science, 33. Amsterdam: Elsevier, pp. 141–169.

Passalacqua P, Tarolli P, Foufoula-Georgiou E. 2010. Testing spacescale methodologies for automatic geomorphic feature extraction from LiDAR in a complex mountainous landscape. Water Resources Research 46: W11535. DOI:10.1029/2009WR008812.

Picco L., Mao L, Cavalli M, Buzzi E, Rigon E, Moretto J, Delai F, Ravazzolo D, Lenzi M, 2012. Using Terrestrial Laser Scanner to assess the morphological dynamics of a gravel-bed river, IAHS-AISH Publication, Wallingford, 428-437.

Pike, R.J., 2002. A bibliography of terrain modeling (geomorphometry), the quantitative representation of topography — supplement 4.0. Open-File Report 02-465. U.S. Geological Survey, Denver, 116 pp. http://geopubs.wr.usgs.gov.

Pike R. J., Evans, I., Hengl, T., 2009. Geomorphometry: A Brief Guide. In: Geomorphometry - Concepts, Software, Applications, Hengl, T. and Hannes I. Reuter (eds.), Series Developments in Soil Science, vol. 33, Elsevier, pp. 3-33.

Pirotti F, Tarolli P, 2010. Suitability of LiDAR point density and derived landform curvature maps forchannel network extraction. Hydrol Process 24:1187–1197.

Poeppl R.E., Keesstra S. D., Keiler M., Coulthard T., Glade T., 2013. Impact of dams, dam removal and dam-related river engineering structures on sediment connectivity and channel morphology of the Fugnitz and the Kaja Rivers, 5th Symposium Conference Volume for Research in Protected Areas, Mittersill, 10 to 12 June 2013, pp. 607 - 614.

Provincia Autonoma di Bolzano- Alto Adige, 2007. Piano generale di utilizzazione delle acque pubbliche per la Provincia Autonoma di Bolzano. Supplemento n. 2 al B.U. n. 40/III del 2.10.2007, pp. 274.

Poeppl R.E., Keesstra S., Keiler M., Coulthard T., Glade T., 2013. Impact of dams, dam removal and dam-related river engineering structures on sediment connectivity and channel morphology of the Fugnitz and the Kaja Rivers, 5th Symposium for Research in Protected Areas, Conference Volume, pp. 607-614.

Quattrochi D.A., Goodchild M.F., 1997. Scale in Remote Sensing and GIS, CRC Lewis Publishers, Boca Raton .

Raich H., 2011. Analisi della pericolosità del bacino del rio Gadria attraverso indagini storico-documentali, Tesi di laurea magistrale in Scienze forestali e ambientali, pp. 135.

Rasemann S., Schmidt J., Schrott L., Dikau R., 2004. Geomorphometry in mountain terrain. In: Bishop, M.P., Shroder, J.F. (Eds.), GIS & Mountain Geomorphology, Springer, Berlin, pp. 101–145.

Renard, K., Foster, G.R., Weessies, G.A., Mc Cool, D.K., Yodler, D.C., 1997. Predicting soil erosion by water—a guide to conservation planning with the Revised Universal Soil Loss Equation (RUSLE). U.S. D.A.- A.R.S., Handbook No 703. 384 pp.

Rippin D, Willis I, Arnold N, Hodson A, Moore J, Kohler J, Björnsson H. 2003. Changes in geometry and subglacial drainage of Midre Lovénbreen, Svalbard, determined from digital elevation models. *Earth Surface Processes and Landforms,* **28**: 273-298. DOI: 10.1002/esp.485.

Ritter P., A vector-based slope and aspect generation algorithm, Photogrammetric Engineering and Remote Sensing, 53 (8), pp.1109-1111.

Roehl, J. E., 1962. Sediment source areas-, delivery ratios and influencing morphological factors. In: Commission of Land Erosion (Symposium of Bari, 1-8 October 1962), 202-213. IAHS Publ. no. 59.

Rumsby, B. T., Brasington, J., Langham, J. A., McLelland, S. J., Middleton, R., Rollinson, G. (2008). Monitoring and modelling particle and reach-scale morphological change in gravel-bed rivers: Applications and changes. Geomorphology, 93(1-2), 40-54. Sponsorship: NERC ARSF, the BGRG Research Fund, and The University of Hull.

Scheidl C., Rickenmann D., Chiari M., 2008. The use of airborne LiDAR data for the analysis of debris flow events in Switzerland, Natural Hazards Earth System Science, 8, pp. 1113–1127.

Schenk I., 1966. Un contributo alla conoscenza delle conoidi nelle valli alpine. La Geografia nelle scuole, vol. 11, pp. 97-104.

Schlunegger F., Badoux A., McArdell B.W., Gwerder C., Schnydrig D., Rieke-Zapp, D., Molnar P., 2009. Limits of sediment transfer in an alpine debris-flow catchment, Illgraben, Switzerland. Quaternary Science Reviews 28, 1097-1105.

Schmid U.G., Sardemann S., High-frequency avalanches: release area characteristics and run-out distances, Cold Regions Science and Technology 37, pp. 439-451.

Schrott, L., Hufschmidt, G., Hankammer, M., Hoffmann, T., Dikau, R., 2003. Spatial distribution of sediment storage types and quantification of valley fill deposits in an alpine basin, Reintal, Bavarian Alps, Germany. Geomorphology 55, 45–63.

Schumm S.A., 1955. The relation of drainage basin relief to sediment loss. International Association of Scientific Hydrology Publication, 36, pp. 216-219.

Schürch, P., Densmore, A. L., Rosser, N. J., Lim, M. and McArdell, B. W., 2011. Detection of surface change in complex topography using terrestrial laser scanning: application to the Illgraben debris-flow channel. Earth Surf. Process. Landforms, 36, pp. 1847–1859.

Sharpnack D.A., Akin G., 1969. An algorithm for computing slope and aspect from elevations, Photogrammetric Engineering, 35 (3) , pp. 247–248.

Shary, P.A., 1995. Land surface in gravity points classification by a complete system of curvatures. Mathematical Geology 27, 373–390.

Shary, P.A., Sharaya, L.S., Mitusov, A.V., 2005. The problem of scale-specific and scale free approaches in geomorphometry. Geografia Fisica e Dinamica Quaternaria 28, 81–101.

Shepard, M.K., Campbell, B.A., Bulmer, M.H., Farr, T.G., Gaddis, L.R., Plaut, J.J., 2001. The roughness of natural terrain: a planetary and remote sensing perspective. Journal of Geophysical Research 106, 777–795.

Singh, S. and Singh, M.C., 1997. Morphometric analysis of Kanhar river basin, National Geographical J. of lndia, (43), 1: 31-43.

Smrecek, R., Danihelová, Z., 2013. Forest stand height determination from low point density airborne laser scanning data in Roznava Forest enterprise zone (Slovakia). iForest - Biogeosciences and Forestry, 6(1), 48-54.

Sofia G, Tarolli P, Cazorzi F, Dalla Fontana G., 2011. An objective approach for feature extraction: distribution analysis and statistical descriptors for scale choice and channel network identification. Hydrology and. Earth System Science 15: 1387–1402. DOI:10.5194/hess-15-1387-2011.

Sougnez, N., Van Wesemael, B, V. Vanacker, 2011. Low erosion rates measured for steep, sparsely vegetated catchments in southeast Spain. In: Catena 84: 1-11.

Stampfly G. M., 2001. Geology of the western Swiss Alps, a guide book. Memoires de Geologie, Lousanne, 36, pp. 174.

Stock J., Dietrich W.E., 2003.Valley incision by debris flows: evidence of a topographic signature Water Resour. Res., 39, p. 1089.

Strahler, A.N., 1964. Quantitative geomorphology of drainage basins and channel networks In. Handbook of Applied Hydrology, McGraw Hill Book Company, New York, Section 4-II.

Tarboton, D.G., Bras, R.L., Rodríguez-Iturbe, I., 1989. The analysis of river basins and channel networks using digital terrain data, Report 326, Ralph M. Parson Lab.,Dept.of Civil Engineering. MIT, Cambridge, Mass.

Tarboton D.G., Bras R.L., Rodríguez-Iturbe I., 1991. On the extraction of channel networks from digital elevation data, Hydrol. Process., 5, pp. 81–100

Tarboton DG., 1997. A new method for the determination of flow directions and upslope areas in grid digital elevation models. Water Resour Res 33:309–319.

Tarolli P, Dalla Fontana G, 2009. Hillslope to valley transition morphology: new opportunities from highresolution DTMs. Geomorphology 113:47–56.

Tarolli P., Sofia G., Dalla Fontana G., 2012. Geomorphic features extraction from high-resolution topography: landslide crowns and bank erosion, Nat Hazards , 61:65–83.

Tate J.N., Atkinson P.M., 2001. Modelling Scale in Geographical Information Science, John Wiley and Sons, Chichester.

Taylor J., 1997. An Introduction to Error Analysis: the Study of Uncertainties in Physical Measurements, volume Second Edition, University Science Books, Sausalito, California, second edition edition, 327 pp.

Tralli D, Blom G., Zlotnicki V., Donnellan A., Evans L. D., 2005. Satellite remotesensing of earthquake, volcano, flood, landslide and coastal inundation hazards, Journal of Photogrammetry & Remote Sensing, 59, 185-198.

Theler D., Reynard E., Lambiel C., Bardou E., 2010. The contribution of geomorphological mapping to sediment transfer evaluation in small alpine catchments. Geomorphology 124, 113-123.

Theule J.I., F. Liebault , , A. Loye, D. Laigle, M. Jaboyedof, 2012. Sediment budget monitoring of debris-flow and bedload transport in the Manival Torrent, SE France, Nat. Hazards Earth Syst. Sci., 12, 731–749.

Thommeret N., Bailly J.S., Puech C., 2010. Extraction of thalweg networks from DTMs: application to badlands. Hydrology and Earth System Sciences Discussions, Copernicus Publications, 14 (8), p. 1527 - p. 1536.

Thompson, C., Croke, J., Grove, J., Khanal, G., 2013. Spatio-temporal changes in river bank mass failures in the Lockyer Valley, Queensland, Australia (2013) *Geomorphology*, 191, pp.129-141.

Toy, T.J., G.R. Foster, and K.G. Renard. 1999. RUSLE for mining, construction and reclamation lands: Journal of Soil and Water Conservation v. 54, no. 2, p. 462-467.

Travis, M. R., Elsner, G. H., Iverson, W. D. and Johnson, C. G., 1975. VIEWIT computation of seen areas, slope and aspect for land-use planning. U.S. Dept. of Agriculture Forest Service Gen. Techn. Rep. PSW 11/1975. Pacific Southwest Forest and Range Experimental Station, Berkley, California, 70 pp.

Tucker DG, Bras R.L., 1998 Hillslope processes, drainage density, and landscape morphology Water Resour. Res., 34, pp. 2751–2764.

Unwin, D., 1981. Introductory Spatial Analysis. Methuen, London and New York, 212 pp.

Vale, S.S. and Fuller, I.C., 2009. Morphological budgeting in the Motueka River: analysis of technique. GeoScience, 2009/1, Understanding river sediment dynamics for catchment and coastal management 17 Downloaded by [Massey University Library] at March 2014 1 – 17. Available from: http://muir.massey.ac.nz/handle/10179/1119

Verstraeten G., Poesen, J., 2001. Factors controlling sediment yield from small intensively cultivated catchments in a temperate humid climate, Geomorphology, Volume 40, Issues 1–2, pp. 123-144.

Vianello A., Cavalli M., Tarolli P., 2009. LiDAR-derived slopes for headwater channel network analysis, Catena 76, 97–106.

Vigiak, O., Borselli, L., Newham, L.T.H., McInnes, J., Roberts, A.M., 2012. Comparison of conceptual landscape metrics to define hillslope-scale sediment delivery ratio. Geomorphology 138, 74–88.

Wack, R., Selzl, H., 2005. Laser DTM generation for South-Tyrol and 3D visualization. Proceedings of the ISPRS Workshop "Laser scanning 2005". ISPRS, Enschede, the Netherlands, pp. 48–53.

Walling, D.E. 1983. The sediment delivery problem, Journal of Hydrology, 65, 209–23.

Walling D.E., Zhang, Y., 2004. Predicting slope-channel connectivity: a national-scale approach, *Sediment Transfer through the Fluvial System* (Proceedings of a symposium held in Moscow. August 2004). IAHS Publ. 288. 2004.

Wasklewicz T., Staley D.M., Reavis K., Oguchi T., 2013. Digital Terrain Modeling, In Treatise on Geomorphology, edited by John F. Shroder, Academic Press, San Diego, 2013, pp 130-161.

Walstra J., Chandler J.H., Dixon N., Dijkstra T.A., 2004. Time for change – quantifying landslide evolution using historical aerial photographs and modern photogrammetric methods, In International Archives of Photogrammetry, Remote Sensing and Spatial Information Sciences, 35:475–480. International Society for Photogrammetry and Remote Sensing (ISPRS). Commission IV. Working Group 8.

Wechsler SP. 2007. Uncertainties associated with digital elevation models for hydrologic applications: a review. Hydrology and Earth System Science 11: 1481–1500.

Wehr A., Lohr U., 1999. Airborne laser scanning – an introduction and overview, Journal of Photogrammetry and Remote Sensing, 2-3, 68-82.

Wester T, Wasklewicz T., Staley D., 2014. Functional and structural connectivity within a recently burned drainage basin, Geomorphology 206 (2014) 362–373.

Wheaton J.M., 2008. Uncertainty in Morphological Sediment Budgeting of Rivers. PhD Thesis, University of Southampton, Southampton, 412 pp.

Wheaton JM, Brasington J, Darby SE, Sear DA. 2010. Accounting for uncertainty in DEMs from repeat topographic surveys: improved sediment budgets. *Earth Surface Processes and Landforms,* **35**: 136-156. DOI: 10.1002/esp.1886.

Whishmeier, W.H., Smith, D.D., 1978. Predicting Rainfall Erosion Losses—A Guide to Conservation Planning. U.S. department of Agriculture. 537.

Wilcock, P. R., 2001. Toward a practical method for estimating sediment-transport rates in gravel-bed rivers, *Earth Surf. Processes Landforms*, **26**,1395–1408.

Wilson, J.P., Gallant, J.C., 2000. Digital terrain analysis. In: Wilson, J.P., Gallant, J.C. (Eds.), Terrain analysis: principles an applications. Wiley, New York, 1-27.

Williams RD., 2012. DEMs of difference, Geomorphological techniques (Ed.), British Society for Geomorphology, p. 17.

Wolman, M.G., Miller, J.P., 1960. Magnitude and frequency of forces in geomorphic processes. The Journal of Geology 68, 54-74.

Wood, J. W., 1996. The geomorphological characterization of digital elevation models. Ph.D. Dissertation, Department of Geography, University of Leicester, Leicester, U.K., 456 pp.

Zadeh LA, 1965. Fuzzy Sets, Information and Control, 8(3): 338-353.

Zevenbergen L. W., Thorne C.R., 1987. Quantitative analysis of land surface topography Earth Surface Processes and Landforms, 12 , pp. 47–56.

http://www.pcn.minambiente.it/GN/progetto_pst.php [2/01/2015]